Feedback mechanisms between PAR polarity effectors and the actomyosin cytoskeleton

Alicia Gascón Fernandez-Gubieda

Doctor of Philosophy

Submitted: May 2021

ABSTRACT

The *Caenorhabditis elegans* zygote is polarised into an anterior and a posterior domain thanks to PAR proteins and the actomyosin cytoskeleton. These proteins are well conserved and play a central role in polarising different animal cell types. In the *C. elegans* zygote cortex, the actomyosin cytoskeleton organises into 'foci' structures, which depend on the RHO-1/ LET-502 pathway (orthologues of the human RHO-A and ROCK) and polarise the PAR proteins thanks to actomyosin flow. Although this process has been well described, very little is known so far about how PAR proteins could in turn regulate the actomyosin cytoskeleton.

In the anterior domain, PAR proteins organise in two distinct complexes: a PAR-3 dependent complex, and the CDC-42 dependent complex. The kinase PKC-3 can bind both, and is active when bound to CDC-42. In this thesis we explore the dynamics of the CDC-42/PKC-3 complex and identify PKC-3 as a positive regulator the actomyosin flow via regulation of the RHO/LET-502 pathway, and via phoshoryation of CDC-42.

Furthermore, we identify two feedback mechanisms between LET-502 and anterior PARs: LET-502 can regulate the organisation of anterior PARs and is required for recruitment of phosphorylated CDC-42 to actomyosin foci.

Graphical Abstract

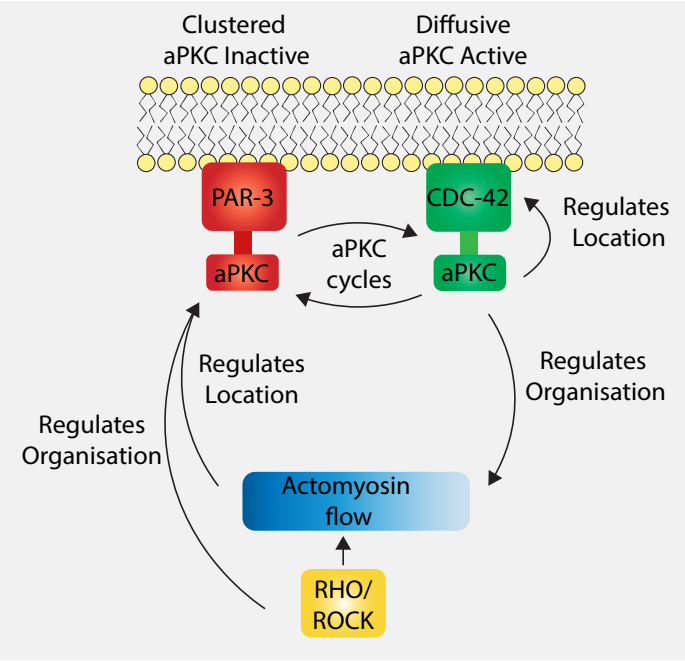

ACKNOWLEDGEMENTS

First, I would like to thank my supervisor Dr Josana Rodriguez for the opportunity to work on this project and for her overall insight and guidance.

I would also like to thank our collaborators Sundar Naganathan and Natasha Savage for their help with data analysis and their helpful comments. As well as Newcastle University and the former ICaMB for providing the funding for my PhD.

Thank you also to other members the lab: Iolo, John, and Jack; as well as the other members of our shared lab and office space, past and present: Beccy, Diana, Tyrell, Beth, Chris, Nik, Ben, Mark, Connor. Thanks specially to Jack and Beccy, who started their PhDs with me, and have made me feel sane throughout it.

Finally, I would like to thank my family and friends, this would not have been possible without you. Gracias a mis bios de Mansión, especialmente Sandra, Alba, Bea, Leire y Paula, por los casi 10 años de compañía y amistad. A mi hermana, Aruna, y sobre todo a mis padres, Josu y Malú, por 27 años de apoyo y por brindarme los recursos que necesitaba para llegar aquí.

Gracias a todos, eskerrik asko danoi, thank you.

PUBLICATIONS

Work from this thesis has lead to the publication of the following articles and reviews:

Rodriguez J*, Peglion F*, Martin J, Hubatsch L, Reich J, Hirani N, **Gubieda AG**, Roffey J, Fernandes AR, St Johnston D, Ahringer J, Goehring NW. (August 2017) aPKC Cycles between Functionally Distinct PAR Protein Assemblies to Drive Cell Polarity. *Dev Cell.*

Gubieda AG*, Parker J*, Squire I, Martin J, Rodriguez J. (August 2020) Going with the flow: insights from *Caenorhabditis elegans* zygote polarisation. *Philos Trans R Soc B.*

Gubieda AG, Parker J, Naganathan S, Squire I, Savage N, Martin J, Rodriguez J. (2021) aPKC regulates actomyosin flow and anterior PAR organisation via phosphorylation of the small GTPase CDC-42. (To submit)

Martin J, Chumakova L, Parker J, Squire I, **Gubieda AG**, Rodriguez J. (2021) The novel role of chromokinesin KLP-19 in cell polarity. (To submit)

TABLE OF CONTENTS

LIST OF TABLES AND FIGURES

ABBREVIATIONS

3' utr	Three prime untranslated region
A/P	Anterior/Posterior
AJ	Adherens Junction
Amp	Ampicillin
ANI-1	Anillin-1 (C. elegans)
aPKC	atypical Protein Kinase C (*Drosopila*, mammalians; PKC-3 orthologue)
APS	Ammonium persulphate
ASI	Asymmetric Index
ATP	adenosine triphosphate
Baz	Bazooka (*Drosophila*, PAR-3 orthologue)
C. elegans	Caenorhabditis elegans
CDC-42	Small GTPase Cell Division Cycle 42 (*C. elegans*)
Cdc42	Small GTPase Cell Division Cycle 42 (mammalians, yeast, *Drosophila*)
CDK	Cyclin-dependent kinase
CGEF-1	cdc-42 GEF
CHIN-1	Chimaerin
CRIB	Cdc42 and Rac interactive binding motif
CV	Coefficient of Variation
CYK-4	Cytokinesis defect protein
DAPI	4′,6-diamidino-2-phenylindole
ddH_2O	double distilled water
Dlg	Discs-large
DNA	deoxyribonucleic acid
Drosophila	Drosophila melanogaster
DSHB	Developmental Studies Hybridoma Bank
dsRNA	double stranded RNA
E. coli	Escherichia coli
ECT-2	Epithelial Cell Transforming 2 protein
EtOH	Ethanol
F-Actin	Filamentous actin
Farp1	FERM, ARH/RhoGEF And Pleckstrin Domain Protein 1
Fwd	Forward
GAP	GTPase activating factor
GBP	G-protein binding domain
GDP	Guanosin Diphosphate
GEF	Guanine exchange factor
GFP	Green fluorescent protein
GMC	Ganglion mother cell
GTP	Guanosin Triphosphate
GTPase	GTP hydrolase
Insc	Inscuteable
IPTG	Isopropyl β-D-thiogalactoside
LB	Luria Bertani Broth

LET-502	Lethal-502 (*C. elegans*, ROCK orthologue)
Lgl	Lethal(2)giant larvae
LGL-1	Lethal Giant Larva (*C. elegans*, Lgl orthologue)
MDCK	Madin-Darby Canine Kidney cells
MetOH	Methanol
Mira	Miranda
miRNA	micro RNA
MRCK	Myotonic dystrophy kinase-related Cdc42-binding kinase
mRNA	messenger RNA
Mud	Mushroom body defect (*Drosophila*, LIN-5 and NuMa orthologue)
N-WASP	Neural Wiskott-Aldrich syndrome protein
NB	Neuroblast
NEBD	Nuclear envelope breakdown
NGM	Nematode Growth Medium
NMY-2	Non Muscular Myosin II
NuMa	nuclear mitotic apparatus protein (mammalians, LIN-5 and Mud orthologue)
ORF	open reading frame
PAK	p21-activated kinase
PALS1	Proteins Associated with Lin Seven 1
Par	Partitioning defective protein effectors (*Drosophila* and mammalians)
PAR	Partitioning defective protein effectors (*C. elegans*)
PATJ	PALS1-Associated Tight Junction protein
PBS	phosphate buffer salinum
PCR	polymerase chain reaction
PFA	Paraformaldehyde
Pins	Partner of Inscuteable
PIV	Particle Imagine Velocimetry
PKC-3	Protein Kinase C 3 (*C. elegans*, aPKC orthologue)
PKN	Protein Kinase N
Pros	Prospero
RAC-1	Ras-related C3 botulinum toxin substrate 1 (*C. elegans*; Rac1 orthologue)
Rac1	Ras-related C3 botulinum toxin substrate 1 (mammalians; RAC-1 orthologue)
RDE	RNAi Defective protein
Rev	Reverse
RGA-3/4	RhoGAP proteins 3 and 4
RHO-1	Ras-like GTP-binding protein (*C. elegans*, RhoA orthologue)
RhoA	Ras-like GTP-binding protein (mammalians, RHO-1 orthologue)
RISC	RNA induced silencing complex protein
RNA	Ribonucleic acid
RNAi	RNA interference
ROCK	Rho-associated protein kinase (*Drosophila*, mammalians; LET-502 orthologue)
S. cerevisiae	Saccharomyces cerevisiae
Scrb	Scribble
SDS-PAGE	Sodium dodecyl sulfate-poly-acrylamide gel
Ser	Serine
SJ	Septate Junction

TBS	Tris Buffered Saline
TEMED	N, N, N', N'-Tetramethylethylenediamine
Thr	Threonine
TJ	Tight Junction
Tx	Triton X
WASP	Wiskott–Aldrich syndrome protein
WSP-1	Wiskott-Aldrich syndrome protein homolog 1 (*C. elegans*; WASP orthologue)

CHAPTER 1. INTRODUCTION

1.1. Asymmetric Cell Division and Cell Polarity

Asymmetric cell division is a process employed both by prokaryote and eukaryote cells to generate cellular diversity and control cell fate (Sunchu and Cabernard, 2020), and often involves the segregation of different RNA and/or cell fate determinants to two daughter cells (Dworkin, 2009, Knoblich, 2010). It is an essential process for the correct development of multicellular organisms and its dysregulation can lead to processes such as tumorigenesis (Knoblich, 2010).

A lot of the key players and regulators of asymmetric cell division are well-conserved in all animals, such as the invertebrates *Caenorhabditis elegans* and *Drosophila melanogaster* (hereafter referred to as *C. elegans* and *Drosophila*), which have served as the main models for its study. These organisms require of three key events for asymmetric cell division (Goldstein and Macara, 2007, Hoege and Hyman, 2013, Devenport, 2014, Ajduk and Zernicka-Goetz, 2016, Mazel, 2017):

1. The presence of a symmetry breaking cue; which is followed by
2. The asymmetric segregation of proteins for the establishment of cell polarity; and
3. The maintenance of cell polarity and translation of polarity signals into polarised outputs.

Cell polarity is the asymmetric localisation or organisation of components along an axis within the cell, and besides being required for asymmetric cell division it is also required for the formation of different and specialised regions within a cell, such as axons or cilia, and processes such as directed cell migration or cell-cell communication (Goldstein and Macara, 2007, Hoege and Hyman, 2013, Devenport, 2014, Ajduk and Zernicka-Goetz, 2016, Mazel, 2017). The establishment of these distinct regions depends on both spacial and temporal information, and as above mentioned, is initiated by a symmetry breaking cue. The nature of the symmetry breaking cue varies depending on the organisms: from the sperm-donated centrosome in *C. elegans* zygotes (Wright and Hunter, 2003, Cowan and Hyman, 2004), to

interactions with somatic follicle cells in the formation of the *Drosophila* oocyte (Roth and Lynch, 2009) or the position of the chromosomes during meiosis I in mouse oocytes (Yi et al., 2013a, Yi et al., 2013b).

Despite the differences in the symmetry breaking cue in these organisms, many of the proteins that mediate polarity and translate polarity cues seem to be highly conserved. Among these key effectors are the PAR proteins, identified in 1988 because of the partitioning-defective phenotype (symmetric division) that arises from their deletion in the *C. elegans* zygote (Kemphues et al. 1988).

1.4. Mechanisms for Polarity Establishment and Maintenance in the *Caenorhabditis elegans* zygote

One of the best characterised systems for the study of cell polarity is the *C. elegans* zygote (**Figure 1.1**), in which the anterior and posterior domain are determined by PAR proteins. PAR proteins are divided into two groups based on their localisation along the anterior/ posterior axis: anterior PARs (aPARs, in orange) which localise at the anterior cortex of the embryo, and posterior PARs (pPARS, in blue) which localise at the posterior cortex upon polarisation.

Anterior PARs (which include the scaffolding protein PAR-3, PAR-6 and the atypical protein kinase C homologue aPKC) are located all throughout the egg cortex before fertilisation, whereas posterior PARs (such as the kinase PAR-1, PAR-2 and LGL-1) are located in the cytoplasm (**Figure 1.1 A-C**). Upon fertilisation, the side of the egg contacted by the sperm becomes the posterior domain via two semi-redundant pathways: first, the parentally donated centrosome induces a cortical actomyosin flow, which pushes anterior PARs towards the anterior domain (Cowan and Hyman, 2004, Munro et al., 2004). At the same time, the microtubules emanating from the centrosome protect posterior PAR-2 from phosphorylation by PKC-3, allowing PAR-2 and other pPARs to load to the membrane (Zonies et al., 2010, Motegi et al., 2011). In this text these two pathways are referred to as the flow-dependent and the microtubule-dependent pathways, respectively.

The two domains established in the A/P axis at the first stages after fertilisation are then maintained for the rest of the first cell division thanks to the mutual inhibition between anterior and posterior PARs (**Figure 1.1 D**). Once pPARs have loaded into the cortex of the zygote, anterior and posterior PARs mutually exclude each other: on the posterior domain PAR-1 kinase can further exclude aPARs by phosphorylating PAR-3, which acts as a membrane anchor for the other aPARs (Benton and St Johnston, 2003, Motegi et al., 2011);

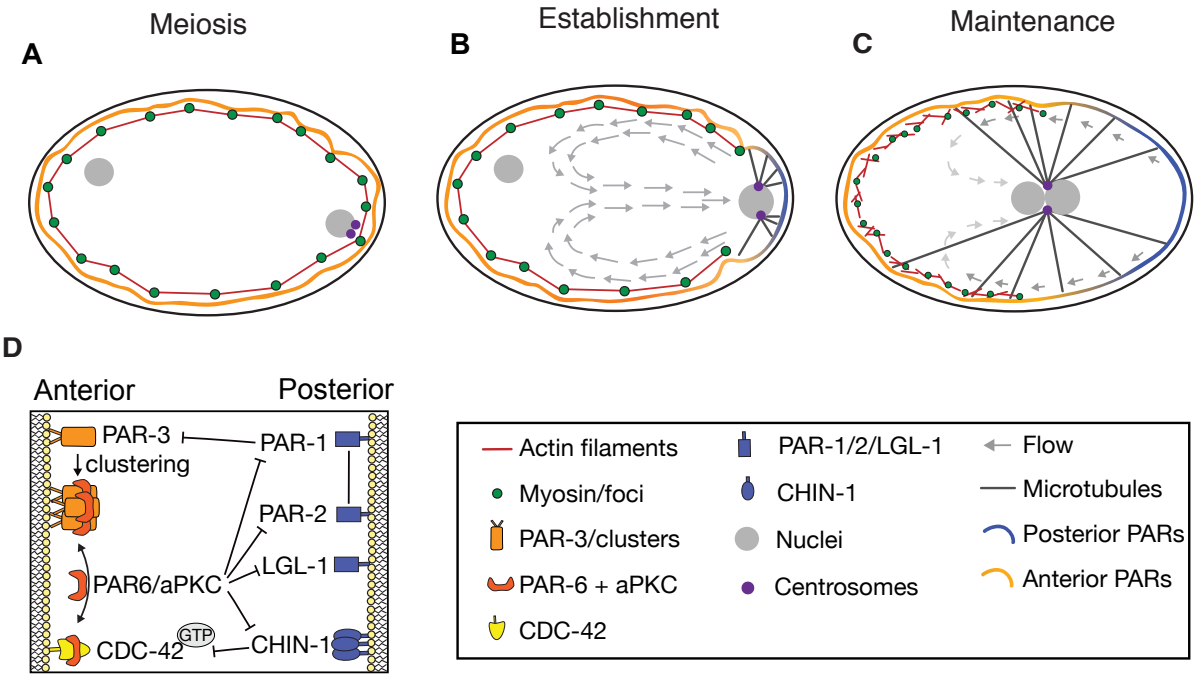

Figure 1.1. Organisation of PAR proteins and their interactions in the worm zygote. A-C. Before the worm zygote becomes polarised, anterior PAR proteins (in orange) localise all over in the membrane, and actomyosin foci (myosin foci in green, actin filaments in red) localise all over the cortex. Soon after fertilisation the zygote becomes polarised into an anterior and a posterior domain thanks to the sperm centrosome. Anterior PARs (in orange) will localise to the anterior domain together with the actomyosin cytoskeleton, and posterior PARs (in blue) will load at the posterior. Once polarity has been established, the actomyosin network dissasembles. The PAR domains are then maintained for the rest of the cell divisions thanks to mutual inhibition between anterior and posterior PARs. **D**. Known interactions between anterior and posterior PARs, interactions between PARs and the membrane, and known clusters. PAR-3 can form clusters, which bind to the PAR-6/aPKC heterodimer. This heterodimer can also exist in a complex with CDC-42, which does not form clusters and diffuses freely in the membrane. CDC-42 can be inhibited by CHIN-1, which localises at the posterior. And PAR-1 (posterior) can inhibit PAR-3 clustering. At the meantime, the anterior kinase aPKC can phosphorylate and prevent CHIN-1, LGL-1, PAR-2 and PAR-1 from localising to the anterior. (Similar version of this figure already published in Gubieda et al. 2020)

and on the anterior domain PKC-3 can phosphorylate pPARs, such as PAR-2 and LGL-1, and release them from their association with the membrane (Betschinger et al., 2003, Zonies et al., 2010, Visco et al., 2016).

The asymmetric localisation of anterior and posterior PARs mediates several processes that eventually lead to an asymmetric cell division, in which one of the daughter cells becomes the somatic cell line precursor and the other cell becomes the germ line precursor. Some of the downstream processes governed by PAR asymmetry include: spindle positioning (determined by PAR-3 and the kinase activity of PKC-3 (Etemad-Moghadam et al., 1995, Colombo et al., 2003, Galli et al., 2011, De Simone et al., 2016)) and the asymmetric concentration of cell fate determinants (which depends on the kinase activity of PAR-1) (Griffin et al., 2011, Wang and Seydoux, 2013, Seydoux, 2018); and abnormalities in PAR polarity are known to lead to processes such as tumorigenesis and metastasis (Knoblich, 2010, Gandalovicova et al., 2016).

1.5. Actomyosin Cortical Flow as a Mechanism for Polarity in the *Caenorhabditis elegans* zygote

1.5.1. The Actomyosin Cytoskeleton: Structure and Function

Actomyosin networks are fundamental elements of eukaryotic cells, and participate in all sorts of morphogenic and mechanosensor processes, from polarity establishment to cell migration (Koenderink and Paluch, 2018). In *C. elegans* the actomyosin cytoskeleton is required both for the retraction of PAR proteins in polarity establishment and for maintaining the PAR domains during polarity maintenance stages (Munro et al., 2004, Goehring et al., 2011b, Small and Dawes, 2017). The actomyosin cytoskeleton is formed by non muscular myosin II (NMY-2 in *C. elegans*, Myosin II in mammalian cells), actin filaments (F-actin), and several cross-linkers, scaffolding and regulatory proteins (Zaidel-Bar et al., 2015), which have self-organising properties and respond and adapt to both chemical and physical stimuli (Misteli, 2001, Levayer and Lecuit, 2012, Zaidel-Bar et al., 2015).

Actomyosin networks are contractile and have very complex dynamics, with movements that range from oscillatory waves to flow (Levayer and Lecuit, 2012). The contraction of the

actomyosin network is a result of the action of the motor protein NMY-2 “walking” on actin filaments (Koenderink and Paluch, 2018). NMY-2 is made up of three different monomers (**Figure 1.2 A**): the NMY-2 heavy chain (formed by two globular heads joined by a long tail), a regulatory light chain (RLC, which can be phosphorylated and regulates the activity of the protein, also known as MLC-4 in *C. elegans*) and an essential light chain (ELC, which stabilises the structure, also known as MLC-5 in *C. elegans*). These heads bind the actin filament and move from its minus to its plus end in a “walking” motion (with one head attached while the other one detaches and advances). NMY-2 can dimerise via its tail, generating a dimer that can assemble into antiparallel oligomers that can bind actin in its two ends and slide in parallel actin filaments. Depending on the organisation of the actin filaments, the forces will pull the actin filaments together, apart, or a mixture of both (Koenderink and Paluch, 2018).

Most studies on the generation of tension and force have been performed in muscular sarcomeres, in which actomyosin is highly organised and not very dynamic. But the structure of actomyosin can vary, and the mechanisms that govern contractility in muscular cells cannot be used to explain the tension generated in non muscular cells, such as the cortex of individual cells or the apical surface of epithelia. Actomyosin structures can be very organised and stable (as sarcomeres), disorganised but stable (as in stress fibres), organised but very dynamic (as in apical constrictions) or both disorganised and dynamic (as in the cell cortex) (Koenderink and Paluch, 2018). In many of these cell types, such as the *Caenorhabditis elegans* zygote or the epithelial cells of *Drosophila melanogaster*, actin filaments arrange themselves in aster-like structures with compact myosin foci in the centre which are constantly going through assembly and disassembly cycles (**Figure 1.2 B-D**) (Coravos and Martin, 2016). In the *C. elegans* zygote, the movement of the cortical actomyosin network towards the anterior domain generates advective actomyosin flows, which are essential for the establishment of polarity. Briefly: contraction of actomyosin towards the anterior domain results in the bulk movement of fluid (the cytoplasm) towards the anterior, which in turn results in the transport of other molecules to anterior (Munro et al., 2004, Goehring et al., 2011b, Reviewed in Gubieda et al., 2020). The following sections describe why the actomyosin network moves

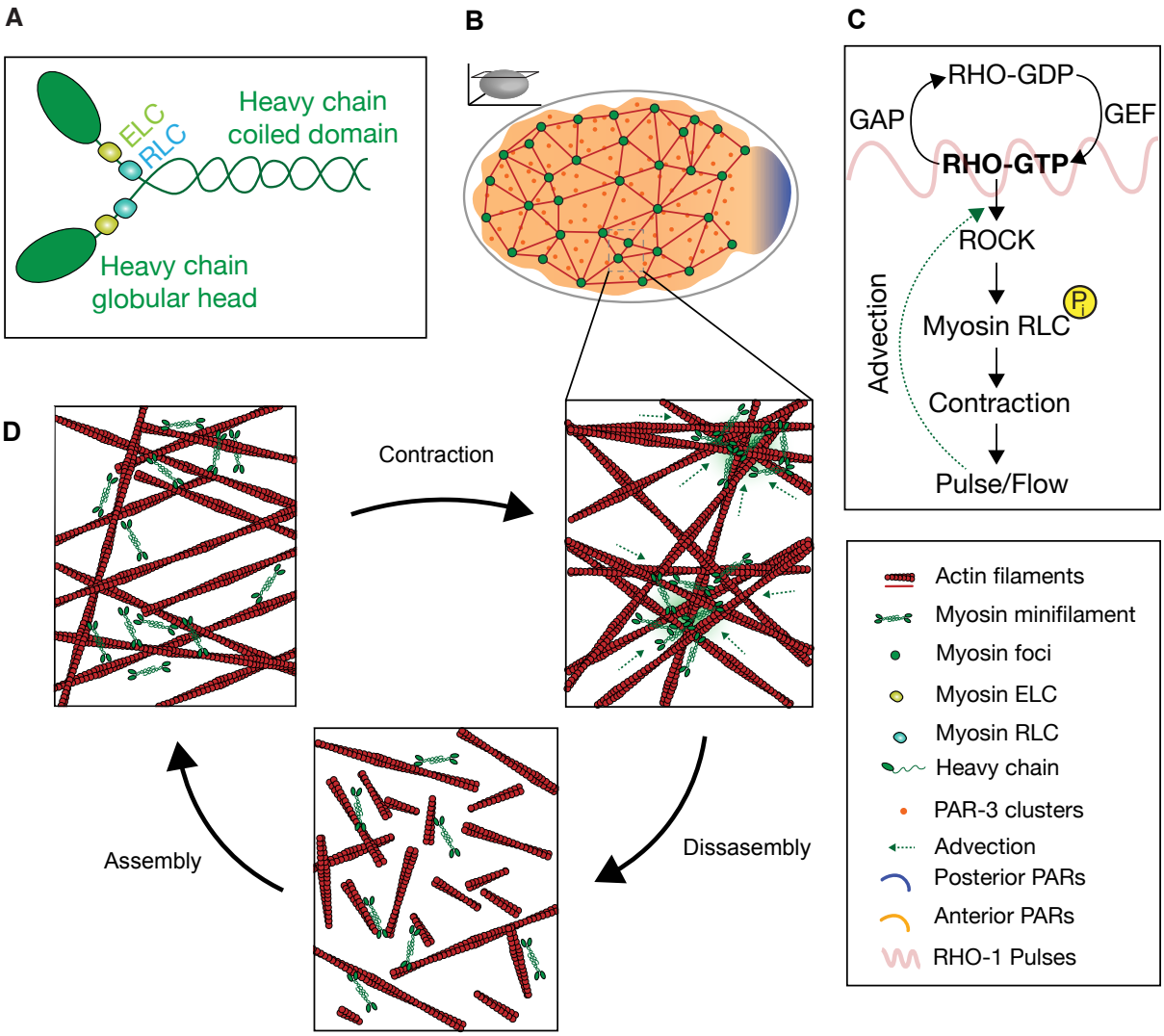

Figure 1. 2. Actomyosin structure, organisation and the RHO pathway. **A.** Non muscular myosin II (NMY-2) is formed by three different peptides: the heavy chain (with a globular head and a coiled tail), an essential light chain (ELC), and a regulatory light chain (RLC). The RLC can be phosphorylated to regulate myosin activity. **B.** In the *C. elegans* embryo, cortical actomyosin organises in foci structures, which can contract and are constantly assembling and dissasembling. This property, called pulsatility, might help accumulate components in the foci by advection. **C.** The RHO pathway regulates actomyosin constriction and flows. The small GTPase RHO is regulated by its GAPs (CYK-4 and RGA-3/4) and its GEF (ECT-2). Active RHO can activate its downstream kinase ROCK (LET-502 in *C. elegans*), which can in turn phosphorylate the RLC (known as myosin light chain-4 or MLC-4 in the worm), leading to NMY-2 mediated contraction. RHO also presents pulsatile activity, with RHO-GTP intensity levels increasing and decreasing every 30 seconds. **D.** NMY-2 foci go through contraction and dissasemby cycles in the *C. elegans* embryo. When active RHO pulses activate ROCK, it will phosphoylate MLC-4, leading to contraction of actomyosin. When the cycle finishes F-actin filaments dissasemble, and the network becomes more disorganised. The network then assembles again with long actin filaments, and the cycle re-starts with another RHO pulse. (Section D based on Selwin Wu et al. 2014's illustration).

towards the anterior, and why some proteins sense this actomyosin flow.

1.5.2. The RHO/LET-502 Pathway and Aurora A as a Symmetry Breaking Cue

One of the key proteins involved in promoting cortical actomyosin flow towards the anterior side of the *C. elegans* zygote is the small GTPase RHO-1, which is located all around the cortex before fertilisation and can activate the myosin regulatory light chain subunit MLC-4, known as RLC in mammals (**Figure 1.2 A**) (Amano et al., 1996, Motegi and Sugimoto, 2006, Schonegg and Hyman, 2006). RHO-1 can act as a molecular switch thanks to its ability to cycle between an active GTP-bound state and an inactive GDP-bound state (Mack and Georgiou, 2014). Small GTPases are activated by guanine nucleotide exchange factors (known as GEFs) and inhibited by guanosine triphosphatase activating proteins (known as GAPs), and their activity can also be affected by post-translational modifications such as phosphorylations (Mack and Georgiou, 2014).

When the sperm-donated centrosome contacts the cortex, it inhibits the activity of RHO-1 GTPase by displacing ECT-2 (a RHO GEF) to the anterior side of the zygote and increasing the concentration of CYK-4 (a RHO GAP) in the posterior (Jenkins et al., 2006, Motegi and Sugimoto, 2006, Schonegg et al., 2007). This is predicted to lead to an increased amount of active GTP-bound-RHO in the anterior side of the cell, and an increased amount of inactive GDP-bound-RHO in the posterior. The RHO effector kinase LET-502 (orthologue of vertebrate ROCK) can then phosphorylate the myosin regulatory light chain (MLC-4), leading to increased non-muscular myosin II (NMY-2) activity and cortex contractions in the anterior domain (Amano et al., 1996, Jenkins et al., 2006, Motegi and Sugimoto, 2006, Schonegg and Hyman, 2006, Nishikawa et al., 2017) (**Figure 1.2 C**). The activity of RHO-1 during the first cell division of *C. elegans* is regulated by another two GAPs too: RGA-3 and RGA-4, which as opposed to CYK-4 (which regulates symmetry breaking), can regulate the contractile activity of the cortex (Schonegg et al., 2007).

This change in contractile activity of actomyosin in the embryo depends on a polarity cue that comes from the sperm-donated centrosome (**Figure 1.3**) (Cowan and Hyman, 2004). This

centrosomal signal has been difficult to characterise, since affecting the components of the centrosome often affects centrosome maturation and the structure of microtubules. But three recent papers have identified the Aurora A homologue AIR-1 (shown as a purple gradient) as the symmetry breaking cue (Kapoor and Kotak, 2019, Klinkert et al., 2019, Zhao et al., 2019). The effect of the cue depends on the proximity of the centrosomes to the cortex (Zhao et al., 2019) and does not require of Aurora to localise to the centrosomes (Zhao et al., 2019) or of centrosomal maturation (Kapoor and Kotak, 2019).

However there is some controversy surrounding the role of AIR-1 as a polarity cue: namely, *air-1* silencing does not result in loss of polarity, as would be expected when removing the polarity cue, and instead results in a bipolar phenotype in which PAR-2 localises to both poles

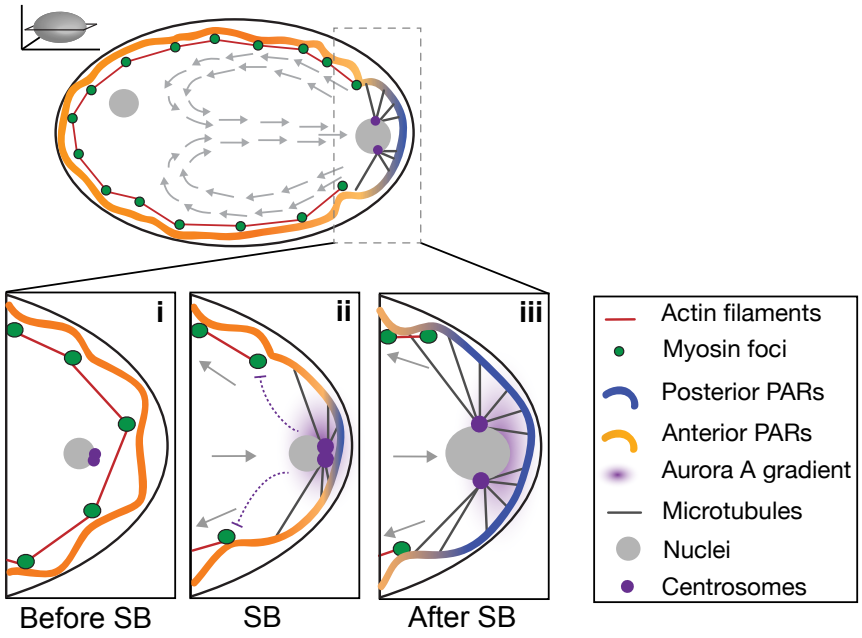

Figure 1. 3. Aurora A as the polarising cue. Midplane view of the embryo during polarity establishment **i**. aPARs initially occupy the membrane, and the centrosomes (purple spheres) are positioned close to the cortex at the future posterior pole. **ii**. A diffusive cue of Aurora A from the centrosomes inhibits actomyosin contractility at the posterior, resulting in cortical flow towards the anterior domain. Microtubules are thought to aid deposition of PAR-2 at the membrane. **iii**. The cortical actomyosin flow also generates a cytosolic backflow, which contributes to placing the posterior male pronucleus closer to the membrane. This simultaneously holds the cue in place to promote cortical flow and, synergising with membrane-bound microtubules, facilitates separation of the centrosomes around the male pronucleus. (Similar version of this figure already published in Gubieda et al. 2020)

of the zygote and the actomyosin cortex flows towards both poles (Schumacher et al., 1998, Noatynska et al., 2010, Klinkert et al., 2019). Due to this inconsistency, other papers postulate that Aurora A is just a regulator of cortical tension and that it protects the zygote from early symmetry breaking during oocyte maturation (Reich et al., 2019).

The molecular pathway by which Aurora A regulates actomyosin flow has not been described yet, but it seems AIR-1 is involved in the regulation of the RHO pathway, as when *C. elegans* embryos are treated with RNAi against AIR-1, the RHO activator ECT-2 does not clear from the posterior membrane as it does in wild type (Motegi and Sugimoto, 2006, Kapoor and Kotak, 2019). Furthermore, Aurora A has previously been described to phosphorylate and inhibit Rok (the kinase downstream of RHO and ROCK homolgue) in *Drosophila* (Moon and Matsuzaki, 2013).

1.5.3. Actomyosin flow requires of PAR oligomerisation to polarise the cell

The actomyosin flow initiated by the sperm centrosomes can push large PAR-3 oligomers (which carry PAR-6 and PKC-3) to the anterior, leading to the formation of an anterior PAR domain (**Figure 1.4 A**) (Munro et al., 2004, Goehring et al., 2011b, Dickinson et al., 2016, Rodriguez et al., 2017). But why do PAR-3 oligomers follow the cortical flow while other PAR proteins do not?

The location of membrane bound proteins is affected by a combination of three factors (Goehring et al., 2011a, Goehring et al., 2011b):

1. The rate of binding and unbinding to the membrane,
2. The rate of lateral diffusion in the membrane, and lastly by
3. Advection by the cortical flow.

Since the actomyosin cortex can act as a fluid, some of the PAR proteins embedded in it will be transported by advection towards the anterior domain without requiring of direct interaction with the cortical network (Goehring et al., 2011b). The best described case of a PAR protein moving with the cortical flow is that of PAR-3, the anteriorly localised scaffolding protein. PAR-3 moves towards the anterior during polarity establishment stage,

when cortical flow is present, even though no physical interactions have been described between PAR-3 and the actomyosin meshwork (Sailer et al., 2015, Dickinson et al., 2017, Rodriguez et al., 2017, Wang et al., 2017).

The key mechanism that allows PAR-3 to follow the cortical flow is its ability to form clusters (Dickinson et al., 2017, Rodriguez et al., 2017, Wang et al., 2017). Monomeric PAR-3 does not bind to the membrane, but PAR-3 oligomerisation results in synergy between monomers, which increases their avidity for the membrane. As a result, cortical clustering of PAR-3 slows down the exchange rate with monomeric PAR-3 in the cytoplasm and stabilises the clusters in

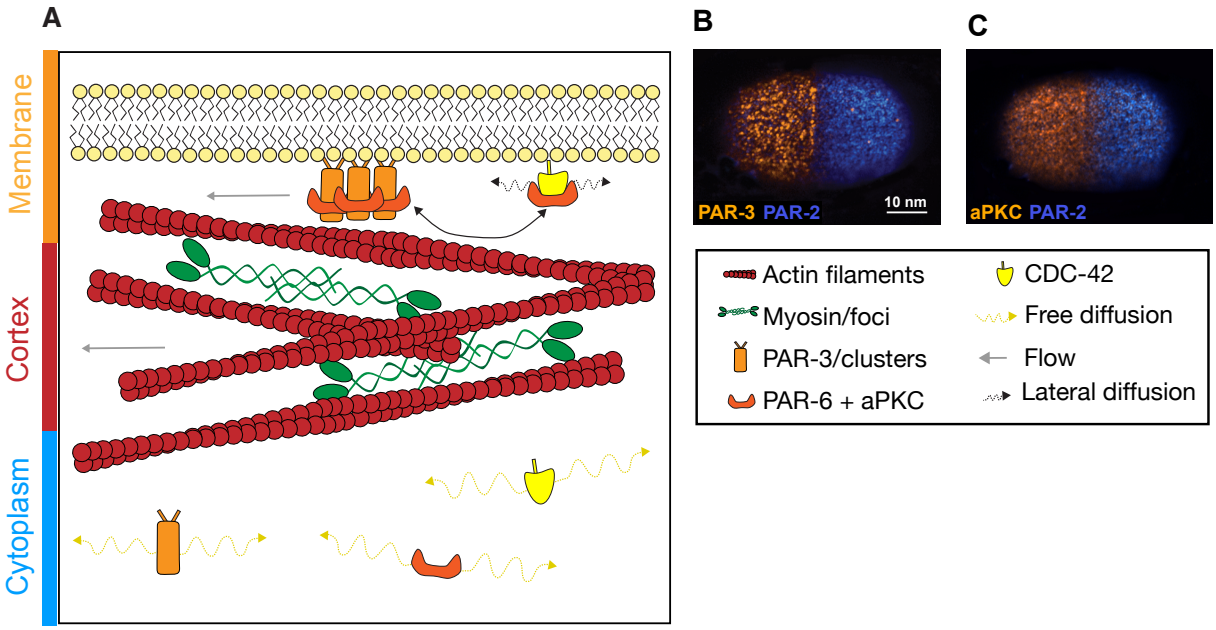

Figure 1. 4. Anterior PAR protein organisation. **A**. Anterior PARs exist in two different membrane-bound complexes: a PAR-3 dependent complex and a CDC-42 dependent complex. PAR-3 clusters can follow advective actomyosin flow even if they are not in direct contact with the actomyosin cytoskeleton, and have high affinity for the PAR-6/aPKC heterodimer. PAR-6/aPKC can also associate with CDC-42, which diffuses laterally in plane of the membrane, not following advective flows. Below the membrane domain, the actomyosin cortex flows towards the zygote anterior, leading to the anterior actomyosin dependent cytoplasmic flow that transports PAR-3 clusters. PAR proteins are also present in the cytoplasm, where they can freely diffuse with high mobility. **B**. Cortical image of PAR-3 and PAR-2 during polarity maintenance PAR-3 forms clustes in the anterior. **C**. Cortical image of aPKC and PAR-2 during early polarity maintenance, aPKC exists both in a clustered state (with PAR-3) and in a diffusive state (with CDC-42), as can be seen by the less punctated organsiation of PKC-3 (as opposed to PAR-3). (Similar version of this figure already published on Gubieda et al. 2020)

the membrane, effectively increasing the length of time that PAR-3 spends of the membrane and thus the time in which it can be advected by cortical flow (Dickinson et al., 2017, Rodriguez et al., 2017, Wang et al., 2017).

However, a stable interaction with the membrane is not enough for advective flow (Rodriguez et al., 2017). When monomeric PAR-3 is forced to localise to the membrane it diffuses freely and does not follow advective flow (Rodriguez et al., 2017). Furthermore, the size of PAR-3 clusters directly correlates with their association with actomyosin flow (Dickinson et al., 2017). This suggests that an increase in cluster size might contribute to flow dependency in two ways: first, by increasing the residency time of the cluster at the membrane, and second, by decreasing the ability of the cluster to freely diffuse on the membrane. The combination of these two factors might allow the directional advection of PAR-3 to surpass its diffusion in the membrane, and results in movement of PAR-3 towards the anterior of the zygote.

Beyond their role in determining their own localisation, PAR-3 clusters are also essential for the regulation of other PAR proteins. Clustering of PAR-3 increases its affinity to PAR-6, which allows PAR-3 clusters to bind the PAR-6/aPKC heterodimer and transport it to the anterior (Dickinson et al., 2017). This PAR-6/aPKC heterodimer exists in two forms: the PAR-3 bound punctate form that follows advective flows and a freely diffusing form bound to CDC-42 (**Figure 1.4 B-C**) (Robin et al., 2014, Sailer et al., 2015, Dickinson et al., 2017, Rodriguez et al., 2017, Wang et al., 2017). Even though CDC-42 can also interact with the membrane and localise to the anterior, its inability to form clusters means that it is not affected by advective flow. CDC-42 localises to the anterior by transiently binding other anterior PARs, and since it is not affected by advective flow it can laterally diffuse in the membrane (Sailer et al., 2015, Dickinson et al., 2017, Rodriguez et al., 2017, Wang et al., 2017).

The presence of PAR-6/aPKC in the anterior is essential for PAR regulation and organisation, and both the punctuate and the diffusive populations are essential to regulate aPKC activity. As our group has previously shown, the kinase aPKC can only phosphorylate its downstream

targets when in complex with PAR-6 and CDC-42 (Rodriguez et al., 2017), and having the ability to switch between the clustered PAR-3 complex and the diffusive CDC-42 complex allows aPKC to localise to the anterior domain when bound to PAR-3 (Dickinson et al., 2017), and to become active and phosphorylate its targets when bound to CDC-42 (Rodriguez et al., 2017).

3.1. CDC-42 and Cortical Flow as a Mechanisms for Polarity Maintenance

While actomyosin flow has mainly been described during establishment, similar but weaker actomyosin flow also occurs during maintenance (at a speed of approx. 2µm/min, compared to approx. 7µm/min during establishment) (Sailer et al., 2015). However regulation of NMY-2 during polarity maintenance depends on different pathways than during establishment: the small GTPase CDC-42 has been reported to control the actomyosin network at polarity maintenance stages as opposed to RHO-1, which generates cortical flow at polarity establishment stages (Gotta et al., 2001, Kay and Hunter, 2001, Aceto et al., 2006, Schonegg and Hyman, 2006).

Besides RHO, CDC-42 is the only other small GTPase known to play a role in the first cell division of the *C. elegans* embryo. The downstream effectors of CDC-42 (such as the actin associated proteins Formins and WASP, or the kinases MRCK or PAK) control actin polymerisation and organisation (Cotteret and Chernoff, 2002), and *cdc-42* RNAi disrupts polarised cortical NMY-2 during maintenance (Motegi and Sugimoto, 2006, Schonegg and Hyman, 2006, Small and Dawes, 2017).

It should be noted however that the cortical actomyosin flow speed in CDC-42 deficient embryos is lower than in wild type embryos during establishment stage, indicating that a positive feedback mechanisms involving CDC-42 is required for initial polarity establishment too (Motegi and Sugimoto, 2006). Even though the role for CDC-42 in regulating polarising flows has not been described before, recent papers have hinted towards a role in NMY-2 recruitment (Small and Dawes, 2017, Gross et al., 2019). Furthermore, removing *nmy-2* with

RNAi results in CDC-42 not segregating into the anterior, pointing to a crosstalk loop between actomyosin and the small GTPase CDC-42 (Schonegg and Hyman, 2006).

Flow of the actomyosin network during maintenance is independent of RHO-1 activity, as seen in *rho-1* RNAi embryos, which fail to establish polarity at early stages but still form a retracted cortical actin network in the absence of RHO-1 during maintenance stage (although this actin network is not properly polarised) (Motegi and Sugimoto, 2006). CDC-42 is also required for normal PKC-3 and PAR-6 cortical localisation. Normally, PKC-3 and PAR-6 load to the membrane by binding PAR-3 and are weakly present in a CDC-42 bound form (**Figure 1.4 A-C**), but PKC-3/PAR-6 can be induced to load to the membrane in a PAR-3 independent and CDC-42 dependent way upon depletion of the HSP90 co-chaperone CDC-37 (Beers and Kemphues, 2006, Rodriguez et al., 2017).

CDC-42 has its own GAP (CHIN-1) and GEFs (CGEF-1), which can regulate the localisation of myosin during the polarity maintenance stages and play a crucial role in cellular processes such as generation of cell morphology, cell motility and cell adhesion (Cotteret and Chernoff, 2002, Kumfer et al., 2010). Besides the regulation of cortical myosin, CHIN-1 has another known roles: it can maintain the asymmetry of the active CDC-42 and regulate the size of the anterior cortical domain in a pathway independent of the posterior LGL-1 and PAR-2 (Beatty et al., 2013). Interestingly, CHIN-1 forms cortical clusters during polarity maintenance stage (Sailer et al., 2015), which can associate with the membrane for even longer than PAR-3 clusters and are coupled to the weak actomyosin flow that occurs during polarity maintenance (Sailer et al., 2015).

3.2. Cross-regulation of PAR proteins and the actomyosin cytoskeleton

Besides CDC-42, other PAR proteins have been reported to regulate NMY-2 in polarity maintenance phase (Small and Dawes, 2017). PAR-1 and PAR-3, for example, are required to ensure that NMY-2 is restricted to the anterior side of the embryo, with PAR-2 and PAR-6 acting downstream of PAR-3 in this process (Small and Dawes, 2017). Likewise, NMY-2 is required to maintain the zygote polarised at maintenance phase, as aPARs expand and pPARs

retract upon its silencing (Liu et al., 2010), suggesting cross-regulation between NMY-2 and PAR proteins (Small and Dawes, 2017).

Anterior PARs have been shown to regulate the dissociation levels of NMY-2 in the anterior domain of the embryo: NMY-2 associates to the cortex at similar rates both in the anterior and posterior domain (anterior k_{on}= 0.19 ± 0.03 μm s^{-1}; posterior k_{on} = 0.21 ± 0.03 μm s^{-1}), but it dissociates from the cortex twice as much as in the posterior (anterior k_{diss}= 0.14 ± 0.01 s^{-1}; posterior k_{diss} = 0.072 ± 0.009 s^{-1}) (Gross et al., 2019). Dissociation rate depends on anterior PAR proteins, as can be observed with *par-6* RNAi treatment (Gross et al., 2019). Furthermore, the anterior aPKC has been identified in fly epithelia and in epithelial cell cultures as a regulator of actomyosin activity (Ishiuchi and Takeichi, 2011, Roper, 2012, Zaidel-Bar et al., 2015), but nothing has been reported about its role in *C. elegans* or in non-epithelial cells yet.

3.3. Cortical Contraction and Flow are Required for Cytokinesis

Following chromosome segregation in anaphase, many molecules assemble into a contractile ring in the equator of the cell to ensure cytokinesis (**Figure 1.5**). Small GTPases, RHO-1 in particular, are essential for the assembly and constriction of this ring (Kamijo et al., 2006, Miller and Bement, 2009). RHO-1 can promote cytokinesis via two separate pathways: first, it can bind the formin-homologous protein DIA and promote the nucleation of filamentous actin (F-Actin); then, it activates the motor activity of non muscle myosin-II (NMY-2) via its canonical LET-502 pathway (**Figure 1.2**). These pathways drive the formation and constriction of the actomyosin ring, respectively (Jaffe and Hall, 2005, D'Avino et al., 2015, Zhuravlev et al., 2017).

Cortical flows also contribute to the assembly of the contractile ring, as they can compress and align actin filaments at the equator (White and Borisy, 1983). During cytokinesis, actomyosin flows from the poles towards the equator, as a result of astral microtubules relaxing contractility in the poles of the zygote (D'Avino et al., 2006, Nishimura and Yonemura, 2006, Khaliullin et al., 2018, Verma et al., 2019). Even though the molecular

mechanism by which microtubules regulate actomyosin in the poles is still unclear, recent research in the *C. elegans* zygote suggests that dynein mediated transport can remove NMY-2 from the poles (Chapa-Y-Lazo et al., 2020). The flow towards the equator can then compress myosin into the equator of the cell, and this compression pulls the nearby cortex into the equator (Menon et al., 2017, Khaliullin et al., 2018). The increase in myosin in the equator would then generate a stronger pull, result in the recruitment of even more myosin into the contractile area (Menon et al., 2017, Khaliullin et al., 2018). This process generates what is called an active RHO zone in the equator of the zygote (Piekny et al., 2005).

Regulation of RHO-1 activity via its GAPs and GEFs is essential for cytokinesis too. The GAP CYK-4, which functions at polarity establishment silencing RHO-1 activity in the posterior domain, has been reported to act non-canonically in cytokinesis: phosphorylated CYK-4 can interact with ECT-2, a RHO-1 GEF, in the spindle mid zone to activate RHO-1 (Wolfe et al., 2009, Zou et al., 2014). CYK-4 can also interact with RHO-1 via two basic

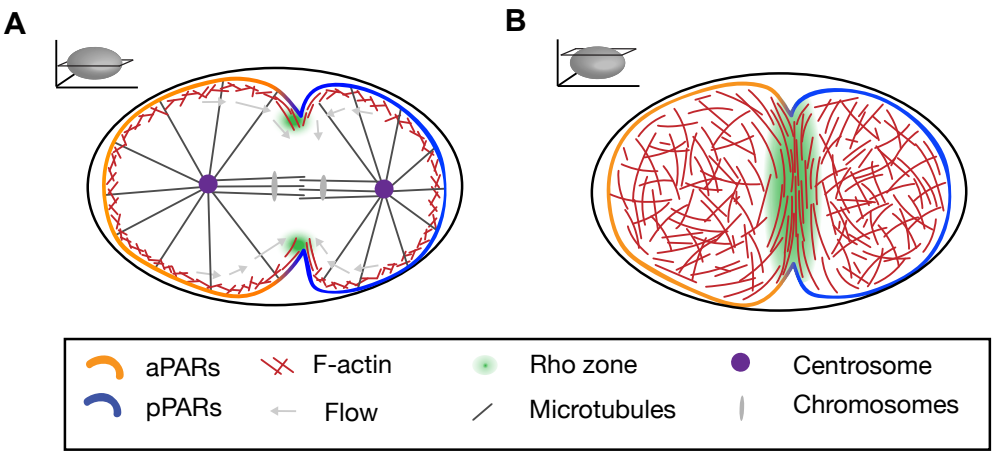

Figure 1.5. Cytokinesis in the worm zygote. A. The zygote midplane during anaphase. Astral microtubules decrease cortical tension in the poles, and the active RHO zone in the equator increases myosin activity. The tension anistropy leads to cortical flow towards the cell equator. **B.** The zygote cortex during cytokinesis, with actin filaments aligning in the equator. (Similar version of this figure already published on Gubieda et al. 2020)

residues, and mutation of these two residues to glutamate exhibits both decreased binding of CYK-4 to RHO-1 and the cortex, and results in slower and less completed furrow ingression (Zhang and Glotzer, 2015).

3.4. Regulation of the Actomyosin Network: Pulsatile Activity

Cortical actomyosin can generate strong forces, and these strong forces can result in instabilities: during contraction the components of the actomyosin network collapse into the contracting clusters, and thus the network becomes disconnected (Alvarado et al., 2013). To avoid the collapse of the network the cells can employ oscillatory/pulsing behaviour (Nishikawa et al., 2017). Pulsatile behaviour is considered an intrinsic characteristic of contractile networks, and has been studied in many developmental processes, such as epithelial cells in *Drosophila*, where they are essential to keep the integrity of the tissue; and the developing mouse, where pulses drive the compaction of the embryo (Martin et al., 2009, Solon et al., 2009, Maitre et al., 2015, Mason et al., 2016). In the *C. elegans* zygote both NMY-2 and RHO pulse, with their intensities increasing and decreasing cyclically in a period of 30 s (**Figure 1.2 C**) (Nishikawa et al., 2017, Naganathan et al., 2018, Saha et al., 2018). Furthermore, these changes in the concentration of the actomyosin components are accompanied by oscillations in the average speed of the cortical flow (Nishikawa et al., 2017).

There are currently two models that explain how pulsatility is achieved (Reviewed in Gubieda et al., 2020): in this thesis, the first model is referred to as the ‘mechanochemical feedback model’, and the second one as the ‘cyclic Rho’ model.

In the mechanochemical feedback model, the actomyosin pulse results in the recruitment of both myosin and activators to the actomyosin network by advection, promoting further contraction (**Figure 1.2 B-C**) (Vasquez et al., 2014, Munjal et al., 2015). At the same time, inhibitors are recruited to the actomyosin network by advection, allowing RHO to become inactive and the actomyosin clusters to dissipate. This delayed negative feedback system results in relaxation of the force, allowing the contraction cycle to restart. This model is based

on behaviour observed in *Drosophila* embryonic cells (Vasquez et al., 2014, Munjal et al., 2015).

In the second model, which is based on data from the *C. elegans* zygote, RHO-1 can coordinate NMY-2 pulses regardless of the motor protein (Nishikawa et al., 2017, Michaux et al., 2018). In this model RHO-1 promotes its own activity, which precedes NMY-2 activity and does not depend on it. This model is supported by single-molecule tracking of NMY-2::RFP in the *C. elegans* zygote, which shows that advection does not contribute to NMY-2 assembly cycles . This pulse is then terminated by the delayed recruitment of RHO inhibitors (like RGA-3/4) to F-actin (Michaux et al., 2018). Due to its independent oscillatory behaviour, RHO is referred to as a 'pacemaker' in this model (Nishikawa et al., 2017, Michaux et al., 2018).

3.5. Regulation of Actomyosin Flow By Other Components of the Network

The amounts of cross-linkers and motor proteins can also affect the behaviour of the actomyosin cytoskeleton, with both increases and decreases in cross-linker and motor levels decreasing contractility (Ding et al., 2017, Descovich et al., 2018). Lack of the actin bundling and crosslinking protein Plastin, for example, results in less coordinated and persistent actomyosin flow during polarity establishment and in polarity defects (Ding et al., 2017). The optimal ratio for constriction has been calculated to be 2:1 (motor to cross-linker), and both increases and decreases in the amount of Plastin from the normal threshold decrease flow velocity (Ding et al., 2017). A similar effect has been described with other cross-linkers during cytokinesis in the *C. elegans* zygote: intermediate levels of Anillin (an F-actin binding protein required for cortical ruffling and cytokinesis in the zygote) have been shown to result in the fastest ring closure, with both higher and lower levels of Anillin resulting in a 'braking' effect (Descovich et al., 2018). Similarly, an increase in the motor protein NMY-2 provides resistance against cytoskeleton remodelling in cytokinesis, indicating that NMY-2 can act both as a motor and as a cross-linker (Descovich et al., 2018).

Another cortical component that can affect the velocity of flow is the E-Cadherin homologue HMR-1 (Padmanabhan et al., 2017). Even though Cadherins are known for their role in cell-cell contacts, they also exist in the form of clusters outside of the junctions, and the single cell zygote allows for the study of this Cadherin population (Wu et al., 2015b, Padmanabhan et al., 2017). During polarisation in the *C. elegans* embryo Cadherin clusters are dragged to the anterior domain by actin filaments, and the HMR-1 clusters decrease the mobility of cortical actomyosin in a way that has been described as a 'picket fence', with HMR-1 clusters acting as a fence against cortical flow (Padmanabhan et al., 2017).

1.4. PAR Exclusion and Activation as a Mechanisms for Polarity Maintenance in the *Caenorhabditis elegans* zygote

As above mentioned, once the anterior and posterior domains have been established, the maintenance of PAR proteins relies on the PAR protein themselves. On one hand, anterior and posterior PARs will mutually exclude each other from their respective domains: the anterior PKC-3, for example, can phosphorylate PAR-1, PAR-2 and LGL-1, limiting their membrane localisation (Zonies et al., 2010, Motegi et al., 2011, Visco et al., 2016); similarly, the posterior PAR-1 has been reported to phosphorylate PAR-3 in *Drosophila*, affecting its membrane binding abilities (Benton and St Johnston, 2003); and lastly, the posterior CHIN-1 inhibits CDC-42 in the posterior domain in the *C. elegans* zygote (Sailer et al., 2015).

On the other hand, anterior and posterior PARs will mutually activate each other: activity of the aPKC homologue PKC-3, for example, is driven by its interaction with CDC-42 in the *C. elegans* zygote (Rodriguez et al., 2017); clustering of PAR-3 can recruit other anterior PARs (Dickinson et al., 2017); and in the posterior PAR-2 helps recruit the kinase PAR-1 (Hao et al., 2006).

1.4.1. Mechanisms of Action and Regulation of the Atypical Protein Kinase C

aPKC phosphorylation of its targets is one of the main mechanisms for the regulation of polarity, to the point where it has even been referred to as 'the kinase that phosphorylates cell polarity' (Hong, 2018). aPKC can phosphorylate its substrates in short stretches of basic and

hydrophobic (BH) amino acids (Bailey and Prehoda, 2015). BH motifs of several aPKC substrates, such as LGL-1, Miranda and Numb, have multiple residues with positive charges which allow for their selective binding to negatively charged phospholipids (Bailey and Prehoda, 2015, Visco et al., 2016). Phosphorylation by aPKC in BH motifs or in regions close enough to the BH to be able to influence the electrostatics of the region can decrease the affinity of said aPKC substrates to the plasma membrane or the cortex, leading to the displacement of proteins from opposite membrane and cortical domains (Bailey and Prehoda, 2015, Hong, 2018). aPKC phosphorylation can also stabilise its substrates in the actomyosin cortex: in the *Drosophila* neuroblast, for example, aPKC phosphorylation of Miranda has been reported to remove it from the apical membrane while favouring its anchoring to the actomyosin cortex in the basal domain (Hannaford et al., 2018).

Other targets of aPKC include: PAR-2, which in the *C. elegans* zygote is excluded from the anterior cortex after phosphorylation by aPKC affects its electrostatic interaction with the membrane (Hao et al., 2006, Goehring et al., 2011a); PAR-1, which in *Drosophila* and mammalian epithelial cells will bind the adaptor protein 14-3-3 (also known as Par-5) instead of the apical membrane upon aPKC phosphorylation (Suzuki et al., 2004, Göransson et al., 2006, Jiang et al., 2015); and Dlg, whose conformation changes upon aPKC phosphorylation, resulting in an activated conformation that allows Dlg to bind its downstream effectors (McGee et al., 2001, Golub et al., 2017).

Given the many substrates of aPKC, the regulation of its activity and location are critical for correct cell polarity (Hong, 2018). Interaction with other proteins is essential for controlling the activity of aPKC, as members of the PKC family (including aPKC) are considered to be self-inhibited in the absence of interactions with other proteins, since the kinase domain of the protein can bind it pseudo-substrate region (Zhang et al., 2014). CDC-42 has been reported to regulate the activity of aPKC in the *C. elegans* zygote (explained in detail in the paragraph below) (Rodriguez et al., 2017); while in the Drosophila embryos both interaction with Cdc42 and Par-6 are believed to be enough to activate aPKC (Hong, 2018).

The correct sub-cellular location and activity state of aPKC is also achieved by interactions with different proteins: in the *C. elegans* zygote, for example, the PAR-6/PKC-3 heterodimer exists in two states (**Figure 1.4 A**) (Robin et al., 2014, Sailer et al., 2015, Rodriguez et al., 2017, Wang et al., 2017): a clustered form bound to PAR-3 (PAR-3/PKC-3/PAR-6) that segregates anteriorly in response to actomyosin flow and in which PKC-3 is does not phosphorylate its downstream targets, and a more diffused CDC-42 dependent assembly (CDC-42/PKC-3/PAR-6) in which PKC-3 can phosphorylate its downstream targets (Dickinson et al., 2016, Rodriguez et al., 2017, Wang et al., 2017). This way, the flow-following PAR-3 assembly promotes a polarised membrane docking of PAR-6/PKC-3, from which PAR-6/PKC-3 can load into the CDC-42 dependent assembly. This CDC-42 dependent assembly can diffuse 5-10 um away from its loading sites to antagonise posterior PARs, and then dissociates to return PKC-3 into the cytoplasm, from where the cycle can start again.

Therefore, the CDC-42 dependent assembly generates an anterior homogenous domain of active PKC-3 based on the spatial information provided by the PAR-3 bound assembly (Rodriguez et al., 2017). The balance between the PAR-3 and the CDC-42 bound assemblies is driven directly by PKC-3, as inactivation of PKC-3's kinase activity stabilises PAR-6/ PKC-3 into its CDC-42 dependent assembly. Interestingly, the RHO-1 effector LET-502 can phosphorylate the PAR-3 in four different residues in migrating cells, inhibiting the interaction between PAR-3 and aPKC and potentially favouring the CDC-42 dependent/active form (Nakayama et al., 2008).

1.4.2. Mechanisms of Action and Regulation of the small GTPase CDC-42

Besides being essential for the correct regulation of aPKC in cell polarity, CDC-42 is also one of the main regulators of the actomyosin cytoskeleton, via effectors such as N-WASP, MRCK-1 or diaphanous related formins (Pichaud et al., 2019).

Most small GTPases, like CDC-42, can associate with the membrane via their C-terminal domain; and in eukaryotes CDC-42 is often found in the plasma membrane, in trafficking vesicles or in the Golgi complex (Erickson et al., 1996, Roberts et al., 2008). Once CDC-42

reaches these locations, it can activate its downstream effectors by binding to their Cdc42 and Rac interactive binding motif (CRIB) domain (Pichaud et al., 2019).

Activation of CDC-42 depends on the aforementioned guanine exchange factors (GEFs) and GTPase activating factors (GAPs), which regulate its association with GTP and GDP (Jaffe and Hall, 2005). Binding to GTP occurs via a GTP binding and hydrolysing domain, domain comprised of 5 α-helices that connect six parallel β-strands (Reviewed in Sprang, 2016). This GTP binding domain consists of two regions that can change their conformation depending on the activation state of the protein and that are key for its specific binding to effector proteins: the Switch I and Switch II domains, comprised respectively of residues 30 to 38 and 60 to 76 in the human CDC-42 (Milburn et al., 1990). In most small GTPases, binding to GTP changes the conformation of the Switch regions, from a signalling-inactive conformation to a signalling-active conformation (Ye et al., 2005). In the case of CDC-42, however, it is the effector proteins that promote conformational changes in GTP bound CDC-42 by interacting with the Phe-37 of the Switch I region. This interaction then leads to an interaction between the Thr-35 and Thr-32 and the γ-phosphate of the GTP molecule (Phillips et al., 2008). For example, interaction of GTP bound CDC-42 with PAK-3 generates a change in the conformation of the Switch I domain, allowing for the Switch I to interact with the γ-phosphate of the GTP, and locking PAK-3 in a complex with CDC-42 (Phillips et al., 2008).

Binding to GTP and GDP might also affect the mobility of CDC-42. The constitutively active Cdc42(Q61L) in budding yeast, for example, has significantly less mobility (membrane exchange) than the wild type Cdc42 (Woods et al., 2016). Therefore inactive GDP-bound Cdc42 could be mobilised (and extracted from the membrane) at a higher rate than active Cdc42, contributing to Cdc42 polarisation (Woods et al., 2016). Similar studies in fission yeast using a photo-activatable form of Cdc42 (mEOS-Cdc42) found that the diffusion rate of GDP-bound Cdc42 at the membrane was higher than that of active GTP-bound Cdc42 (Bendezú et al., 2015). The molecular basis for differential diffusion and/or extraction of GDP- and GTP-bound Cdc42 is still unknown, however it has been hypothesised that the

ability of GTP-bound Cdc-42 to bind effectors could slow down the mobility of these complexes (Woods and Lew, 2019).

1.5. Different Cell Polarity Models

Cell polarity and asymmetric cell division can be established autonomously or as a response to extracellular signalling. Both the worm first cell division and the fruit fly neuroblast cell (the neural stem cell) division have been previously considered to be established autonomously (Knoblich, 2001), although recently the cell-cell contact between the neuroblast and its daughter cells has been shown to orient the division axis (Loyer and Januschke, 2018).

On the other side, the establishment of cell polarity in epithelial cells is more complicated, as it requires both interaction to the extracellular matrix and to neighbouring cells (Yeaman et al., 1999), and has mostly been studied in mammalian cell cultures, *Drosophila* imaginal discs and *Drosophila* ovarian follicular epithelium (Muller, 2000). Finally, budding yeast (which lacks PAR proteins) has served as a good model for the study of Cdc42, which is essential for its polarisation and proliferation (Chiou et al., 2017). Here we will briefly review the polarity machinery of these systems.

1.5.1. *Cell Polarity and Asymmetric Cell Division in Drosophila melanogaster Neuroblast*

The asymmetric cell division of neuroblasts (NB) in the fruit fly is essential for the development of a functional central nervous system. Neuroblasts divide asymmetrically following the apical-basal axis, and in each asymmetric cell division, each NB generates a new NB and a ganglion mother cell (GMC), which will only divide once and generate either a pair of neurons or glial cells (Knoblich, 2001) (**Figure 1.6 A**). The source of the cue that determines the orientation of the NB division depends on the life stage of the fruit fly (Loyer and Januschke, 2020): in embryos, a signal from the overlaying epithelium is essential for recruiting the apical polarity effectors (Siegrist and Doe, 2006, Yoshiura et al., 2012); whereas in larvae in which the NBs are no longer in contact with the epithelium, the contact between NBs and their daughter cells determines orientation (Loyer and Januschke, 2018).

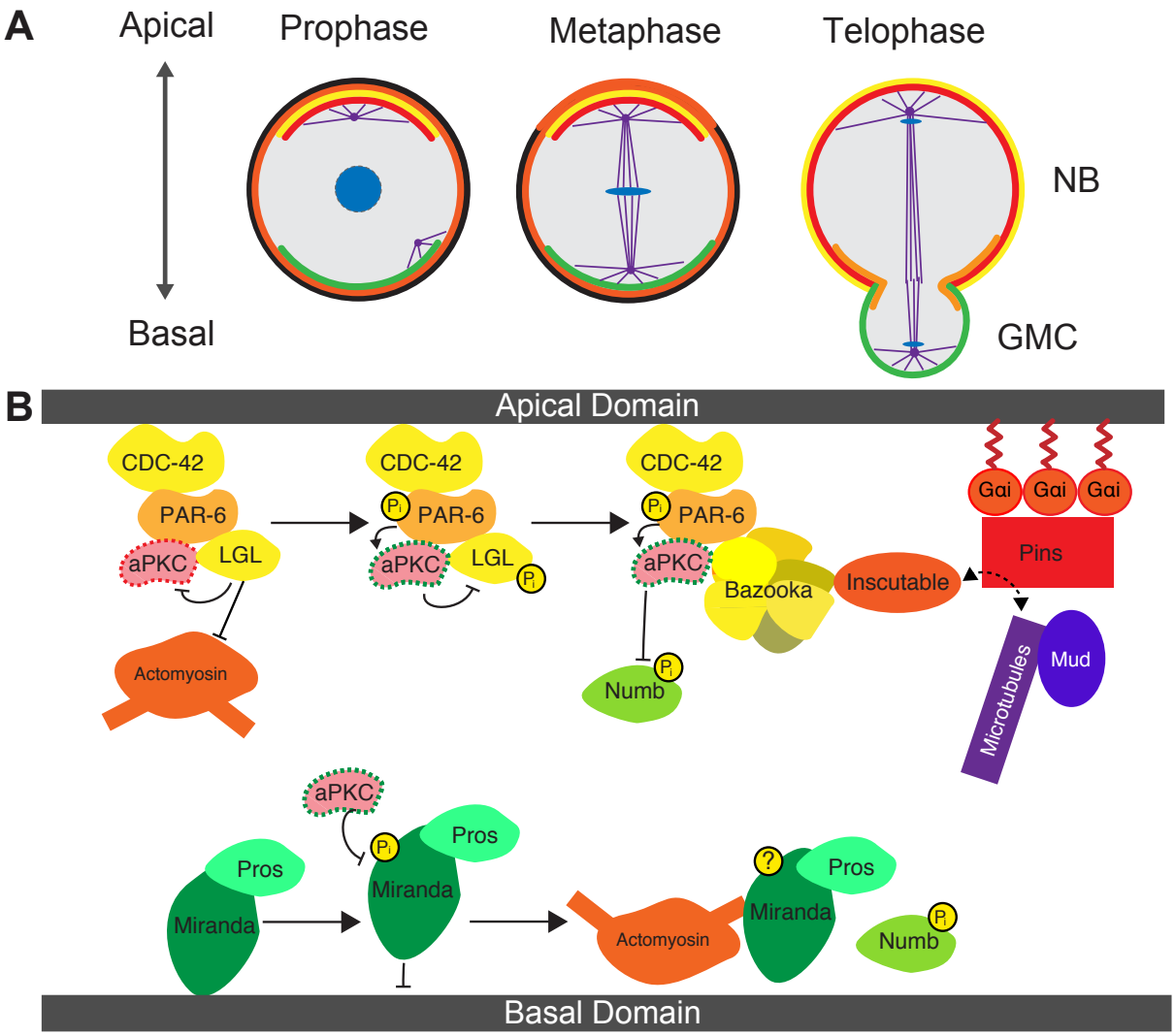

Figure 1.6. Polarity and asymmetric cell division in the fly neuroblast. A. *Drosophila* neuroblasts (NB) divide asymmetrically to generate a new NB and a Gangial Mother Cell (GMC). NBs are polarised during mitosis, with PAR proteins (in yellow) and the Inscutable/Pins/Galfa (in red) complex localising to the apical domain, and the basal determinants Miranda, Prospero and Numb (in green) localising to the basal domain. The Inscutable/Pins/Galfa complex serves as a link between the PAR complex and microbutules (in purple) via the NuMa homologue Mud, with Pins only being able to bind Inscutable when it is not bound to Mud. Actomyosin polarises during metaphase, becoming enriched in the apical domain. It is later cleared from the basal and the apical domain during anaphase, and by telophase it becomes enriched in the equator of the cell, on the future site of cleavage. **B**. The PAR complex varies in composition throughout the cell cycle, during interphase it is composed of aPKC, LGL and PAR-6 (which localise to the membrane via CDC-42). Upon entry into mitosis, Aurora A phosphorylates PAR-6, leaving to aPKC activation. aPKC can then phosphotylate LGL, affecting its interaction with the complex and restricting LGL to the basal domain. LGL is then substituted by Bazooka in the apical PAR complex. Bazooka can then interact with the Inscutable/Pins/Gai complex, which can interact with microtubules via Mud. The composition of the basal domain also varies in composition throughout the cell cycle, during interphase Miranda associates directly with the cortex all over the cell, and during prophase aPKC phosphorylates Miranda and removes it from the membrane. During metaphase, actomyosin allows Miranda to bind into the basal domain. The cell fate determinant Numb becomes enriched in the basal domain after aPKC (bound to Bazooka) phosphorylates it and removes it from the apical domain.

The cell fate determinants that localise basally and segregate into the GMC include Prospero (transcription factor that will promote expression of GMC genes and stop the expression of NB genes), Miranda (segregating factor that binds to Prospero and ensures its segregation to the GMC) and Numb (segregating determinant that prevents cell renewal by suppressing Notch signalling) (Rhyu et al., 1994, Hirata et al., 1995, Knoblich et al., 1995, Shen et al., 1997, Schuldt et al., 1998, Shan et al., 2018); whereas the apically localised polarity effectors include Bazooka (PAR-3 homologue), aPKC, Par-6 and Lgl; as well as the spindle orientation complex: Pins (LGN in mammals), GαI, and Mud (Numa in mammals). Interestingly, and as it occurs in *C. elegans*, Bazooka polarisation is also actin dependent, with actomyosin cortical flows concentrating Baz foci in the apical pole (Oon and Prehoda, 2019), and so it has been hypothesised that the basal cue from the daughter cell that controls Bazooka polarity could be initiating the cortical actomyosin flow (Loyer and Januschke, 2020).

In the apical domain, Bazooka con interact with other Pars. The Par complex varies in composition in the *Drosophila* neuroblast throughout the cell cycle (**Figure 1.6 B**): before the cell enters mitosis it is composed of aPKC, Lethal(2)giant larvae (the fly homologue of LGL), and PAR-6, which localise to the apical cortex thanks to the interaction of PAR-6 with the small GTPase Cdc-42 (which is apically enriched) (Betschinger et al., 2003, Atwood et al., 2007, Wirtz-Peitz et al., 2008). When the NB enters mitosis, the Aurora A kinase phosphorylates Par-6, leading to the activation of aPKC. aPKC can then phosphorylate its target Lgl, which affects its interaction with the membrane and other Par proteins, restricting Lgl to the basal domain of the cell (Betschinger et al., 2003, Wirtz-Peitz et al., 2008). Furthermore, and since aPKC phosphorylation of Lgl disrupts its interaction with Par-6 and aPKC, this allows Bazooka to substitute Lgl as part of the apical complex. Besides phosphorylating Lgl to remove it from the apical membrane (Betschinger et al., 2003), active aPKC can also affect the localisation of basal determinants, such as Miranda and Numb.

The basal determinant Miranda contains seven aPKC phosphorylation sites in its C-terminal domain, which is required for cortical association (Fuerstenberg et al., 1998). Miranda localises uniformly across the cortex during interphase, and is cleared from the apical

membrane during prophase by aPKC phosphorylation in its S96 (Hannaford et al., 2018). After nuclear envelope breakdown, Miranda reappears asymmetrically in the basal domain, due to lack of local aPKC activity, and also to its interaction with the actomyosin cytoskeleton, which helps retain Miranda in the basal pole (Hannaford et al., 2018, Hannaford et al., 2019).

Numb, on the other side, needs to interact both with Bazooka and with aPKC to become phosphorylated (Smith et al., 2007, Wirtz-Peitz et al., 2008). When Bazooka enters the apical Par complex, the substrate specificity of aPKC changes and allows aPKC to phosphorylate Numb in its positively charged N-terminus domain, thus removing it from the apical domain (Knoblich et al., 1997, Smith et al., 2007, Wirtz-Peitz et al., 2008).

Besides interacting with cell fate determinants, the apical Par complex can also recruit the key players for spindle orientation: Inscuteable (Insc), Partner of Inscuteable (Pins), the heterotrimeric G-protein subunit $G_{\alpha i}$ and Mushroom body defect (Mud, the homologue of the vertebrate NuMa and the *C. elegans* LIN-5) (Kraut and Campos-Ortega, 1996, Kraut et al., 1996, Parmentier et al., 2000, Schaefer et al., 2000, Yu et al., 2000, Siller et al., 2006). Bazooka can directly bind Inscuteable (Schober et al., 1999), which in turn binds to Pins, which is bound to the membrane via its interaction with inactive (GDP bound) $G_{\alpha i}$, and to the microtubules via Mud (Schaefer et al., 2000, Schaefer et al., 2001, Nipper et al., 2007). These interactions between the Par complex, the Inscuteable/Pins complex, and NuMa allow for the spindle orientation to be finely controlled; a process that is necessary for correct placement of the cleavage furrow (Roubinet et al., 2017).

Similar to what our lab has described with anterior PARs in the *C. elegan*s zygote, there seems to be a 'division of labour' for the spindle orientation complex in the fly neuroblast: Inscuteable and Mud can bind competitively to the LGN orthologue Pins, and are mutually exclusive (Culurgioni et al., 2011), creating one complex in which Pins could 'sense' its localisation via interaction with the apical PAR compex, and another complex that is 'functional'. This division into two complexes has also recently been observed in murine

mammary stem cells, were Inscuteable forms tetramers with LGN, which bind PAR-3 and $G_{\alpha i}$, and cannot be dissociated by NuMA (Culurgioni et al., 2018).

As in *C. elegans* embryos, the actomyosin network is asymmetrically distributed in *Drosophila* neuroblasts. Non Muscular Myosin II (usually referred to as Myosin II in *Drosophila*) is uniform in the cortex during interphase, and concentrates on the apical domain during prophase and metaphase, as the actomyosin network flows towards the apical domain (Oon and Prehoda, 2019), and basal determinants move towards the basal axis (Barros et al., 2003). In anaphase, cortical flows move Myosin II away from the apical domain and concentrate in the equator of the cell, where the cleavage site will be formed during telophase (Barros et al., 2003, Roubinet et al., 2017). After the asymmetric cell division, Myosin II will be inherited by the GMC (Barros et al., 2003).

The correct localisation of actomyosin requires of crosstalk between Par proteins and the actomyosin network. Lgl and has been shown bind the heavy chain of myosin II, inhibits the assembly of contractile myosin filaments (Strand et al., 1994, Kalmes et al., 1996). aPKC phosphorylation of Lgl can block the interaction between Lgl and actomyosin (Kalmes et al., 1996, Betschinger et al., 2003). This phosphorylation allows for the apical Par proteins to directly regulate actomyosin activity during metaphase, as Lgl phosphorylation in the domain leads to myosin accumulation in the apical cortex (Barros et al., 2003). Furthermore, the progressive recruitment of Pins to the apical domain by Bazooka from prophase to metaphase results in Protein Kinase N (PKN, a negative regulator of myosin (Ferreira et al., 2014)) being recruited to the apical domain towards the end of metaphase, which mediates the dephosphorylation of Myosin II and results in the clearance of myosin in anaphase and its accumulation in an equatorial ring (Tsankova et al., 2017) .

1.5.2. *Epithelial Cell Polarity*

Epithelial cells are polarised along the apical-basal axis (**Figure 1.7**), and this polarity is essential for the cells to carry out their functions and generate correct tissue morphogenesis. Besides having an apical domain, epithelial cells have basolateral domains that are essential for their functions. Epithelial cells form sheets of cells, linked by intercellular junctions that

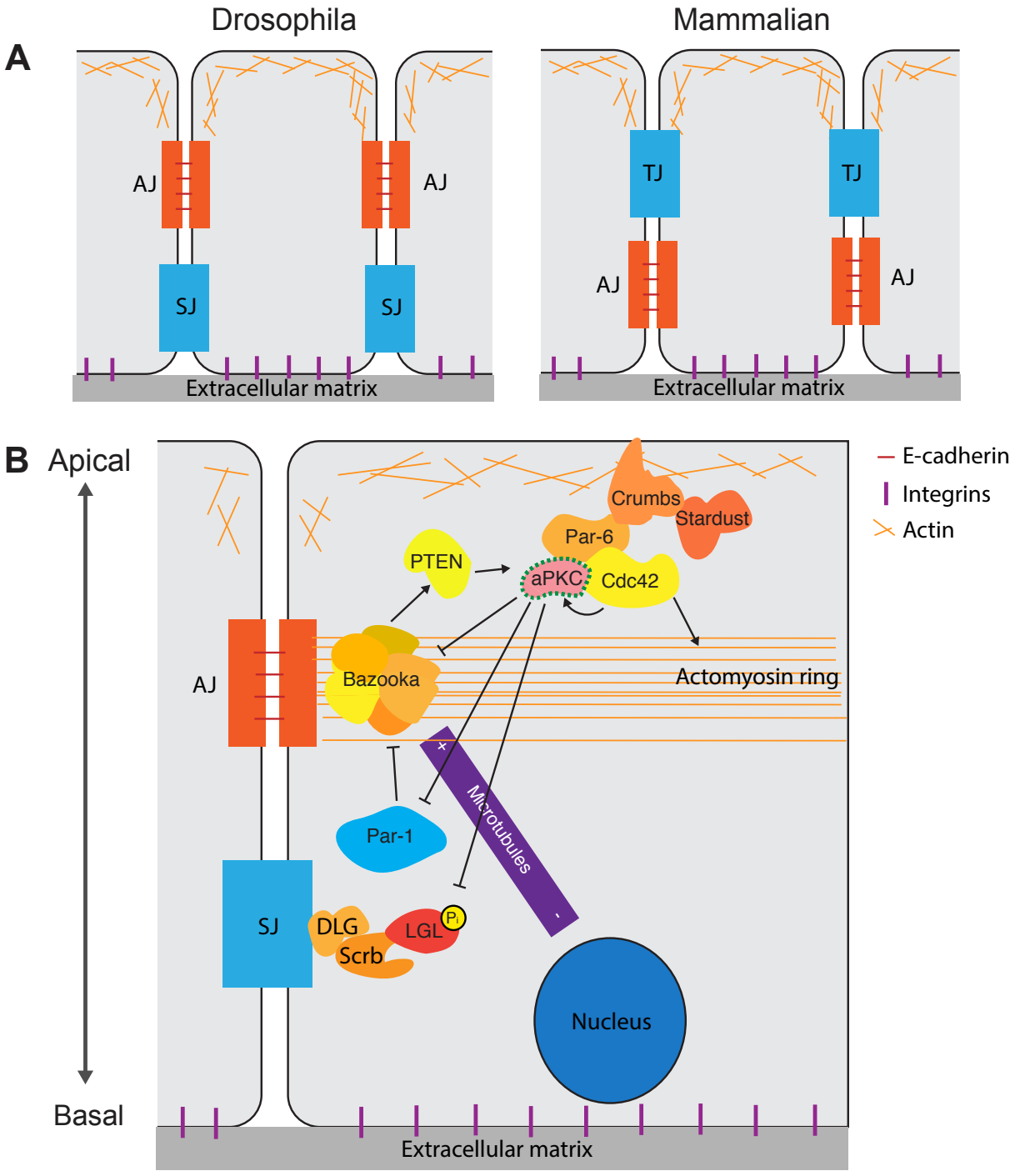

Figure 1.7. Epithelial cell polarity. A. Epithelial cells have apicobasal polarity; the apical side is enriched in actomyosin and the basal domain is attached to the extracellular matrix via integrins. Epithelial cells are attached to each other by adherens junctions (AJ) and septate junctions (SJ) in *Drosophila*, and by tight junctions (TJ) and AJ in vertebrates. **B.** Representation of polarity proteins and structures in a fly epithelial cell. The actomyosin ring, at the apical domain of epithelial cells, is regulated by the apically localised Cdc42. Cdc42 activates aPKC, which can inhibit Bazooka and inhibit its localisation in the apical domains. Bazooka can also regulate apical PARs via PTEN, and is removed from the more basal SJ by phosphorylation of the kinase PAR-1.

both provide adhesion in between the cells and act as a barrier by controlling the permeability (**Figure 1.7 A**) (Reviewed in Goldstein and Macara, 2007, and Rodriguez-Boulan and Macara, 2014). In mammalians a specialised region called adherens junctions (AJ) keeps the epithelial cells together; and another specialised region called tight junction (TJ), located apical to the AJs, serves as a barrier between the interior of the epithelial sheet and the outside environment. Invertebrates have a similar organisation: the epithelia of *Drosophila melanogaster* is linked by AJ and septate junctions (SJ, which serve the function of TJ), but the AJ are located apical to the septate junctions (with the exception of fly midgut epithelia, in which the SJ are located apical to AJ (Chen et al., 2018)). The *C. elegans* epithelia, on the other hand, has a single combined apical junction (*Ce*AJ; which combines the properties of both mammalian AJ and TJ), but even in this single *Ce*AJ junction subdomains can be observed, with the more apical domain being enriched in cadherin and catenins (as are the AJs) (Armenti and Nance, 2012). The presence of these junctions in the lateral domain leads to a very different membrane composition to that in the basal axis: the basal domain of epithelial cells is enriched on extracellular matrix receptors, such as integrins, and contains no intercellular adhesion molecules, such as cadherins (St Johnston and Ahringer, 2010).

Epithelial cell polarity has mostly been studied in *Drosophila* and in mammalian cell cultures; the two systems share many similarities, but get polarised in different ways. The cues that help establish polarity in mammalian epithelia seem to come from neighbouring cells and the extracellular matrix: MDCK cells, for example, require of interactions with the extracellular matrix and with each other to polarise (Yeaman et al., 1999). *Drosophila* epithelium, on the other hand, seem to get their polarity cue from apical actin and apico-basal microtubules, as Bazooka gets transported to the apical axis via dynein dependent transport, and gets stabilised there thanks to the apical actin enrichment (which originates from the geometry of the developing zygote) (Harris and Peifer, 2005, St Johnston and Ahringer, 2010). It should be noted that the mechanisms for polarisation of the fly midgut epithelial is fundamentally different to other *Drosophila* epithelia, where the canonical PAR polarity pathway is not required for polarisation (Chen et al., 2018), perhaps due to it being an absorptive, instead of secretory epithelia.

The key players for polarity establishment and maintenance in secretory epithelia are the same as in *C. elegans* embryos and *Drosophila* neuroblasts (PAR proteins, small GTPases such as CDC-42 and RHO, and the actomyosin cytoskeleton), but also include other groups of proteins, such as the Crumbs complex, which consists of Crumbs, PALS1 (called Stardust in *Drosophila*) and PATJ (PALS-1 associated TJ protein), and the Scribble complex, which consists of Discs-large (Dlg), Lethal Giant larvae (Lgl) and Scribble (Scrb) (**Figure 1.7 B**) (Reviewed in Goldstein and Macara, 2007, and Rodriguez-Boulan and Macara, 2014).

The Scribble complex locates to SJ and TJ, and its essential for the maintenance of their structure (Woods et al., 1996). Its component Dlg is responsible for maintaining the integrity of the TJ/SJ, and has been well characterised in *Drosophila*, where it has no paralogues (vertebrates have four orthologues of Dlg, which are believed to have redundant functions and are thus harder to study) (Woods et al., 1996, Bergstralh et al., 2013). The kinase aPKC is key for the regulation of this complex, as the localisation of Lgl is directly regulated by aPKC phosphorylation. aPKC binds to the apical cortex via a Crumbs/PAR-6/PALS1 complex, and can be activated by PAR-6 (Yamanaka et al., 2001, Graybill et al., 2012). Similar to what has been shown in *Drosophila* neuroblast, the kinase activity of aPKC controls selective interaction with LGL or PAR-3 (Yamanaka et al., 2003). When active, aPKC can phosphorylate LGL in both mammalian and *Drosophila* epithelial cells (Plant et al., 2003), as it does in *Drosophila* neuroblasts. Furthermore, LGL can also inhibit the activity of aPKC by binding the PAR complex in epithelial cells (Elsum et al., 2012).

Similar to what our lab has described in the *C. elegans* embryo (Rodriguez et al., 2017), in which anterior PARs exist in two separate complexes, PAR proteins also exist in different complexes in *Drosophila* epithelial cells: a complex with Bazooka, which localises to the adherent junctions; and the PAR-6/aPKC/CDC-42 complex, in the apical domain (Harris and Peifer, 2005). A similar distribution is present in vertebrate epithelial cells, with Par-3 localising to tight junctions (the most apical lateral structures) in epithelial cell cultures (Mack et al., 2012). Bazooka is restricted to this domain via two mechanisms: on the area basal to adherent junctions the kinase Par1 can phosphorylate Bazooka preventing both clustering of

Bazooka and its binding to aPKC, and therefore inhibiting the presence of the apical Pars in the basal domain (Benton and St Johnston, 2003); at the same time aPKC phosphorylation of Bazooka in the apical domain releases Bazooka from the apical Par complex, allowing Bazooka to interact with the lipid phosphatase PTEN and regulating the phosphoinositide turnover (von Stein et al., 2005).

The resulting increase in PIP2 in the apical domain leads to increased Cdc42 (Martin-Belmonte et al., 2007). Active Cdc42 can bind Par6 and recruit the Par6/aPKC complex to the apical domain (in which it will interact with the Crumbs complex) and activate aPKC (Yamanaka et al., 2001), as binding of aPKC to the CR3 regions of Par3 inhibits its kinase activity (Soriano et al., 2016). As in *C. elegans* embryos, Cdc42 is essential for Par6/aPKC localisation, as it promotes apical recruitment of the heterodimer (Nunes de Almeida et al., 2019). However, unlike in *C. elegans* embryos, Cdc42 is not essential for aPKC activity, as both in *Drosophila* and mammalian cell cultures aPKC has been shown to bind to the membrane via a polyphasic domain, which becomes exposed upon interaction with Par6 (Dong et al., 2019).

The apical Par complex has also been shown to control E-cadherin regulation via endocytosis, and is thus required to maintain the integrity of AJ (Georgiou et al., 2008, Leibfried et al., 2008). Furthermore, active Cdc42 can lead to the nucleation of actin via the Arp2/3 complex (Rohatgi et al., 2000), and this remodelling of the actomyosin cytoskeleton can further regulate endocytosis and AJ integrity (Georgiou et al., 2008, Leibfried et al., 2008). The PAR-3 homologue Bazooka can also interact directly with E-Cadherin, and this interaction is essential for cell-cell adhesion (Zhang et al., 2009). This interaction is promoted by microtubules, which inhibit Rho signalling (Bulgakova et al., 2013). Interestingly, aPKC has been shown to phosphorylate ROCK and suppress its localisation to the adherent junctions of epithelial cell culture, thus inhibiting actomyosin contractility (Ishiuchi and Takeichi, 2011); and similarly, in *Drosophila* epithelia Crumbs has been shown to recruit aPKC and negatively regulate Rok, the fly homologue of ROCK, during tubulogenesis (Roper, 2012), suggesting that this negative interaction might be well conserved.

1.5.3. *Cell Polarity and Symmetry Breaking in Yeast: the Role of Cdc-42*

The unicellular yeasts *Saccharomyces cerevisiae* (*S. cerevisiae*, also known as budding yeast) and *Schizosaccharomyces pombe* (S. pombe, also known as fission yeast) has served as important model for the study of polarity (Martin and Arkowitz, 2004). More specifically, *S. cerevisiae* has been used for the study of symmetry breaking, as it can easily be induced to polarise at random sites (Irazoqui and Lew, 2004, Johnson et al., 2011). In wild type yeast the selection of this polarisation site depends on proteins that act as spatial landmarks, such as the GTPase Rsr1 and its interactors: Bud3, Bud4, septins, Axl1 and Axl2 (Park and Bi, 2007). Removing Rsr1 allows to ignore these predetermined spatial cues, and has allowed for the study of symmetry breaking at a random site (Johnson et al., 2011).

Polarisation and symmetry breaking in yeast depend on the small GTPase Cdc42, which was first characterised in *S. cerevisiae* (Johnson and Pringle, 1990). Cdc42 is activated locally during G1 phase, leading to the activation of several of its downstream effectors (**Figure 1.8 A**). This, in turn, leads to the activation of several feedback loops that can regulate Cdc42 and the rest of the polarisation machinery (Etienne-Manneville, 2004, Chiou et al., 2017). Cdc42 becomes depolarised within the bud in G2, when the bud stops growing apically and starts growing within itself, in a process that is suspected to involve regulation of Cdc42 GAPs (Chiou et al., 2017). It later becomes inactive and concentrates in the neck of the bud, where cytokinesis will take place.

The local activation of Cdc42 in budding yeast uses a positive feedback loop to assemble the budding site (**Figure 1.8 B**) (Chiou et al., 2017). The Cdc42 effector PAK can bind the Cdc42-directed GDP/GTP exchange factor (that is, the Cdc42 GEF) via the scaffolding protein Bem1, leading to the recruitment of GEF into sites that are already enriched in active Cdc42 (Chiou et al., 2017). The recruitment of the Cdc42 GEF depends on the cell cycle: during the G1 phase the GEF is sequestered in the nucleus by Farp1, and only in the late G1, when CDK complex triggers Far1p degradation can the GEF leave the nucleus and get recruited to the budding site, beginning the polarisation of the cell and growing of the bud (Etienne-Manneville, 2004, Chiou et al., 2017).

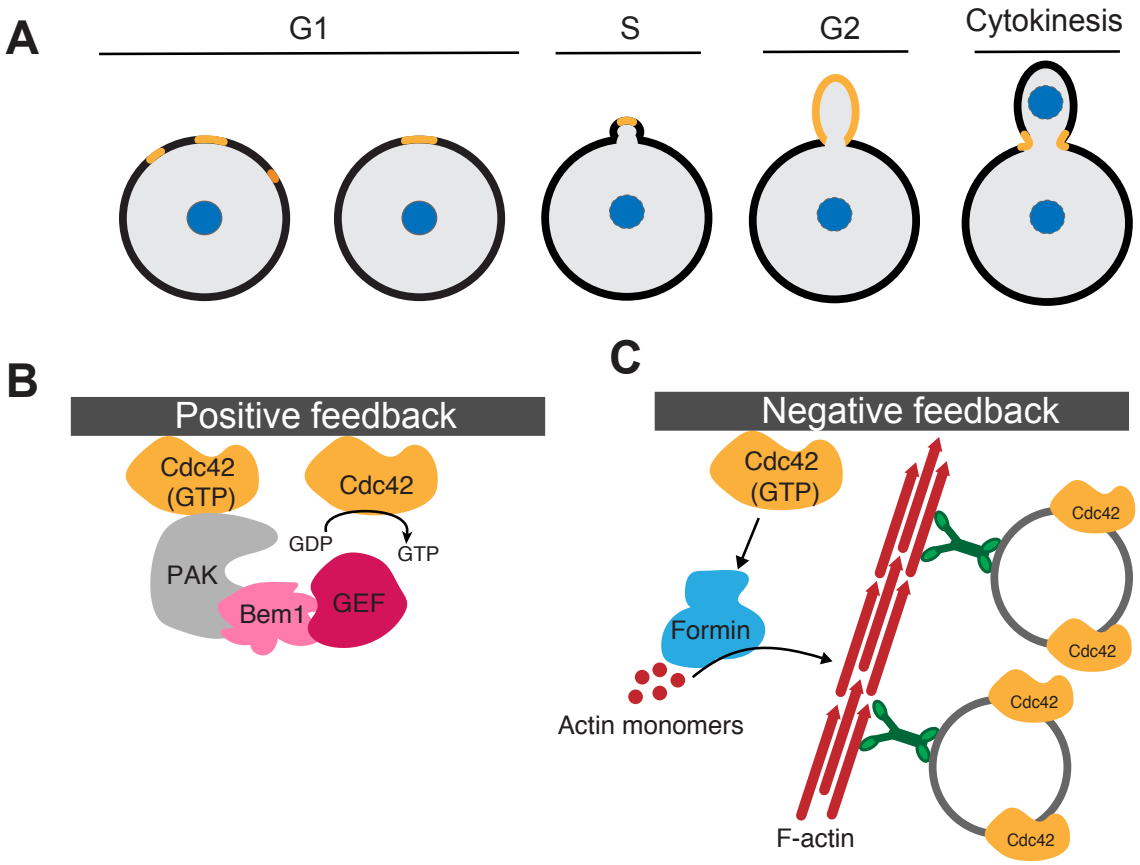

Figure 1.8. Polarity in the budding yeast. A. Active Cdc42 forms clusters (in orange) in the membrane of *S. cerevisiae* during G1 phase. These clusters compete for the cytoplasmatic components until only one cluster is left. This cluster will generate the budding site, and the bud will start to grow apiclally thorought G1 phase. At G2, Cdc42 becomes depolarised within the bud, and localises all over the bud's membrane. At this stage the bud starts to grow isotropically (in all directions) instead of apically. During cytokinesis, Cdc42 becomes inactive and localises to the neck of the bud. **B**. At the budding site a positive feedback look helps gather more active Cdc42. The Cdc42 effector PAK can bind the scaffolding protein Bem1, which can bind the Cdc42 GEF. This GEF exchanges GDP for GTP in Cdc42, contributing to increased active Cdc42 in the cluster. **C**. A negative feedback loop controls the location of the Cdc42 cluster. Active Cdc42 can bind its effector Formin, which nucleates actin and orients actin filaments towards the budding site, the motor protein Myosin V (in green) delivers vesicles along this filaments. The vesicles are less enriched in Cdc42 than the cluster site is, so their fusion to the budding site dilutes Cdc42 and displaces the polarity site.

A longstanding question in yeast polarity is how does Cdc42 generate one single budding site, if its presence in the membrane could (via the positive feedback loop above describe) grow a polarisation site in any place in which Cdc42 is activated. Cell imaging has shown that even though two to four clusters of Cdc42 are present at early polarity establishment, only one cluster develops further and generates a budding site (Wu et al., 2015a, Chiou et al., 2017, Witte et al., 2017). This single cluster is a result of competition of all clusters for the recruitment of cytoplasmic components, which will favour the bigger clusters, as they recruit more effectively (Chiou et al., 2017).

Besides breaking symmetry, active Cdc42 also orients actin filaments towards the budding site thanks to its effector Bni1 (a Formin that nucleates actin) (**Figure 1.8 C**) (Johnson et al., 2011, Chiou et al., 2017), and the motor protein Myosin V delivers secretory vesicles along this actin cables, promoting exocytosis in the budding site (Chiou et al., 2017). These vesicles carry Cdc42, and were believed to further enrich Cdc42 at the polarisation site; new research however has shown that Cdc42 is less concentrated in the vesicles than it is the the budding site, therefore vesicle fusion to the polarity site adds more membrane than Cdc42 to the polarity site, diluting Cdc42 and generating a negative feedback loop (Johnson et al., 2011, Layton et al., 2011, Chiou et al., 2017). This negative feedback loop has been hypothesised result in a displacement of the polarity site, which has been observed in yeast cells, but its role is still unclear (Dyer et al., 2013, Hegemann et al., 2015, Chiou et al., 2017).

Another negative feedback mechanism controls the size of the Cdc42 polarisation site: active Cdc42 clusters recruit septin to the budding site (Iwase et al., 2006) and lead to the assembly of septin filaments around this site. This in turn can recruit the Cdc42 GAPs (Bem2 and Rga1) and set a boundary to avoid the spreading of active Cdc42 (Caviston et al., 2003, Chiou et al., 2017).

Lastly, some recent papers have described differences in how binding to GTP and GDP might also affect the mobility of Cdc42 in both budding yeast and fission yeast (see **Section 1.4.2** for a comparison of Cdc42 mobility in both yeast species). In budding yeast, binding to GTP results in lower membrane exchange rate of Cdc42 with the cytoplasm, as seen with the

constitutively active Cdc42(Q61L) mutant (Woods et al., 2016). Therefore inactive GDP-bound Cdc42 could be extracted from the membrane at a higher rate than active Cdc42, allowing for recycling of GDP-Cdc42 while contributing to a gradient of GTP-Cdc42 in the membrane (Woods et al., 2016, Moran and Lew, 2020). The molecular basis for differential diffusion and/or extraction of GDP- and GTP-bound Cdc42 is still unknown, however it has been hypothesised that the ability of GTP-bound Cdc-42 to bind effectors could slow down the mobility of these complexes (Woods and Lew, 2019). Given that diffusion of CDC-42 in the membrane has been recently identified as a key part of polartiy establishment and maintenance in *C. elegans* zygotes (Rodriguez et al., 2017), these recent papers on Cdc42 mobility in yeast could be highly significant for the study of polarity in other animal systems.

1.6. Technical Approach to *Caenorhabditis elegans*

1.6.1. *Caenorhabditis elegans* as a model organism

Caenorhabditis elegans is a small nematode found in soil, which was first described in 1900 by a librarian with a personal interest in biology (Maupas, 1900), and first used as a model organism for research by Sydney Brenner in the 1970s (Brenner, 1974). *C. elegans* are mostly hermaphrodites (XX chromosomes), allowing for easy maintenance of different strains, but also generate males (X0 chromosomes), allowing to cross strains.

C. elegans also has a very short life cycle (it can lay eggs after 3 days at 25 °C), a very small size, and can feed on bacteria such as *Escherichia coli*, making its cultivation in laboratories very easy. *C. elegans* also has a constant (and very small) number of cells. This property, named eutely, has made this nematode a very useful system for the study of the nervous system, as every hermaphrodite *C. elegans* only has 302 cells in its nervous system (383 for males) (Hobert, 2013).

Furthermore, *C. elegans* larvae can be frozen and stored for up to decades. They also have a relatively small genome (with only 12 chromosomes and 20000 genes in hermaphrodites), and in 1998 it became the first animal to have its full genome sequenced (Consortium, 1998). Despite its small genome, around 40% of genes have humans orthologues, and 80% of these

genes are targeted by RNAi libraries, allowing for their study and screening (Shaye and Greenwald, 2011).

1.6.2. RNAi silencing in *Caenorhabditis elegans*

RNA interference (RNAi) was first observed in *C. elegans*, in the form of micro RNA (miRNA) (Fire et al., 1991), a discovery for which Andrew Fire and Craig Mello were awarded the Nobel Prize for Physiology in 2006.

RNAi relies on small non coding RNAs (siRNA, of 21 to 28 nucleotides in length) that control the expression of genes, and is a process essential for development, tissue differentiation and cell division (Wilson and Doudna, 2013). In *C. elegans*, double stranded RNA (dsRNA) can induce silencing of genes at both the transcriptional and post transcriptional stages (Grishok, 2005). Gene silencing with dsRNA can be achieved both by injecting dsRNA into the gonad of the worms and looking at the the next generation; or by feeding the worms bacteria expressing dsRNA (Grishok, 2005).

Feeding-based gene silencing has allowed for genome-wide screens based on silencing genes with specific RNAi clones (Fievet et al. 2013). This method relies on dsRNA molecules reaching the cells of interest. Upon entering the cells, the dsRNA gets processed into siRNA (a double strand of 21-28 nucleotides) by the ribonuclease DICER (Meister and Tuschl, 2004). DICER has both a RNAse domain and a dsRNA binding domain, and is part of the DICER complex (which also contains the dsRNA binding protein RDE-4, the siRNA binding protein of the Argonaute family RDE-1, and the helicase DRH-1) (Meister and Tuschl, 2004). This process can be amplified by RNA dependent RNA polymerases, which use the siRNA from the DICER complex to generate more siRNA (Grishok, 2005).

The siRNA duplex generated by the DICER complex is then loaded into the RNA induced silencing complex (RISC), where one of the RNA strands is cleaved and degraded, leading to a functional RISC with a single antisense RNA strand (Grishok, 2005). The antisense strand of siRNAs can then serve as a template for the RISC to recognise complementary mRNA and cleave it, leading to its degradation (Yamamoto-Hino and Goto, 2013).

1.7. Aims

Our research group has previously described a temperature sensitive PKC-3 mutant in which the kinase activy of PKC-3 is significantly decreased at 25 °C (Rodriguez et al. 2017) (See **Figure 1.9 A** for images of the PAR domains in this mutant).

In the zygotes of this kinase mutant, actomyosin flow is significantly affected, resulting in weaker retraction of PAR-3 to the anterior domain (**Figure 1.9 A**). Furthermore, the CDC-42 dependent PAR complex loses its asymmetry: instead of localising to the anterior domain, it becomes symmetric and localises all over the zygote's membrane, suggesting that the kinase activity of PKC-3 plays a role in regulating the membrane localisation of CDC-42.

The main objectives for this project were to determine how PKC-3 could be regulating actomyosin flow in the *C. elegans* zygote, as PKC-3 has never been described as an activator of actomyosin and contractility before. Another aim was to describe how the localisaton of

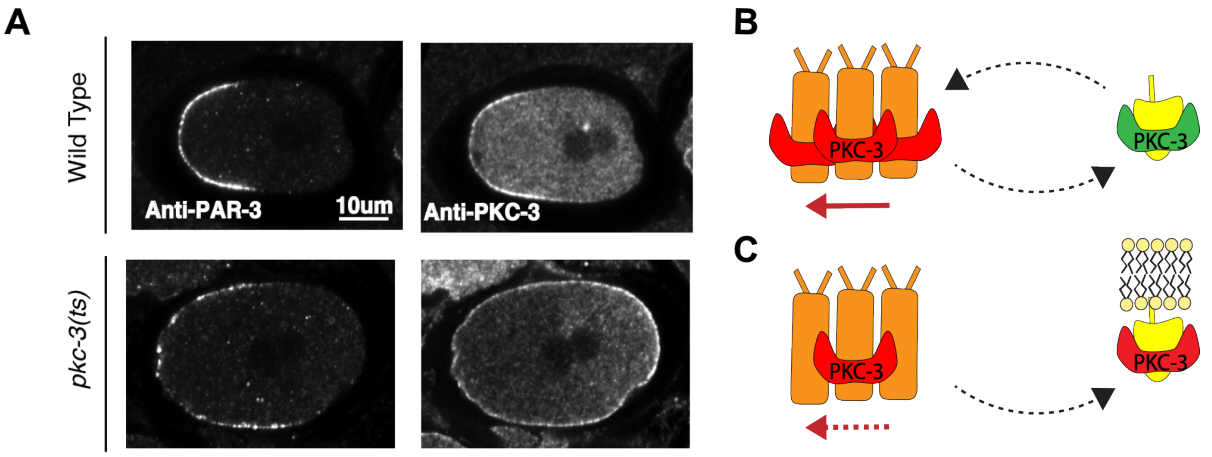

Figure 1.9. Polarity deffects in the *pkc-3(ts)* mutant . A. Immunofluorescent stainings of PAR-3 and PKC-3 in embryos during polarity maintenance stage. In wild type embryos PAR-3 retracts to the anterior domain thanks to actomyosin flow, and PKC-3 expands a little bit from the PAR-3 domain, closer to posterior. In the *pkc-3(ts)* mutant, PAR-3 and PKC-3 domains are affected, as described in Rodriguez et al 2017. **B.** Model of anterior PAR domains in wild type embryos. In wild type embryos PAR-3 oligomers have high affinity for PKC-3. PAR-3 oligomers can sense flow, and move to anterior with actomyosin flows. PKC-3 can also interact with CDC-42, which expand a bit furter into posterior. PKC-3 can bind both PAR-3 and CDC-42, and the CDC-42 complex can turnover (detach from the membrane and go into the cytoplasm). **C.** Model of anterior PAR domains in *pkc-3(ts)* mutant. Actomyosin flow is weaker, and so PAR-3 retraction to the anterior domain is affected. PKC-3 has increased affinity for CDC-42 than for PAR-3, and it is present in a complex with CDC-42 all over the membrane, and not just in anterior, with lower levels of membrane turnover.

CDC-42 is regulated by PKC-3, and to identify new ways in which PAR proteins and the cytoeskeleton regulate each other. Previous research has focused on how the cytoskeleton regulates PAR localisation (see Gubieda et al., 2020 for a review), but very little is known so far about how the cytoskeleton could be regulated by PAR proteins.

The results are split in four chapters, each with the following aim:

- To identify the signalling pathways in which PKC-3 is involved in regulating actomyosin flow (CHAPTER 3)
- To study PKC-3 regulation of the RHO/LET-502 pathway and determine if this pathway regulates anterior PARs (CHAPTER 4)
- To identify the mechanisms that regulate the membrane diffusion/exchange rate of CDC-42/PAR-6/PKC-3 complex in which PKC-3 is active (CHAPTER 5)
- To increase our understanding on the crosstalk between PAR proteins and the actomyosin cytoskeleton (CHAPTER 6)

CHAPTER 2. MATERIALS AND METHODS

2.1. Reagents, buffers and media used

A list of all buffers and media used can be seen in **Table 2.1,** with references to source of reagents, and protocols for preparation and storage.

2.2. Handling of *Caenorhabditis elegans*

Strains: A list of strains can be seen in **Table 2.2**. All strains are now available from the Caenorhabditis Genetic Center (CGC), except for the lines specifically generated for this study.

Stock keeping: Worms were grown on 60 mm NGM plates (Triplered, #TCD010060) seeded with OP50 *E. coli* (Brenner, 1974), with 300 worms in each NGM plate. Wild type and temperature sensitive (*ts*) worms were kept at 15 °C. Worm strains expressing fluorescent reporters were kept at 25°C to avoid silencing of the recombinant proteins.

Bleaching: Strains were bleached once a week for sterilisation and synchronisation. Worms and eggs were washed off one NGM plate with 1 ml M9-Tx buffer into an ependorff tube and pelleted for 40 seconds at 3,000 rpm in a tabletop centrifuge. The resulting pellet was then washed once with 1 ml M9 buffer and once with 1ml fresh bleach solution (**Table 2.1**) before bleaching. Embryos were incubated in 500 µl of bleach solution at room temperature with hand-shaking for 4 minutes, pelleted for 40 seconds at 3,000 rpm and washed three times with 1 ml M9-Tx buffer and once with 1 ml M9 buffer.

Storage of bleached embryos: The bleached embryos were kept in an microfuge tube with 300 µl of M9 buffer at 15 °C (wild type and temperature sensitive strains) or 20 °C (recombinant strains) for 48 h to obtain a synchronised population of starved L1 worms.

2.3. Storage and thawing of *Caenorhabditis elegans* strains

Long term storage: long term storage of young larvae (L1) was performed as described by Brenner (1974). Briefly, bleached eggs were plated on six 60 mm NGM plates (300 eggs each, no OP50) at 15 °C (wild type and temperature sensitive strains) or 20 °C (recombinant

Name	Use	Composition	Preparation and storage
Bleach	Synchronising worms.	20% v/v Bleach (Sigma #239305), 5% v/v HCl (Sigma #320331), double distilled H2O (ddH2O)	Mixed reagents, stored at room temperature for up to 7 days.
M9	Washing worms	22 mM KH2PO4 (Fisher #P/4800/53), 42 mM NaHPO4 (Fisher #10028-24-7), 86 mM NaCl (Melford #S23020),1 mM MgSO4 (Fisher #M/1050/53)	Mixed reagents (except MgSO4). Autoclaved and stored at room temperature. Filtered MgSO4 (0.22 µm pore size, Agilent, #5190-5116) added from a 1M stock after autoclave step next to flame.
M9-Tx	Washing worms	M9 buffer with 0.1 % v/v Triton X (Sigma #T9284)	M9 prepared as stated above, Triton added before use from a 10% Triton X stock.
PBS	Immunofluorescence	137 mM NaCl (Melford #S23020), 2.7 mM KCl (Sigma #P9541), 8 mM Na2HPO4 (Sigma #S9763), and 2 mM KH2PO4 (Fisher #P/4800/53), pH 7.5	Mixed reagents, pH adjusted to to 7.5, and autoclaved. Stored at room temperature.
PBST	Immunofluorescence	PBS buffer with 0.05% Tween 20 (Sigma #P1379)	PBS prepared as stated above, Tween added before use from a 10% Tween 20 stock.
TBS	Western blotting	150 mM NaCl, 50 mM TrisHCl (Sigma, #648317), pH 7.6	Mixed reagents, pH adjusted to to 7.6, and autoclaved. Stored at room temperature.
TBST	Western blotting	TBS buffer with 0.1% Tween 20	TBS prepared as stated above, Tween added before use from a 10% Tween 20 stock.
NGM	Growing worms	0.25% Tryptone (Sigma #T7293), 0.3% NaCl, 1.5% Agar (Melford, #A20020), 1 mM CaCl2 (Fisher, #C/1500/53), 1mM MgSO4, 25 mM KPO4, 5 µg/mL Cholesterol (Sigma, #C8667), 25 µg/ml Nystatin (Merk, #475914)	Tryptone, NaCl and Agar were mixed and autoclaved. Once sterilised, the other reagents were added to the melted NGM, under a flame to ensure sterile conditions.
RNAi plates	RNAi treatment for worms	NGM supplemented with 10 µg/mL carbenicillin (Melford, #C0109), 12.5µg/mL tetracycline (Sigma, #87128), 1 mM IPTG (Melford, #MB1008)	Antibiotics and IPTG were supplemented to melted NGM right before use, under a flame to ensure sterile conditions.
LB	Growing bacteria	5 g/L NaCl, 10 g/L tryptone , 5 g/L yeast extract (VWR, #J850). final pH 7.0	Mixed reagents, pH adjusted to to 7.0, and autoclaved. Stored at room temperature.
Egg buffer	Live imaging of embryos	2mM CaCl2, 118 mM NaCl, 48 mM KCl, 2 mM MgCl2, 25 mM HEPES (pH 7.4), in ddH2O	Prepared 1M stock solutions of CaCl2, NaCl, KCl (Sigma, #P9541), MgCl2 (Sigma, #M1028) and HEPES (Sigma, #H3375). Mixed reagents, stored at 4 °C.
DNA extraction buffer	Extracting DNA for PCR	25 mM Tris HCl (pH 7.5), 0.5 µg/mL Proteinase K (Fisher, #AM2546), in ddH2O	Mixed reagents right before use.
Lysis Buffer	Extracting protein for immunochemistry	25 mM Tris HCl (pH 7.5), 100 mM NaCl, 0.05% NP40 (Sigma #74385), with Protease inhibitors (Roche Applied Science #1873580)	Mixed reagents and stored at -20 °C.

Table 2.1: Names and composition of buffers employed, source of reagents, and protocols for preparation and storage.

ID	Name	Genotype	Use	Source	Description
EU1295	*act-2(ts)*	*act-2(or621)*	Mutation in *act-2* gene, resulting in excess actin activity at 25°C.	Caenorhabditis Genetics Center (CGC)	Willis et al, 2006
HR1157	*rock(ts)*	*let-502(sb118)*	Strain with mutation in *let-502* gene, resulting in no kinase activity at 25°C. Used for immunofluorescence.	Paul Mains Laboratory	Raharjo et al, 2011
JA1641	NMY-2::gfp x *pkc-3(ts)*	*zuIs45 [nmy-2::NMY-2::GFP + unc-119(+)] V; pkc-3(ne4246)II*	NMY-2::GFP crossed with *pkc-3(ts)* , used for in vivo imaging and immunofluoresnce.	Generated by Josana Rodriguez	Fievet et al, 2012
JA1685	GFP::CDC-42(S71)	unc-119(ed3);ttTi4348 [Pmex-5::gfp/cdc-42(gDNA)/tbb-2 3'UTR, unc-119(+)] chrI	GFP::CDC-42 strain used as a control for strains JA1686 and JA1687. Used for immunofluorescence and crosses.	Generated by Josana Rodriguez for this project	Methods section 2.4
JA1686	GFP::CDC-42(S71A)	*unc-119(ed3);ttTi4348 [Pmex-5::gfp/cdc-42_S71A(gDNA)/tbb-2 3'UTR, unc-119(+)] chrI*	Non-phosphomimetic GFP::CDC-42 strain with a mutation in Serine 71 to Alanine. Used for immunofluorescence and crosses.	Generated by Josana Rodriguez for this project	Methods section 2.4
JA1687	GFP::CDC-42(S71E)	*unc-119(ed3);ttTi4348 [Pmex-5::gfp/cdc-42_S71E(gDNA)/tbb-2 3'UTR, unc-119(+)] chrI*	Phosphomimetic GFP::CDC-42 strain with a mutation in Serine 71 to Glutamine. Used for immunofluorescence and crosses.	Generated by Josana Rodriguez for this project	Methods section 2.4
JH2689	*ect-2(ts)*	*ect-2(ax751)*	Mutation in *ect-2* gene, resulting in no ECT-2 activity at 25°C.	Seydoux Laboratory	Zonies et al, 2010
JJ1473	NMY-2::gfp	*zuIs45 [nmy-2::NMY-2::GFP + unc-119(+)] V*	NMY-2::GFP, used for in vivo imaging and immunofluoresnce.	CGC	Nance et al, 2003
JRS008	GFP::CDC-42(S71) x *pkc-3(ts)*	*pkc-3ts(ne4246) II;unc-119(ed3);ttTi4348 [Pmex-5::gfp/cdc-42(gDNA)/tbb-2 3'UTR, unc-119(+)] chrI*	GFP::CDC-42 strain crossed with *pkc-3(ts)* . Used for immunofluorescence and crosses.	Generated by Josana Rodriguez for this project	Methods section 2.5
JRS009	GFP::CDC-42(S71A) x *pkc-3(ts)*	*pkc-3ts(ne4246) II;unc-119(ed3);ttTi4348 [Pmex-5::gfp/cdc-42_S71A(gDNA)/tbb-2 3'UTR, unc-119(+)] chrI*	Non-phosphomimetic GFP::CDC-42 strain with a mutation in Serine 71 to Alanine. Crossed with *pkc-3(ts)* . Used for immunofluorescence.	Generated by Josana Rodriguez for this project	Methods section 2.5
JRS013	GFP::CDC-42(S71E) x *pkc-3(ts)*	*pkc-3ts(ne4246) II;unc-119(ed3);ttTi4348 [Pmex-5::gfp/cdc-42_S71E(gDNA)/tbb-2 3'UTR, unc-119(+)] chrI*	Phosphomimetic GFP::CDC-42 strain with a mutation in Serine 71 to Glutamine. Crossed with *pkc-3(ts)* . Used for immunofluorescence.	Generated by Josana Rodriguez for this project	Methods section 2.5
JRS14	GFP::CDC-42(S71E) x PH-GBP Nanobody	*unc-119(ed3);ttTi4348 [Pmex-5::gfp/cdc-42_S71E(gDNA)/tbb-2 3'UTR, unc-119(+)] chrI; unc-119(ed3) III; crkEx1 [pNG19:mex5p::PH(PLC1D1)::GBP::mKate::nmy-2UTR + unc-119(+)].*	Phosphomimetic GFP::CDC-42 (S71E) strain crossed to PH-GBP Nanobody, resulting in membrane bound GFP::CDC-42.	Generated for this thesis	Methods section 2.5
JRS16	GFP::CDC-42(S71) x PH-GBP Nanobody	*unc-119(ed3);ttTi4348 [Pmex-5::gfp/cdc-42(gDNA)/tbb-2 3'UTR, unc-119(+)] chrI; unc-119(ed3) III; crkEx1 [pNG19:mex5p::PH(PLC1D1)::GBP::mKate::nmy-2UTR + unc-119(+)].*	GFP::CDC-42 strain crossed to PH-GBP Nanobody, resulting in membrane bound GFP::CDC-42.	Generated for this thesis	Methods section 2.5
KK725	*nop-1*	*nop-1(it142), chrIII*	Mutation in *nop-1* gene.	CGC	Rose et al, 1995
MG617	RhoBiosensor	*xxSi5 [pie-1p::GFP::ani-1(AH+PH)::pie-1 3'UTR + Cbr-unc-119(+)], chrII.*	GFP::ANI-1, biosensor against active (GTP bound) RHO. Used for life imaging and immunofluorescence.	CGC	Tse et al, 2012
N2	Wild Type		Wild type ancestral worm. Used for immunofluorescence and western blots.	CGC	Brenner 1974
NWG038	PH-GBP Nanobody	*unc-119(ed3) III; crkEx1[pNG19:mex5p::PH(PLC1D1)::GBP::mKate::nmy-2UTR + unc-119(+)].*	GFP binding nanobody with PH domain. Used to bring the GFP bound protein in other strains to the membrane. Used for crosses.	Nate Goehringer Laboratory. Described in Rodriguez et al, 2017.	Rodriguez et al, 2017
SA131	GFP::CDC-42(S71)	*tjIs6 [pie-1p::GFP::cdc-42 + unc-119(+)]*	GFP:CDC-42 strain used as a control against WH423. Used for western blots.	Sugimoto Laboratory. Described in Motegi and Sugimoto, 2006	Motegi and Sugimoto, 2006
VC506	*cgef-1*	*cgef-1(gk261), chrX*	Strain with mutation in the CDC-42 GEF *cgef-1*.	CGC	Kumfer et al, 2010
WH423	mCherry::CDC-42(Q61L)	*Ppie-1::mcherry::cdc-42(Q61L)*	mCherry:CDC-42 strain with a constitutively active CDC-42. Used for western blots.	Alina Skop. Described in Kumfer et al, 2010	Kumfer et al, 2010

Table 2.2: *C. elegans* strains employed, source of the strain, and reference to paper in which the strain has been described or the Methods section in which generation of the strain is disucssed (for strains generated in this project).

strains). Larvae were allowed to hatch and starve for 1 week (if kept at 15 °C) or 4 days (if kept at 20 °C). The young starved larvae were collected with 1 mL of M9, and pelleted for 60 s at 3,000 rpm in a tabletop centrifuge. The supernatant was removed and worms were resuspended in 3 ml of freezing solution (6.5 mM K_2HPO_4, 43.5 mM KH_2PO_4, 100 mM NaCl) with 30% glycerin (Thermofisher, #17904). The solution with the worms was split into three 1.8 ml cryovials (Sigma Aldrich, #V7884) labelled with the date and the strain name. The three cryovials were stored at -80 °C. At all times, three extra cryovials of each worm strain were stored in liquid nitrogen for permanent storage. For permanent storage, the same freezing protocol was followed, and worms that had been frozen at -80 °C for at least 12 hours were then transfered to liquid nitrogen.

Thawing of frozen worms: One vial from -80 °C was thawed at room temperature until the top layer of ice detached from the walls of the vial. 1 ml of M9Tx buffer was then used to softly pipette the sample up and down, until the entire sample thawed. Worms were washed with 1 ml of M9Tx with 1 minute of centrifugation at 3,000 rpm in a microfuge. Supernatant was removed and the remaining 50 to 100 µl were plated in a 60 mm NGM plate seeded with OP50 bacteria.

2.4. Generating new lines of *Caenorhabditis elegans* by MosCI

Three new lines were generated for this study with the the *Mos1*-mediated Single Copy transgene Insertions, or MoSCI, method (Frøkjær-Jensen et al, 2012). The lines were generated by Josana Rodriguez with the following protocol. One lined contained CDC-42::GFP (as a control), one contained an alanine mutation CDC-42(S71A)::GFP, and one contained a phosphomimmetic mutation CDC-42(S71E)::GFP.

2.4.1.Generation of the plasmid containing *cdc-42*

Amplification of genomic cdc-42: First, *cdc-42* (1024 bp) was amplyfied, using the Fwd 5' *cdc-42* and Rev 3' *cdc-42* primers (See **Table 2.3** for primer sequence), which include the *att* sequences for MosCI insertions. Amplification was performed in a PCR tube, with 4 µl of HighFidelity Buffer 5x (ThermoFisher), 10 µM of each primer, 2.5 mM dNTP, 1 µl of a genomic DNA extract (See Section 2.5.3 for further details in how genomic DNA is

extracted), and 0.2 µl of Phusion enzyme (ThermoFisher, #F530) at a concentration of 0.02 U/µl, and ddH_2O for a final concentration of 20 µl. The DNA was denatured for 30 seconds at 98 °C, followed by 30 cycles of denaturation (also at 98 °C), annealing (20s, at 59 °C) and extension (72 °C, for 45 seconds). Followed by a final extension step of 10 minutes at 72 °C.

Cloning of genomic cdc-42 *into the* pDONR221 *plasmid*: 1 µl of the PCR product was incubated with 1 µl of the *pDONR221* plasmid (from a 150 ng/µl stock), with 6 µl TE buffer

Name	Sequence	Tm (°C)	Use
Fwd 5' cdc-42 co	ATGCAGACGATCAAGTGC	50	Amplifying endogenous cdc-42, as control
Rev 3' cdc-42 control	CACGTCGGTCTGTGGATACTCTAGAGGCCTTAATCGATCG	52	Amplifying endogenous cdc-42, as control
Fwd 5' cdc-42	GACCATGATTACGCCAAGC	56	Amplifying overexpressed cdc-42 inserted with MosCi method, to strains generated with this method
Rev 3' cdc-42	CGGCCAGTGAATTATCAACTATG	51	Amplifying overexpressed cdc-42 inserted with MosCi method, to strains generated with this method
Fwd 5' alanine	GATCGATTAAGGCCTCTA**GCC**TATCCACAGACCGACGTG	61	Adding the alanine mutation to MosCi inserts
Rev 3' alanine	CACGTCGGTCTGTGGATA**GGC**TAGAGGCCTTAATCGATC	61	Adding the alanine mutation to MosCi inserts
Fwd 5' glutamic acid	CGATCGATTAAGGCCTCT**AGAG**TATCCACAGACCGACGTC	60	Adding the glutamic acid mutation to MosCi inserts
Rev 3' glutamic acid	CACGTCGGTCTGTGGATA**CTC**TAGAGGCCTTAATCGATCG	61	Adding the glutamic acid mutation to MosCi inserts
Fwd 5' GFP	CCTGAAGTTCATCTGCACCA	59	Amplifying GFP genes, to check new crossed strains
Rev 3' GFP	AGCAGAAGAACGGCATCAAG	60	Amplifying GFP genes, to check new crossed strains

Table 2.3: Oligonucleotide sequences used for amplification and sequencing of new strains generated in this thesis.

and 2 µl BP clonase II enzyme (Invitrogen), in a final volume of 10 µl. The sample was incubated at 25 °C overnight. The enzyme was then deactivated with 1 µl of Proteinase K (Invitrogen #59895) for 10 minutes at 37 °C.

Transformation of DH5alpha with the pDONR221_gCDC42attB *plasmid*: 100 µl of the DH5alpha bacteria were thawed on ice. 4 µl of the cloned *pDONR221_gCDC42attB* reaction was added to the bacteria and incubated on ice for 20 minutes. The sample was heat shocked at 42 °C for 40 seconds in a water bath, and then incubated for a further 2 minutes at 4 °C. 500 µl of LB media (at 37 °C) were then added to the sample and incubated for 1 h at 220 rpm. 50 µl of the reaction were plated on a LB-Kanamycin (50 mg/mL) plate, and incubated overnight at 37 °C. Five colonies were picked from the plate, and grown overnight in liquid LB with Kanamycin (50 mg/mL).

Digestion of pDONR221_gCDC42attB *plasmid*: The plasmid was isolated from each clone with a MiniPrep Kit (ThermoFisher, #K0503). The plasmids from each clone were checked with digestion, to confirm the presence of pDONR221_gCDC42attB: 2 µl of the purified plasmid (around 200 ng), 2 µl of 10x Sure/Cut Buffer H, and 1 U of PvuI enzyme (Roche) were incubated in a final concentration of 15 µl, and incubated at 37 °C for 1 h. The digestion was checked by gel electrophoresis on gels of 1% (w/v) agarose in TBE stained with ethidium bromide (0.2 µg/mL). The DNA ladder Bioline HyperLadder I (Ecogen #BIO-33053, for DNA products over 1000 bp) was used to determine DNA size. Samples were visualised with UV light in a Syngene G:BOX, and samples with 2099 and 1471 bp fragments were sequenced for further confirmation.

2.4.2.Generation of the plasmid containing alanine and glutamic acid mutations

Adding the alanine and glutamic acid mutation to pDONR221_gCDC42attB: To add the mutations to the plasmid, two different PCR reactions were set up: one for the alanine mutation (primers Fwd 5' Alanine and Rev 3' alanine, see **Table 2.3** for sequence), and one for the glutamic acid mutation (primers Fwd 5' Glutamic acid and Rev 3' Glutamic acid, see **Table 2.3** for sequence). The PCR reactions were set up in PCR tubes with the QuickChange II XL Site directed mutagenesis kit manual (Agilent Technologies#200521), with 5 µl of

Buffer 10x, 2 µl of the template plasmid (at a 5 ng/µl concentration), 100 ng/µl of each primer, 1 µl of the dNTP mix (2.5 mM), and 3 µl of the QuickSol reagent, topped up to 50 µl with ddH_2O. As a control, another PCR was performed with the control plasmid *pBluescript II SK(-)*, which contains a β-galactosidase mutation. The DNA was denatured for 60 seconds at 95 °C, followed by 18 cycles of denaturation (also at 95 °C), annealing (50 s, at 60 °C) and extension (68 °C, for 4 minutes). Followed by a final extension step of 7 minutes at 68 °C.

Dpn1 digestion: To each PCR tube, 1 µl of Dpn1 (Agilent Technologies, #200521) enzyme was added. The sample was centrifuged at 10,000 rpm for 1 minute in a tabletop centrifuge. And incubated at 37 °C for 1 hour.

Transformation of XL10-Gold ultracompetent cells with the pDONR221_gCDC42attB *control and mutants*: The XL10-Gold ultracompetent bacteria were thawed on ice, and 40 µl of bacteria were transfered to 14 ml round bottom propylene tubes (one tube per reaction). 2 µl of β-mercaptoethanol mix were added to the sample, and the sample was incubated for 10 minutes on ice. To each tube, 2 µl of each Dpn I treated DNA and 1 µl of 0.01 ng/µl pUC18 (control) were added, and the sample was incubated for 30 mins on ice. The sample was then heatshocked for 30 seconds at 42 °C, followed by a 2 minute incubation on ice. 500 µl of NZY broth (Fisher BioReagents, #BP2465-2) at 42 °C was added, and the sample was incubated at 37 °C for 1 hour with 220 rpm agitation. 2.5 µl of the transformed bacteria were plated on a LB-Kanamycin (50 mg/mL) plate, and incubated overnight at 37 °C. A LB-Amp-XGal-IPTG (50 mg/mL Amp, with 100 µl 2% XGal and 100 µl 10mM IPTG) plate was used for the control. Three colonies of each plate were picked, and grown in 5 ml of LB for a Miniprep. Of the extracted plasmid, 20 µl at 100ng/µl were sent to sequence at EuroFins, to ensure that the contained the desired sequences.

2.4.3.Injection of plasmid into *C. elegans* for MosCI insertion

Preparation of injection mix: To inject the plasmid into young adult worms, a 200 mM potassium phosphate and 30 mM potassium citrate buffer was used (pH 7.5), for a 10x buffer. This 10x buffer was then combined with pie-1 promoter transposase (pCFJ103, at a final concentration of 50 ng/µl), and the pMYO-3_mCherry-unc-54 (pCFJ04, at a final

concentration of 10 ng/µl) and the myo-2-mCherry-unc-54 (pCFJ90, at a final concentration of 5 ng/µl) reporters, to create a 2x injection mix. To the final injection mixes, 80 ng/µl of the plasmid generated (pDONR221_gCDC42attB) was added. All three injection mixes were stored at -20 °C.

Injection of plasmids into the worm germline: Injection was done on very young adult worms with an *unc-119* mutation (*unc-119(ed3);ttTi4348* genotype). The *unc-119* mutation makes worms paralysed and causes an egg-laying defect, and so it can be used for selection of transformed animals. Injection was performed as described by Mello et al. (1991), with 1 µl of the injection mix with a microinjection needle. Injected animals were then transfered to 60 mm NGM plates and grown at 15 °C, and plates were checked for phenotypically rescued F1 worms 72 hours after the injection. The presence of the desired gene was checked with sequencing, and by presence of wild type phenotype (as opposed to *unc-119* phenotype) and lack of red fluorescence, as described in **Section 2.5.2**.

2.5. Generating new lines of *Caenorhabditis elegans* by crossing

Eight new lines were generated for this study: CDC-42(S71)::GFP, CDC-42(S71A)::GFP and CDC-42(S71E)::GFP (previously generated by Josana Rodriguez with the *Mos1*-mediated Single Copy transgene Insertions, or MoSCI, method (Frokjaer-Jensen et al., 2012), see **Section 2.4**), and crosses of this strains to the *pkc-3(ts)* (previously generated by Josana Rodriguez) and PH-GBP::mKate strains. A ninth cross between the RhoBiosensor and *pkc-3(ts)* strains was attempted, but not successful due to silencing of the GFP-tagged protein at 15 °C.

Generation of males: Stage 4 larvae were picked from a plate of unsynchronised worms into a new plate. The worms were then heat shocked for 6 hours at 30 °C and then recovered at 25 °C until descendants reached young adult stage. For the CDC-42(S71)::GFP mutant and PH-GBP::mKate crosses, males were generated from the PH-GBP::mKate strain (NWG0038). For the crosses CDC-42(S71)::GFP mutant and *pkc-3(ts)* crosses, males were generated from the CDC-42(S71)::GFP mutant strains, to avoid heat shocking the temperature sensitive strain.

Crossing ratio: Six young adult males were crossed to two stage 4 hermaphrodites of the desired phenotype. The plates were kept at either 25 °C (for crosses without temperature sensitive mutants) or 15 °C (for crosses with temperature sensitive mutants) until the progeny reached young adult stages. The F1 hermaphrodites were singled out into eight 6-well-plates (Triplered, #TCP011006) to start the selection process.

2.5.1.Selection of worms with temperature sensitive *pkc-3(ts)* crosses

Selection of F2: The F1 hermaphrodites were kept in the 6-well-plates at 25 °C for 24 hours (or until 40-80 eggs had been laid) and then transferred into replicate 6-well-plates at 15 °C. Singled worms from the wells in which survival (indicative of heterozygous *pkc-3(ts)*/+ worms) was observed were kept as F2.

Selection of F3: Singled young adult F2 worms were placed into ten 6-well-plates and kept in the 6-well plates at 25 °C for 24 hours (or until 40-80 eggs had been laid) and then transferred into replicate 6-well-plates at 15 °C. Singled worms from the plates in which high lethality was observed (indicative of homozygous for *pkc-3(ts)*/*pkc-3(ts)*) were kept for F4.

Selection of F4 and onwards: Singled young adult F4 worms were plated into 6-well-plates at 15 °C for 24 hours (or until 40-80 eggs had been laid). Worms from each well were then observed under a Zeiss Axioimager microscope with a x20 lens. Worms from wells in which fluorescence was observed were kept and analysed for 2 more generations to ensure that both the GFP reporter and *pkc-3(ts)* were in homozygosis.

2.5.2.Selection of worms in non temperature sensitive crosses (two fluorescent reporters)

Selection of F2: The F1 hermaphrodites were kept in the 6-well-plates at 25 °C for 48-72 hours. The F2 worms were analysed under a Zeiss Axioimager microscope with a x20 lens. Wells in which both fluorescent reporters (GFP in green and mKate in red) were observed were kept for further analysis.

Selection of F3 and onwards: The F2 worms were kept in the 6-well-plates at 25 °C for 48-72 hours. The F3 progeny were analysed under a Zeiss Axioimager microscope with a x20 lens. Wells in which all worms (with progenies larger than 20) carried both fluorescent reporters

were kept for further analysis. This step was repeated for 2 more generations to ensure that both GFP and mKate reporters are in homozygosis.

2.5.3.Confirming the presence of the desired genes by PCR

DNA extraction: To further confirm the genotype of crossed lines, 3 adult worms were picked and placed in a PCR tube with 10 µl of DNA extraction buffer. The tube was frozen over night at -80 °C, and Proteinase K (Fisher, #AM2546) was added at a final concentration of 0.5 µg/mL, for lysis of the worms. Lysis was performed at 60 °C for 90 minutes, followed by inactivation of the Proteinase K at 95 °C for 15 minutes.

PCR: High fidelity PCR was performed in using Phusion High Fidelity DNA polymerase (ThermoFisher, #F530) at a concentration of 0.02 U/µl, with HF Buffer, 200 µM of a nucleotide mix (50 µM of each nucleotide triphosphate), 0.5µM of each primer (see **Table 2.3**) and with 1µl of DNA extract, in a final volume of 20 µl (topped up with ddH_2O). The DNA was denatured for 30 seconds at 98 °C, followed by 30 cycles of denaturation (also at 98 °C), annealing (10s, 5 °C below the temperature of the less stable primer) and extension (72 °C, for 30s/Kb of DNA generated). Followed by a final extension step of 10 minutes at 72 °C.

Visualisation: The PCR results were visualised by gel electrophoresis on gels of 1% (w/v) agarose in TBE stained with ethidium bromide (0.2 µg/mL). To determine the size of the PCR product (in base pairs, bp) DNA ladders Bioline HyperLadder I (Ecogen #BIO-33053, for DNA products over 1000 bp) or Bioline HyperLadder IV (Ecogen #BIO-33029, for DNA products under 1000 bp) were used to determine DNA size. Samples were visualised with UV light in a Syngene G:BOX. Positive results were purified with a PCR purification Kit (Quiagen) and sent to sequence to Eurofins Genomics Tube Sequencing service (using the primers listed in **Table 2.3**).

2.6. RNAi Preparation and Feeding

RNAi sequences and source: All RNAi clones (HT115 RNAse-deficient *E. coli* expressing dsRNAi) were acquired from the Ahringer library (Kamath and Ahringer, 2003). The primer

sequences used to generate the dsRNAi of each clone can be seen in **Table 2.4**. Genomic fragments obtained with the primers listed are cloned into the L4440 vector.

Preparation of Plates: HT115 RNAse-deficient *E. coli* expressing dsRNAi were streaked onto LB-agar plates (10 μg/ml of carbenicillin, 10 μg/ml tetracycline, 100 U/ml nystatin) and incubated over night at 37 °C. Resulting individual colonies were selected and grown in 10 ml of liquid LB (10 μg/ml of carbenicillin, 10 μg/ml tetracycline, 100 U/ml nystatin) over night at 37 °C with 220 rpm agitation and an inclination of 45°. The RNAi was induced in the liquid LB for 4 h with 4 mM of IPTG at 37 °C with agitation and concentrated five fold. 300 μl of the resulting bacteria mix was spotted onto NGM plates (with 10 μg/ml of carbenicillin, 10 μg/ml tetracycline, 1mM IPTG, 100 U/ml nystatin) and left to dry for 72 hours at room temperature before use.

Name	GenePairs Name	Fwd Primer Seq	Rev Primer Seq
akt-1	C12D8.10	GTAAGATGCCTTCAGTGGACAAC	CTTCATCGTCGAACCTTCATATC
ced-10	C09G12.8	TAGTAATTTTCAGCCGATTTGGA	ATTTTTAAGCCAATTTTTCCAGC
cdc-42	R07G3.1	TTCTTCGATAATTATTGCTCCCA	AACGACGACGAAAATGTTAAAGA
chin-1	BE0003N10.2	AAAATTTCGGAATTCAACG	AAAATTTCCCCAATTCCA
cnt-2	Y39A1A.15	ATACGTGTGCCTGTACAGTGATG	AATCTCCGAATAACCTACCCAAA
csnk-1	Y106G6E.6	TCATCACAGATACGGAAATGATG	ACTTTCTGATCGGACGTTATTCA
ect-2	T19E10.1	CTCTGATTTCTGCCAAAGC	GGCAAAGAAATCCGATT
let-502 (rock)	C10H11.9	GCATTATCTCGATCACGGG	ATTTGAACTCCGACCGAA
mlc-5	T12D8.6	CTCATTCTCTCTTTTATCGCCAA	CTGGGAGAGAGCGAATAAGAAAT
nop-1	F25B5.2	ATCACACAATGATTCAGCAGATG	TCATTAAGACTTTTCAAGCTCGC
pkc-3	F09E5.1	CATTTCCAACCACAATTCC	TGTTCCAAAGCTTCCCAA
rga-3/4	K09H11.3	GCAAGGAAGGCAACTCTG	GTTATTTCTCGGTGTGGC

Table 2.4: Primers used to obtain the genomic fragments that are cloned into an L4440 vector to express dsRNAi. GenePairs name for each gene shown. All clones are sourced from the Ahringer RNAi library (Kamath et al., 2003).

RNAi Feeding: Synchronised L1 larvae were grown until reaching L4 stage on NGM plates with OP50. Worms were then collected of the plates with M9-Tx buffer and washed 3 times with 1 ml of M9-Tx to remove remaining OP50 bacteria, and then plated onto the RNAi plates and grown for 70 h at 15 °C. Adult worms were shifted at 25 °C for 2 h right before embryo collection.

2.7. Immunofluorescence

2.7.1. Slide Preparation

Microscopy slides (Erie Scientific, 10-2066a) were washed with distilled water and detergent (Fairy Original Washing Up Liquid), rinsed with distilled water and 70% EtOH, and left to dry at 70 °C in an oven. The slide was covered with 200 µl of 0.1% poly-lysine solution with a pippete and incubated at room temperature for 30 minutes. The poly-lysine solution was recovered with a pipette tip and the excess solution removed with a paper tissue (Kimberly Clark). The slide was incubated in an oven at 70 °C for 10 minutes to allow for the poly-lysine to dry and then cooled at room temperature for 30 minutes.

2.7.2. Embryo Extraction

Adult *C. elegans* were collected with 1 ml of M9-Tx and washed twice with M9-Tx, pelleting the worms by gravity in an 1.5 ml microfuge tube for 60 s. After a final wash of 1 ml of M9 the worms were re-suspended in 300 µl of M9. 7-10 µl of worms were collected from the tube and added to the poly-lysine coated slides. Worms were cut in between the two gonads under the microscope with a syringe and squashed with a 22 mm x 40 mm coverslip over the middle square.

2.7.3. Embryo Fixation

Embryos were fixed either with 100% methanol or with 2% paraformaldehyde (v/v, from frozen 4% stock, Sigma #158127). For most experiments 100% methanol fixation was used, experiments using 2% paraformaldehyde fixation are indicated throughout the text.

For the methanol fixation, the slide was placed on a metal surface cooled with dry-ice and incubated for 30 minutes right after the squashing of the embryos. The embryos were then

fixed in 100% methanol for 30 minutes at room temperature and then washed once in PBS and once in PBST for 5 minutes each.

For the paraformaldehyde fixation, after squasing the worms, 10 µl of 4% paraformaldehyde was added to the 10 µl of worms to acchieve a 2% concentration of paraformaldehyde (v/v). Worms were then fixed for 30 minutes at room temperature. The slide was then place on a metal surface cooled with dry-ice and incubated for 10 minutes. The embryos were then washed once in PBS and once in PBST for 5 minutes each.

2.7.4. Staining

The embryos were incubated with the primary antibodies diluted in PBST overnight at 4 °C. Embryos were then washed three times in PBST for 5 minutes each and incubated with secondary antibodies and DAPI for 45-60 minutes at room temperature. A full list of the antibodies employed can be seen in **Table 2.5**.

Embryos were then washed twice in PBST and once in PBS for 5 minutes each, and rinsed in distilled water previous to mounting in 20-30 µl of Mowiol (Sigma #81381). Samples were covered with a 22 mm x 22 mm coverslip and kept at room temperature in the dark for 48 h before being stored at 4 °C.

2.7.5. Image Acquisition

Microscope settings: Embryos were imaged with a Nikon A1R Upright confocal microscope and a x60 oil immersion lens with a Numerical apperture (NA) of 1.4, equipped with 4 Multi-Alkali PMT detectors and a Nikon A1plus camera.

Imaging settings: Images were acquired with the NIS-Elements software, with the scanner set to Galvano mode. And the pinhole set to 52 µm. The wavelenghs used for the laser were: 405 nm (for DAPI imaging), 488 nm (for Alexa 488 secondary antibodies and GFP imaging), 561 nm (for Alexa 594 secondary antibodies), and 640 nm (for Alexa 647 secondary antibodies).

Image analysis and processing: Images were labelled with a four digit code before analysis to ensure blind-analysis of the data. Images were analysed with Fiji (Schindelin et al, 2012), and secondary processing of images was performed with Adobe Photoshop CC 2015 (with a 437 x

PRIMARY ANTIBODIES FOR IMMUNOFLUORESCENCE (IFs)			
Target	**Animal**	**Conditions**	**Source**
PAR-2	Rabbit (polyclonal)	1:500 in PBST	Generated as described in Dong et al. 2007
PAR-3	Mouse (polyclonal)	1:35 in PBST	Developmental Studies Hybridoma bank (P4A1)
PKC-3	Rat (polyclonal)	1:500 in PBST	From Kemphues laboratories
PKC-3	Rabbit (polyclonal)	1:2500 in PBST	From Tabuse et al. 1998. Animal ID: 94630
LET-502 (ROCK)	Rabbit (polyclonal)	1:10.000 in PBST	From Ahringer laboratories, ID: 904 SDI (genomic antibody technology)
pS71 CDC-42	Rabbit (polyclonal)	1:100 in PBST	Invitrogen, 44214G
Tubulin	Rat (monoclonal)	1:1000 in PBST.	Chemicon MAB1864
GFP	Rabbit (polyclonal)	1:5000 in PBST	Abcam, ab6556
NMY-2	Rabbit (polyclonal)	1:50.000 in PBST	From Pickel laboratories, animal ID: Rb20417
CDC-42	Mouse (polyclonal)	1:500 in PBST	Santa Cruz B-9 (sc-390210)

SECONDARY ANTIBODIES FOR IMMUNOFLUORENSCENCES (IFs)		
Name	**IF conditions**	**Source**
Alexa Fluor 488 Rabbit	1:5000 in PBST	Molecular probes, A11034, from goat
Alexa Fluor 594 Rabbit	1:5000 in PBST	Molecular probes, A11037, from goat
Alexa Fluor 647 Rabbit	1:5000 in PBST	Molecular probes, A21245, from goat
Alexa Fluor 488 Mouse	1:5000 in PBST	Molecular probes, A11029, from goat
Alexa Fluor 594 Mouse	1:5000 in PBST	Molecular probes, A11032, from goat
Alexa Fluor 647 Mouse	1:5000 in PBST	Molecular probes, A21236, from goat
Alexa Fluor 488 Rat	1:5000 in PBST	Molecular probes, A11006, from goat
Alexa Fluor 594 Rat	1:5000 in PBST	Molecular probes, A11007, from goat
Alexa Fluor 647 Rat	1:5000 in PBST	Molecular probes, A21247, from goat

ANTIBODIES FOR WESTERN BLOTS			
Target	**Animal**	**Primary**	**Secondary**
Tubulin	Mouse (monoclonal)	alpha-tubulin (SIGMA T9026) 1:20.000 in TBST 5% milk	anti-mouse HRP, 1:5.000 in TBST with 5% milk, DAKO (P0447)
CDC-42	Mouse (polyclonal)	CDC-42 (Santa Cruz, B9), 1:500 in TBST with 5% BSA	anti-mouse HRP, 1:5.000 in TBST with 5% BSA, DAKO (P0447)
CDC-42 pS71	Rabbit	pS71 Rac/Cdc-42 (Invitrogen 44214G), 1:2500 in TBST 5% BSA and 10 mM NaF	anti-rabbit HRP, 1:5.000 in TBST with 5% BSA and 10 mM NaF, DAKO (P0447)

Table 2.5: Antibodies employed.

291.85 pixel selection, and posterior adjustments of Brightness/Contrast) and Adobe Illustrator CC2015.

2.7.6. Image Analysis

2.7.6.1. Determining Cell Stage

In fixed images the cell stage was determined by DAPI staining (see **Figure 2.1** for examples in wild type embryos). Unless otherwise stated, embryos were classified as: Meiosis (if the

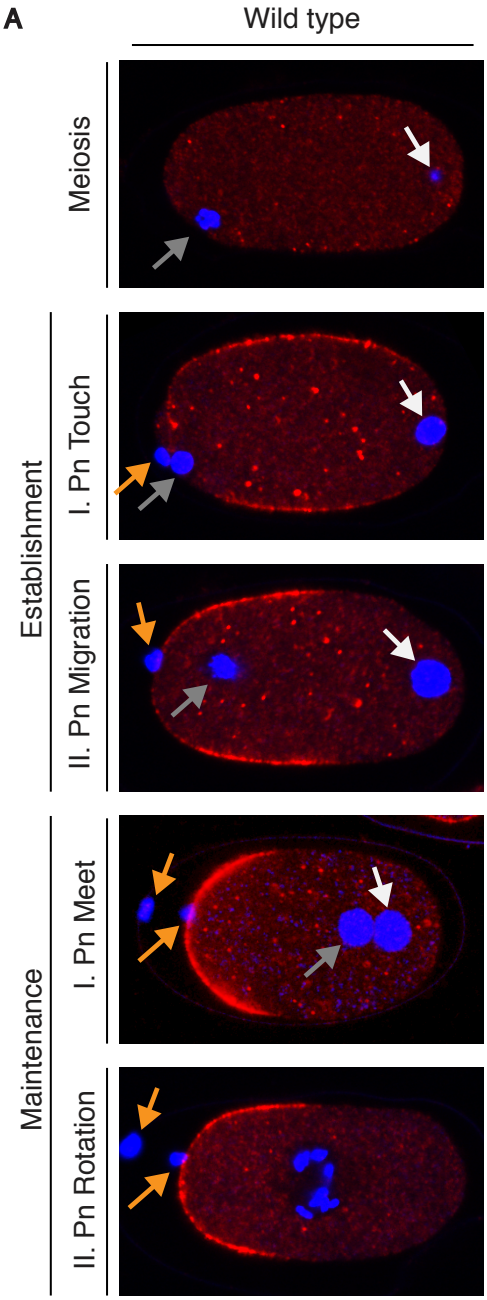

Figure 2.1. Embryo staging with DAPI staining. A. Embryos stained with DAPI (in blue) and PAR-3 antibodies (red). The anterior side is shown in the left side, and the posterior side on the right side. Grey arrows point to the female-derived DNA, orange arrows point to the polar bodies, and white arrows point to the sperm- derived DNA.

Meiosis. The *C. elegans* oocyte is polarised while the female pronucleus is still undergoing meiosis, and different chromosomes can be observed with DAPI staining (blue, grey arrow). The male pronucleus (blue, white arrow) localises to the posterior domain, not touching the posterior membrane.

Establishment. Polarity establishment stage starts when the male pronucleus (white arrow) contacts the posterior membrane (***Pn Touch***). At this stage the female pronucleus (white arrow) has completed meiosis, and polar bodies have been formed (orange arrows). Note that two polar bodies are formed during meiosis of the oocyte, but the first polar body tends to detach from the zygote, and thus only one polar body is visible in some of the images. Polarity establishment continues as the male and female pronuclei migrate towards each other (***Pn Migration***)

Maintenance. Polarity maintenance stage starts when the male and female pronuclei (white and grey arrows, respectively) meet in the posterior domain. The pronuclei then rotate and center in the middle of the zygote. Maintenance can be divided in two stages: an earlier stage (***Pn Meet, or Maintenance I***) where the pronuclei meet, and a later stage (***Pn Rotation, or Maintenance I***) where the pronuclei rotate and centre. During Maintenance II, the chromosomes condense, and different chromosomes are visible (in blue).

female pronucleus is undergoing meiosis and the male pronucleus has not touched the membrane yet), Establishment (after fertilisation, from the point the male pronuclei touches the membrane until its migration to the anterior side of the zygote), Maintenance (when the male and female pronuclei meet and rotate to the centre of the cell) and Late Stages (anaphase and metaphase).

For some experiments, maintenance was also analysed as two separate stages: Maintenance I (when the male and female pronuclei meet) and Maintenance II (when the male and female pronuclei rotate and move to the centre of the zygote).

2.7.6.2.Ensuring unbiased analysis

To make sure analysis was done in an unbiased way, all images were saved using a two letter and two number code that did not reflect their genotype/RNAi condition. The analysis of all conditions for each experiment was performed at the same time, blindly.

2.7.6.3.Determining the Asymmetric Index

For analysis of images in Fiji (Schindelin et al., 2012), the Segmented Line tool was employed with a width of 2 px to select the cortex (manually). Intensity for PARs calculated with an Asymmetric Index (ASI), calculated with the following formula:

$$ASI = \frac{[PAR\ Intensity\ In\ Anterior\ domain] - [PAR\ Intensity\ In\ Rest\ Of\ Cortex]}{2x[[PAR\ Intensity\ In\ Anterior\ domain] + [PAR\ Intensity\ In\ Rest\ Of\ Cortex]]}$$

The raw ASI values were normalised to the mean ASI value of control embryos, so that a value of 1 indicates wild type asymmetry and a value of 0 indicates complete loss of asymmetry (same intensity all over the membrane).

2.7.6.4. Analysing differences in PAR-3 and PKC-3 retraction

When analysing mid plane images of embryos to determine how much the PKC-3 domain extended from the PAR-3 domain, the images were opened in Image J and the cortex was straightened employing an ImageJ macro and the resulting images were then analysed with a Matlab scrip to determine the length of the PAR-3 and the PKC-3 domains in an unbiased way (as described by Rodriguez et al. 2017).

This type of analysis was used to determine PAR-3 and PKC-3 retraction in embryos of the wild type, *let-502* RNAi (also refered to as *let-502* RNAi) and *let-502(ts)* (also refered to as *let-502 (ts)*) background.

For analysis of CDC-42::GFP mutants, PAR-3 and PKC-3 retraction were determined manually in Image J, employing the Segmented Line tool width of 2 px to select the cortex.

2.7.6.5.Determining whether a structure is present or not

When analysing cortical images to determine whether a structure was present or not, all images of the desired staged were opened in Image J at the same time, and blindly separated into 'present' or 'not present' categories. These results where then analysed with a Fisher's exact test in GraphPad Prism 6.

This type of analysis was used to determine presence of pS71 CDC-42, LET-502 and NMY-2 foci.

2.7.6.6.Determining whether structures are foci or dots

When analysing cortical images to determine whether a structure formed foci or dots, all images of the desired staged were opened in Image J at the same time, and blindly separated into 'foci' or 'dotty' categories. These results where then analysed with a Fisher's exact test in GraphPad Prism 6.

This type of analysis was used to determine the shape of ANI-1::GFP structures.

2.7.6.7.Determining size and shape of foci

To determine the size and shape of actomyosin structures, the Analyse Particles command was used. The Analyse Particles command requires setting a threshold (**Figure 2.2**), and the lower this value, the lower the number of 'particles' it will detect. A value too high will often result in thousands of 1-2 pixel size sections from the bakground being selected as 'particles' by the software. Therefore, and to simplify the analysis, we set the threshold as the minimum value that allowed for the selection of all the visible foci in the image (that is, all foci visible to the eye).

To select a threshold, a cortical ROI was selected for the IF images of interest in Image J. A threshold was manually set for each ROI (see **Figure 2.2** for example of threshold), to select the structures of interest, and then analysed with the Analyse Particles command, set to analyse shape descriptors (roundness and solidity) and size.

This type of analysis was used to determine the shape and size of NMY-2 foci in wild type embryos, embryos treated with *mlc*-5 RNAi, and in embryos of CDC-42(S71)::GFP and CDC-42(S71E)::GFP strains.

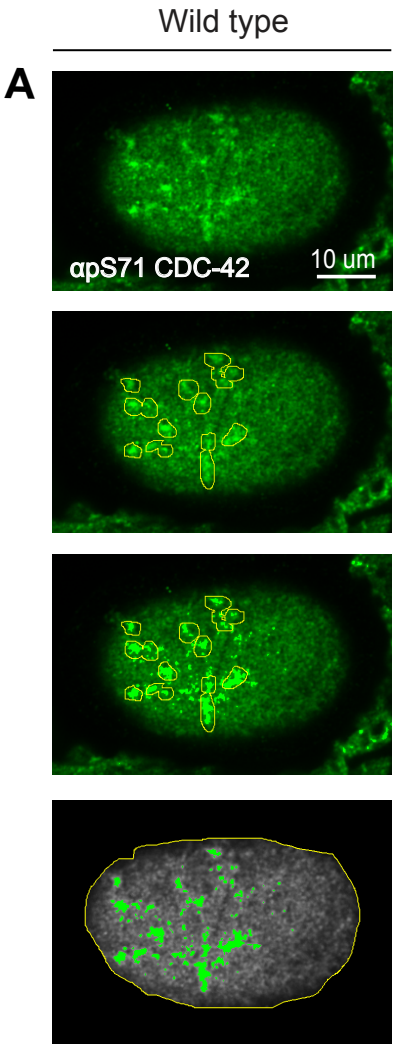

Figure 2.2 Setting of threshold for particle analysis in ImageJ.

Images of a wild type embryo of establishment stage stained with αpS71 CDC-42 (#44214G, Invitrogen).

The most obvious foci are shown with a yellow circle around them (Freehand selection tool).

The threshold is increased manually, until all the foci surrounded by the yellow circle have been selected. Once this minimum threshold is determined, that value is saved.

Once the threshold has been determined, the embryo is selected and copy/pasted into a new image with black background, to ensure that no particles outside the embryo are being analysed. The 'Analyse Particles' command is then used to determine particle shape and size, with the threshold value determined in the previous step.

2.7.6.8.Analysis of degree of organisation of cortical structures

To determine if cortical structures were well defined/organised or disorganised, we measured the coefficient of variation for the cortex of each embryo (CV) by selecting a 10 um section of the anterior cortex and measuring its mean intensity and the standard deviation.

The CV is the ratio of standard deviation to the mean of intensity, and has been previously used as an indicator of the heterogeneity of actomyosin networks (Sonal et al., 2018), with homogenous distributions resulting in lower levels than the heterogeneous distribution observed in the presence of foci.

$$CV = \frac{[StandarDeviationIntensity]}{[MeanIntensity]}$$

We used this type of analysis to determine the degree of organisation of NMY-2 foci from both *in vivo* NMY-2::GFP samples and fixed embryos stained for NMY-2; and also to compare the degree of organisation of ANI-1::GFP in samples treated with different RNAis. Values were normalised to the mean CV value of the respective controls to allow for easier comparison of stained and *in vivo* samples, so that the CV value of the control is 1. A value of 0, on the other hand, would represent completely homogenous distribution (with a value of 0 for the Standard Deviation).

2.7.6.9.Analysis of colocalisation

Colocalisation analysis of LET-502, pS71 CDC-42 and PAR-3 with NMY-2 were performed in ROIs of the anterior cortex of the imaged zygotes. The Pearson's correlation coefficient (r) was obtained with the Coloc 2 plugging of Image J, and the significance of the results was calculated with an ordinary one way ANOVA in GraphPad Prism 6. Pearson's coefficient is a measure of the linear correlation between two variables, and has values between +1 (total positive correlation, i.e. correlation) to -1 (total negative correlation, i.e. exclusion), with a value of 0 indicating neither correlation nor exclusion.

2.8. Live Imaging

2.8.1. Sample Preparation

Adult worms were collected from NGM plates with a pick and cut in between the two gonads with a syringe on top of a 30 mm circular coverslip (Bioptechs, #1.5 thickness). The coverslip was then mounted on agar pads with egg buffer (see Table 2.1 for composition).

2.8.2. Video Acquisition

Images were acquired using a Nikon A1R Eclipse inverted microscope with a custom-made temperature control stage (designed by Life Science Imaging Ltd.) set up to regulate temperature and a x60 oil immersion lens. Images were acquired with the NIS-Elements software.

For NMY-2::GFP and GFP::ANI-1 analysis, images were taken every 5 s. For GFP::GBPwsp-1 and CDC-42::GFP analysis, images were taken every 30 s. All strains were imaged at 25 °C, with the exception of GFP::GBPwsp-1, which was not fluorescent at 25 °C and was therefore imaged at 15 °C. In all cases, bright-field images were acquired to track the movement of the nuclei and stage the embryos.

2.8.3. Video Analysis

2.8.3.1. Analysis of velocity

To quantify the velocity of NMY-2::GFP retraction we performed Particle Imagine Velocimetry (PIV) using the PIVlab MATLAB algorithm (Thielicke, 2014, Thielicke and Stamhuis, 2014), as detailed in Naganathan et al. (2018). Analysis was done in collaboration with S. Naganathan (the acquired videos were sent to S. Naganathan for analysis).

This software analyses the images by separating them into small regions (or tiles). Separating the image of an embryo into smaller regions is essential, as uniform exposure of the entire embryo cannot be guaranteed due to the distribution of intensity of the laser beam (Thielicke, 2014). The different regions can then be optimised independently of the intensity values of other regions, and once this equalisation is completed the neighbouring tiles are combined

again using bilinear interpolation (Thielicke, 2014). For the analysis presented in this thesis the embryo was divided into 18 tiles along the anterior/posterior axis (Naganathan et al., 2018).

Once the image is equalised, particles above a certain value of intensity are selected, and once this upper limit of the intensity is selected, all pixels exceeding that value are replaced by this upper limit value (Thielicke, 2014). This process is called intensity capping, and ensures that the brighter particles of the image do not contribute statistically more to the correlation single that other weaker particles (Thielicke, 2014).

Once the particles with the intensity value of interest have been selected and capped, small sub-images of the image of interest are cross-correlated, so that a particle from the sub-image 'A' is looked for in the sub-image 'B', to determine the more likely displacement of particles from tile 'A' to 'B' (Thielicke, 2014). The average velocity in each sub-image is then averaged over time across the entire period with flow (Naganathan et al., 2018). For the analysis presented in this thesis the sub-image size was of 16 pixels with a step of 8 pixels (Naganathan et al., 2018).

2.8.3.2.Analysis of degree of organisation of cortical structures

To determine if cortical structures were well defined/organised or disorganised, we measured the coefficient of variation (CV) in live videos. As mentioned above, the CV is the ratio of standard deviation to the mean of intensity, and has been previously used as an indicator of the heterogeneity of actomyosin networks (Sonal et al., 2018).

We used this type of analysis to determine the degree of organisation of NMY-2 foci and active RHO (ANI-1::GFP) structures.

2.8.3.3.Making kymographs

Kymographs were generated for the entire flow period with a1 px line across the length of the embryo, from anterior to posterior. For every time-frame (taken every 5 seconds) a line was plotted along the Y axis using the KymographBuilder plugin in Image J.

We used kymographs to represent the velocity of NMY-2 retraction in NMY-2::GFP embryos.

2.9. Protein Chemistry

2.9.1. Embryonic Protein Extraction

Embryos from four 60 mm plates (300 worms per plate) were collected with 1 ml M9-Tx and washed twice before bleaching as described in **Section 2.1**. The clean embryos were washed once with 1 ml of the Lysis buffer (see composition in **Table 2.1**), and loading buffer (NuPAGe MOPS SDS kit) was added for a final volume of 100 ul. The embryos were lysed by sonication in a Diagenode Bioruptor Sonicator in a 5 minutes cycle of 30sON/30sOFF. Sample was boiled at 70 °C for 10 minutes and centrifuged at maximum speed for 20 minutes in a tabletop centrifuge. The supernatant was then recovered with a fine tip, frozen with liquid nitrogen and stored at -80 °C.

2.9.2. Generation of Bris-Tris gels for electrophoresis

Bis-Tris acrylamide gels were used for electrophoresis, poured right before use.

Preparation of 3.5x Bis-Tris stock solution: 13 g of Bis-Tris (Melford #B7500) were dissolved into 50 ml of distilled water, and pH was adjutsted to 6.8. The bis-tris solution was stored at 4 °C for a up to 6 months.

Preparation of 10% Ammonium persulphate (APS) solution: 1 g of Ammonium persulphate (Sigma #A3678) was dissolved in 10 ml of water. The solution was split into microfuge tubes, with 150 µl per tube, and stored frozen at -20 °C.

Preparation of resolving and stacking solutions and gel pouring: For the resolving section of the gel, a 12% acrylamide concentration was used, and for the stacking section of the gel, a 4% solution. For preparation of 1 gel, 7.5 ml of resolving solution were prepared with 2.14 ml bis-tris stock solution, 2.25 ml of 40% acrylamide (Sigma, #A4058), and 3.11 ml distilled water. Once the first three reagents were mixed together, the polymerisation process was initiated with 33.6 µl 10% APS and 8.6 µl TEMED (Sigma #T9281). As soon as the APS and TEMED were added to the solution, the solution was poured into a 1.5 mm wide Mini-Protean Glass Cassette and Casting Stand (Bio-Rad), as instructed by the manufacturer. The resolving solution was coverd with 1ml of distilled water, and left to set for 1 h. The stacking

solution was then prepared with with 2.14 ml bis-tris stock solution, 0.75 ml of 40% acrylamide and 4.61 ml of distilled water. Once the first three reagents were mixed together, the polymerisation process was initiated with 80 µl 10% APS and 18 µl TEMED. The distilled water sitting on top of the resolving gel solution was removed, and substituted with the stacking solution. 1.5 mm wide and 10 well spacers were placed into the solution, and the gel was alloed to set for a further 45 minutes.

2.9.3. Protein Visualisation Techniques

Extracted embryonic protein was loaded into a 12% Bis-Tris gel and run with NuPAGE MOPS (Invitrogen) buffer at 100V-170V. Gel was stained with Instant Blue stain (Expedeon) for total protein visualisation, or transferred into a PVDF membrane (Millipore, Immobilon-P membrane, 0.45 µm) for Western blotting. Previous to use, the PVDF membrane was activated by wetting the membrane with 100% methanol for 30 seconds, followed by a 2 minute incubation in distilled water, and a 10 minute equilibration in the transfer buffer (Towbin buffer, Biorad 10x TG #161-0771). Before transfer, the gel was also incubated in transfer buffer for 10 minutes.

Transfer was performed under semi-dry conditions with a Trans-Blot Turbo Blotting System (Biorad) at 25V for 30 minutes (mounting instructions as detailed by the company, using thick filter paper for the mounting). After transferring, the membrane was blocked in 10% BSA or 5% Milk in TBST for 1 hour at room temperature (see **Table 2.5** for a list of all antibodies and corresponding buffers/blocking agents) with gentle agitation. The membrane was then incubated with a primary antibody in 5% BSA or 5% Milk over night at 4 °C, washed 3 times with TBST and then incubated with secondary antibody linked to horseradish peroxidase for 1 hour at room temperature. The membrane was then washed 3 times with TBST and once with TBS before incubating for 5 minutes with the ECL Prime (Amersham) detection reagent. The resulting light reaction signal was then captured with an X-ray film (Amersham Hyperfilm ECL, 8 x10 in, #28906838).

2.10.Kinase Assay

A kinase assay was performed to detect phosphorylation of CDC-42 (Cytoskeleton, #CD01) by PKCz (Calbiochem, Millipore #14-525). The kinase assay was peformed by Josana Rodriguez with the following protocol:

To perform the kinase assay, 100 ng, 50 ng and 0 ng of PKCz were pipetted into an microfuge tube, 5X kinase buffer was added to the mix, and 1 µg/µl of the CDC-42 substrate. 10 mM ATP-gamma-S were added for the reaction, and ddH2O was added for a final volume of 30 µl. The sample was incubated at 30 °C for 1 h, and after the incubation 1 µl of 50 mM PNBM was added (for a final concentration of 1/5 mM), and incubated for a further 1 h at room temperature.

To detect the phosphorylation, 31 µl of 2x Laemmli buffer was added, and the sample stored at -20 °C over night. The sample was then boiled at 95 °C for 5 minutes, centrifuged at 13,000 rpm for 5 minutes in a tabletop centrifuge, and run in a NuPAGE novex gel Bis-Tris 10% (Invitrogen) 10 lane x 1mm (#NP030), with NuPAGE MOPS (SDS running buff NuPAGE Invitrogen NP0001) buffer. 18 µl of each sample was added to each well, with 6 µl of PageRuler Plus Prestained Protein Ladder (26619, Pierce) as a marker.

Transfer was performed into a PVDF membrane, as described in **Section 2.9.3**. After the transfer, the membrane was blocked with 5% milk in TBST 0.05% Tween for 40 min at room temperature with agitation. The anti-thiophosphate ester antibody was used as a primary antibody (1:10,000 in 5% Milk TBST (abcam #ab92570)) for an overnight incubation at 4 °C, the membrane was then washed 3 times with TBST, and anti-rabbit HRP (1:20,000 in 5% Milk TBST (abcam #ab136636)) was used as a secondary antibody, with a 2 h incubation at room temperature.

As detailed in section **Section 2.9.3**., the membrane was then washed 3 times with TBST and once with TBS before incubating for 5 minutes with the ECL Prime (Amersham) detection reagent. The resulting light reaction signal was then captured with an X-ray film (Amersham Hyperfilm ECL, 8 x10 in, #28906838) .

2.11. Statistical Analysis

Graphical representation of data and statistical analysis were performed with GraphPad Prism, Version 7.0a for Mac OS X.

Gaussian distribution was tested with a D'Agostino-Pearson omnibus normality test. When the N value of a group was too low to run this normality test, non parametric distribution was assumed.

Unpaired t tests and Mann-Whitney tests were used when comparing two groups of data of parametric and non parametric distribution, respectively. Ordinary one-way ANOVAs and Kruskal-Wallis tests were employed to calculate significance of three or more groups of parametric and non parametric distribution, respectively. Fisher's exact tests were employed for the analysis of nominal (categorical) data. $P<0.05$ (*), $P<0.01$ (**), $P<0.001$ (***) and $P<0.0001$ (****) were considered significant results.

CHAPTER 3. PKC-3 ACTIVITY IS REQUIRED FOR REGULATION OF ACTOMYOSIN FLOW

3.1. Introduction

The partitioning defective PAR proteins are key regulators of polarity across several species (Knoblich, 2001) (See **Chapter 1** for full introduction). In *Caenorhabditis elegans* PAR proteins are essential to polarise the zygote, and are traditionally split into two groups (anterior or posterior) based on their localisation along the A/P axis. As described in the introduction, the anterior PAR proteins include PAR-3, PAR-6, the small GTPase CDC-42 and the kinase PKC-3 (homologue of the human atypical protein kinase C, aPKC). And posterior PAR proteins include the kinase PAR-1, PAR-2, LGL-1 and CHIN-1.

The kinase PKC-3 is one of the key effectors of polarity, and can cycle between two anterior PAR complexes: a PAR-3 dependent complex that generates clusters and segregates to the anterior in response to actomyosin flow, and a diffusive CDC-42 dependent complex in which PKC-3 can phosphorylate its downstream targets (Dickinson et al., 2017, Rodriguez et al., 2017, Wang et al., 2017).

The *C. elegans* strain *ne4246*, hereafter referred to as *pkc-3(ts)*, contains a temperature sensitive mutation in a well conserved Asp residue (D386V) close to the active site. This mutation renders PKC-3 inactive at 25 °C and affects the localisation of the CDC-42/PAR-6/ PKC-3 complex. In wild type embryos, the CDC-42/PAR-6/PKC-3 complex is enriched in the anterior membrane, and this membrane pool is constantly exchanged with the cytoplasmic pool (Goehring et al., 2011a, Goehring et al., 2011b). In this thesis we refer to the exchange between membrane and cytoplasmic PAR pools as ‘turnover’.

At the restrictive temperature in *pkc-3(ts)* embryos, the turnover of the CDC-42 complex is affected, and PKC-3 becomes locked in the membrane, in a complex with CDC-42. This results in the CDC-42 dependent complex localising all over the cortex of the *C. elegans* zygote (Rodriguez et al., 2017). Furthermore, this strain also presents other defects, such as

decreased actomyosin flow and PAR-3 retraction during establishment (Rodriguez et al., 2017).

Interestingly, aPKC has only been previously reported as an inhibitor of actomyosin contractility in epithelial cell cultures and *Drosophila* amnioserosa cells (David et al., 2010, Ishiuchi and Takeichi, 2011, David et al., 2013, Durney et al., 2018); and to our knowledge, no mechanisms have been reported that could explain how lack of PKC-3 activity leads to actomyosin flow defects in the *C. elegans* zygote (Rodriguez et al., 2017).

3.1.1.Objectives

The main objectives of the work presented in this chapter were the following:

- To describe the ways in which PKC-3 and CDC-42 affect actomyosin flow and structure.
- To identify the signalling pathways in which PKC-3 activity affects actomyosin flow with an RNAi screen.
- To validate the results of the RNAi screen.

3.2. Results

3.2.1. *pkc-3* and *cdc-42* regulate actomyosin flow

In the mutant *pkc-3(ts)* strain actomyosin flow is decreased during establishment (Rodriguez et al., 2017). In this strain PKC-3 is locked in a complex with CDC-42 all over the embryo membrane, making it hard to determine which one of these signalling molecules is responsible for changes in flow. To analyse the role of CDC-42 and PKC-3 in regulating actomyosin flow we analysed non muscular myosin II (NMY-2) *in vivo* in wild type embryos, *pkc-3(ts)* embryos, and embryos treated with *pkc-3* RNAi and *cdc-42* RNAi, to understand if PKC-3 and CDC-42 play different roles in regulating actomyosin and determine which one of these proteins is responsible for the decreased flow observed in *pkc-3(ts)* embryos.

Live imaging of NMY-2::GFP showed a very clear lack of retraction of the actomyosin network in *pkc-3(ts)* embryos (**Figure 3.1 A**), with *pkc-3(ts)* and *pkc-3* RNAi presenting very similar kymographs. *cdc-42* RNAi, on the other hand, still had visible actomyosin flow, although a bit slower than wild type embryos.

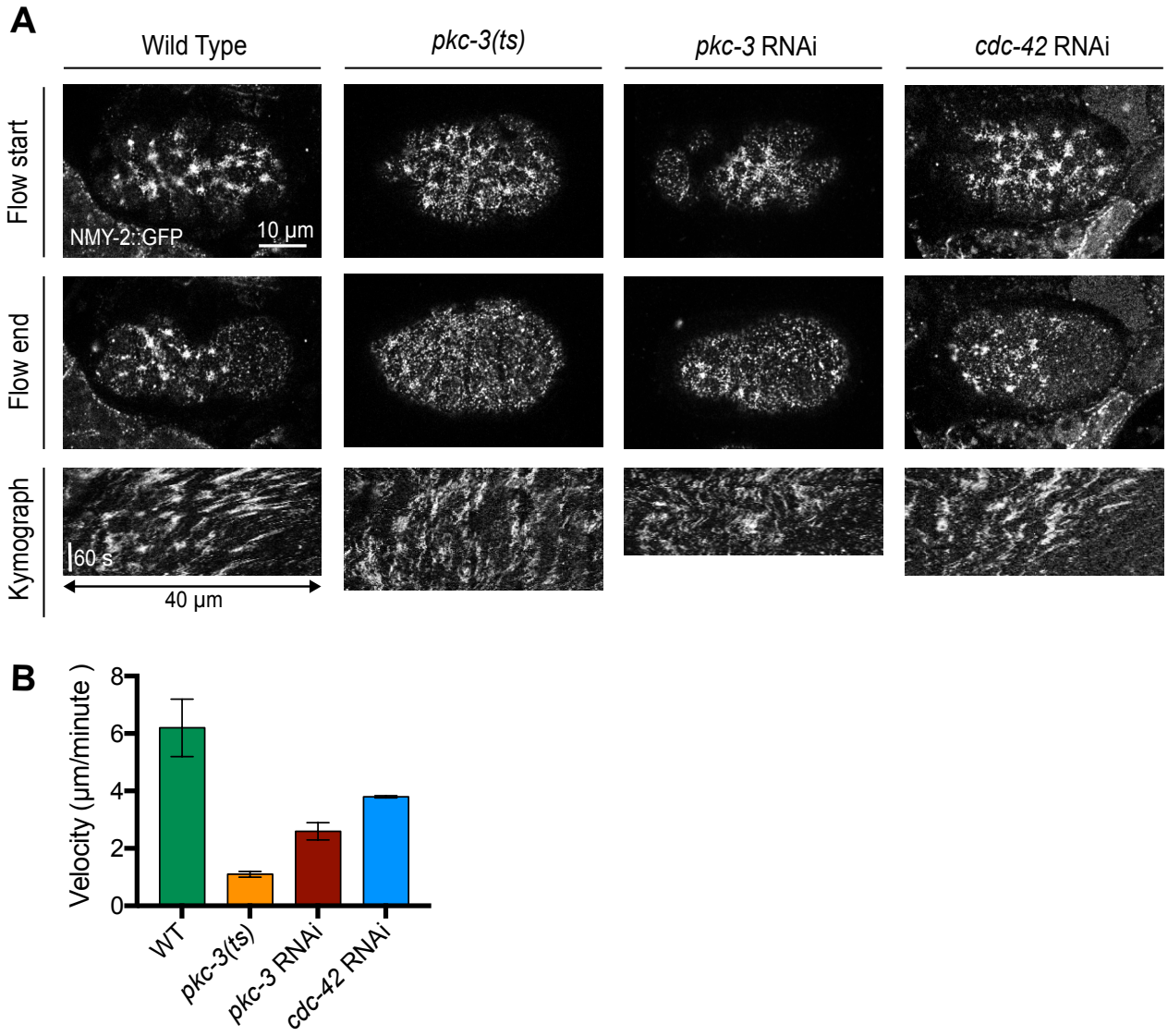

Figure 3.1. Analysis of flow velocity of NMY-2::GFP and its dependence on *pkc-3* and *cdc-42*. A. Representative live images of embryos expressing NMY-2::GFP (JJ1473) at the time of flow start (while the male pronuclei is in contact with the membrane, as seen in bright field images) and flow end (around the time the pronuclei meet, as seen in bright field images), and the kymographs corresponding to the entire flow period. The y-axis length of the kymograph reflects the time-length of the flow period in the embryo analysed, with this being 235 seconds for the wild type embryo kymograph, 270 s for the *pkc-3(ts)* embryo, 190 s for the *pkc-3* RNAi embryo, and 240 s for the *cdc-42* RNAi embryo. The x-axis length of the kymograph is a 40 µm section of length of the embryo (the full length size as seen in the cortical images). NMY-2::GFP foci retract to anterior in wild type embryos and NMY-2::GFP embryos treated with *cdc-42* RNAi, but retraction is not clearly visible in kymographs of NMY-2::GFP crossed to *pkc-3(ts)* and NMY-2::GFP embryos treated with *pkc-3* RNAi. **B.** Flow velocity towards anterior in µm/minute. In wild type embryos NMY-2::GFP retracts towards the anterior at a velocity of 6.2 µm/minute (n=4), in *pkc-3(ts)* embryos it retracts at 1.1 µm/minute (n=3). Silencing of *pkc-3* with RNAi results in NMY-2::GFP retracting at 2.6 µm/minute (n=3), and *cdc-42* silencing with RNAi results in flow velocity of 3.8 µm/minute (n=3).

To quantify the velocity of NMY-2::GFP retraction we performed Particle Imagine Velocimetry (PIV) using the PIVlab MATLAB algorithm, as detailed in Naganathan et al. (2018) and in collaboration with S. Naganathan (**Figure 3.1 B**), with the videos being acquired in our lab and then sent to S. Naganathan for their analysis with the PIV software. In wild type embryos NMY-2::GFP retracted towards the anterior at a velocity of 6.2 μm/minute (n=4), whereas in *pkc-3(ts)* embryos NMY-2::GFP retracted much slower at 1.1 μm/minute (n=3). Similarly, in embryos treated with *pkc-3* RNAi NMY-2::GFP retracted much slower, at 2.6 μm/minute (n=3). Finally, in embryos treated with *cdc-42* RNAi NMY-2::GFP retracted at 3.8 μm/minute (n=3), a velocity much lower than in wild type embryos but higher than in *pkc-3(ts)* embryos and embryos treated with *pkc-3* RNAi. The n values were too low to determine if these differences were statistically significant.

The differences we observed suggest that both PKC-3 and CDC-42 play a role in regulating the actomyosin network and flow during polarity establishment, with PKC-3 perhaps having a stronger effect in regulating flow.

3.2.2.PAR-3 retraction and asymmetry requires *pkc-3* and *cdc-42*

At polarity establishment stage actomyosin flow retracts PAR-3 to the anterior half of the zygote, and the levels of PAR-3 retraction and asymmetry (as determined in immunofluorescent images) can be used as a proxy for actomyosin flow, and therefore as a way of inferring actomyosin flow defects (Rodriguez et al., 2017). This avoids using embryos with NMY-2::GFP over expression to analyse flow, since we know NMY-2 over expression can affect the actomyosin network (see **Section 3.2.4**).

PAR-3 retraction is indicated as the percentage of the total membrane domain with visible PAR-3; and the asymmetric index (ASI) indicates the asymmetry of PAR-3 membrane intensity on a scale from 0 to 1, with 0 being no asymmetry (same levels in anterior and posterior) and 1 being wild type asymmetry (Rodriguez et al., 2017) (**Figure 3.2**, See **Chapter 2 - Methods** for ASI formula). To further investigate if both PKC-3 and CDC-42 signalling can regulate actomyosin flow, we analysed both PAR-3 retraction and the asymmetric index in wild type embryos, *pkc-3(ts)* mutants, and embryos treated with *pkc-3*

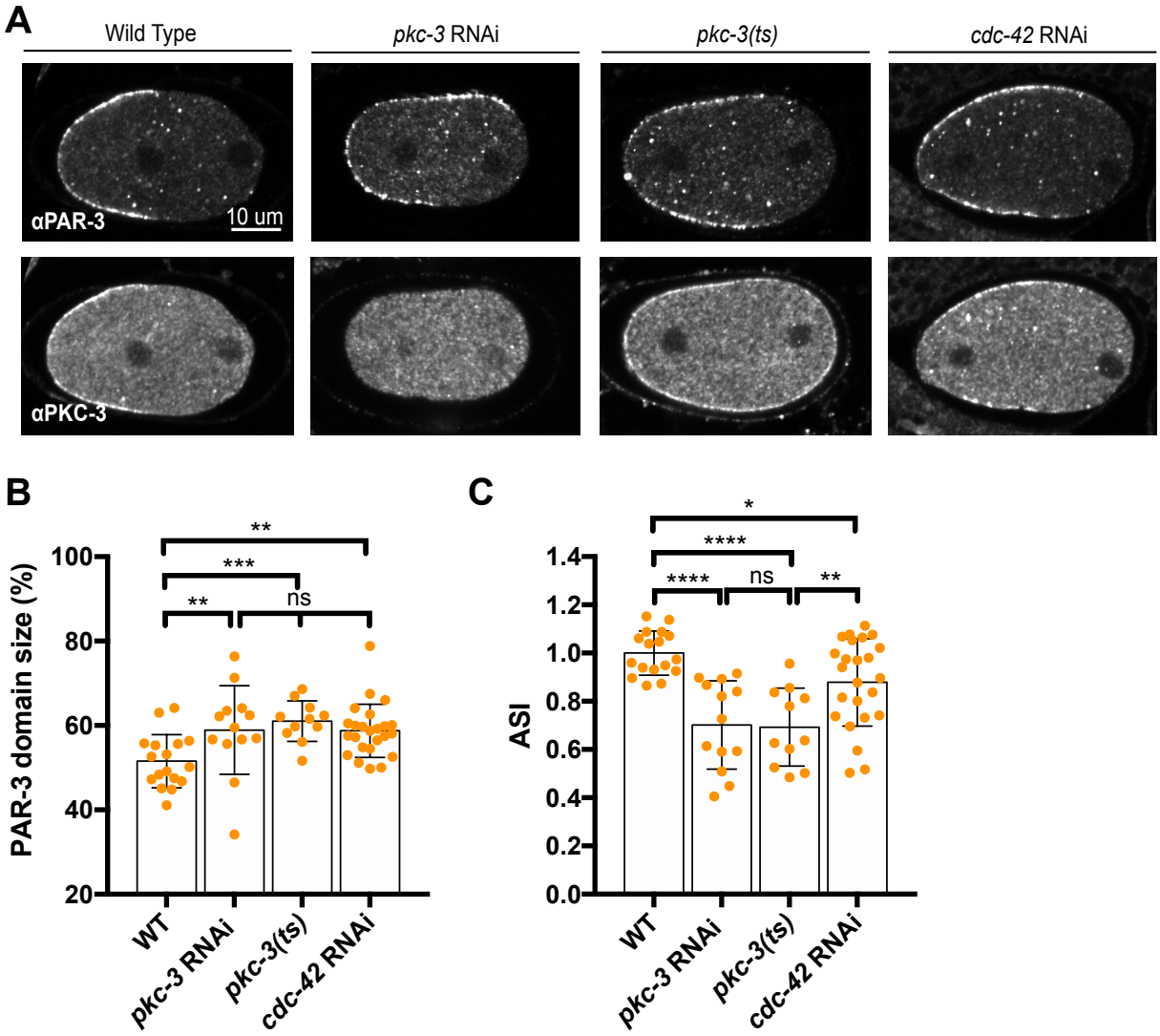

Figure 3.2. Analysis of PAR-3 retraction and dependence on *pkc-3* and *cdc-42*. A. Midplane images of PAR-3 (DSHB, #P4A1) and PKC-3 (Tabuse et al, 1998) stained embryos at establishment stage (as seen by the location of the nuclei). **B.** PAR-3 domain size in wild type embryos (n=17), *pkc-3(ts)* embryos (n=13) and embryos treated with *cdc-42* (n=11) and *pkc-3* RNAi (n=24), as the percentage of the total embryo membrane during polarity establishment stage. Domain size is 19% bigger in *pkc-3(ts)* embryos than in wild type embryos (domain 51% vs 62%, P=0.0003, ordinary one-way ANOVA). There is no significant difference between *pkc-3* RNAi (PAR-3 domain is 57% of the cell), *pkc-3(ts)* and *cdc-42* RNAi (PAR-3 is 58% of the cell) (passed a D'Agostino-Pearson normality test). **C.** Normalised asymetric index (ASI) for PAR-3 in wild type and *pkc-3(ts)* embryos, as well as embryos treated with *pkc-3* and *cdc-42* RNAi, during polarity establisment stage (same embryos as in section B of the figure). Asymmetric index is lower for PAR-3 in the *pkc-3(ts)* background (ASI=1.00 vs 0.69, P<0.0001, ordinary one-way ANOVA) and in embryos treated with *pkc-3* RNAi (ASI=0.70, P<0.0001). And only slighy lower in *cdc-42* RNAi embryos (ASI=0.88, P=0.0198).

and *cdc-42* RNAi (**Figure 3.2**).

During establishment, *pkc-3(ts)* embryos show significantly less PAR-3 retraction than wild type embryos: in wild type embryos actomyosin flow retracts PAR-3 to 51% of the cell, whereas in *pkc-3(ts)* embryos PAR-3 is less retracted and takes up 62% of the cell (P=0.0003, with a one way ANOVA). Similar to *pkc-3(ts)* embryos, PAR-3 only retracts to 57% of the embryo upon *pkc-3* RNAi treatment (P=0.0318), and to 58% of the embryo upon *cdc-42* RNAi treatment (P=0.0017) (**Figure 3.2 A** and **B**). The difference in PAR-3 retraction between *pkc-3(ts), pkc-3* RNAi and *cdc-42* RNAi embryos was not significant, further suggesting that both PKC-3 and CDC-42 could play a role in regulating actomyosin flow during polarity establishment stage.

As for the asymmetric index, it was also significantly smaller in the *pkc-3(ts)* mutant embryos than in wild type embryos (**Figure 3.2 A** and **C**): wild type embryos have an asymmetric index of 1.00 whereas *pkc-3(ts)* embryos have an asymmetric index of 0.69 ($P< 0.0001$). The ASI values for *pkc-3* RNAi were very similar to that of *pkc-3(ts)*, with a mean value of 0.70 (not significantly different to *pkc-3(ts)*, P=0.8895). *cdc-42* RNAi also resulted in smaller ASI, with a mean of 0.88 (P=0.0198, compared to wild type) but significantly higher than *pkc-3(ts)* embryos (P=0.0022).

These results suggest that both PKC-3 and CDC-42 regulate actomyosin flow during polarity establishment stage, with PKC-3 signalling perhaps having a stronger role in regulating flow than CDC-42 signalling.

3.2.3.*pkc-3* and *cdc-42* regulate the structure of the actomyosin network

Another phenotype we observed in *pkc-3(ts)* embryos is a change in the structure of the actomyosin network (**Figure 3.3**), with the foci looking less organised and defined. To analyse this difference, we measured the coefficient of variation (CV) of the cortex of live embryos expressing NMY-2::GFP and of embryos immunostained with αNMY-2 antibodies. The CV is the ratio of standard deviation to the mean of the myosin intensity, and has been previously used as an indicator of the heterogeneity of actomyosin networks (Sonal et al., 2018) (See **Chapter 2.7.6 - Methods** for CV formula).

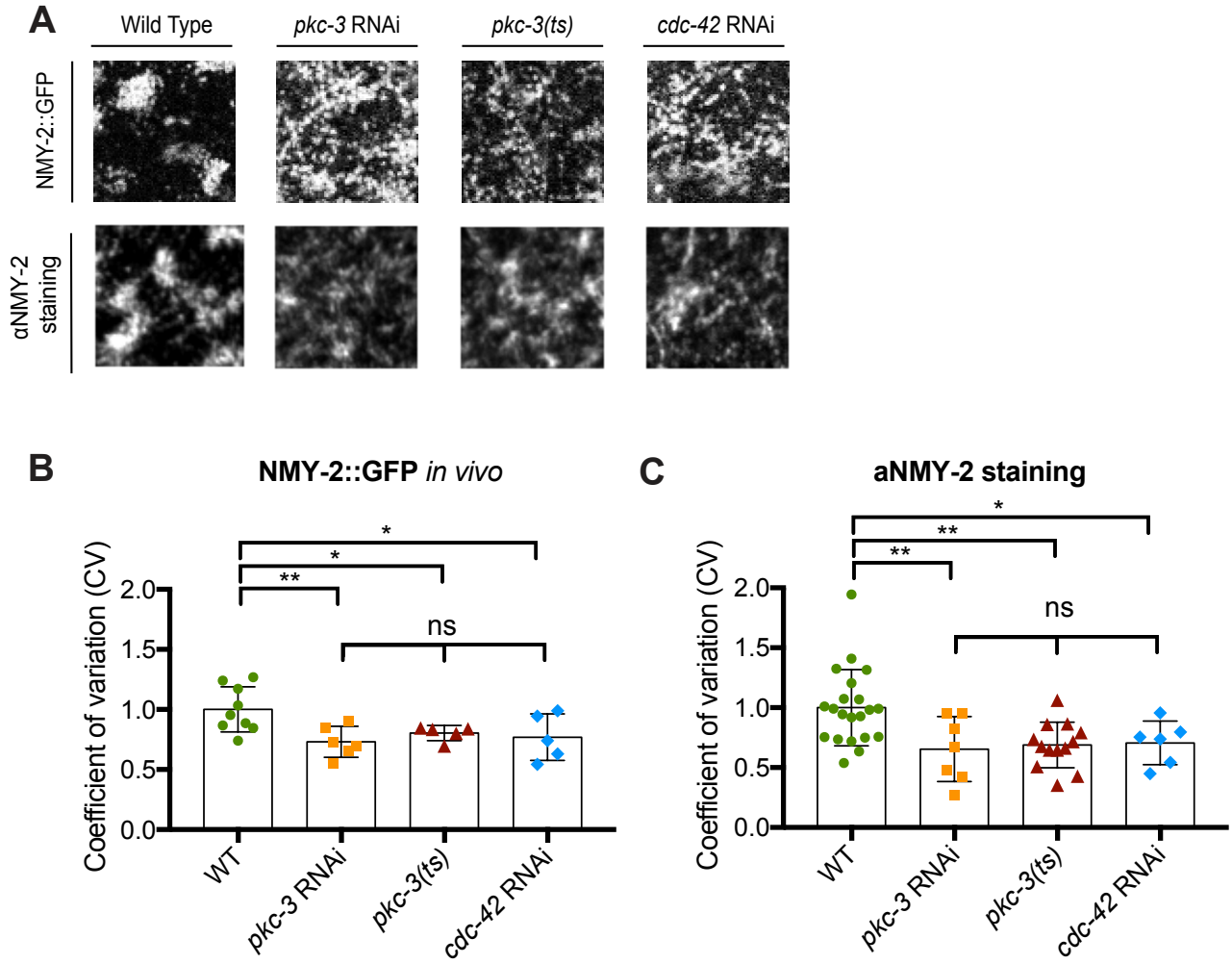

Figure 3.3. Analysis of NMY-2 foci organisation and its dependence on *pkc-3* and *cdc-42* . A. 10 µm square selections of the anterior actomyosin cortex in live wild type embryos expressing NMY-2::GFP (JJ1473) or wild type embryos stained with an anti-NMY-2 antibody (Pickel laboratory, #Rb20417), as well as embryos treated with RNAi against *pkc-3* and *cdc-42*, and embryos with a *pkc-3(ts)* mutation treated with an empty RNAi vector. Embryo stage is early polarity establishment, after flows start. These selections are used for analysis of the coefficient of variation (CV), which can be used to determine the degree of organisation of actomyosin networks (Sonal et al., 2018). **B.** Normalised CV from live embryos expressing NMY-2::GFP during polarity establishment stage, in the aforementioned conditions. In the wild type control the average CV value was 1.00 (n=9), in *pkc-3* RNAi 0.73 (significantly lower than in wild type embryos, P=0.009, n=6), in *pkc-3(ts)* embryos 0.80 (significantly lower than in wild type embryos, P=0.037, n=5), and in *cdc-42* RNAi the CV value was 0.77 (significantly lower than in wild type embryos, P=0.045, n=5) (significance calculated with a Kruskal-Wallis test). **C.** Normalised CV of fixed embryos stained for NMY-2 in the aforementioned conditions, during polarity establishment stage. For wild type embryos the average CV value was 1.00 (n=20), in *pkc-3(ts)* embryos the average CV value was 0.69 (P=0.0021, n=13), for *pkc-3* RNAi the value was 0.65 (P=0.012, n=7) and in *cdc-42* RNAi embryos the average CV value was 0.71 (P=0.05, n=5) (significance calculated with a Kruskal-Wallis test).

In live videos of NMY-2::GFP, the average CV value was of 1.00 at the time of flow start (all values normalised), indicating a strong difference between the actomyosin foci and the background intensity (**Figure 3.3**, see **Figure 3.1** for the full-embryo images of NMY-2::GFP *in vivo*). In embryos treated with *pkc-3* RNAi the CV value was 0.73, significantly lower than in wild type embryos (P=0.009, with a Kruskal-Wallis test), reflecting higher disorganisation of the network. In *pkc-3(ts)* embryos the CV was 0.80, also significantly lower than in wild type embryos (P=0.037). And in embryos treated with *cdc-42* RNAi, the CV was 0.77, also significantly lower than in wild type embryos (P=0.045). There was no significant difference between *pkc-3* RNAi, *pkc-3(ts)* and *cdc-42 RNAi* embryos.

In wild type fixed embryos stained for NMY-2, the average CV value was 1.00 (**Figure 3.3**, see **Figure 3.4** for full-embryo images of NMY-2 staining), and was significantly lower in *pkc-3(ts)* embryos, with a value of 0.69 (P=0.0021). Similarly the CV value was also significantly lower in *pkc-3* RNAi embryos 0.44 (P=0.0012) and in *cdc-42* RNAi embryos 0.71 (P=0.05). The difference between *pkc-3(ts), pkc-3* RNAi and *cdc-42* RNAi embryos was not significant. These results suggest that beyond just affecting the retraction of the network, PKC-3 and CDC-42 play a role in regulating its organisation and structure.

3.2.4.*cdc-42*, but not *pkc-3*, regulates the time of disassembly of the actomyosin network

Another phenotype we found in *pkc-3(ts)* embryos is a change in the timing of disassembly of the actomyosin network (**Figure 3.4**). We analysed this phenotype in embryos stained for NMY-2, and staged the embryos by the position of the nuclei, with the earlier time of the maintenance stage, when the pronuclei meet, being referred to as 'Maintenance I' and the later stage when the pronuclei rotate and centre begins referred to as 'Maintenance II' in the figure (**Figure 3.4 A-C**). As with the analysis of flow and foci structure, we analysed wild type embryos, *pkc-3(ts)* embryos, and embryos treated with *pkc-3* and *cdc-42* RNAi, to determine if the time of disassembly of NMY-2 foci was determined by CDC-42, PKC-3 or a combination of both. We decided not to do this analysis *in vivo*, as NMY-2::GFP is an NMY-2 over expression, and disassembly of the network is delayed compared to wild type (**Figure 3.4 D**).

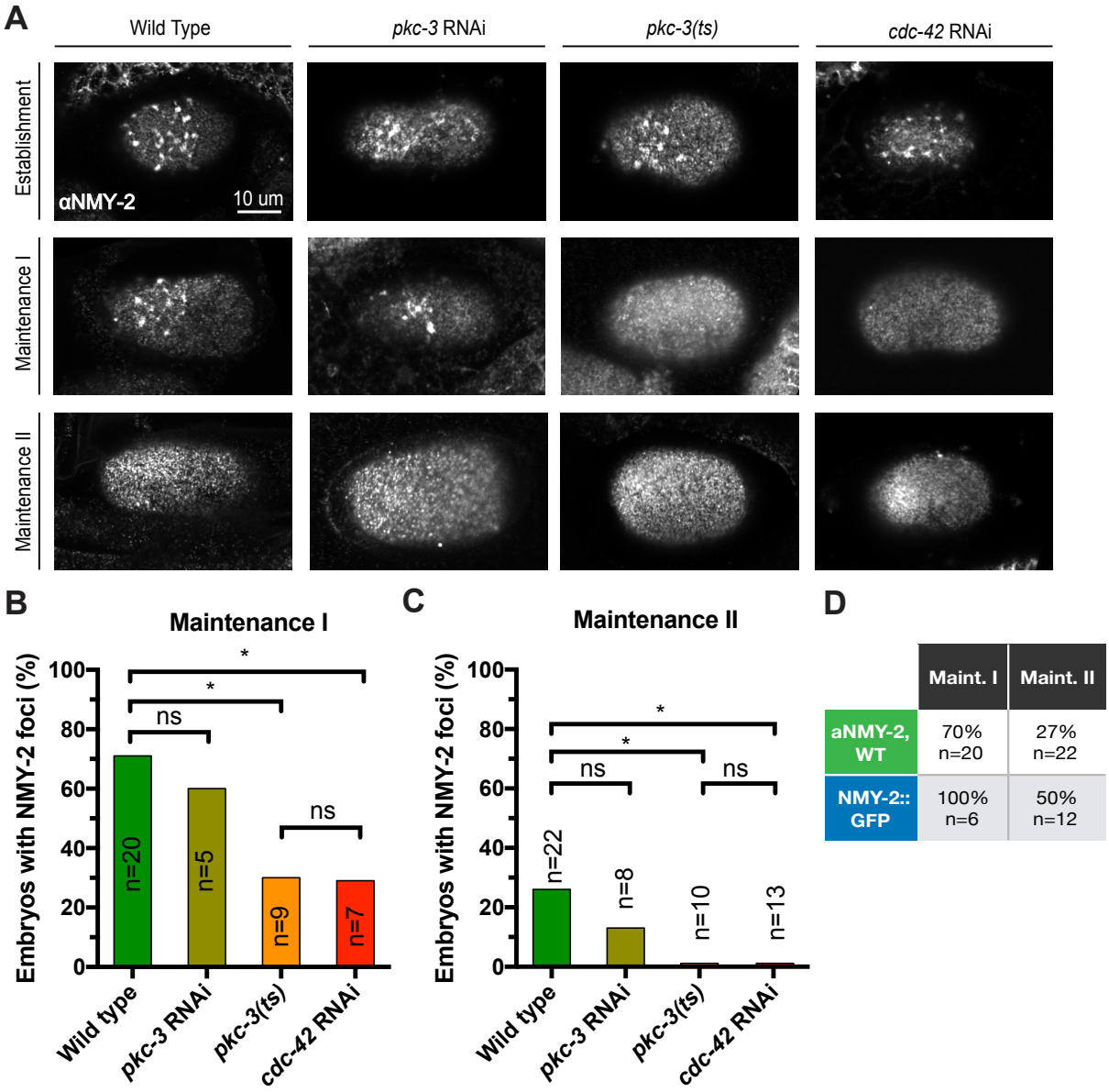

Figure 3.4. Time of dissasembly of the NMY-2 foci network. A. Embryos stained for NMY-2 (Pickel laboratory, #Rb20417) during establishment and maintenance stages I and II. **B.** Analysis of NMY-2 foci presence during Maintenance I (Fisher's exact test). **C.** Analysis of NMY-2 foci presence during Maintenance II (Fisher's exact test). **A-C.** In wild type embryos NMY-2 is present in foci structures during polarity establishment, and the myosin network dissasembles during polarity maitenance stage, with 70% of embryos still having foci during Maintenance I and 27% of embryos during Maintenance II. In embryos treated with *pkc-3* RNAi the time of NMY-2 dissasembly is not significantly different to wild type embryos (60% and 12% for each stage), but in embyros of *pkc-3(ts)* background and embryos treated with *cdc-42* RNAi dissasembly occurs earlier, in Maintenance I (33% and 0% for each stage of *pkc-3(ts)* and 28% and 0% for *cdc-42* RNAi). There is no significant difference between *pkc-3(ts)* embryos and embryos treated with *cdc-42* in the analysis of NMY-2 foci dissasembly. **D.** Table comparing NMY-2 foci present during Maintenance stages I and II in wild type embryos stained for NMY-2 and fixed embryos expressing NMY-2::GFP (JJ1473) .

In wild type embryos actomyosin forms foci during polarity establishment, and these foci polarise to the anterior side of the zygote. Foci are still present in 70% of wild type embryos in the early stages of polarity maintenance, when the pronuclei meet (Maintenance I), and disappear in most embryos when the pronuclei rotate and centre (Maintenance II), with only 27% of embryos presenting foci at this stage. In *pkc-3(ts)* embryos however, NMY-2 foci disappear earlier in the cell cycle, with only 33% of embryos presenting foci in Maintenance I and no embryos presenting foci in Maintenance II. These percentages are significantly different to those from wild type embryos (P=0.0289 and P=0.0437 respectively, with a Fisher's exact test).

Our analysis showed that *cdc-42* RNAi resulted in a phenotype similar to *pkc-3(ts)*, with 28% of embryos presenting foci during Maintenance I and no embryos presenting foci during Maintenance II (P=0.0444 and P=0.0437 when compared to wild type, and not significantly different to *pkc-3(ts)*). Lastly, embryos treated with *pkc-3* RNAi were not significantly different to wild type embryos, with 60% of embryos presenting foci during Maintenance I and 12% of embryos presenting foci during Maintenance II.

Given that *pkc-3* RNAi does not show any defects in the disassembly of the actomyosin network, these results suggest that CDC-42 signalling regulates the time of disassembly of the actomyosin network, and that the lack of CDC-42/PAR-6/PKC-3 turnover observed in *pkc-3(ts)* embryos (Rodriguez et al., 2017) is the reason for the early disassembly of foci observed in this strain.

3.2.5.RNAi screen to identify actomyosin pathways affected by *pkc-3*

To identify the pathways by which the kinase activity of PKC-3 can affect the generation of actomyosin flow we performed a RNAi screen, silencing five flow regulating molecules that control actomyosin flow in different ways in both wild type and *pkc-3(ts)* background. These genes were: the RHO-1 activating proteins *rga-3* and *rga-4*, the casein kinase *csnk-1*, the ARF activating protein *cnt-2*, and the small GTPase CDC-42 activating protein *chin-1*. All of these molecules had been identified in a *C. elegans* genome-wide RNAi screen as actomyosin flow regulators (Fievet et al., 2013).

To determine if silencing these genes was restoring actomyosin flow to a wild type level, we stained embryos for PAR-3 and inferred changes in flow from the analysis of PAR-3 retraction and asymmetry (as previously shown in **Figure 3.2**).

3.2.5.1.Increasing RHO-1 activity generates a cortical ruffling phenotype

The first genes in our screen were *rga-3* and *rga-4*, the GAPs of the small GTPase RHO-1 (**Figures 3.5** and **3.6**). The RNAi employed to silence these genes targets the ORFs of both the *rga-3* and *rga-4* genes, silencing both genes at the same time (Schmutz et al., 2007). Knockdown of either *rga-3* or *rga-4* results in a weaker hyper-contractile cortex phenotype than that observed for *rga-3/4* RNAi, suggesting that both genes share the same function in the first cell division of *C. elegans* (Schmutz et al., 2007; Schonegg et al., 2007). Due to the strong effects observed in *rga-3/4* RNAi, we used the RNAi at both 50% and 100% strengths

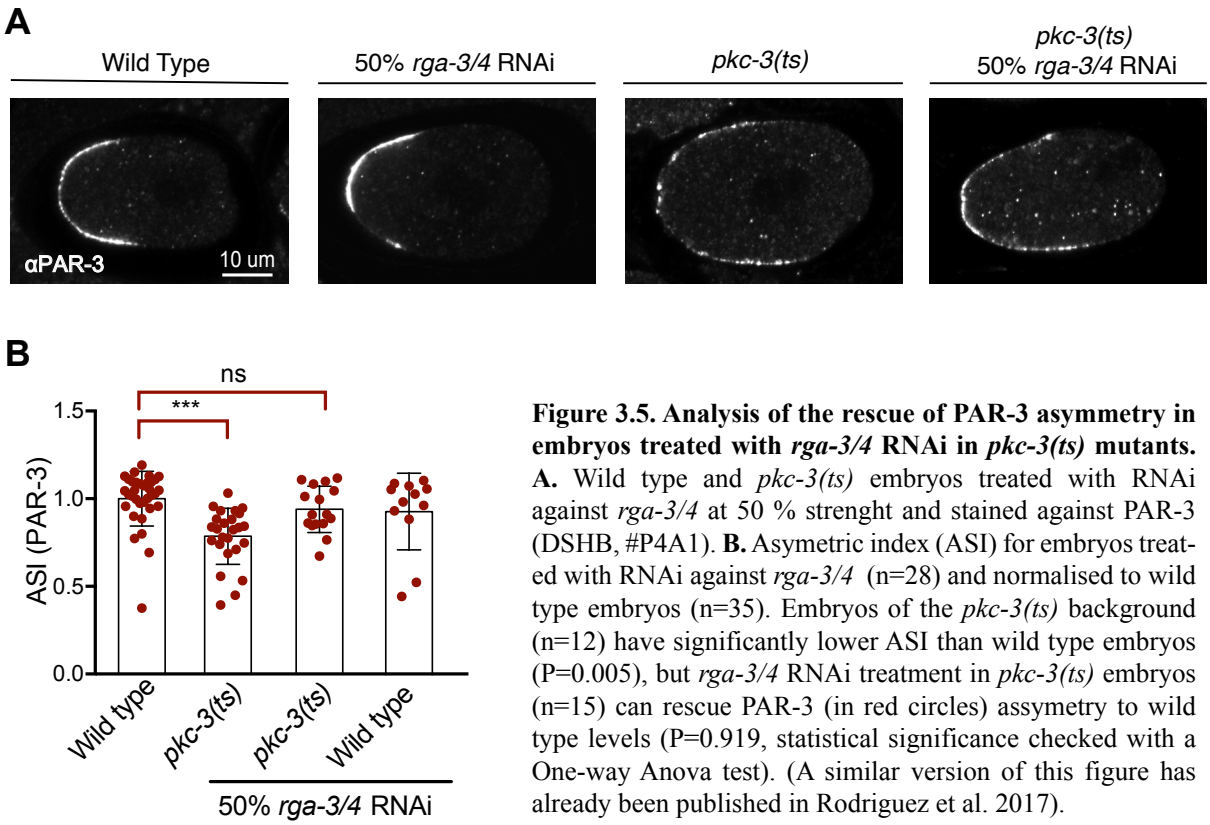

Figure 3.5. Analysis of the rescue of PAR-3 asymmetry in embryos treated with *rga-3/4* RNAi in *pkc-3(ts)* mutants. **A.** Wild type and *pkc-3(ts)* embryos treated with RNAi against *rga-3/4* at 50 % strenght and stained against PAR-3 (DSHB, #P4A1). **B.** Asymetric index (ASI) for embryos treated with RNAi against *rga-3/4* (n=28) and normalised to wild type embryos (n=35). Embryos of the *pkc-3(ts)* background (n=12) have significantly lower ASI than wild type embryos (P=0.005), but *rga-3/4* RNAi treatment in *pkc-3(ts)* embryos (n=15) can rescue PAR-3 (in red circles) assymetry to wild type levels (P=0.919, statistical significance checked with a One-way Anova test). (A similar version of this figure has already been published in Rodriguez et al. 2017).

(50% strength is achieved by diluting the bacteria expressing the RNAi of interest with bacteria not expressing RNAi, at 50% v/v).

Silencing the RHO-1 GAPs *rga-3/4* at a 50% strength was enough to increase flow and rescued the intensity of PAR-3 in the anterior of *pkc-3(ts)* embryos (**Figure 3.5**, published in Rodriguez et al. 2017), indicating that increased RHO-1 activity can partly rescue the decrease in flow of *pkc-3(ts)* and suggesting that PKC-3 could be a regulator of the RHO/ LET-502 pathway.

We could not use the 100% strength RNAi against *rga-3/4* to analyse the rescue of PAR-3 as this strength results in cortical defects, which make analysis of the PAR-3 domain difficult. These cortical defects fit into two categories (**Figure 3.6 A)**: membrane 'blebs' phenotype, in which the cortex generates bubble-like structures, and a membrane invagination phenotype. Neither of these phenotypes can be seen in wild type or *pkc-3(ts)* embryos.

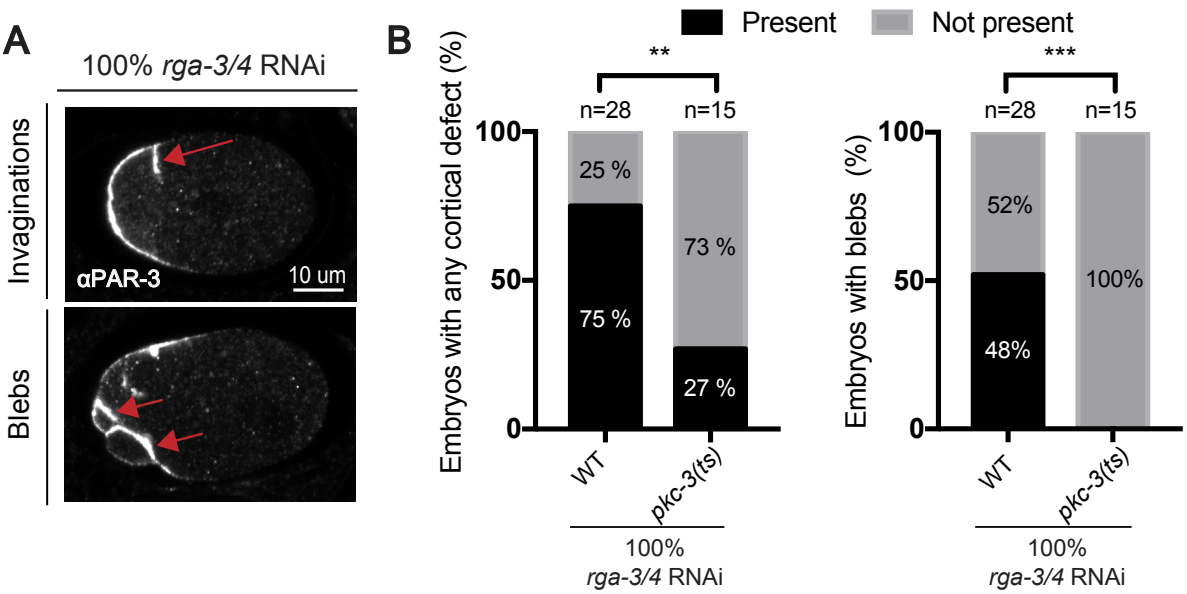

Figure 3.6. Analysis of cortical defects generated by *rga-3/4* RNAi. A. Midplane images of wild type embryos treated with full strenght RNAi against *rga-3/4*, the GAP for the small GTPase RHO, and stained for PAR-3 (DSHB, #P4A1) . Red arrows point to invatinations and blebs. Treating wild type embryos with this RNAi affects the structure of the cortex and generates structures such as invaginations of the cortex and ruffles. **B.** Percentages of embryos with any cortical defects (includes both invaginations and blebs) and with bleb defects during maintenance. The lack of kinase activity in *pkc-3(ts)* significantly reduces the rate of cortical defects upon *rga-3/4* RNAi (P=0.002 for all cortical defects phenotypes and P=0.006 for bleb phenotype, calculated with Fisher's exact test).

Furthermore, these cortical defect phenotypes might depend on the kinase activity of PKC-3 (**Figure 3.4 B**), with 75% of embryos of the wild type background (n=28) presenting cortical defects and only 25% of embryos of the *pkc-3(ts)* background (n=15) presenting these cortical defects (P=0.002, Fisher's exact tests) upon *rga-3/4* knock down. The bleb phenotype was observed in 48% of the embryos of the wild type background, but it was not observed in any of the *pkc-3(ts)* embryos imaged (P=0.006).

We hypothesised that two mechanisms could be responsible for the observed cortical defects: first, the RNAi against *rga-3/4* could increase RHO-1 activity, leading to an increased activity of it's effector kinase LET-502 (Schonegg et al., 2007). This kinase is known to phosphorylate the myosin light chain 4 (MLC-4), increasing contractility of non-muscular myosin II (NMY-2) in the anterior domain of the embryo (Amano et al, 1996).

Silencing the *rga-3/4* genes could thus lead to increased LET-502 activity and cortical flow, as previously reported (Schonegg et al., 2007), and the increased activity of this pathway could generate the observed perturbations on the cortex. Second, the increase in RHO-1 activity could be affecting it's role in cytokinesis, and generating a cytokinetic-like rings at earlier stages.

To understand how the cortex is disrupted when increasing RHO-1 activity via *rga-3/4* silencing, we stained for NMY-2 in wild type embryos and embryos treated with the *rga-3/4* RNAi (**Figure 3.7**). NMY-2 organises in foci, which polarise to the anterior side of the zygote during polarity establishment stages. This foci then disappear during polarity maintenance stages, and finally, NMY-2 becomes organised in a cytokinetic ring during the late stages of the first cell division. In embryos treated with *rga-3/4* RNAi, NMY-2 still segregates to the anterior domain, but the foci structure are very disorganised. The blebs observed when employing the *rga-3/4* RNAi do not show any sign of a contractile NMY-2 ring, indicating that the observed ruffling phenotype is a result of disorganised cortical NMY-2, rather than a change in the function/timing of RHO-1's cytokinetic activity.

3.2.5.2.Silencing csnk-1 changes PAR domain localisation and affects polar body extrusion in a PKC-3 activity dependant manner

Another one of the targets selected to test for changes in flow was the casein kinase CSNK-1 (**Figure 3.8**). CSNK-1 has been suggested to decrease cortical forces downstream or in parallel to PAR proteins, as zygotes treated with *csnk-1* RNAi divide symmetrically and show increased cortical activity and spindle pulling (Panbianco et al., 2008).

CSNK-1 is a casein kinase that antagonises the PIP_2 synthesis enzyme PPK-1 in anterior to increase the levels of PIP_2 in the posterior, leading to changes in the membrane composition of the posterior domain and different regulation of heterotrimeric G proteins (Panbianco et al., 2008).

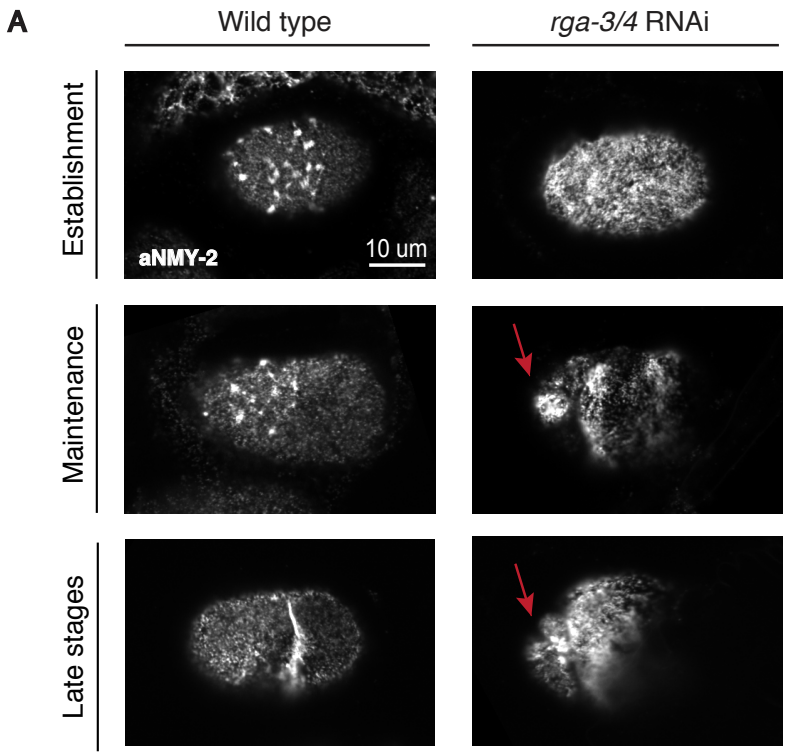

Figure 3.7. The actomyosin network in embryos treated with *rga-3/4* RNAi. A. Cortical planes of embryos stained for NMY-2 (Pickel laboratory, #Rb20417). NMY-2 organises in punctae in polarity establishment stages in wild type embryos and in a cytokinetic ring in later stages of the zygote. The foci structure are disorganised upon treatment with *rga-3/4* RNAi. Blebs in embryos treated with *rga-3/4* RNAi are indicated with the red arrows.

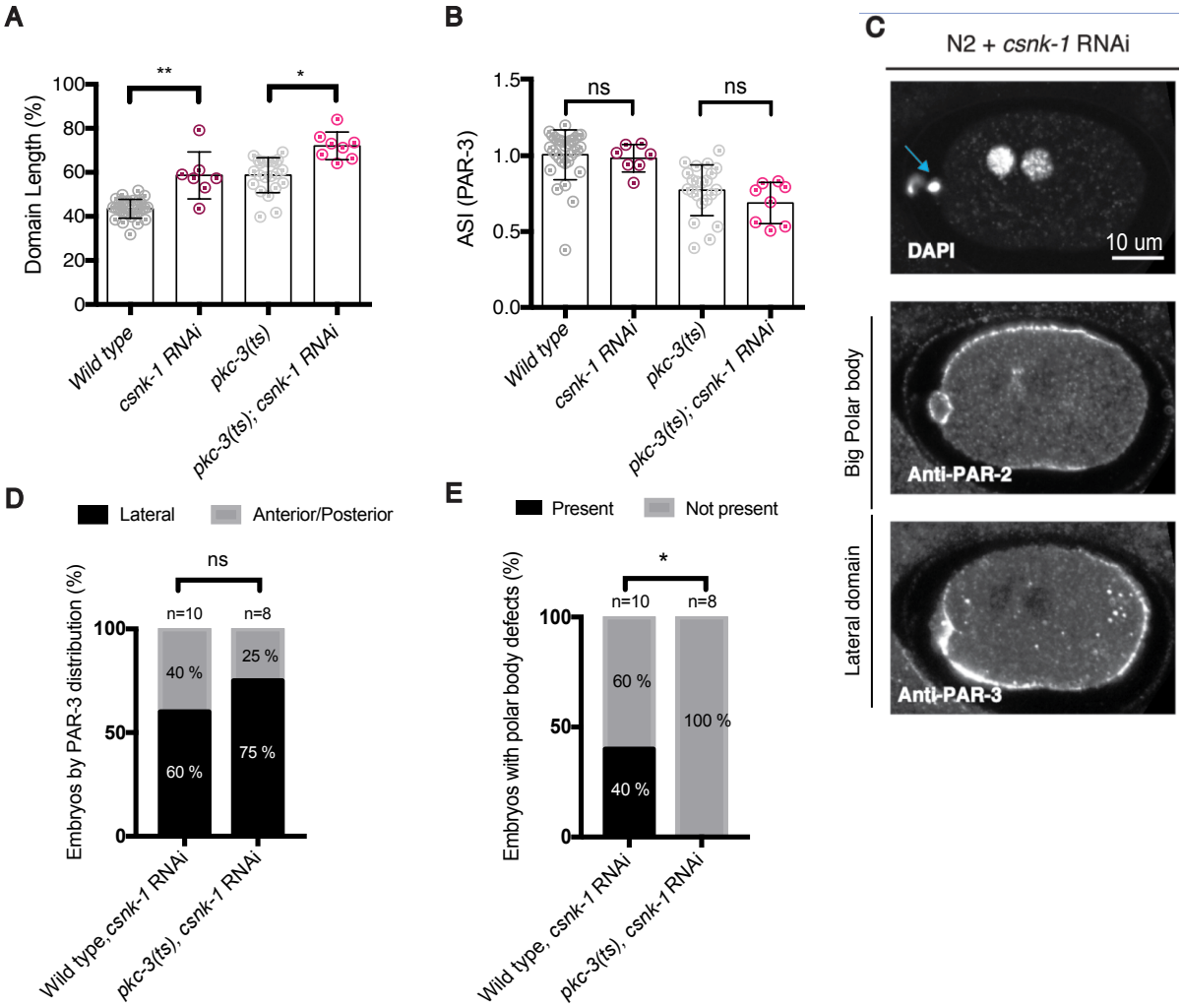

Figure 3.8. Effect of *cnsk-1* RNAi in wild type and *pkc-3(ts)* embryos. A. Length of the PAR-3 domain (as a percentage of the total membrane domain) upon *csnk-1* silencing in wild type and *pkc-3(ts)* background embryos, changes upon *csnk-1* silencing are significant both in the wild type (P=0.0049, Kruskal Wallis test) and the *pkc-3(ts)* (P=0.047, Kruskal Wallis test) background embryos. Embryos of maintenance stage. **B.** Intensity of the PAR-3 domain during maintenance as measured by the asymmetric index in wild type and *pkc-3(ts)* background upon *csnk-1* silencing. Effects are not significant in any case (P=0.5150 and P=0.3641). **C**. Images of wild type background embryos upon *csnk-1* silencing. Polar body size (shown with the blue arrow) increases, as can be seen in the PAR-2 staining (DSHB, #P4A1) , and PAR domains become lateral rather than anterior/posterior, as visible by the PAR-3 staining (DSHB, #P4A1) . **D**. Analysis of PAR-3 domain in embryos treated with *csnk-1*. Lateral and A/P domains were observed both in wild type backgroud and *pkc-3(ts)* backgroup uopn *cnsk-1* silencing, with no significant differences between the two. **E**. Analysis of embryos with polar body defects. Polar body deffects are only visible in the wild type background upon *cnsk-1* silencing, but not in the *pkc-3(ts)* background (P=0.0425, Fisher's exact test).

When performing *csnk-1* silencing with RNAi we observed an increase in PAR-3 domain length both in a wild type and a *pkc-3(ts)* backgrounds (P=0.0049 and P=0.047, respectively) (**Figure 3.8 A** and **B**). This change in domain size was accompanied by a change in domain localisation: PAR-3 localised in a lateral domain in 60% of the embryos on a wild type background and 75 % of embryos with a *pkc-3(ts)* background (**Figure 3.8 C-D**).

We hypothesised that there could be two reasons for the change from anterior/posterior to lateral polarity upon *csnk-1* silencing: first, changes in phosphoinositide asymmetries could affect localisation of anterior PARs (as has been shown in rat neurites (Jiang et al., 2005) and epithelial cells (Martin-Belmonte et al., 2007)) or more likely, it could be caused by *csnk-1* RNAi affecting chiral flows (weak flows along the Left/Right axis, described in Naganathan et al. 2014), which also depend on myosin activity (Naganathan et al., 2014). Recent research analysing the effect of *csnk-1* RNAi in chiral flow supports the second theory (Naganathan et al., 2018).

Since lack of PKC-3 activity does not seem to prevent the lateral PAR-3 phenotypes observed in *csnk-1* RNAi, PKC-3 might not be involved in chiral flow regulation and is more likely just involved in the establishment of anterior/posterior polarity.

Another phenotype observed when employing the *csnk-1* RNAi is a change in polar body size/localisation (**Figure 3.8 C** and **E**). In wild type embryos, the polar body is extruded in the anterior domain of the zygote via a RHO-1 dependant contractile ring (which is recruited by anilin) that moves inwards down the length of the meiotic spindle, in a process that requires correct CDC-42 localisation (Zhang et al., 2008).

When treating wild type embryos with *csnk-1* RNAi, we observed changes in the size and extrusion of the polar body extruded (**Figure 3.8 C** and **E**), with 40% of embryos having a visibly bigger polar body accompanied of a disorganised cortex in the area where the polar body was extruded. Interestingly, none of the *pkc-3(ts)* embryos treated with the same RNAi showed this change in their polar body. This difference was significant (P= 0.0425, Fisher's exact tests), suggesting a role for PKC-3 in polar body extrusion.

Previous research on *csnk-1* RNAi and polar body extrusion suggest that CSNK-1 is a regulator of the RHO/LET-502 pathway (Flynn and McNally, 2017), so we hypothesised that the change in polar body size observed could be related to changes in regulation of the RHO-1 dependant contractile ring, once again suggesting that PKC-3 might be a positive regulator of the RHO-1 pathway.

3.2.5.3.Silencing of the ARF GAP cnt-2 increases actomyosin flow in a PKC-3 independent manner

The ARF GAP Centaurin-2 has previously been reported to affect asymmetric cell division in *C. elegans* neuroblast by affecting vesicle trafficking (Singhvi et al., 2011), and cortical actomyosin dynamics (Fievet et al., 2013). Furthermore it's human homologue centaurin-alpha(2) has been shown to regulate by binding PIP_2 and PIP_3 and preventing cortical actin formation (Venkateswarlu et al., 2007).

In our RNAi screen, silencing of *cnt-2* with RNAi resulted in a significant increase in PAR-3 retraction in wild type background (P=0.0465) (**Figure 3.9 A**). Retraction in the *pkc-3(ts)* background was also increased, although not significantly (P=0.0946).

The asymmetric index for PAR-3 was not significantly affected in either background (**Figure 3.9 B**). The similar changes in PAR-3 retraction in both the wild type and *pkc-3(ts)* background suggests that PKC-3 is not involved in flow regulation via CNT-2.

3.2.5.4.Increasing CDC-42 activity favours the CDC-42 bound state of anterior PARs

Finally, the last target selected for the screen was *chin-1*, a GAP for CDC-42 (**Figure 3.10**). Removal of *chin-1* with RNAi results in an increase in GTP bound CDC-42, so given the role of CDC-42 in keeping actomyosin flow at maintenance (Motegi and Sugimoto, 2006; Schonegg and Hyman, 2006) and having observed lower actomyosin flow in *cdc-42* RNAi, we expected to observe increased PAR-3 asymmetry upon *chin-1* silencing.

The PAR-3 domain we observed, however, was not affected by *chin-1* silencing in either the wild type or the *pkc-3(ts)* domain (**Figure 3.10 B**), suggesting that *chin-1* silencing does not affect actomyosin flow in a significant way in the zygote.

PAR-3 intensity (as measured by the asymmetric index) even seems to be decreased in the *pkc-3(ts)* background (ASI goes from 0.77 in *pkc-3(ts)* embryos to 0.60 in *pkc-3(ts)* treated with *chin-1* RNAi), although not significantly (P= 0.39) (**Figure 3.10 B**).

This decrease could be explained however by the fact that in the mutant *pkc-3(ts)*, the CDC-42 bound state is favoured in anterior PARs, as opposed to the PAR-3 state being favoured. So an increase in GTP bound CDC-42 might favour even further the CDC-42 state as opposed to favouring the PAR-3 bound state.

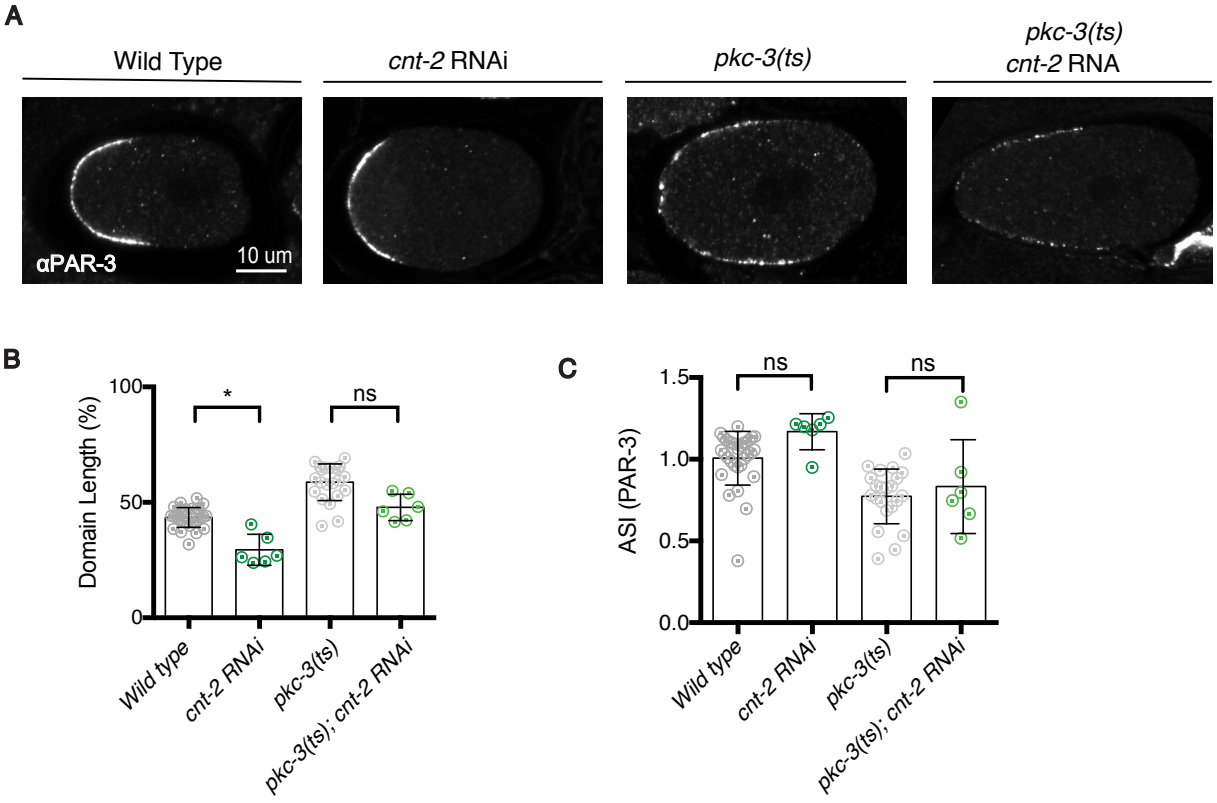

Figure 3.9. Effect of *cnt-2* RNAi in wild type and *pkc-3(ts)* embryos. A. Images of wild type and *pkc-3(ts)* embryos, with and without *cnt-2* RNAi, and stained for PAR-3 (DSHB, #P4A1). Embryos are of maintenance stage. **B**. Length of PAR-3 domain upon *cnt-2* silencing in wild type and *pkc-3(ts)* background embryos during polarity maintenance stage, changes upon *cnt-2* silencing are significant only in the wild type (P=0.0305, n=31 and n=6), and not in the *pkc-3(ts)* bacground embryos (P=0.0946, n=22 and n=6) (calculated with Kruskal Wallis test). **C.** Intensity of the PAR-3 domain as measured by the assymetric index in wild type and *pkc-3(ts)* background upon *cnt-2* silencing. Effects are not significant in either background.

Interestingly, *chin-1* RNAi rescues the lethality observed in *pkc-3(ts)* embryos: *pkc-3(ts)* embryos show a lethality of 43% and *chin-1* RNAi on its own shows a lethality of 13%, whereas *pkc-3(ts)* embryos treated with *chin-1* RNAi only show a lethality of 17%. This suggests that the increase in CDC-42 activity generated when removing the CDC-42 GAP rescues the activity of the PKC-3 bound CDC-42 in *pkc-3(ts)* embryos.

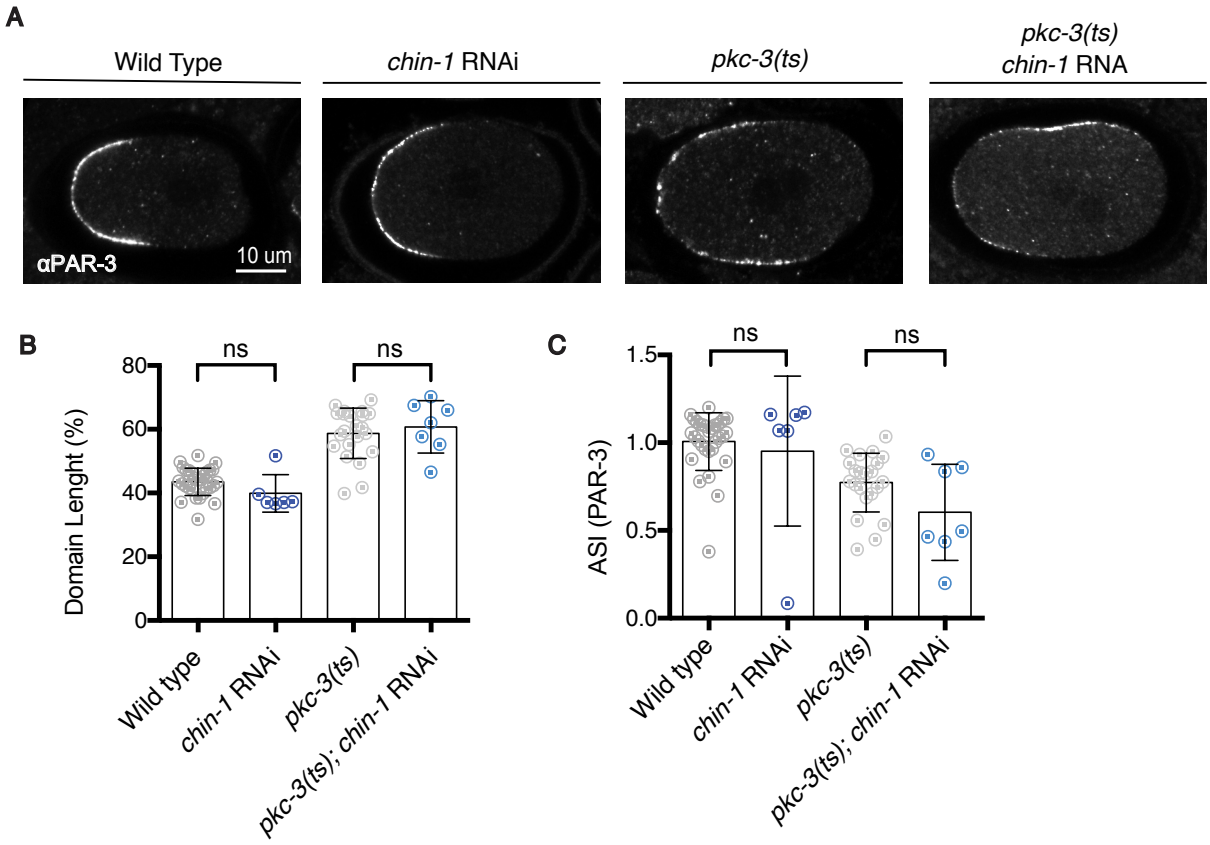

Figure 3.10. Effect of *chin-1* RNAi in wild type and *pkc-3(ts)* embryos. A. Images of wild type and *pkc-3(ts)* embryos, with and without *chin-1* RNAi, and stained for PAR-3 (DSHB, #P4A1). Embryos are of maintenance stage. **B**. Lenght of PAR-3 domain upon *chin-1* silencing in wild type and *pkc-3(ts)* background embryos during polarity maintenance, changes upon *chin-1* silencing are not significant either in wild type (P=0.39, n=31 and n=6), not in the *pkc-3(ts)* background (P>0.999, n=22 and n=7, Kruskal Wallis test) embryos. **C.** Intensity of the PAR-3 domain as measured by the assymetric index in wild type and *pkc-3(ts)* background upon *chin-1* silencing during polarity maintenance. Effects are not significant in either background (P>0.999 for both comparisons shown, Kruskal Wallis test).

3.3. Discussion

3.3.1. PKC-3 and CDC-42 regulate actomyosin flow and structure during polarity establishment

PAR proteins are key effectors of polarity in many metazoan cells, and their localisation to discrete cortical domains is essential for their proper function. In the *pkc-3(ts)* strain, inactive PKC-3 localises symmetrically all over the membrane in a CDC-42 bound complex, and PAR polarity and actomyosin flow are affected (Rodriguez et al., 2017). Given the tight link between PKC-3 and CDC-42, analysing the mutant *pkc-3(ts)* in which both proteins are affected, as well as embryos treated with *pkc-3* RNAi and *cdc-42* RNAi allows us to determine which actomyosin defects are caused by lack of PKC-3 or its activity, which by lack CDC-42 or its activity, and which defects might be a result of more than one pathway/ pathways involving both proteins.

To analyse the decreased flow phenotype, we analysed live videos of NMY-2::GFP and fixed embryos stained for PAR-3, as PAR-3 retraction and asymmetry depends on actomyosin flow (Munro et al., 2004). In NMY-2::GFP embryos all conditions resulted in slower actomyosin flow during polarity establishment stage, with *pkc-3(ts)* and *pkc-3* RNAi showing a stronger flow defect (**Figure 3.1 B**). Furthermore, all three conditions resulted in lower levels of PAR-3 retraction and asymmetry, with *pkc-3* and *pkc-3(ts)* having a stronger phenotype than *cdc-42* RNAi (**Figure 3.2 B-C**).

These results suggest that both PKC-3 and CDC-42 play a role in regulating actomyosin flow during polarity establishment, with PKC-3 playing a stronger role in regulating actomyosin flow. These results are very interesting, as no role has been described before for PKC-3 in regulating the polarising flow, and CDC-42 has mostly been studied as a regulator of the actomyosin network during the later maintenance stage (Sailer et al., 2015, Small and Dawes, 2017), even though *cdc-42* RNAi has been reported to be required for clearing of the CDC-42 GEF ECT-2 at the start of actomyosin flow (Motegi and Sugimoto, 2006) (See **Chapter 1** for information on CDC-42 GEFs and their regulation).

Another phenotype we identified in the *pkc-3(ts)* mutant was a change in actomyosin structure, with NMY-2 foci looking more disorganised than in the wild type control (**Figure 3.3 B-C**). To analyse this phenotype we imaged NMY-2::GFP *in vivo*, as well as in fixed embryos stained for NMY-2. In all cases, *cdc-42* RNAi, *pkc-3* RNAi and the *pkc-3(ts)* mutant had significantly more disorganised foci than in wild type embryos. These results suggest once again that both CDC-42 and PKC-3 could be involved in regulating actomyosin foci structure, and, given how similar the *pkc-3(ts)*, *pkc-3* RNAi and *cdc-42* RNAi phenotypes are, perhaps regulating it in the same way/together (See **Chapters 5 and 6** for further discussion).

The role of PKC-3 in regulating actomyosin foci has not been studied before, but *cdc-42* RNAi has previously been reported to result in bigger average NMY-2 foci size (Naganathan et al., 2018), which reflects the 'more disorganised' foci structure we detected. However no mechanism has been yet identified for CDC-42 regulation of actomyosin during establishment.

3.3.2. CDC-42, but not PKC-3, regulates the time of disassembly of the actomyosin network

The last phenotype we identified in the *pkc-3(ts)* strain was a change in the time of disassembly of the actomyosin network, with NMY-2 foci disassembling earlier during maintenance in *pkc-3(ts)* embryos than in the wild type control (**Figure 3.4 B-C**), suggesting that PKC-3 or CDC-42 could be required for the regulation of NMY-2 foci formation/ stabilisation. As with the previously mentioned phenotypes, we analysed time of foci disassembly in embryos treated *cdc-42* RNAi and *pkc-3* RNAi, as well as *pkc-3(ts)* embryos, to determine if the change in timing was a result of the lack of PKC-3 activity, or a result of CDC-42 being locked in the CDC-42/PAR-6/PKC-3 complex (in *pkc-3(ts)* embryos).

Interestingly, *cdc-42* RNAi resulted in the same phenotype as *pkc-3(ts),* with actomyosin foci disassembly happening at the time of pronuclear meet (Maintenance I) as opposed to when the pronuclei rotate and centre (Maintenance II) (**Figure 3.4 A-C**). Treatment with *pkc-3* RNAi, on the other hand, did not result in a significantly different change in time of NMY-2

foci disassembly, suggesting that neither PKC-3 as a protein nor its kinase activity are involved in this process. Furthermore, these results indicate that CDC-42 signalling regulates the time of disassembly of the actomyosin network. The fact that the phenotype is also visible in *pkc-3(ts)* embryos suggests that PKC-3 being locked in the CDC-42/PAR-6/PKC-3 complex prevents CDC-42 from regulating the time of actomyosin foci disassembly.

cdc-42 RNAi has been previously shown to be required to restrict NMY-2::GFP to the anterior after the actomyosin foci disassemble (Motegi and Sugimoto, 2006, Small and Dawes, 2017), but its effect in regulating the time of disassembly has not been reported before. However these studies used over-expressed NMY-2::GFP for analysis, which we have shown has different disassembly times than the wild type NMY-2 (as seen in fixed wild type embryos and fixed embryos expressing NMY-2::GFP) (**Figure 3.4 D**). The difference between these two strains might be the reason this phenotype has previously gone unnoticed.

3.3.3. The results from our RNAi screen point to PKC-3 as a regulator of the RHO/ LET-502 pathway

The PKC-3 homologue aPKC has been reported to phosphorylate the RHO kinase LET-502 in epithelial adherents junctions, inhibiting its activation of Myosin II and thus protecting the epithelial apical domains from excessive constriction (Ishiuchi and Takeichi, 2011). Similarly, Crumbs mediated recruitment of aPKC is required to negatively regulate Rok (the fly homologue of ROCK/LET-502) and prevent the formation of myosin cables in *Drosophila* epithelial cells during tubulogenesis (Roper, 2012). Interestingly, Cdc42 has also been reported to inhibit RhoA by regulating its GTP level (Sander et al., 1999, Møller et al., 2019). And while the mechanisms underlying this regulation have not been described yet, they have been hypothesised to involve competition in binding to the GDP dissociation inhibitors (GDI), required for GDP/GTP exchange (Møller et al., 2019).

In the *C. elegans* zygote the small GTPase RHO has been well characterised as key regulator of actomyosin flow (via its effector kinase LET-502) (Schmutz et al., 2007, Nishikawa et al., 2017), so if this negative interaction between aPKC/CDC-42 and LET-502 were conserved in the first cell division of the *C. elegans* embryos, we would expect *pkc-3(ts)* embryos to show

increased LET-502/actomyosin activity. However in *C. elegans*, anterior PARs have been reported to promote actomyosin flow (Motegi and Sugimoto, 2006, Schonegg and Hyman, 2006), and we have shown that the mutant *pkc-3(ts)* strain and *pkc-3* RNAi result in slower actomyosin flow.

For our RNAi screening we employed the *pkc-3(ts)* mutant and combined it with individual RNAis against different actomyosin regulating pathways, to determine if knockdown of any of the target genes suppressed or enhanced the actomyosin cortical defects observed in *pkc-3(ts)*. Using the *pkc-3(ts)* mutant and combining it with a single RNAi at a time allows for greater knock down levels than using two RNAis at the same time (Fievet et al., 2013).

The screen revealed that PKC-3 is required for full function of the RHO pathway, since even though partially increasing RHO-1 activity by removing *rga-3/4* with 50% strength RNAi could rescue PAR-3 retraction in *pkc-3(ts)* embryos (**Figure 3.5 B**), using 100% RNAi generated a hyper contractile 'bleb' phenotype that was only present in the wild type background but not in the *pkc-3(ts)* background (**Figure 3.6 B**), suggesting that the activity of PKC-3 is required for the RGA/RHO pathway.

Another phenotype we identified that suggests a role for PKC-3 activity in the RHO pathway is the change in polar body size in embryos treated with *csnk-1* RNAi: wild type background embryos presented polar body extrusion defects upon *csnk-1* silencing, while *pkc-3(ts)* background embryos did not (**Figure 3.8 E**).

Polar body extrusion depends on a RHO-1 contractile ring, and CSNK-1 regulates this process by its regulating RGA-3/4 (Flynn and McNally, 2017). Furthermore, CSNK-1 has also been shown to regulate the disassembly of myosin and anilin foci in the *C. elegans* oocyte (Flynn and McNally, 2017). Given the role for CSNK-1 in regulating the RHO/ LET-502 pathway, these results from our screen further support that either PKC-3, CDC-42 or the CDC-42/PAR-6/PKC-3 complex are required for full activity of the RHO/LET-502 pathway (See **Chapter 4** for further discussion).

3.3.4.PKC-3 is not required for phosphoinositide dependant regulation of the actomyosin flow

Although the main role of phosphoinositide (PIP) asymmetries seems to be linked to the localisation of the mitotic spindle (Panbianco et al., 2008, Afshar et al., 2010, Kotak et al., 2014), links to PAR polarity have been suggested in several organisms. Both the PI3-kinase (phosphorylates PIP_2 to PIP_3) and the PTEN phosphatase (dephosphorylates PIP_3 to PIP_2) have been shown to affect localisation of PAR-3 and aPKC in rat neurites (Jiang et al., 2005). And PTEN has also been shown to affect the localisation of CDC-42 in epithelial cells (Martin-Belmonte et al., 2007). The role of PIPs in regulating polarity in *C. elegans* zygote is still not well understood, nevertheless the posterior PAR-1 and PAR-2 are known to associate with phosphoinositides (but only when they are not phosphorylated by PKC-3) (Motegi et al., 2011, Ramanujam et al., 2018). And more recently, PIP_2 has been shown to direct the distribution of actin filaments in *C. elegans* embryos (Scholze et al., 2018).

Two of the proteins silenced in the screen targeted PIP regulation: CSNK-1 and CNT-2. CSNK-1 acts with the PIP_2 synthesis enzyme PPK-1 to increase the levels of PIP_2 in the posterior (Panbianco et al., 2008), and CNT-2 is recruited to the plasma membrane via its interaction with the phosphoinositide 3-kinase, and regulates binding of phosphoinositide 3-kinase to PIP_2 and PIP_3 to prevent cortical actin formation (Venkateswarlu et al., 2007).

In our screen, RNAi against *csnk-1* and *cnt-2* resulted in increases in PAR-3 domain length in both wild type and *pkc-3(ts)* backgrounds (**Figure 3.8** and **3.9**), suggesting that the pathways by which *csnk-1* and *cnt-2* regulate PAR-3 retraction do not require PKC-3 or CDC-42 activity, and therefore suggesting that the kinase activity of PKC-3 is not required for polarisation pathways involving PIP regulation.

3.3.5.Silencing *chin-1* does not rescue PAR-3 asymmetry

The last gene silenced in the RNAi screen was *chin-1*, the CDC-42 GAP. Silencing of *chin-1* favours the CDC-42/PAR-6/PKC-3 complex, allowing it to expand further from the PAR-3 domain than in wild type embryos (Rodriguez et al., 2017).

We could not detect a significant change in PAR-3 asymmetry upon *chin-1* silencing in wild type or *pkc-3(ts)* embryos (**Figure 3.10 B-C**), suggesting that favouring GTP bound CDC-42 or the CDC-42/PAR-6/PKC-3 complex does not significantly increase flows and hence rescue PAR-3 retraction. This, however, does not rule out a role for CDC-42 in regulating actomyosin flow, as the localisation of the CDC-42/PAR-6/PKC-3 in *pkc-3(ts)* embryos treated with *chin-1* is still affected, and therefore increasing CDC-42 activity might not be sufficient to gain wild-type function of CDC-42.

CHAPTER 4. CROSS-REGULATION BETWEEN PKC-3, CDC-42 AND THE RHO/LET-502 PATHWAY

4.1. Introduction

The small GTPase RhoA, and its *C. elegans* homologue RHO-1, are well known regulators of Myosin II activation and F-actin assembly (Jaffe and Hall, 2005). As other small GTPases, RhoA cycles between an active GTP-bound form and an inactive GDP-bound form thanks to its GEFs (Guanine Nucleotide Exchange Factors) and GAPs (GTPase-Activating Proteins) (Jaffe and Hall, 2005). GTP bound RhoA can activate its downstream effectors, one of which is the Rho-associated coiled-coil containing kinase (Rock) (Jaffe and Hall, 2005). Active Rock can then phosphorylate the myosin regulatory light chain subunit (RLC, known as MLC-4 in *C. elegans*), leading to contractility of the actomyosin network (Amano et al., 1996).

Before fertilisation, RHO-1 localises all around the membrane in *C. elegans* oocytes, as seen with YFP-RHO-1 (Schonegg et al., 2007). When the sperm centrosome contacts the posterior cortex, it inhibits the activity of RHO-1 GTPase by displacing ECT-2 (its GEF) to the anterior side of the zygote (Motegi and Sugimoto, 2006, Schonegg et al., 2007). This is proposed to lead to an increased amount of active GTP-bound-RHO in the anterior side of the cell, and an increased amount of inactive GDP-bound-RHO and decreased cortical tension in the posterior (Jenkins et al., 2006, Motegi and Sugimoto, 2006, Schonegg et al., 2007).

The imbalance in the cortical tension due to reduced contractility in the posterior causes the actomyosin cortex to flow towards the anterior, as if it were an elastic band in which one end had been cut off, causing the entire band to retract (Jenkins et al., 2006, Motegi and Sugimoto, 2006, Mayer et al., 2010, Gubieda et al., 2020). As the cortex retracts from the posterior, RHO-1 controls actomyosin contractility and flow (Nishikawa et al., 2017, Michaux et al., 2018).

As discussed in **Chapter 3**, the PKC-3 homologue aPKC has been reported to phosphorylate ROCK in epithelial adherents junctions, inhibiting its activation of Myosin II and thus protecting the epithelial apical domains from excessive constriction (Ishiuchi and Takeichi, 2011), similarly, PAR proteins have been reported to be inhibitors of actomyosin contractility in *Drosophila* amnioserosa cells (David et al., 2010, David et al., 2013, Durney et al., 2018). Interestingly, Cdc42 has also been reported to inhibit RhoA by regulating its GTP level (Sander et al., 1999, Møller et al., 2019). The mechanisms underlying this regulation have not been described yet, but might involve competition in binding to the GDP dissociation inhibitors (GDI), required for the GDP/GTP exchange (Møller et al., 2019).

Our results suggest that the interaction between anterior PARs and RHO/LET-502 in *C. elegans* might be different, with the CDC-42/PAR-6/PKC-3 complex activating this pathway (See **Section 1.4** of the Introduction for detailed descriptions of how PKC-3 and CDC-42 can regulate each other).

4.1.1.Objectives

The aims of this chapter were the following:

- To investigate if *pkc-3(ts)* regulates the RHO/LET-502 pathway, as suggested by data from the previous chapter.
- To determine if PKC-3 regulates the RHO/LET-502 pathway via CDC-42, or via a different pathway.

4.2. Results

4.2.1.Validating an antibody against LET-502

To analyse the role of PKC-3/CDC-42 in regulating the RHO pathway and actomyosin flow, we validated an antibody against LET-502, the RHO effector that regulates actomyosin flow and retraction during polarity establishment in the *C. elegans* zygote (Jaffe and Hall, 2005).

To validate the antibody we stained both wild type embryos and embryos treated with *let-502* RNAi (**Figure 4.1 A-B**). The only stage in which we could identify any structures was in meiosis (staged with DAPI) before polarity establishment (as seen with PAR-3 staining). 69%

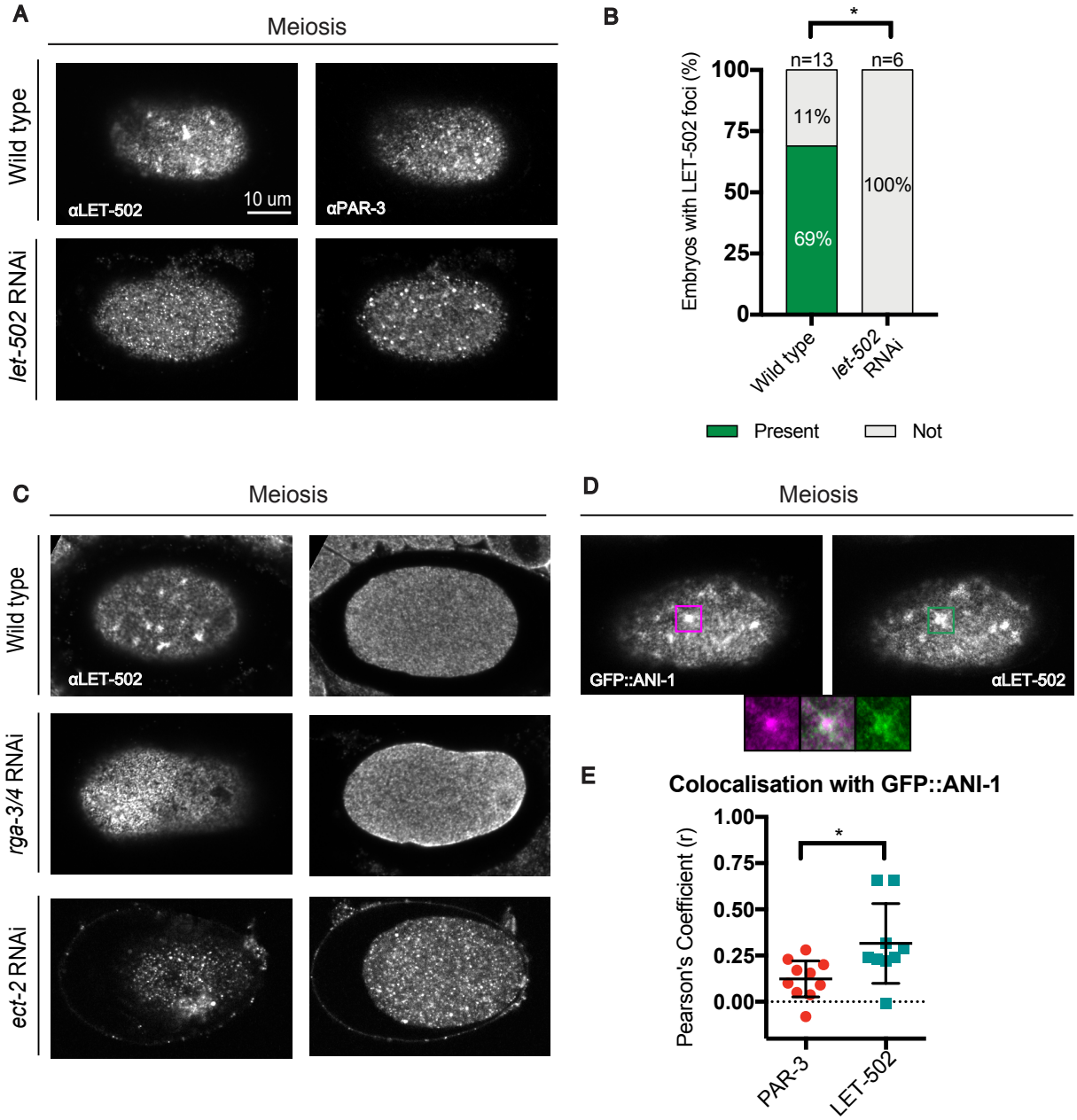

Figure 4.1. Validation of the antibody against LET-502. **A.** Cortical images of wild type embryos and embryos treated with *let-502* RNAi during meiosis, stained with LET-502 (Ahringer laboratory, #904) and PAR-3 (DSHB, #P4A1) antibodies. The RHO effector kinase LET-502 is present in foci structures during meiosis in the cortex of wild type embryos, before polarity is established and PAR-3 starts to retract. **B**. These foci are present in 69% of imaged embryos in the wild type strain. No embryos treated with *let-502* RNAi showed these foci (P=0.0108, Fisher's exact test). **C**. Increasing RHO activity with *rga-3/4* RNAi results in LET-502 localising homogeneusly all over the cortex (as visible in midplane images), whereas decreasing RHO activity with *ect-2* RNAi results in lack of LET-502 foci on the cortex. **D**. Cortical images of GFP::ANI-1 (active RHO reporter), stained for LET-502. LET-502 foci colocalise with GFP::ANI-1 foci. **E**. Pearson's Coefficient for LET-502 and PAR-3 colocalisation with GFP::ANI-1. The difference is statistically significant (P=0.0429, n=9, Mann-Whitney's test).

of wild type embryos showed foci that resembled NMY-2 at this stage, while none of the *let-502* RNAi embryos analysed had LET-502 foci (P=0.0108, Fisher's exact test).

To further confirm that the foci cortical structures detected were LET-502, we silenced *rga-3/4* (the RHO GAP) and *ect-2* (the RHO GEF) with RNAi (**Figure 4.1 C**). As described in the previous chapter, *rga-3/4* RNAi generates increased levels of RHO-GTP (Schmutz et al., 2007, Schonegg et al., 2007), which change the organisation of the actomyosin cortex, resulting in NMY-2 localising all over the cortex. *ect-2* RNAi, on the other hand, would result in lower levels of RHO-GTP (Motegi and Sugimoto, 2006). *rga-3/4* RNAi resulted in LET-502 becoming disorganised and localising all over the cortex, as observed for NMY-2 in the previous chapter, and *ect-2* RNAi, on the other hand, resulted in no embryos with LET-502 foci, as would be expected.

Even though LET-502 stainings in the *C. elegans* embryo have not been published, different groups have analysed the organisation of active RHO with an anillin reporter (GFP::ANI-1): anillin is a downstream effector of RHO, and this anillin reporter has been shown to bind GTP-bound RHO, and therefore can be used to determine the localisation of active RHO. These studies report that active RHO forms foci in the cortex for ~5 seconds, in which NMY-2 starts to accumulate in the foci too. The RHO foci then disappear, and the NMY-2 foci stay in the cortex for a total of ~30 seconds (Nishikawa et al., 2017, Michaux et al., 2018). To confirm that the observed LET-502 foci are consistent with the previous reports of active RHO, we stained for LET-502 in embryos expressing GFP::ANI-1 (**Figure 4.1 D-E**). The LET-502 foci we observed colocalised with GFP::ANI-1, indicating that the LET-502 foci we observe are generated from the active RHO foci other groups have reported (Nishikawa et al., 2017, Michaux et al., 2018). The colocalisation was statistically significant, when compared to colocalisation of GFP::ANI-1 with PAR-3 (P=0.0429, n=9, Mann-Whitney's test) (**Figure 4.1 E**).

4.2.2.PKC-3 activity, but not CDC-42, affects LET-502 immunolocalisation

Having confirmed that PKC-3 affects actomyosin flow and suspecting it might be a regulator of the RHO pathway (see previous chapter), we looked at the organisation of the RHO kinase

LET-502 in wild type embryos, embryos of the *pkc-3(ts)* strain, and in embryos treated with *pkc-3* and *cdc-42* RNAi, to determine if PKC-3 or CDC-42 were affecting this pathway **(Figure 4.2)**.

Staining for LET-502 in wild type embryos resulted in cortical foci structures during meiosis (staged with DAPI) and before polarity establishment (as seen with PAR-3 staining) in 62% of wild type embryos **(Figure 4.2 B)**. In embryos of the *pkc-3(ts)* strain the punctae where

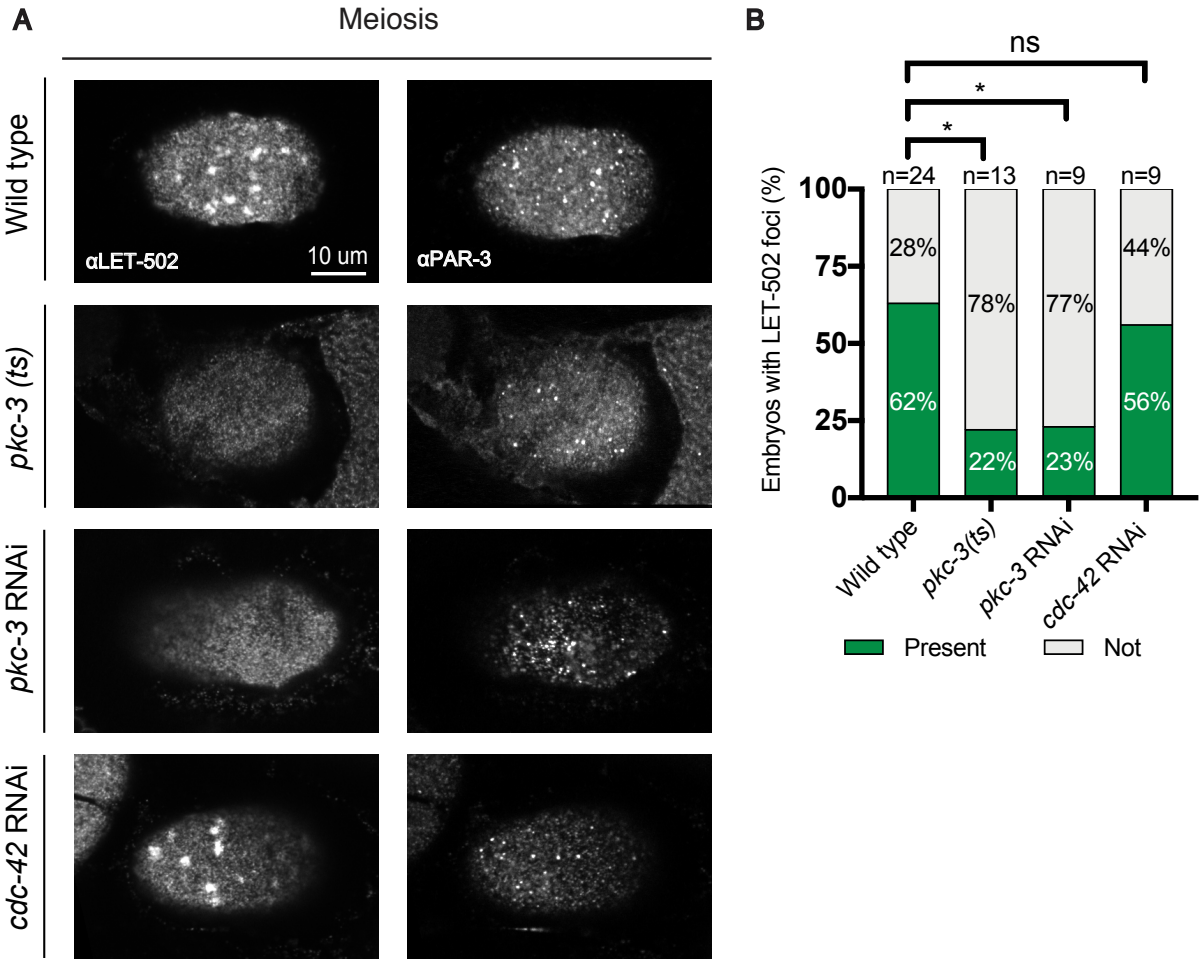

Figure 4.2. PKC-3 and CDC-42 are required for LET-502 foci. A. Cortical images of LET-502 (Ahringer laboratories, #904) and PAR-3 (DSHB, #P4A1) staining during meiosis in embryos of different backgrounds. The RHO effector LET-502 is present in foci during meiosis in the cortex of wild type embryos, before polarity is established and PAR-3 starts to retract. **B**. These foci are present in 62% of imaged embryos in the wild type strain, but only in 22% of embryos of the *pkc-3(ts)* background (P=0.038) and 23% of embryos treated with *pkc-3* RNAi (P=0.05). 56% of embryos treated with *cdc-42* RNAi show LET-502 punctae, a number not significantly different to the wild type percentage (P>0.99), all embryos are from the same experiment (Statistical significance calculated with Fisher's exact tests) .

present in meiosis too, but only in 22% of embryos. This difference is significant (P=0.038, Fisher's exact test). In *pkc-3* RNAi, this difference was also visible, with 23% of embryos showing LET-502 foci (P=0.05), whereas in *cdc-42* RNAi the rate of LET-502 punctae was 56%, similar to that of wild type embryos (P>0.999). These results suggest that PKC-3 might regulate actomyosin flow via the RHO/LET-502 pathway.

Even though LET-502 stainings in the *C. elegans* embryo have not been published, active RHO has been reported to be present in foci from meiosis until maintenance (Nishikawa et al., 2017, Michaux et al., 2018). Our stainings (**Figure 4.1**), on the other hand, only show LET-502 and active RHO during meiosis, probably due to the foci during establishment having a different organisation (and being more susceptible to fixation) than the foci during meiosis.

We hypothesised that the difference observed in *pkc-3(ts)* and *pkc-3* RNAi could be due to changes in LET-502 organisation, with LET-502 foci in *pkc-3(ts)* and *pkc-3* RNAi being less stable or resistant to fixation than those in wild type embryos, as might be occurring with the establishment foci. Alternatively, PKC-3 activity could be required to recruit LET-502 to foci, in a more directed manner. However, we did not analyse LET-502 expression levels in embryos treated with *pkc-3* RNAi, and therefore cannot rule out effects in LET-502 or RHO expression levels as the reason for the decrease in LET-502 cortical structures.

4.2.3.PKC-3, but not CDC-42, regulates active RHO

To bypass the limitations of the LET-502 antibody (the fact that it only shows cortical foci during meiosis, suggesting issues with fixation of later cortical structures), and increase our understanding of PKC-3's regulation of the RHO/LET-502 pathway, we analysed the Rhobiosensor (anillin reporter, GFP::ANI-1), which indicates the presence of active, GTP bound, RHO (**Figure 4.3**). We analysed this strain under wild type conditions, as well as with *cdc-42* and *pkc-3* RNAi treatments, but were unable to analyse it crossed with the *pkc-3(ts)* strain, as keeping the strain at 15 °C (as required for temperature sensitive strains) resulted in the quick loss of the fluorescent signal.

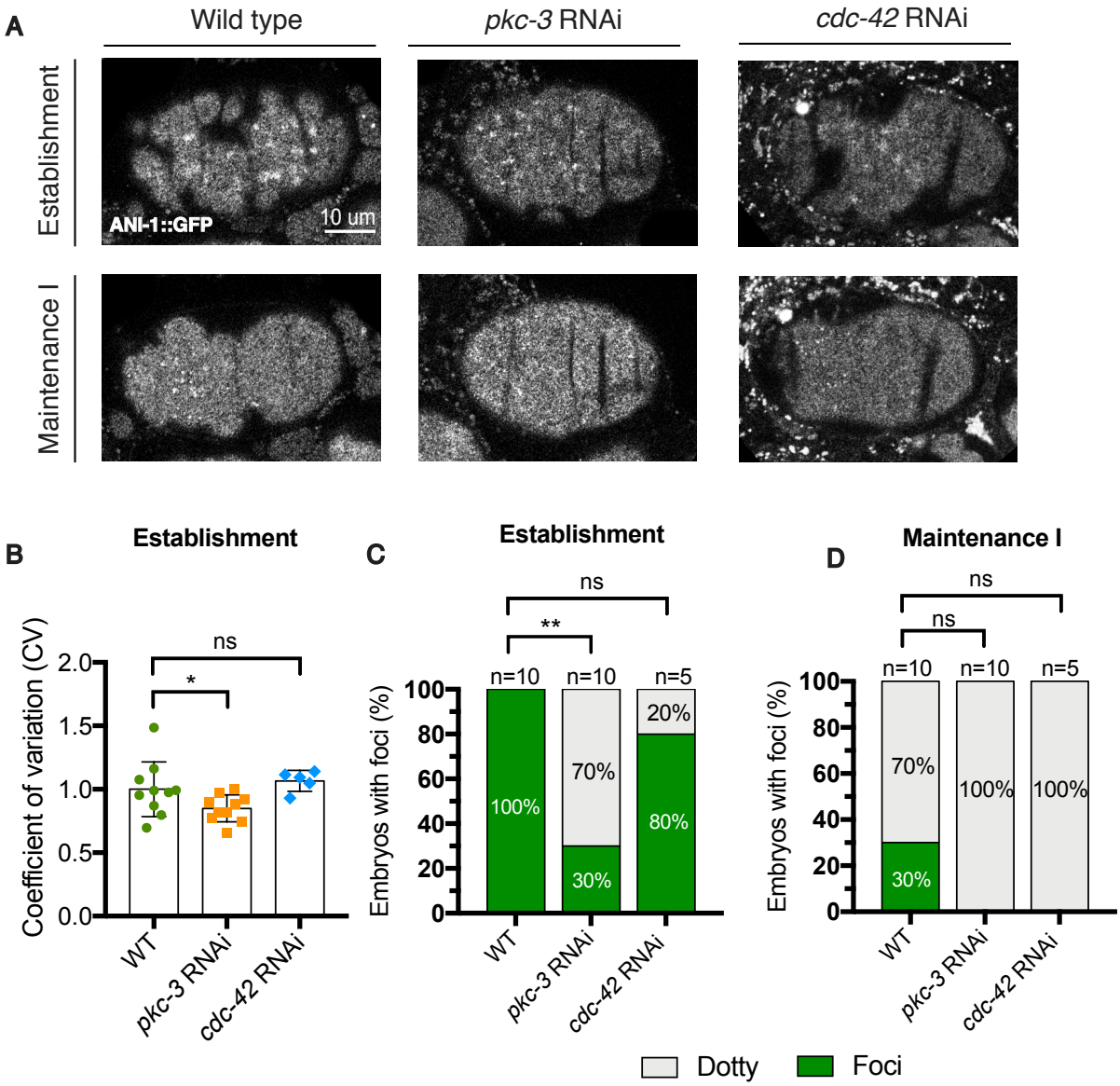

Figure 4.3. Anylisis of the RHO-biosensor ANI-1::GFP and its dependence on *pkc-3* and *cdc-42*. **A.** The Rhobiosensor ANI-1::GFP organises in foci during establishment, and in dotty structures during early maintenance. In embryos treated with *pkc-3* RNAi, the dotty structures are present during establishment too, whereas embryos treated with *cdc-42* RNAi resemble those in wild type conditions. **B**. The coefficient of variation (CV) for the Rhobiosensor during establishment. In wild type embryos the average CV value is 1.00 (n=10), with *pkc-3* RNAi resulting in a significantly lower average value (CV=0.84, P=0.05, n=10, Kruskal-Wallis) and *cdc-42* not being significantly different (CV=1.06, P=0.224, n=5, Kruskal-Wallis). **C**. During establishment, ANI-1::GFP organises in foci in all wild type embryos, whereas only 30% of embryos treated with *pkc-3* RNAi organise in the same foci, with the remaining 70% embryos showing dotty structures. This difference is highly significant (P=0.0031, Fisher's exact test). Under *cdc-42* RNAi treatment 80% of embryos showed foci structure, a number not significantly different to wild type embryos (P=0.333). **D**. During the early stages of maintenance, ANI-1::GFP organises in dotty structures in 70% of embryos in wild type conditions. In embryos treated with *pkc-3* and *cdc-42* RNAi, ANI-1::GFP organises into dotty structures in all embryos of this stage. This difference is not significant (P=0.211 and P=0.505 with a Fisher's exact test, respectively).

As previously reported by other groups (Nishikawa et al., 2017, Michaux et al., 2018), we observed active Rho foci from meiosis until polarity maintenance. With the foci moving to the anterior and becoming more 'dotty' as the zygote enters the Maintenance I stage (**Figure 4.3 A**). In embryos treated with *pkc-3* RNAi, the structure seemed more disorganised, with smaller and more 'dotty' foci, from establishment phase and not only in maintenance phase. To analyse the disorganisation caused by *pkc-3* RNAi we calculated the CV value of each embryo during early establishment and Maintenance I stages, and to determine if the structure change from foci to dotty structures we manually sorted embryos in to 'dotty' vs 'foci' categories (**Figure 4.3 B-D)**.

The average CV value under wild type conditions during establishment stage was 1.00 (**Figure 4.3 B**), significantly higher than in embryos treated with *pkc-3* RNAi (CV=0.84, P=0.05, Kruskal-Wallis), but not significantly different from embryos treated with *cdc-42* RNAi (CV=1.06, P=0.224), further suggesting that PKC-3 plays a role in regulating the RHO pathway independently of its role in the CDC-42 anterior complex.

As for the foci/dotty structure, all embryos under wild type conditions showed ANI-1::GFP organised into foci structures during polarity establishment (n=10), whereas only 30% of embryos treated with *pkc-3* RNAi organised in foci, with the remaining 70% embryos showing dotty structures (**Figure 4.3 C-D)**. This difference was highly significant (P=0.0031, n=10, Fisher's exact test). Under *cdc-42* RNAi treatment, on the other hand, 80% of embryos showed foci structures, a number not significantly different to wild type embryos (P=0.333, n=5).

During the early stages of maintenance, ANI-1::GFP organised in dotty structures in 70% of embryos in wild type conditions (n=10). Whereas in embryos treated with *pkc-3* and *cdc-42* RNAi, ANI-1::GFP organised into dotty structures in all embryos of this stage (n=10 and n=5, respectively), not significantly different to embryos under wild type conditions (P=0.211 and P=0.505 with a Fisher's exact test, respectively). It should be noted, however, that we did not analyse the expression levels of ANI-1::GFP under *pkc-3* and *cdc-42* RNAi, and therefore we cannot rule out that the changes oversed in *pkc-3* are not caused by a change in ANI-1::GFP expression.

4.3. Discussion

4.3.1.PKC-3, but not CDC-42, regulates the RHO/LET-502 pathway

The RHO/ROCK pathway (RHO/LET-502 in *C. elegans*) is a well known regulator of actomyosin flow and contractility (Jaffe and Hall, 2005). When the *C. elegans* zygote is fertilised, ECT-2 is cleared from the posterior cortex and active GTP-bound RHO becomes enriched in the anterior, where its downstream effector LET-502 phosphorylates the myosin light chain MLC-4, leading to contractility of actomyosin and flow towards the anterior (Amano et al., 1996, Motegi and Sugimoto, 2006, Schonegg et al., 2007, Nishikawa et al., 2017, Wang et al., 2017).

The only interactions previously described between aPKC and the RHO/ROCK pathway have been negative. aPKC, for example, has been reported to phosphorylate and inhibit ROCK in epithelial cell cultures, leading to decreased apical constriction (Ishiuchi and Takeichi, 2011). Similarly, in *Drosophila* epithelia, Crumb mediated recruitment of aPKC is required to negatively regulate Rok and generate myosin cables during tubulogenesis (Roper, 2012). And aPKC has also been reported to recruit Smurf1 to cellular protrusions to degrade RhoA and prevent RhoA signalling (Wang et al., 2003).

Furthermore, other PAR proteins (which are essential for correct aPKC localisation and activity) have also been shown to negatively regulate the RHO/ROCK pathway. Cdc42, for example, has been reported to inhibit RhoA by regulating its GTP level in migrating cells (Sander et al., 1999, Møller et al., 2019). And Par6 has also been reported to recruit Smurf1 to trigger RhoA degradation in epithelial tight junctions (Ozdamar et al., 2005).

Our results, however, suggest that in the *C. elegans* zygote PKC-3 is required to activate the RHO/LET-502 pathway (or required for its correct organisation), instead of playing a role in inhibiting it.

To confirm the role of PKC-3 in regulating the RHO/LET-502 pathway we looked at LET-502 staining (with an antibody) and active RHO (with the biosensor ANI-1::GFP). Both sets of experiments confirmed that PKC-3 is required for the correct organisation/activity of the RHO/LET-502 pathway: the antibody we used to look at LET-502 showed cortical foci during

meiosis (the only stage at which we could fix LET-502 foci) (**Figure 4.1**), and these foci were PKC-3 dependent, but CDC-42 independent (**Figure 4.2 B**), indicating that PKC-3 plays a role in the organisation of the RHO/LET-502 pathway independently of its interaction with the CDC-42.

Similarly, active RHO was disorganised and generated dotty structures, instead of foci, upon *pkc-3* depletion but not upon *cdc-42* depletion (**Figure 4.3 C-D**), further indicating that PKC-3 (and not CDC-42) is required for the correct organisation of RHO/LET-502. These results suggest that the lower actomyosin flow velocity and PAR-3 retraction we detected in *pkc-3(ts)* embryos and *pkc-3* RNAi embryos could result (at least partially) from the change in RHO regulation that arises from lack of active PKC-3.

4.3.2.Potential targets for PKC-3 up-regulation of the RHO/LET-502 pathway

It is still unclear which PKC-3 target could be causing the RHO/LET-502 defects we observe in *pkc-3(ts)* embryos and *pkc-3* RNAi embryos. Regulation of small GTPases is complex, with several GAPs and GEFs regulating their activity, and many more proteins regulating the interaction between the small GTPase and its GAPs/GEFs (Marjoram et al., 2014, Choi et al., 2020).

Some kinases are known to directly phosphorylate RhoA and change its activity (Choi et al., 2020). For example EGF dependent phosphorylation of RhoA by ERK has been shown to up regulate RhoA (Tong et al., 2016); and phosphorylation of RhoA in its S188 by protein kinase A (PKA) has been shown to decrease its GTPase activity (Lang et al., 1996). Interestingly, aPKC has a similar target sequence to PKA, and the S188 is conserved in *C. elegans*, making this a potential target for PKC-3 phosphorylation in the *C. elegans* zygote.

Other set of proteins known to regulate Rho are cell adhesion receptors, such as integrins and cadherins (Marjoram et al., 2014). The tyrosine kinase Src for example, has been reported to phosphorylate a RhoA GAP and decrease RhoA activity in an integrin dependent pathway (Arthur et al., 2000).

Even though the *C. elegans* zygote is by definition a single-cell organism with no cell-cell adhesion, clusters of HMR-1, the only *C. elegans* integrin, have been described in the zygote

and shown to regulate NMY-2 retraction (Padmanabhan et al., 2017), making this another possible pathway to study.

CHAPTER 5. PKC-3 PHOSPHORYLATES CDC-42, AFFECTING THE ESTABLISHMENT OF THE ANTERIOR PAR DOMAIN

5.1. Introduction

In the *C. elegans* zygote, PKC-3 localises in two anterior complexes: a PAR-3 bound complex that polarises to the anterior during polarity establishment as a response to actomyosin flow; and a CDC-42 bound complex that can diffuse laterally in the membrane (5-10 um away from the PAR-3 complex) and in which PKC-3 can phosphorylate downstream targets (Dickinson et al., 2017, Rodriguez et al., 2017, Wang et al., 2017).

CDC-42 is a small GTPase of the RHO-family. CDC-42 binds to its effectors via their CDC42/Rac-Interactive-Binding motif (CRIB), but post-translational modifications of CDC-42 can affect the binding to these effectors (Schwarz et al., 2012). Interaction of CDC-42 with its downstream effectors also results in changes in its conformation (Phillips et al., 2008), and changes in conformation can be essential for interaction with other proteins. The anterior PAR-6, for example, contains a semi-CRIB domain and a PDZ domain, which allows it to bind both to CDC-42 and to PKC-3 (Joberty et al., 2000). Binding of CDC-42 to PAR-6's CRIB domain alters the binding affinity of its PDZ domain, which is adjacent to the CRIB domain, and is necessary for its interaction with other effectors, such as Crumbs in epithelia (Whitney et al., 2016a, Whitney et al., 2016b).

Unlike classic and novel PKC, the atypical PKC (aPKC) is not activated by calcium or diacylglycerol (Steinberg, 2008). Instead, aPKC is regulated by its interaction with other proteins, and members of the PKC family (including aPKC) are considered to be self-inhibited in the absence of interactions with other proteins, since the kinase domain of the protein can bind it pseudo-substrate region (Zhang et al., 2014). In *C. elegans*, for example, interaction with CDC-42 via PAR-6 is essential to regulate PKC-3 activity (Joberty et al., 2000, Aceto et al., 2006, Li et al., 2010b); and also to regulate its cellular location (Rodriguez et al., 2017).

When active, PKC-3 and its orthologue aPKC can phosphorylate polarity effectors (such as LGL-1, Miranda and Numb), affecting their localisation (Bailey and Prehoda, 2015). Phosphorylation by aPKC can influence the electrostatics of the phosphorylated region and decrease its affinity with the membrane, leading to the displacement of membrane-bound proteins (Bailey and Prehoda, 2015). In the *C. elegans* zygote, for example, PKC-3 can phosphorylate PAR-2, affecting its electrostatic interaction with the membrane and excluding it from the anterior cortex (Hao et al., 2006, Goehring et al., 2011a).

In *C. elegans* inhibition of PKC-3 decouples PKC-3 from PAR-3 and favours the CDC-42/ PAR-6/PKC-3 complex, as can be seen in *pkc-3(ts)* embryos and in embryos treated with the aPKC inhibitor CRT90. (Rodriguez et al., 2017). This decoupling is also observed in *Drosophila* neuroblasts, with PAR-6 and aPKC distributing over the entire cortex upon aPKC inhibition (Hannaford et al., 2019). We refer to the symmetric localisation of CDC-42 (all over the membrane) as lack of CDC-42 membrane turnover.

What mechanisms could affect the rate of exchange CDC-42 in the membrane? Interestingly, binding to GTP and GDP can affect the rate at which CDC-42 gets extracted from the membrane, as in budding yeast the constitutively active Cdc42(Q61L) has significantly less mobility (membrane exchange) than the wild type Cdc42 (Woods et al., 2016). Therefore inactive GDP-bound Cdc42 can be mobilised (and extracted from the membrane) at a higher rate than active Cdc42, contributing to Cdc42 polarisation (Woods et al., 2016, Moran and Lew, 2020).

Furthermore, the aforementioned research from our labs points to a key role for aPKC activity in regulating membrane turnover (Rodriguez et al., 2017).

5.1.1.Objectives

The objectives of the work presented in this chapter were the following:

- To describe how the membrane turnover of CDC-42 depends on PKC-3.
- To determine if PKC-3 could be phosphorylating CDC-42.
- To describe how CDC-42/PKC-3 turnover affects the organisation of the anterior PAR complexes.

5.2. Results

5.2.1.The conserved S71 of CDC-42 might be a substrate for PKC-3

Given that the anterior CDC-42 complex is favoured in *pkc-3(ts)* embryos and locates all over the membrane (Rodriguez et al., 2017), we considered that the kinase activity of PKC-3 might directly affect the CDC-42 complex by regulating either its stability at the membrane or the rate of recruitment to the membrane.

PKC-3 is known to phosphorylate its substrates in positively charged BH domains, affecting the interactions of the substrates with the negatively charged phospholipid membrane (Visco et al., 2016), and thus providing a mechanisms by which PKC-3's kinase activity could detach the CDC-42 complex from the membrane.

Even though CDC-42 does not contain a classic negatively charged BH domain (Bailey and Prehoda, 2015), it does contain one highly conserved serine (S71) that is identified by the group-based prediction tool (GPS 5.0) software as predicted phosphorylation site for aPKC **(Figure 5.1 A)** (Wang et al., 2020). CDC-42 S71 has previously been reported as a substrate for the kinase AKT (Kwon et al., 2000, Schoentaube et al., 2009, Schwarz et al., 2012). AKT and PKC-3 have very similar substrate motifs (Gnad et al., 2007) and very similar kinase domains (50% identity and 69% similarity) **(Figure 5.1 B-C)**, and so we considered the S71 as a potential target site for PKC-3.

Furthermore, AKT phosphorylation of this site in RAC1 has been shown to inhibit the GTP binding ability of RAC1 in human cell cultures without affecting the GTPase activity of RAC1 (Kwon et al., 2000, Schoentaube et al., 2009, Schwarz et al., 2012), and phosphomimetic mutations of the S71 in both RAC1 and CDC42 have been shown to modulate the binding to specific downstream effectors (Schwarz et al., 2012), thus making this phosphorylation event one of huge biological significance.

Some preliminary results from our research group also showed that the PKC-3 homologue aPKC can phosphorylate CDC-42 *in vitro* (**Figure 5.1 D**), giving further support to the idea

that the S71 of CDC-42 could be a substrate for PKC-3. It would be interesting to replicate this assay with PKC-3 from *C. elegans*, instead of the human orthologue.

5.2.2. An antibody against pS71-CDC-42 shows that CDC-42 phosphorylation is dependent on PKC-3

There is one commercially available antibody against pS71 CDC-42, which is reported to be specific for S71 phosphorylations in CDC-42 and RAC1. CDC-42 and RAC1 have the same

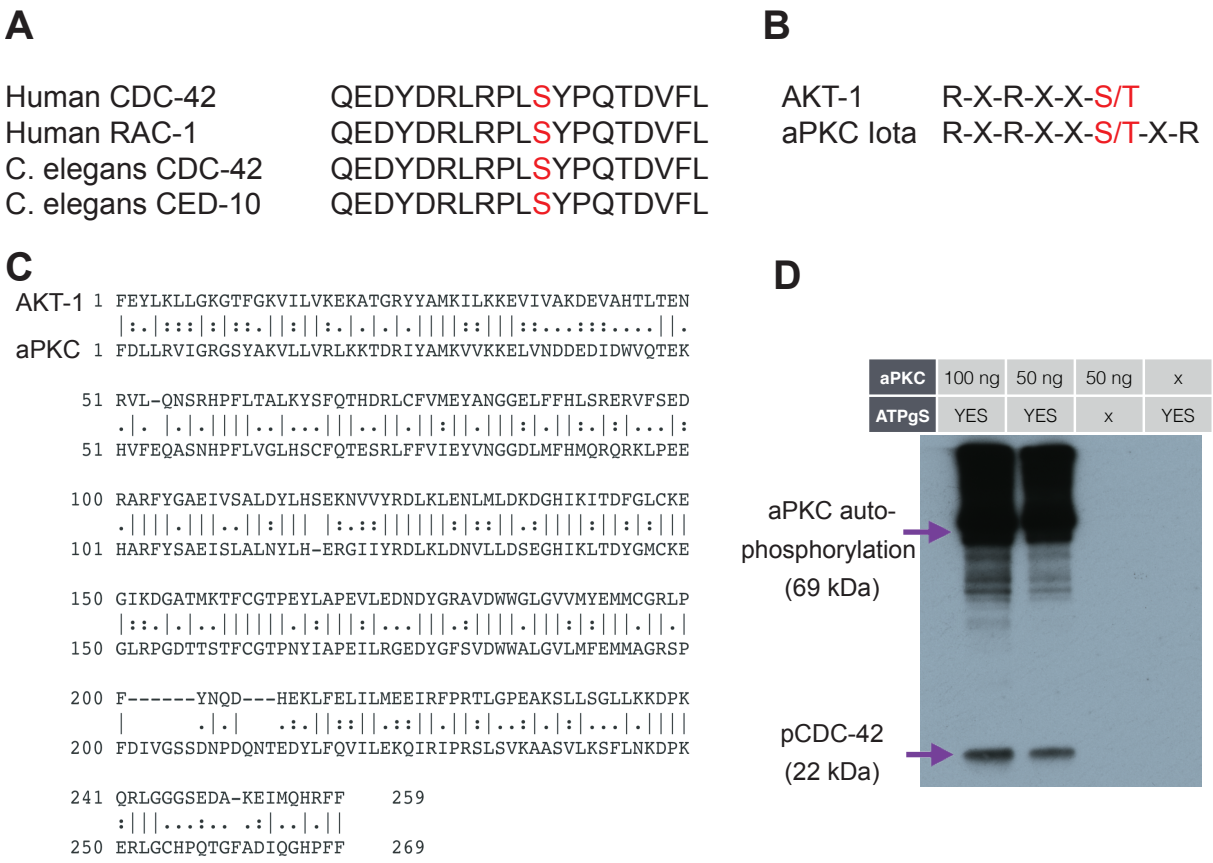

Figure 5.1. The S71 of CDC-42 is a candidate for PKC-3 phosphorylation. A. Phosphorylations site S71 in the small GTPases CDC-42 and RAC-1, and its worm orthologue CED-10. The sequence is well conserved in both human and worm proteins. **B.** The phosphorylation motif for AKT-1, the reported kinase for the S71 phosphorylation site, and the PKC-3 human homologue aPKC iota are highly similar. **C.** The kinase domains of AKT-1 and aPKC iota are very conserved, and have an identity value of 50% and a similarity value of 70%. **D.** Kinase assay with aPKC zeta (Calbiochem, Millipore #14-525). aPKC can phosphorylate CDC-42 (22kDa, Cytoskeleton, #CD01) and itself (69kDa). In negative controls, with no ATPgS or no aPKC, no pCDC-42 is visible.

molecular size and the same conserved domain (see **Figure 5.1 A**). We used this antibody to analyse pS71 CDC-42 phosphorylation in western blots (**Figure 5.2**).

Western blots with this antibody in embryonic protein extracts recognised one band at 27 kDa that has been previously reported to correspond to pRAC1 (Kwon et al., 2000), even though CDC-42 and RAC1 are expected to weight 21 kDa. The intensity of the band, however, did not decrease upon *cdc-42* or *pkc-3* RNAi, and it was not recognised by an antibody against total CDC-42 (**Figure 5.2 A-B**).

The anti pS71 CDC-42 antibody detected another band at 30 kDa (**Figure 5.2 A-B**), which decreased in intensity in *pkc-3* RNAi, we hypothesised that this could be another substrate for PKC-3, or that the high lethality caused by *pkc-3* RNAi could result in decreased levels of some proteins in our extract due to aberrant embryo development or stress (however tubulin staining suggests this is unlikely).

The antibody against CDC-42 only recognised one band in the region associated with CDC-42 (at 21 kDa), which disappeared upon *cdc-42* RNA (**Figure 5.2 A-B**). Likewise, the pS71 CDC-42 phosphoantibody did not recognise 100 ng of recombinant CDC-42::MBP, which was strongly recognised by the antibody against CDC-42 (**Figure 5.2 B**).

We further tested this antibody by blotting high amounts of purified CDC-42::MBP and the non phosphorylated mutant CDC-42(S71A)::MBP previously purified from bacteria (**Figure 5.2 C**). The antibody could recognise amounts between 312 ng and 187 ng of both forms equally, but failed to recognise 72 ng of either of them, indicating that it can recognise non phosphorylated CDC-42 above and equal to 187 ng in western blots, but no smaller amounts. Altogether, these results show that either this phosphoantibody is not specific for the phosphorylation in western blots (perhaps due to CDC-42 being denatured), or that the presence of phosphorylated CDC-42 is too small in embryonic protein extracts to be detected. Further analysis of the specificity of this antibody in native pS71 CDC-42 could be done in native gels, in the future.

Despite the pS71 CDC-42 antibody not seeming specific in western blots, it detected foci structures in the cortex of fixed *C. elegans* zygotes during the polarity establishment stage

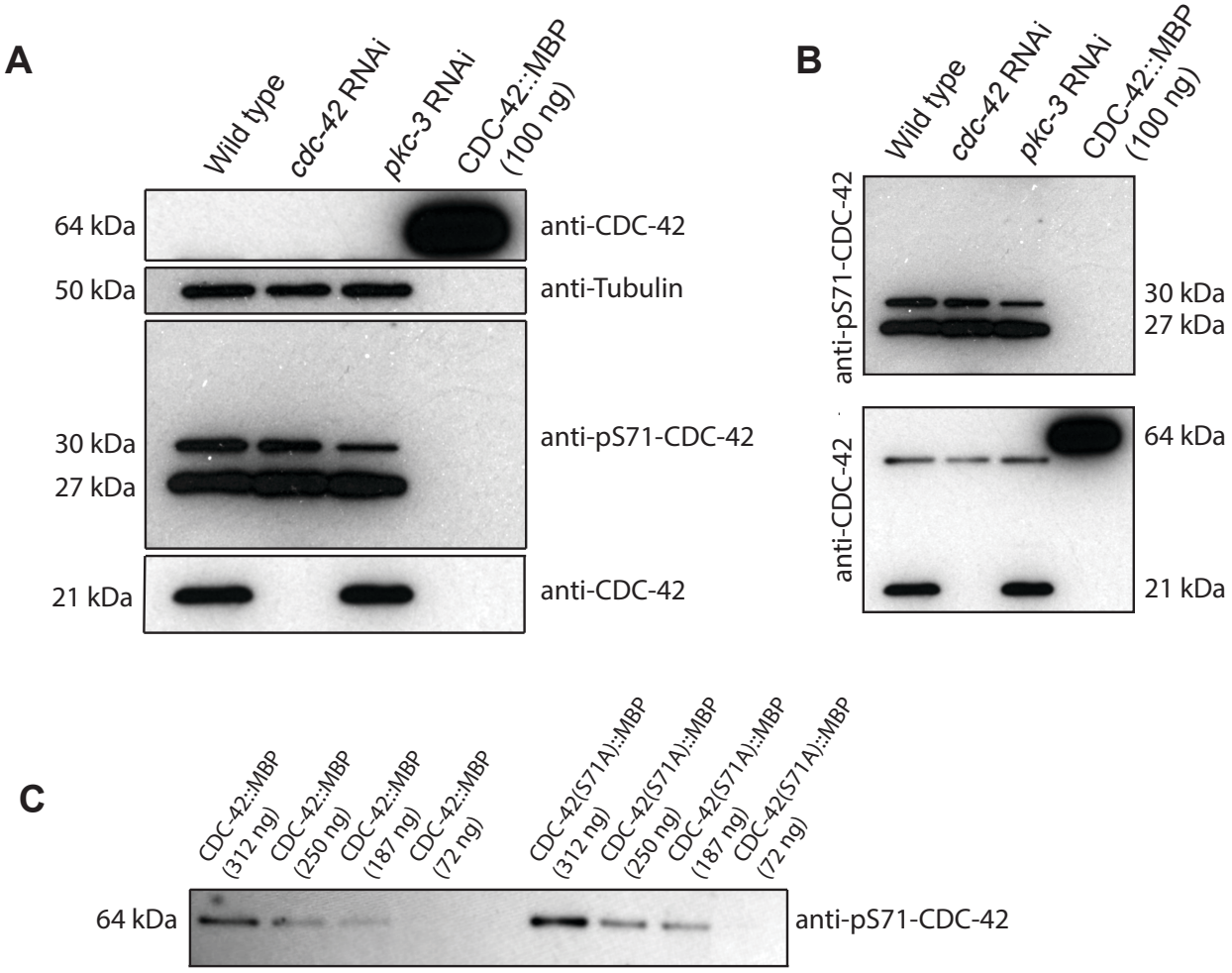

Figure 5.2. Immunoblot analysis of extracts from *pkc-3* and *cdc-42* RNAi-treated *C. elegans* with anti-pS71-CDC-42 . **A**. Western blots of embryonic protein extracts of wild type embryos, embryos treated with *cdc-42* and *pkc-3* RNAi, and purified CDC-42::MBP. The antibody against pS71 CDC-42/RAC-1 (Invitrogen, #44214G) detects one band in all samples at 27 kDa, and one band at 30 kDa that decreases upon RNAi silencing of the PKC-3 kinase, but fails to detect purified CDC-42::MBP. The antibody against CDC-42 (SantaCruz, #B9) detects a CDC-42 band at 21 kDa in the control and *pkc-3* RNAi samples, but not in the *cdc-42* RNAi samples. And it also detects purified CDC-42::MBP at 63 kDa. The tubulin antibody (Sigma, #T9026) is used as loading control, and detects tubulin at 50 kDa. **B**. Full membrane images of the western blots shown in section A of the figure, for the anti CDC-42 and anti pS71 CDC-42 antibody. **C.** Western blot of purified CDC-42::MBP and the non-phosphorylated mutant CDC-42(S71A)::MBP. The antibody against pS71 CDC-42/RAC-1 can detect bands of 312 ng, 250 ng and 187 ng of both forms of the protein equaly, but it does not detect any of the forms at 72 ng.

(90% of embryos, n=25) (**Figures 5.3 A** and **5.4,** note that **Figure 5.3** contains a mixture of data generated for this thesis and data previously generated in our research group) that are reminiscent of NMY-2 cortical foci. The structures disappeared upon *cdc-42* RNAi (21%, n=21), and in the non-phosphomimetic mutant CDC-42(S71A)::GFP in which the endogenous *cdc-42* had been silenced (using RNAi against the *3'utr* end of the *cdc-42* gene) (0%, n=6), indicating that these structures require the phosphorylated form of CDC-42.

Since the pS71 CDC-42 antibody is reported to detect pS71 RAC-1 too, we silenced *ced-10*, the *C. elegans* homologue of *rac-1*. The antibody still recognised the pS71 foci (100%, n=6), indicating that these structures do not correspond to RAC-1, nor require it.

Finally, the pS71 foci were still present after silencing the predicted kinase *akt-1* with RNAi (66%, n=6), but were only present in 8% of embryos of the *pkc-3(ts)* kinase mutant at the polarity establishment stage (n=24), pointing to PKC-3 as the kinase upstream of this phosphorylation (**Figure 5.3 B**). The lack of complete penetrance in *pkc-3(ts)* might be due to residual PKC-3 activity, or could point to another kinase also being able to phosphorylate pS71 CDC-42.

Interestingly, the pS71 foci were stronger in embryos of the WH423 strain (which expresses an overactive CDC-42 (Q61L), in which the GTP-bound CDC-42 is stabilised (Ziman et al., 1991, Aceto et al., 2006)) (**Figure 5.3**). Our group has previously reported that promoting GTP-bound CDC-42 (either with the CDC-42(Q61L) mutation or employing *chin-1* RNAi to silence the CDC-42 GAP) favours the CDC-42/PAR-6/PKC-3 complex, in which PKC-3 is active (Rodriguez et al., 2017). The increased pS71 CDC-42 foci in CDC-42(Q61L) further support the idea that the structures recognised do in fact correspond to PKC-3 phosphorylation of CDC-42. Furthermore, most embryos in which the CDC-42 GEF (*cgef-1*) had been silenced did not have pS71 CDC-42 foci, indicating that the phosphorylation depends on CDC-42 activity (foci present in 45% of embryos, n=11).

As above mentioned, pS71 CDC-42 foci are mostly present during polarity establishment stage (**Figure 5.4 A-B**), with 86% of embryos during this stage showing pS71 CDC-42 foci (n=37), although weak foci and punctae structures are also visible in meiosis (in 68% of

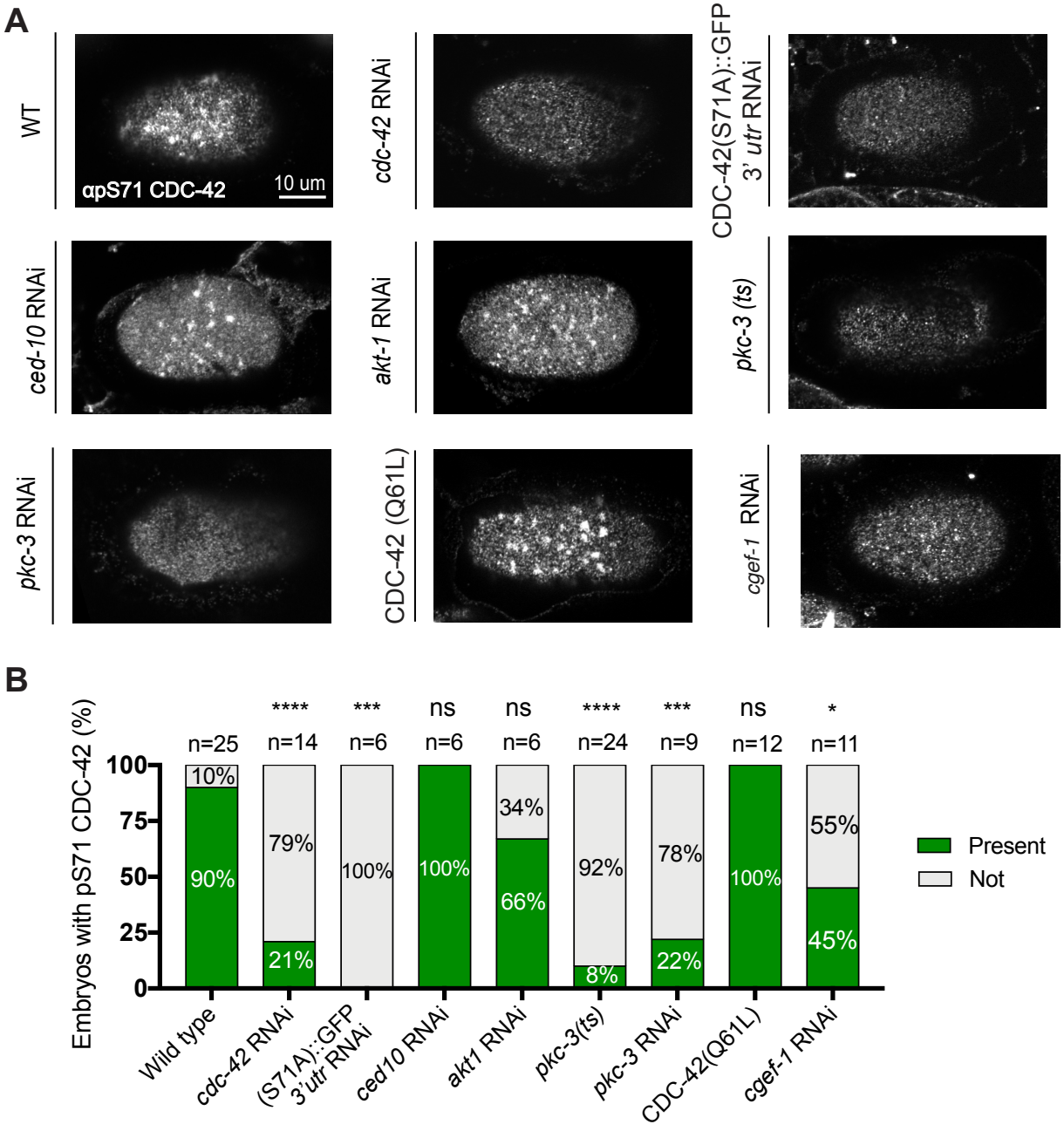

Figure 5.3. Validation of the pS71 CDC-42 antibody in fixed embryos. A. Cortical images of the pS71 CDC-42/RAC-1 antibody (Invitrogen, #44214G). **B**. The antibody detects foci structures in the cortex of wild type embryos during establishment phase that are gone upon silencing of *cdc-42* with RNAi (P<0.0001), and in the non phosphorylated mutant CDC-42(S71A)::GFP in which the endogenous *cdc-42* has been silenced (P=0.0001). The foci are still present upon silencing of the *rac-1* orthologue *ced-10* (P>0.9999), and silencing of the reported kinase *akt-1* (P=0.3406), indicating that the phosphorylation detected is specific for CDC-42 and that is not dependent on the kinase AKT-1. The phosphorylation is gone in the *pkc-3(ts)* mutant (P<0.0001) and in *pkc-3* RNAi embryos (P=0.0007), indicating that PKC-3 might be phosphorylating this site. Finally, the foci are strong and present in 100% of the embryos on the hyperactive CDC-42(Q61L) strain (P=0.5367), in which CDC-42 is constitutively bound to GTP. While the phosphorylation decreases in embryos treated with RNAi against the CDC-42 activator *cgef-1* (P=0.0124).

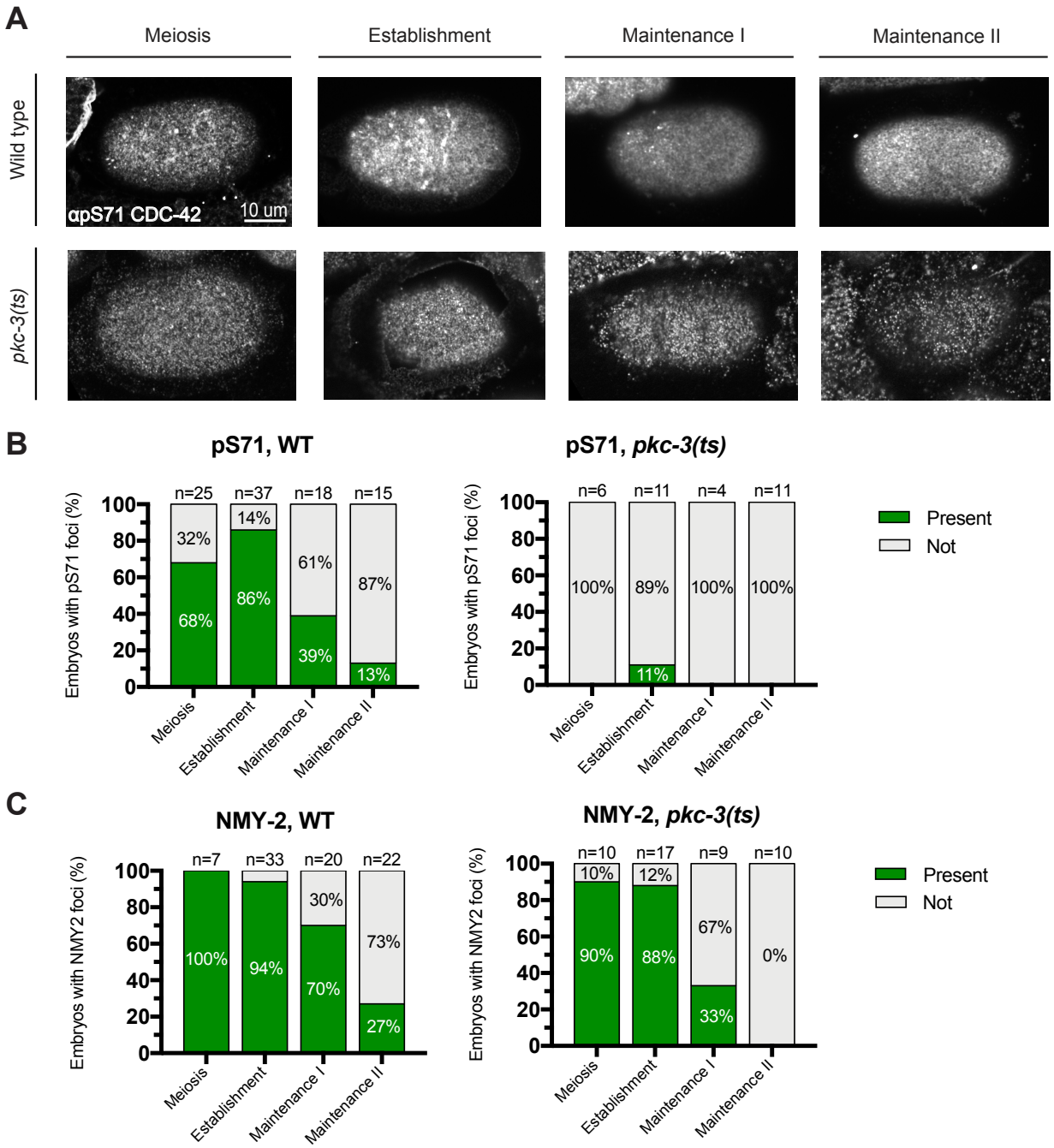

Figure 5.4. Analysis of pS71 CDC-42 foci presence during the first cell division of the *C. elegans* zygote. **A.** Wild type and *pkc-3(ts)* embryos stained with an antibody against pS71 CDC-42 (Invitrogen, #44214G). Phosphorylation of CDC-42 in S71 occurs predominantly during establishment phase, although it is partially visible during meiosis too in wild type embryos. In wild type embryos, pS71 decreases in Maintenance I, when the pronuclei meet, and is gone in most embryos in Maintenance II, when the pronuclei rotate and centre. **B.** Presence of pS71 by cell cycle stage in wild type embryos and *pkc-3(ts)* embryos (present in green, not present in grey). **C.** Presence of NMY-2 by cell cycle stage in wild type embryos and *pkc-3(ts)* embryos (present in green, not present in grey).

embryos, n=25). In most embryos pS71 foci disappear at the start of polarity maintenance stage (Maintenance I), when the pronuclei meet, although some foci and punctae structures are still weakly visible in some embryos at this stage (39%, n=18), and only 13% of embryos still show pS71 cortical structures at later stages of polarity maintenance (Maintenance II), during pronuclei rotation stages (with a single embryo showing the foci, n=15). It should be noted that the difference in pS71 presence in wild type and *pkc-3(ts)* embryos is not due to changes in NMY-2 foci presence, as in *pkc-3(ts)* embryos differences in NMY-2 foci presence are only visible during maintenance stage (when pS71 are mostly gone), and not during establishment stage (when pS71 foci are gone in *pkc-3(ts)* embryos) (**Figure 5.4 B-C**, for images of NMY-2 at different stages see **Chapter 3**).

5.2.3. Phosphomimetic and non phosphomimetic mutations of S71 affect the location of CDC-42::GFP

Post-translational modifications such as phosphorylations are known to affect the membrane binding abilities of some proteins, such as the posterior PAR-2 and LGL-1, which lose their membrane biding ability upon phosphorylation by aPKC (Zonies et al., 2010, Visco et al., 2016). Given the presence of a potential aPKC phosphorylation site in CDC-42, we analysed the cortical localisation of CDC-42 by performing *in vivo* imaging of GFP strains carrying the wild type CDC-42(S71)::GFP, the non-phosphorylatable CDC-42(S71A)::GFP and the phosphomimetic CDC-42(S71E)::GFP (**Figure 5.5**, note that this figure contains a combination of data generated for this thesis, and data of one experiment previously performed in our research group).

The *in vivo* images showed that both CDC-42(S71)::GFP and CDC-42(S71A)::GFP were strongly enriched in the anterior membrane of the embryos and weakly in the posterior membrane. The anterior membrane localisation of the phosphomimetic CDC-42(S71E)::GFP was extremely reduced compared both to wild type ($P<0.0001$, one-way ANOVA) and to the alanine mutant ($P<0.0001$), and its asymmetry is loss, with no clear difference between the posterior and anterior membrane levels of CDC-42 ($P=0.2996$), suggesting that phosphorylation of CDC-42 in S71 could affect its membrane residence time, and pointing to

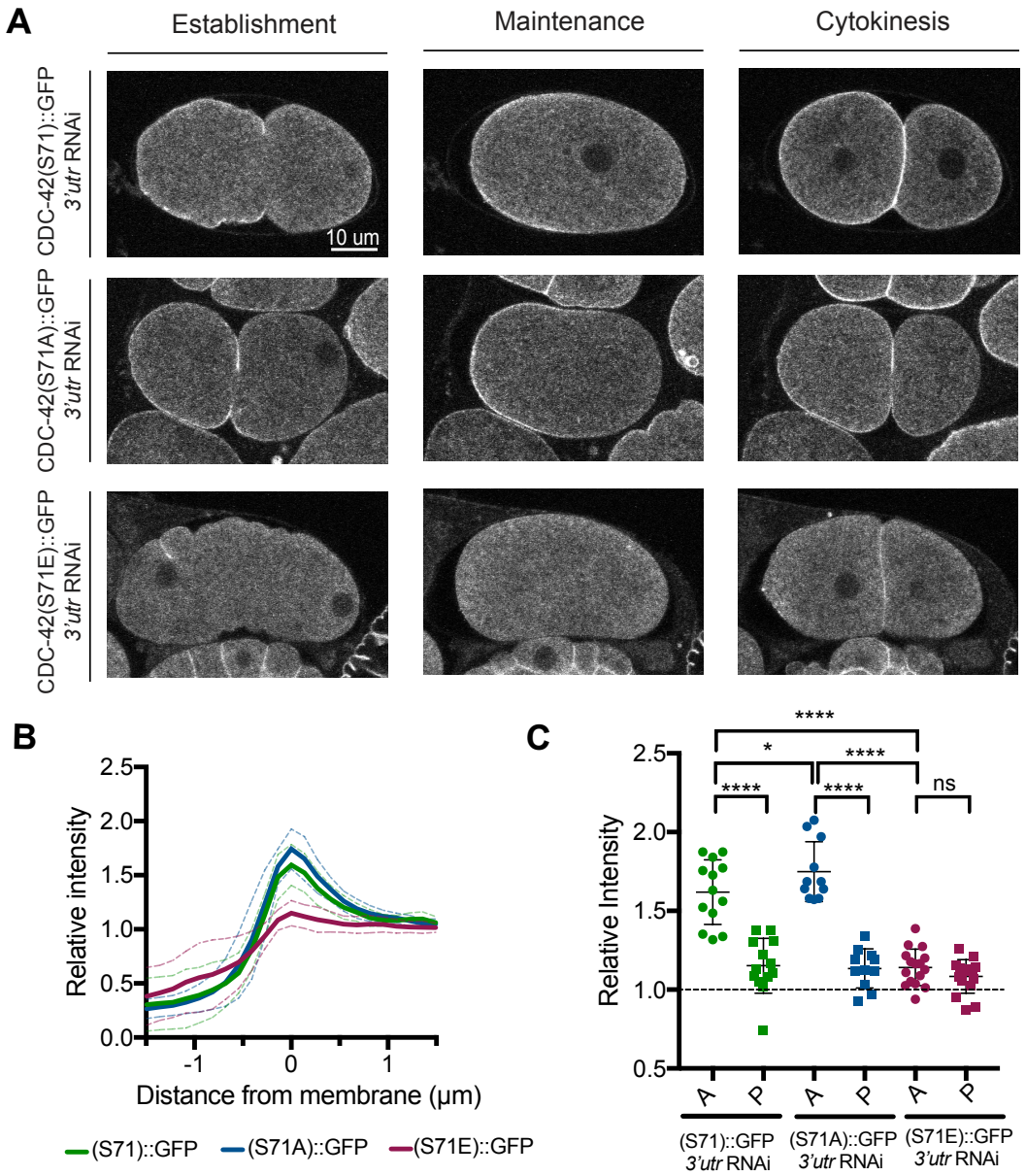

Figure 5.5. Analysis of mutations to S71 and their effect in the membrane binding ability of CDC-42. A. Embryos expressing CDC-42::GFP, CDC-42(S71A)::GFP and CDC-42(S71E)::GFP with endogenous *cdc-42* silenced with RNAi against the *3'utr* region of *cdc-42*. **B.** Intensity in the anterior membrane during polarity maintenance of each mutant normalised to the intensity of each embryo's cytoplasm (cytoplasm is on the right). CDC-42(S71A)::GFP localises more strongly to the membrane than the control CDC-42(S71)::GFP, and CDC-42(S71E)::GFP localies to the membrane more weakly than the control (n=13 for the S71 control, n=11 for the S71A mutant, and n=15 for the S71E mutant). The dashed lines represent the error bars (standard deviation). **C.** Membrane intensity of all mutants in anterior (A, in circles) and posterior (P, in squares) membrane during polarity maintenance. Both the wild type (S71, green) and the alanine mutant (S71A, blue) are asymmetric, with increased intensities in the anterior domain ($P<0.0001$ for both). The phosphomimmentic mutant (S71E, magenta) localises symmetrically all over the membrane, with no difference between the anterior and posterior domains ($P=0.299$). S71A localises to the anterior membrane stronger than the wild type CDC-42 ($P=0.0434$). Statistic tests were perform with a one-way Anova.

CDC-42 phosphorylation as a mechanism for turn-over of the PAR-6/PKC-3/CDC-42 complex in the anterior domain.

Quantification of membrane fluorescence in these mutant strains also showed slightly stronger levels of CDC-42(S71A)::GFP than of CDC-42(S71)::GFP in the anterior membrane (P=0.0434), further suggesting that phosphorylation of CDC-42 affects the stability of the PAR-6/PKC-3/CDC-42 complex in membrane, decreasing its residency time in the membrane (**Figure 5.5 B-C**).

5.2.4.CDC-42 phosphorylation state affects anterior PAR organisation

To further understand the role of this phosphorylation site in the regulation of anterior PARs, we analysed the localisation of PAR-3 and PKC-3 by immunofluorescence assays in the CDC-42::GFP mutant strains (**Figures 5.6** and **5.7**). Staining of PAR-3 and PKC-3 can be used as proxy for the PAR-3 dependant anterior complex (PAR-3/PAR-6/PKC-3) and the CDC-42 dependent anterior complex (CDC-42/PAR-6/PKC-3), respectively, as the expansion of PKC-3 from PAR-3 reflects the expansion of the CDC-42 dependent complex from the PAR-3 complex (Rodriguez et al, 2017). Analysis was performed as described in **Methods Section 2.7.6.4**.

The endogenous *cdc-42* was once again silenced in these CDC-42::GFP mutant strains employing RNAi against the *3' utr* of the *cdc-42* gene. We analysed only the CDC-42::GFP mutant strains treated with *3'utr* against *cdc-42*, instead of analysing the strains expressing both the GFP tagged protein and endogenous CDC-42, as this allows for easier analysis of the phenotypes caused by the S71 mutation. We analysed PKC-3 and PAR-3 staining in embryos of establishment stage, as this stage allows to detect both differences in PAR complex organisation (Rodriguez et al, 2017) and actomyosin flow deffects (as shown in **Chapter 3**).

5.2.4.1.Controls for CDC-42(S71)::GFP and the **3'utr cdc-42** *RNAi*

Before analysing the differences between the CDC-42(S71)::GFP mutant strains, we analysed the differences between wild type embryos and CDC-42(S71)::GFP embryos in which the endogenous *cdc-42* had been silenced employing RNAi against the *3' utr* of the *cdc-42* gene;

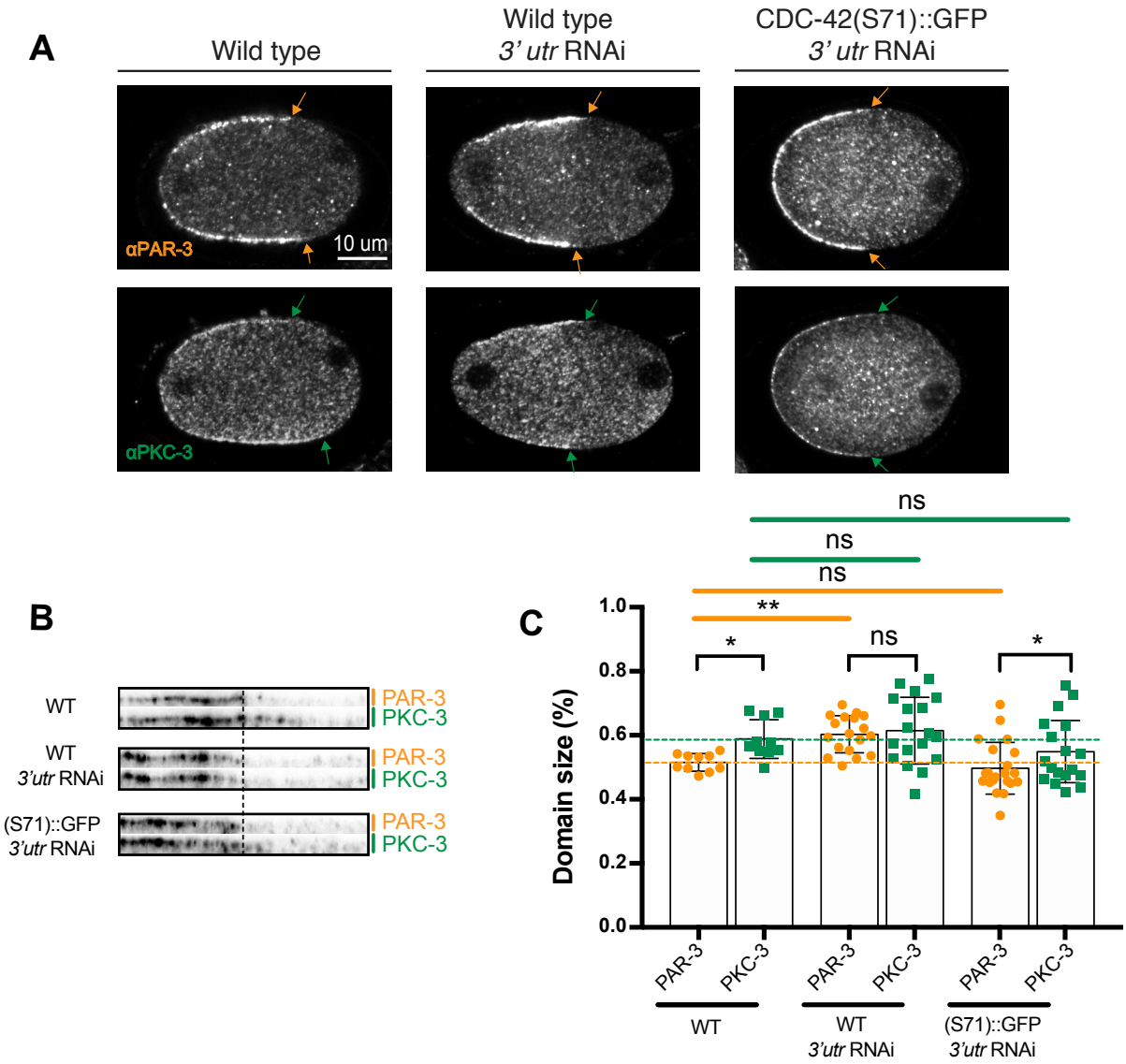

Figure 5.6. Analysis of PAR-3 and PKC-3 localisation in wild type embryos, embryos treated with RNAi against the *3' utr* of the cdc-42 gene, and embryos expressing CDC-42::GFP. A. Midplane images of wild type embryos, wild type embryos in which the endogenous *cdc-42* has been silenced with RNAi against the *3' utr* of *cdc-42* and embryos expressing CDC-42(S71)::GFP in which the same RNAi has been used. The arrows point to the boundaries of the PAR-3 and PKC-3 domain (in orange and green, respectively). **B.** Close-up view of the PAR-3 and PKC-3 boundary region showing PAR-3 on top and PKC-3 on the bottom. The dashed line indicates end of the PAR-3 domain. One example of both PAR-3 and PKC-3 is shown for each genotype. **C.** Domain size of PAR-3 and PKC-3 as a ratio for the full size of the membrane in wild type embryos, embryos treated with *3'utr* RNAi, and CDC-42(S71)::GFP embryos treated with the same RNAi. The expansion of PKC-3 from PAR-3 is significantly visible in wild type embryos (P=0.0271) and in CDC-42(S71)::GFP embryos treated with *3'utr* RNAi (P=0.0439). There is no significant expansion of PKC-3 from PAR-3 in wild type embryos in which endogenous *cdc-42* has been silenced with *3'utr* RNAi. There are no significant differences between wild type embryos and embryos expressing CDC-42(S71)::GFP, whereas removing endogenous *cdc-42* with the *3'utr* RNAi results in decreased PAR-3 retraction (P=0.007) and lack of PKC-3 expansion from PAR-3 (P=0.6767). Statistical significance checked with an ordinary one-way ANOVA.

as well as wild type embryos treated with *3'utr* RNAi, to determine how effective this RNAi was at removing wild type *cdc-42* (**Figure 5.6 A-C**).

In wild type embryos, PAR-3 takes up 52.10% of the zygote membrane, and PKC-3 expands a little bit further into posterior, taking up 58.53% of the zygote membrane (P=0.0271, difference statistically significant). In the CDC-42(S71)::GFP strain treated with *3'utr* RNAi PAR-3 retracted to 50.75% of the cell and PKC-3 expanded to 55.96% of the cell during establishment (n=29) (**Figure 5.6**), this retraction pattern was not significantly different to the retraction pattern observed in wild type embryos (**Figure 5.6 B-C**). However treating embryos with *3'utr* RNAi resulted in colocalisation of the PAR-3 and PKC-3 boundaries, with no difference in domain size (P=0.6767, one-way ANOVA). This lack of PKC-3 expansion from PAR-3 shows that the *3'utr* RNAi is effective at silencing *cdc-42* expression (**Figure 5.6 B-C**).

These results confirmed that *3'utr* was effective at removing endogenous *cdc-42*, and that the CDC-42(S71)::GFP strain has a PAR-3 and PKC-3 retraction phenotype that is not significantly different to that of wild type embryos. So to make comparison of different CDC-42 mutants more simple, we focus on CDC-42(S71)::GFP as a control throughout this section.

5.2.4.2.Lack of CDC-42 phosphorylation promotes the CDC-42 dependent complex and CDC-42 phosphorylation decreases PAR-3 retraction

Once confirmed that CDC-42(S71)::GFP shows no significant differences to wild type embryos in anterior PAR distribution, we analysed the difference between this strain and phospho-mutants, all treated with *3'utr* RNAi (**Figures 5.7 A-C)**.

Embryos of the non-phosphorylatable CDC-42(S71A)::GFP strain treated with *3'utr* RNAi showed increased decoupling of PKC-3 from the PAR-3 complex (P<0.0001, n=21), due to PKC-3 expanding more from the PAR-3 boundary than in the wild type embryos (P=0.0014, n=21; ordinary one-way ANOVA) (**Figure 5.7 A-C**). These results further suggest that lack of phosphorylation might stabilise the CDC-42/PAR-6/PKC-3 complex in the anterior, increasing its residence time at the membrane.

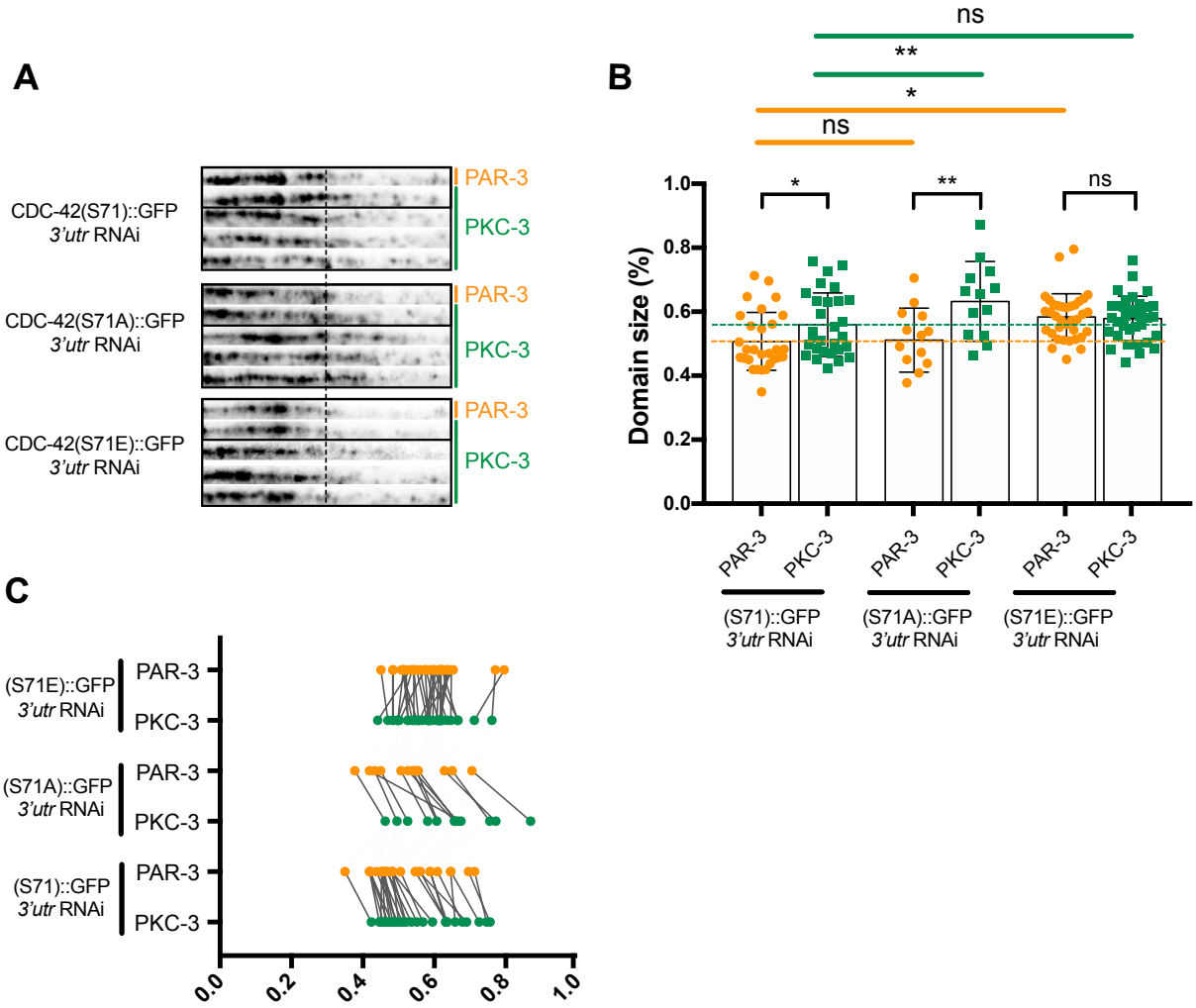

Figure 5.7. Analysis of mutations to S71 CDC-42 and their effect in anterior PAR organisation during establishment. A. Close-up view of the PAR-3 (DSHB, #P4A1) and PKC-3 (Tabuse et al, 1998) boundary regions showing PAR-3 on top and PKC-3 on the bottom. The dashed line indicates end of the PAR-3 domain. One example of both PAR-3 and PKC-3 is shown for each genotype, with a further three examples of PKC-3 only (lined up for PAR-3 domain) shown for each genotype. All embryos are treated with RNAi against the *3' utr* of *cdc-42*, to silence the endogenous *cdc-42*. **B.** PAR-3 and PKC-3 retraction phenotype of CDC-42(S71)::GFP (n=29), the non phosphorylatable CDC-42(S71A)::GFP (n=13) and the phosphomimmetic CDC-42(S71E)::GFP (n=35) strains during polarity establishment stage. In wild type (S71)::GFP embryos PKC-3 domain expands significantly from the PAR-3 domain (P=0.022). This expansion is increased in the non phosphorylatable (S71A)::GFP embryos (P=0.0002) due the increased size of the PKC-3 domain (P=0.0021), and not present in (S71E)::GFP embryos (P=0.365). In phosphomimmetic embryos PAR-3 retraction is significantly lower than in wild type embryos (P=0.0005). **C.** Retraction profiles of PAR-3 and PKC-3. The embryos are the same as the ones shown in panel B, a value of 1.00 indicates no retraction at all of PAR-3 or PKC-3, while a value of 0 indicates no presence of the protein at the membrane. Dark grey lines link values corresponding to the same embryo, so that a vertical line indicates co-locaisation of the PAR-3/PKC-3 boundary, the angle of the diagonal lines indicates the degree of separation between PAR-3 and PKC-3 boundaries.

In the phosphomimetic CDC-42(S71E)::GFP treated with *3'utr* RNAi, on the other hand, we observed very high levels of coupling of PKC-3 and PAR-3 complex boundaries, with no significant levels of expansion of PKC-3 from PAR-3 (P=0.8154, with n=35) (**Figure 5.7 A-C**). Since the phosphomimetic CDC-42(S71E)::GFP localises very weakly to the membrane, the increase in coupling between PAR-3 and PKC-3 might be a result of PKC-3 existing solely on its PAR-3 bound form, due to the lack of enough stable CDC-42 in the membrane to generate the CDC-42 complex.

Furthermore, phosphomimetic embryos treated with *3'utr* RNAi showed significantly less retraction of the PAR-3 domain (P=0.0006) (**Figure 5.7 B**), suggesting that the phosphomimetic strain might have weaker actomyosin flow.

5.2.4.3.CDC-42::GFP is not as effective at forming the anterior PAR complex as the endogenous protein

To further investigate the effect of the S71 mutation in CDC-42 and determine if the phenotypes observed in *pkc-3(ts)* embryos could be solely a result of lack of CDC-42 phosphorylation, we crossed the CDC-42(S71)::GFP mutants to *pkc-3(ts)* and analysed the PAR-3 and PKC-3 domains in these crosses.

In *pkc-3(ts)* embryos PKC-3 expands from the PAR-3 domain and localises all over the membrane (**Figure 5.8 A**), due to CDC-42 localising all over the embryo membrane (Rodriguez et al. 2017), and suggesting that inactive PKC-3 increases the stability of the CDC-42/PAR-6/PKC-3 complex in the membrane. To determine if the over-expression of CDC-42(S71)::GFP and silencing of endogenous *cdc-42* had an effect in anterior PAR organisation in the *pkc-3(ts)* background, we analysed differences between the control *pkc-3(ts)* embryos, *pkc-3(ts)* embryos in which endogenous *cdc-42* had been silenced with RNAi against the *3'utr* of the gene, and embryos expressing CDC-42(S71)::GFP crossed to *pkc-3(ts)* treated with this same RNAi (**Figure 5.8**).

Silencing of endogenous *cdc-42* with RNAi against the *3'utr* of the gene resulted in a much weaker PKC-3 domain (**Figure 5.8 A and C**) (relative intensity 0.729, normalised to wild type intensity of 1.00), in which PKC-3 was only weakly visible in the zygote membrane.

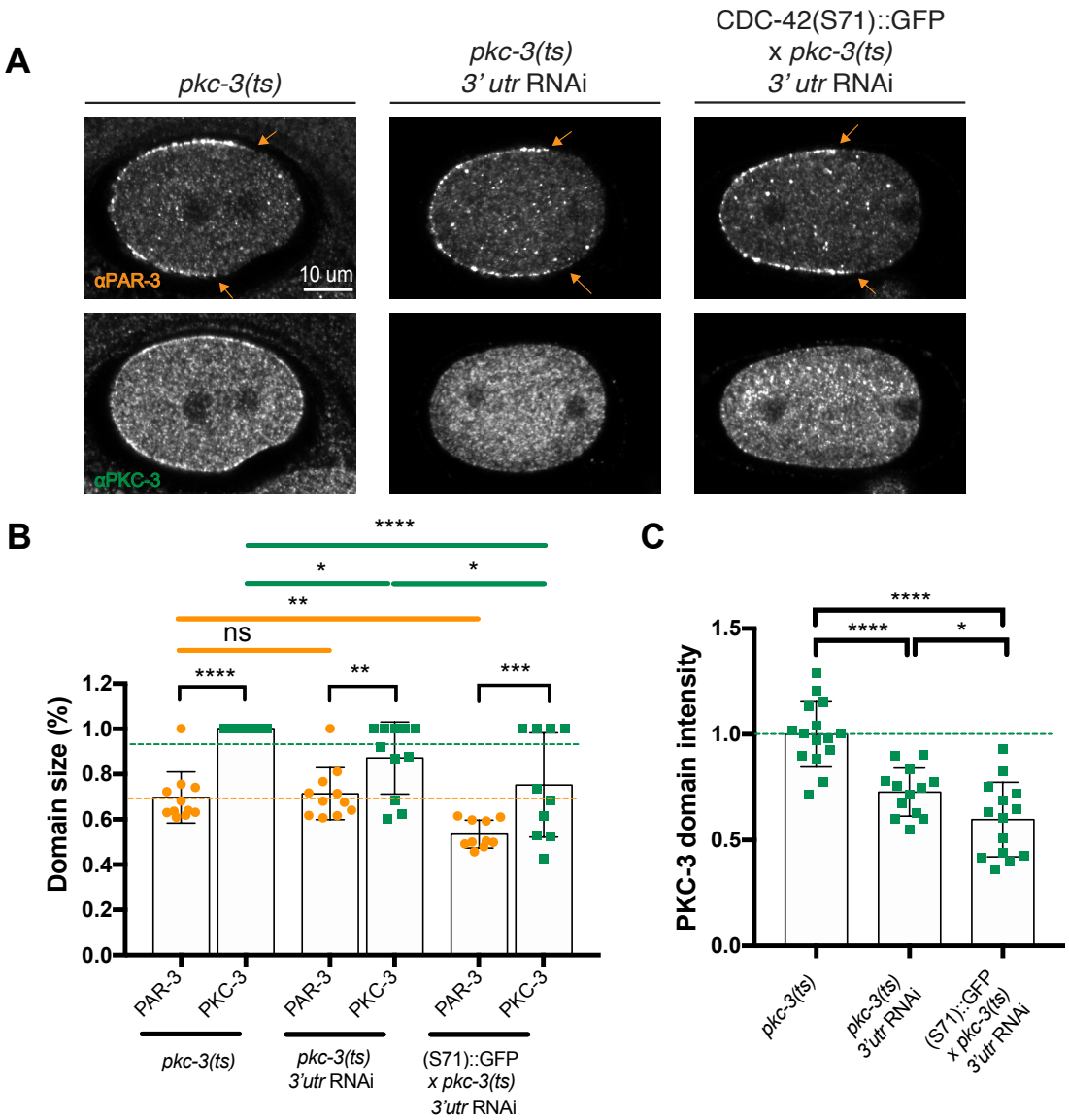

Figure 5.8. Analysis of PAR-3 and PKC-3 retraction in embryos with the *pkc-3(ts)* mutation expressing the recombinant CDC-42(S71)::GFP phosphomutants. A. Midplane images of embryos stained against PAR-3 (DSHB, #P4A1) and PKC-3 (Tabuse et al, 1998), during establishment stage. Genotypes are *pkc-3(ts)*, *pkc-3(ts)* treated with RNAi against the *3'utr* of the *cdc-42* gene, and CDC-42(S71)::GFP x *pkc-3(ts)* embryos treated with the same RNAi. The orange arrows point to the boundary f the PAR-3 domain. **B.** PAR-3 and PKC-3 domains as a ratio of the zygote membrane in *pkc-3(ts)* embryos, *pkc-3(ts)* embryos treated with RNAi against the *3'utr* of the *cdc-42* gene, and CDC-42(S71)::GFP x *pkc-3(ts)* embryos treated with the same RNAi. The PKC-3 domain expands from the PAR-3 domain in all three strains ($P<0.0001$ in all three cases), although PKC-3 is more expanded in untreated *pkc-3(ts)* embryos than in embryos treated with *3'utr* and in embryos of the CDC-42(S71)::GFP x *pkc-3(ts)* strain treated with the same RNAi ($P=0.0259$ and $P<0.0001$, respectively). Overexpression of CDC-42(S71) also results in higher levels of PAR-3 retraction ($P=0.0073$). **C.** PKC-3 domain intensity, normalised to the *pkc-3(ts)* value (1.00). In *pkc-3(ts)* embryos in which endougenous *cdc-42* has been silenced with *3'utr* RNAi PKC-3 intensity is significantly lower (0.729, $P<0.0001$), and similarly, in CDC-42(S71)::GFP x *pkc-3(ts)* embryos treated with the same RNAi, the value is significantly lower than in *pkc-3(ts)* embryos (0.597, $P<0.0001$). Significance checked with an ordinary one-way ANOVA. Statistical significance checked with an ordinary one-way ANOVA.

Interestingly, over-expression of CDC-42(S71)::GFP in this background did not rescue the intensity of the PKC-3 domain, and resulted in even lower PKC-3 intensity (**Figure 5.8 C**), with a relative intensity of 0.597 (P<0.0001 compared to the *pkc-3(ts)* value, and P=0.031 compared to *pkc-3(ts) 3'utr* RNAi value). Suggesting that CDC-42(S71)::GFP might be less stable at the membrane than the endogenous CDC-42 or that CDC-42(S71)::GFP might not be as effective at generating the CDC-42/PAR-6/PKC-3 domain as endogenous CDC-42 is

Furthermore, in CDC-42(S71)::GFP x *pkc-3(ts)* embryos treated with *3'utr* RNAi showed higher levels of PAR-3 retraction compared to *pkc-3(ts)* embryos (P=0.0073, one-way ANOVA) (**Figure 5.8 B**), as we also observed in the control CDC-42(S71)::GFP treated with *3'utr* RNAi (shown in **Figure 5.6 B**), further suggesting that over-expression of CDC-42 might rescue flow during establishment stage in *pkc-3(ts)* embryos. Our analysis also indicated that silencing *cdc-42* with the *3'utr* RNAi did not fully remove endogenous *cdc-42* (**Figure 5.8 B**), as PKC-3 still expanded from the PAR-3 domain in *pkc-3(ts)* embryos treated with *3'utr* RNAi (P=0.0073 for establishment stage) albeit the PKC-3 domain was significantly smaller than in *pkc-3(ts)* embryos not treated with the same RNAi (P=0.0259 for establishment).

To simplify the analysis of S71 mutation defects in aPAR organisation, we focused on CDC-42(S71)::GFP as the control for this experiment.

5.2.4.4.Analysis of pkc-3(ts) crosses with the CDC-42(S71)::GFP mutants

When the non-phosphomimetic mutant CDC-42(S71A)::GFP was crossed with *pkc-3(ts)*, the extension of PKC-3 from the PAR-3 domain was highly significant (P=0.0006, n=10) (**Figures 5.9 A-B**), appearing even more significant than in its control (CDC-42(S71)::GFP crossed to *pkc-3(ts)*). However there was no significant difference between the PKC-3 domain of the control strain and that of CDC-42(S71A)::GFP x *pkc-3(ts)* embryos (P=0.1388) (**Figure 5.9 A-B**).

The cross between the phosphomimetic CDC-42(S71E)::GFP x *pkc-3(ts)* with endogenous *cdc-42* silenced with *3'utr* RNAi resulted in a decrease in the PKC-3 domain (P=0.0013, with n=20), with the PKC-3 domain not being visible at all in some embryos (**Figure 5.9 B-C**).

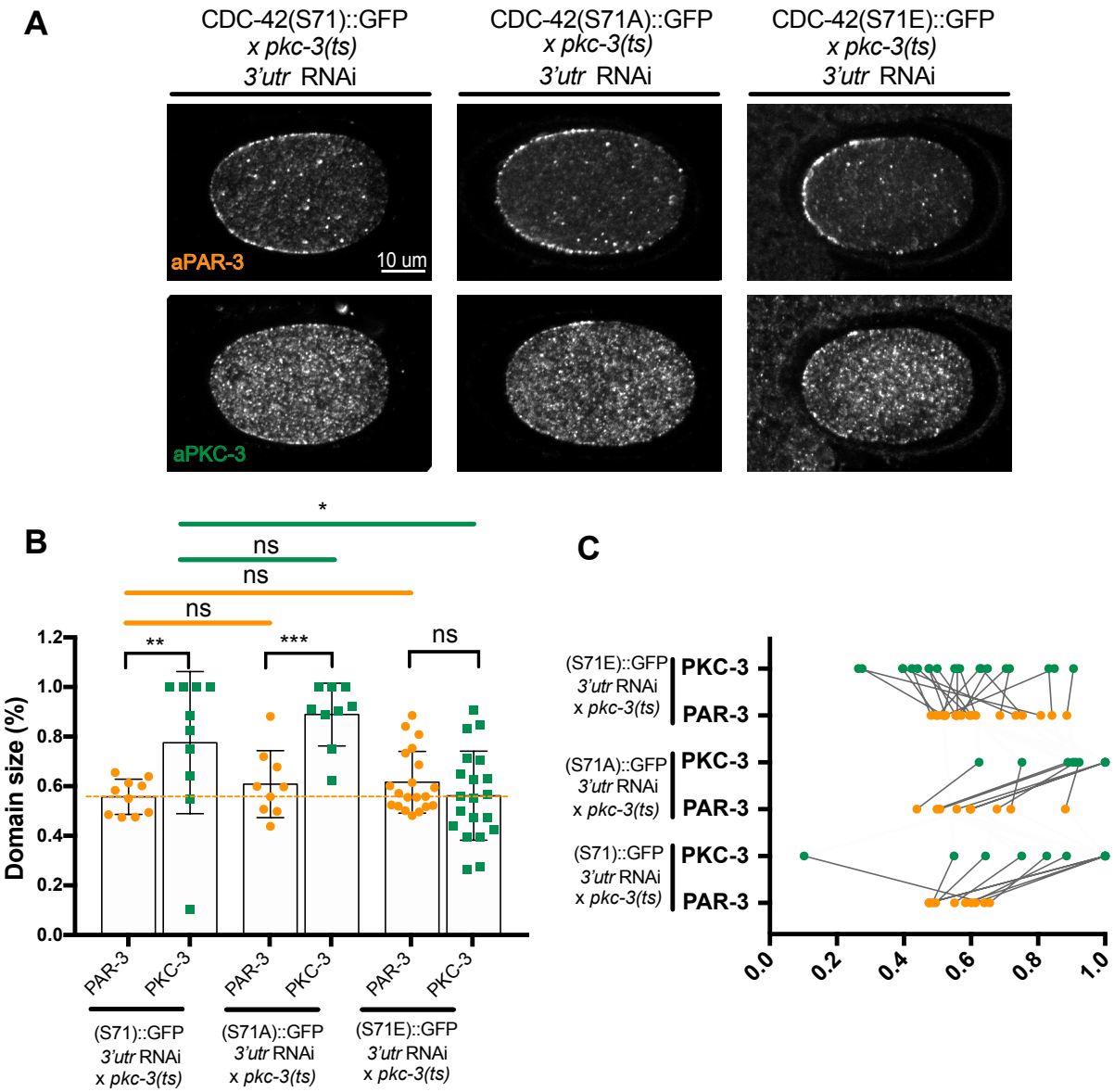

Figure 5.9. Analysis of anterior PAR organisation in *pkc-3(ts)* embryos with phosphomimetic CDC-42(S71) mutations. A. Midplane images of embryos expressing CDC-42::GFP (with S71A and S71E mutations) crossed to *pkc-3(ts)* and with the endogenous *cdc-42* silenced with *3'utr* RNAi, stained for PAR-3 (DSHB, #P4A1) and PKC-3 (Tabuse et al, 1998). Embryos are of establishment stage. **B.** PAR-3 and PKC-3 retraction phenotype of CDC-42(S71)::GFP x *pkc-3(ts)* (n=10), the non phosphorylatable CDC-42(S71A)::GFP x *pkc-3(ts)* (n=10) and the phosphomimmetic CDC-42(S71E)::GFP x *pkc-3(ts)* (n=20) strains during polarity establishment stage. PAR-3 and PKC-3 retraction are shown as the ration of the zygote membrane taken up by the PAR-3 and PKC-3 domain, with 1.00 indicating the entire embryo membrane contains the PAR of interest and 0 indicating no visible PAR in the membrane. Statistical significance checked with an ordinary one-way ANOVA. **C.** Retraction of PAR-3 and PKC-3 as shown in panel B, with grey lines linking values corresponding to the same embryo. Value 0 indicates lack of presence of the protein in the membrane, while a value of 1.00 indicates the protein is visible in the entire embryo membrane.

This lack of expanded PKC-3 domain is likely due to the fact that CDC-42(S71E)::GFP cannot be stabilised in the membrane as effectively as the other CDC-42::GFP strains, and that the PKC-3 of the *pkc-3(ts)* strain depends mainly on CDC-42 to localise to the membrane (Rodriguez et al. 2017).

Lastly, unlike what we have shown in the CDC-42(S71E)::GFP mutant (**Figures 5.7**), in the CDC-42(S71E)::GFP x *pkc-3(ts)* cross embryos the PAR-3 domain was not significantly bigger than in its control (CDC-42(S71)::GFP x *pkc-3(ts)*)(P=0.3483) (**Figures 5.9**).

5.2.5.The phosphomimetic CDC-42(S71E)::GFP cannot recruit PKC-3

To determine if the phosphorylation of CDC-42 could affect interaction with other PAR proteins, and given that the S71E mutant does not localise strongly to the membrane, we promoted the membrane localisation of CDC-42(S71)::GFP and CDC-42(S71E)::GFP (**Figure 5.10**) using the PH-GBP strain, which carries a membrane-tethered (the PH domain binds to $PI(4,5)P_2$) nanobody against GFP (the GBP protein, GFP-binding protein, binds to CDC) (Rodriguez et al., 2017).

We then analysed embryos of these crosses by immunofluorescence and measured the intensity of PKC-3 in the posterior of maintenance stage embryos, since PKC-3 is normally not present in the posterior at this stage (to make sure we were only selecting the posterior membrane we only analysed the furthermost posterior 30% of the embryo) (**Figure 5.10 A**). As control we used CDC-42(S71)::GFP embryos treated with *3'utr* RNAi that had not been crossed with the PH-GBP strain. We also analysed and included wild type embryos, for further reference.

As expected, targeting CDC-42(S71)::GFP to the membrane carried PKC-3 to the membrane, indicating that CDC-42::GFP can recruit the PAR-6/PKC-3 heterodimer (**Figure 5.10 A**). The lower levels of PKC-3 we observe in posterior (relative to levels in the anterior domain) suggest that binding of CDC-42::GFP to the PH-GBP strain might affect its structure or its ability to bind the PAR-6/PKC-3 heterodimer, or that CHIN-1 in the posterior could be affecting PAR-6/PKC-3 recruitment by changing the GTP state of the CDC-42::GFP recruited to the membrane.

Targeting CDC-42(S71E)::GFP to the membrane, on the other hand, did not carry PKC-3 to the membrane, suggesting that the phosphorylation of CDC-42 might result in the disassembly of the CDC-42/PAR-6/PKC-3 complex in *C. elegans* embryos (P>0.0001 compared to the CDC-42(S71)::GFP strain crossed to the same PH-GBP strain, one-way ANOVA) (**Figure 5.10 B**). Furthermore, the levels of PKC-3 in posterior observed in CDC-42(S71E)::GFP embryos were not significantly different to those observed in wild type embryos (P=0.7996, one-way ANOVA), or to those observed in control CDC-42(S71)::GFP

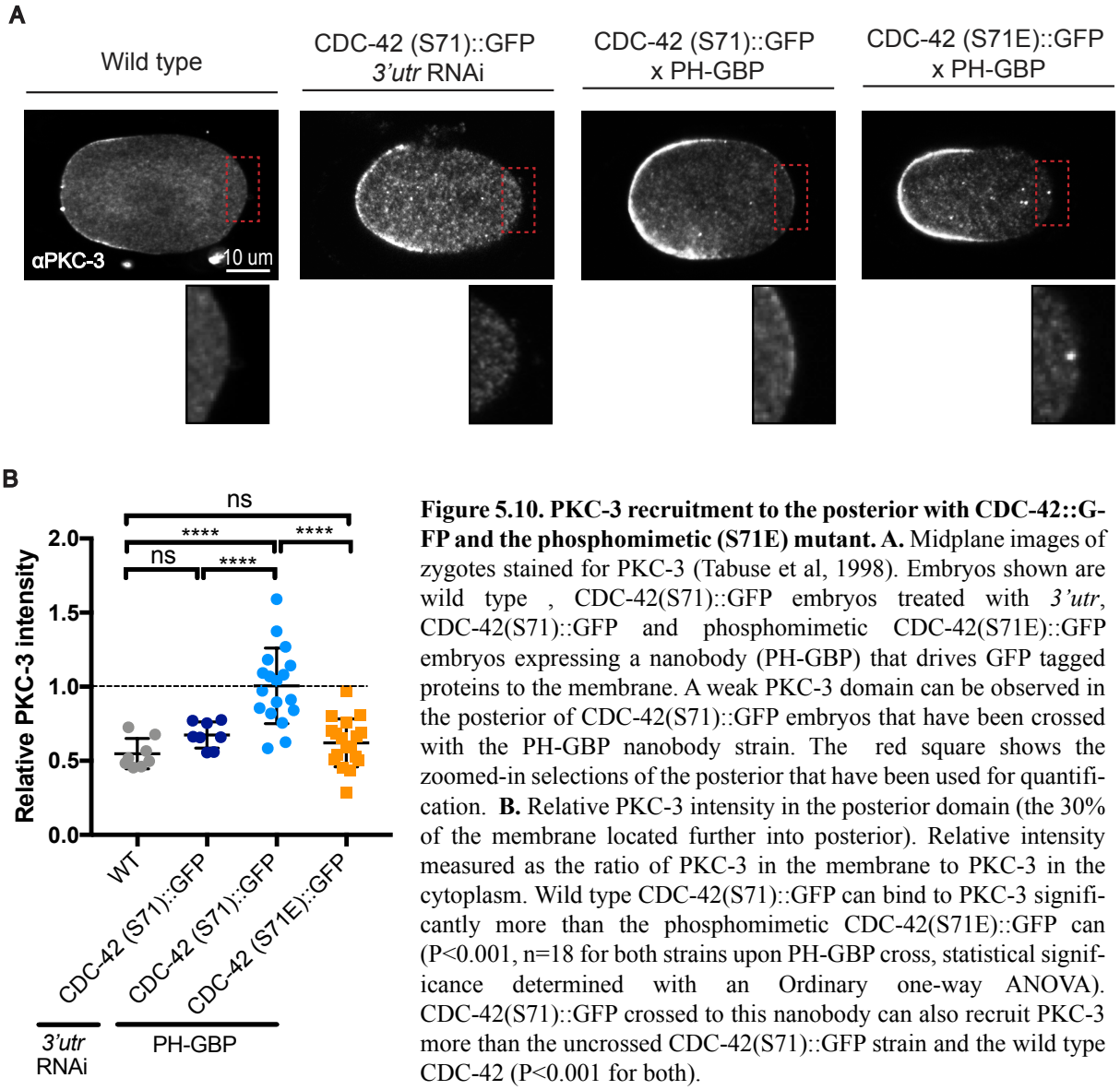

Figure 5.10. PKC-3 recruitment to the posterior with CDC-42::GFP and the phosphomimetic (S71E) mutant. A. Midplane images of zygotes stained for PKC-3 (Tabuse et al, 1998). Embryos shown are wild type , CDC-42(S71)::GFP embryos treated with *3'utr*, CDC-42(S71)::GFP and phosphomimetic CDC-42(S71E)::GFP embryos expressing a nanobody (PH-GBP) that drives GFP tagged proteins to the membrane. A weak PKC-3 domain can be observed in the posterior of CDC-42(S71)::GFP embryos that have been crossed with the PH-GBP nanobody strain. The red square shows the zoomed-in selections of the posterior that have been used for quantification. **B.** Relative PKC-3 intensity in the posterior domain (the 30% of the membrane located further into posterior). Relative intensity measured as the ratio of PKC-3 in the membrane to PKC-3 in the cytoplasm. Wild type CDC-42(S71)::GFP can bind to PKC-3 significantly more than the phosphomimetic CDC-42(S71E)::GFP can (P<0.001, n=18 for both strains upon PH-GBP cross, statistical significance determined with an Ordinary one-way ANOVA). CDC-42(S71)::GFP crossed to this nanobody can also recruit PKC-3 more than the uncrossed CDC-42(S71)::GFP strain and the wild type CDC-42 (P<0.001 for both).

strain treated with *3'utr* RNAi (P=0.9043) (**Figure 5.10 B**). However, although these results are quite promising, they correspond to a single experiment, and are therefore only preliminary.

5.2.6.Active CDC-42 generates cortical foci

To try to determine if phosphorylated CDC-42 was active, we imaged GFP::GBPwsp-1, a biosensor for GTP bound-CDC-42 built with the G-protein binding domain of WASP (a downstream effector of CDC-42) bound to GFP (Kumfer et al., 2010). We did not detect any GFP::GBPwsp-1 structures upon fixation (not shown). However *in vivo* the GFP::GBPwsp-1 strain presented foci structures in the cortex when imaged at 15° C (**Figure 5.11**), which resemble those observed with the pS71 CDC-42 antibody (**Figure 5.3**) and are visible in the same stages of the cell division (during establishment, and in some cases early in maintenance). These foci seemed very unstable and disappeared if imaged for longer than a few seconds, or if the temperature increased, not allowing for the study of their dynamics. Nevertheless the presence of GTP-bound CDC-42 foci in the cortex of the *C. elegans* zygote suggests that the phosphorylated CDC-42 foci we observed in embryos stained with the pS71 CDC-42 antibody correspond to GTP-bound CDC-42. Although, it could also mean the antibody binds to active (GTP-bound) CDC-42.

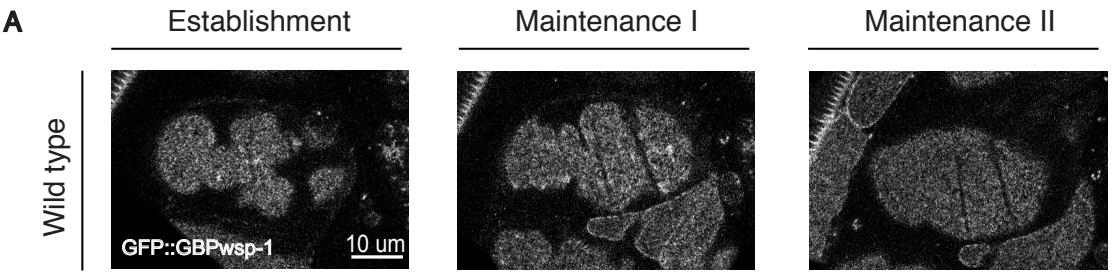

Figure 5.11. *In vivo* cortical structures of GFP::GBPwsp-1. A. Premiminary images of the CDC-42 biosensor GFP::GBPwsp-1 show foci-like cortical structures during establishment and early maintenace stages. These structures are no longer visible at the later stages of maintenance.

5.3. Discussion

PKC-3 and CDC-42 are essential regulators of polarity, and in the *C. elegans* zygote they colocalise at the anterior domain, with PKC-3's kinase activity being linked to its interaction with CDC-42. Our lab has shown that inhibiting the kinase activity of PKC-3 results in CDC-42 and PKC-3 localising together all over the membrane of the embryo (Rodriguez et al., 2017), which suggests that PKC-3 activity regulates the turnover of the CDC-42 complex. Furthermore, this interaction seems to be conserved in some other organisms, as lack of PKC-3 activity decouples aPKC from the PAR-3 complex in *Drosophila* neuroblasts too (Hannaford et al., 2019). Our group has identified the S71 of CDC-42 as a substrate for the regulation of this interaction.

5.3.1.The Kinase Activity of PKC-3 Regulates CDC-42

Although we were not able to use the anti-pS71 CDC-42 antibody to identify pS71 CDC-42 in western blots, this antibody detected foci structures in the cortex of embryos, particularly at polarity establishment stage. These foci structures disappeared upon *cdc-42* RNAi and in CDC-42(S71A)::GFP embryos treated with the RNAi against the *3'utr* of the *cdc-42* gene, suggesting that the antibody is successfully recognising CDC-42 phosphorylation. These foci structure resemble that of NMY-2 (see **Chapter 6** for the analysis of their association with actomyosin); and are gone in the *pkc-3(ts)* embryos and the embryos treated with *pkc-3* RNAi, suggesting that phosphorylation of CDC-42 depends on PKC-3. It should be noted that the NMY-2 foci alteration in *pkc-3(ts)* cannot account for pS71 reduction (as clearly seen in **Figure 5.4**).

Furthremore, the pS71 foci seemed dependent on CDC-42 activity, as most embryos in which the CDC-42 GEF (*cgef-1*) had been silenced did not have pS71 CDC-42 foci and the constitutively active CDC-42 strain (WH423) showed stronger pS71 foci than wild type embryos. This correlation with CDC-42 activity could be due to two reasons: active, GTP-bound CDC-42 is the form of the protein that can be phosphorylated; or increased CDC-42 activity results in increased PKC-3 activity, which can in turn result in increased phosphorylation of CDC-42.

Previous studies on pS71 phosphorylation of RAC-1, CDC-42 and their orthologues have shown mixed results in this regard: Kwon et al. (2000) showed that alanine mutations in the S71 of Rac1(S71A) decrease the GTP binding ability and GTPase activity of purified human Rac1 *in vitro*; similarly, Shoentaube et al. (2009) have shown that phosphomimetic Rac1(S71E) and Cdc42(S71E) have less affinity for GTP in vitro; more recent papers, however report that Cdc42(S71E) has the same GTP binding affinity as wild type Cdc42 (Schwarz et al., 2012).

Our images of active CDC-42 reporter GFP::GBPwsp-1 (**Figure 5.11**) suggest that the pS71 foci we observe during establishment correspond to active CDC-42, however more images and controls of this strain would be needed to confirm that pS71 foci correspond to the GFP::GBPwsp-1 foci we see.

5.3.2.Phosphorylation of S71 regulates CDC-42 location

As for the effect of S71 phosphorylation in CDC-42 localisation, the *in vivo* analysis indicated that phosphorylation of CDC-42 in its S71 changes the localisation of CDC-42. While both CDC-42(S71)::GFP and the non phosphorylatable CDC-42(S71A)::GFP bind the anterior membrane strongly, phosphomimetic CDC-42(S71E)::GFP only localises very weakly to the membrane, and its asymmetry is lost (**Figure 5.5 C**).

The location of proteins in the membrane is affected by the rate of binding and unbinding to the membrane, the rate of lateral diffusion, and (if certain conditions are met) advection by cortical flow (Goehring et al., 2011a, Goehring et al., 2011b). Given that CDC-42 does not form clusters, and a stable interaction with the membrane is not enough for advective flow (Rodriguez et al., 2017), it is unlikely that directional flow advection of CDC-42 surpasses its diffusion rate in the membrane. Leaving the rate of binding and unbinding to the membrane, and the rate of lateral diffusion as the main mechanisms that regulate the membrane localisation of CDC-42(S71)::GFP, CDC-42(S71A)::GFP and CDC-42(S71E)::GFP embryos.

For example, the phosphomimetic mutation might not allow CDC-42(S71E)::GFP to effectively access the membrane; the mutation could increase the rate at which it is extracted from the membrane; or a mixture of both.

This suggests that PKC-3 phosphorylation of CDC-42 might serve as a mechanism for membrane turn-over of the CDC-42/PAR-6/PKC-3 complex, with the phosphorylation potentially releasing CDC-42 from its association with the membrane. This could also explain why the CDC-42/PAR-6/PKC-3 complex is present all around the embryo's cortex in the *pkc-3(ts)* embryos.

Furthermore, the stronger anterior localisation observed in the alanine mutant (**Figure 5.5 B-C**) suggests that the alanine mutation stabilises CDC-42 in the anterior, perhaps by completely removing the possibility of pS71 phosphorylation, even with residual PKC-3 activity.

5.3.3. Phosphorylation of CDC-42 in S71 regulates its interaction with other PAR proteins

Another reason for the increased intensity of CDC-42(S71A)::GFP observed in the anterior domain could be due to increased interaction with other proteins, which could stabilise the complex in the anterior.

Phosphomimetic mutations of Rac1(S71E) and Cdc42(S71E) have been shown to affect the interaction of these proteins with some downstream targets: Cdc-42(S71E), for example, has decreased affinity for its downstream effectors N-Wasp and IQGAP1/2 *in vitro* (Schwarz et al., 2012). The phosphomimetic mutations do not inhibit all interactions to downstream effectors: interaction to MRCKa, for example, is not affected by S71E mutations in Cdc42 , as reported in *in vitro* assays with human HEp2 cell lysates (Schwarz et al., 2012). Results for PAK1 are unclear, with some papers claiming that interaction is not affected by the phosphomimetic mutation (Schoentaube et al., 2009), and other papers claiming that interaction to the kinase domain of PAK1 is not affected, but interaction to the full length protein is (Schwarz et al., 2012). However, all of these results are from *in vitro* assays.

To determine the effect of S71 in the stability of this complex, we crossed the CDC-42(S71)::GFP and CDC-42(S71E)::GFP strains with the anti-GFP nano-body (PH-GBP) strain, which targets GFP bound proteins to the cell membrane and allows to assess CDC-42 recruitment of other proteins at the cell stage of interest. These crosses showed that wild type CDC-42(S71)::GFP can recruit the PAR-6/PKC-3 heterodimer (**Figure 5.10 B**), whereas we

detected no interaction between CDC-42(S71E)::GFP and the PAR-6/PKC-3 heterodimer. These results suggest that phosphorylation of CDC-42 in S71 could disrupt the CDC-42/ PAR-6/PKC-3 complex, allowing for PAR-6 and PKC-3 to be recycled into the cytosol, and potentially generating a pool of phosphorylated CDC-42 that could interact with other proteins.

If this hypothesis were correct, then the non phosphorylatable CDC-42(S71A)::GFP would lead to a more stable CDC-42 complex. Interestingly, our analysis or PAR domains in the CDC-42(S71A)::GFP strain suggests this could be true (**Figure 5.7 B**). Although we did not cross the CDC-42(S71A)::GFP strain to the anti-GFP nano-body (PH-GBP), the analysis of PKC-3 and PAR-3 domains suggests that the S71A mutation in CDC-42 stabilises the interaction with the PAR-6/PKC-3 heterodimer, as the CDC-42 dependent complex expands from PAR-3 further than it does in its wild type control. It would be interesting to cross the PH-GBP strain to the CDC-42(S71A)::GFP strain, to confirm the hypothesis that the S71A mutation stabilises the interaction of CDC-42 with the PAR-6/PKC-3 heterodimer.

Furthermore, changes in how CDC-42 binds PAR-6/PKC-3 could also affect the rate at which it binds the membrane or gets extracted from the membrane: previous studies in budding yeast have reported that inactive GDP-bound Cdc42 can be mobilised (and extracted from the membrane) at a higher rate than active Cdc42, contributing to Cdc42 polarisation (Woods et al., 2016), perhaps due to the ability of GTP-bound Cdc-42 to bind effectors, which could slow down the mobility of these complexes (Woods and Lew, 2019).

5.3.4.Mechanisms for regulation of CDC-42's interaction with the membrane

So how does aPKC phosphorylation regulate the membrane interaction of CDC-42? Phosphorylation of membrane bound CDC-42 could increase the rate at which it is extracted from the membrane, decrease the rate at which CDC-42 binds the membrane in the first place, stabilise it by affecting its interaction with other proteins, or affect the response of CDC-42 to actomyosin flows.

Therefore there are three different hypothesis that could explain the different localisations we observe in the three CDC-42(S71)::GFP mutants:

1. The rate at which the different mutants bind the membrane is different (being highest for S71A, and lowest for S71E), while in the posterior CHIN-1 clears CDC-42(S71)::GFP and CDC-42(S71A)::GFP from the membrane; or
2. All three CDC-42::GFP mutants can bind the membrane at similar rates, but CDC-42(S71)::GFP and CDC-42(S71A)::GFP become stabilised at the anterior by their interaction with PAR-6/PKC-3, while the phosphomimetic CDC-42(S71E)::GFP cannot be stabilised in the membrane; or
3. By interacting with the PAR-6/PKC-3 heterodimer, wild type CDC-42(S71)::GFP and mutant CDC-42(S71A)::GFP could be stabilised in the membrane enough to follow actomyosin flow.

As described in the introduction, whether a membrane bound complex can follow advective flows or not depends on the rate at which it can sense flows and the rate at which it can diffuse in the membrane (Goehring et al., 2011a, Goehring et al., 2011b). The only proteins that have been reported to follow advective flows in the *C. elegans* zygote are CHIN-1 and PAR-3, both of which form oligomers (Sailer et al., 2015, Gubieda et al., 2020). And as it has been shown for PAR-3, oligomerisation is essential for it to follow flow, as oligomerisation decreases the rate of lateral diffusion in the membrane, and also increases the time of residence of the complex in the membrane (Dickinson et al., 2017, Rodriguez et al., 2017). Furthermore, it has been shown that increasing the time of residence of monomeric PAR-3 in the membrane is not enough for it to follow flow (Rodriguez et al., 2017), and the size of PAR-3 oligomers has been shown to directly correlate to the rate at which they follow flow (Dickinson et al., 2017). The size of each PAR3 monomer is 149kDa, while the size of CDC-42 is 21kDa, and of the PAR-6/PKC-3 heterodimer is 102 kDA (with the respective sizes of each monomer being 34 kDa and 68 kDa). It therefore seems unlike that the size of the CDC-42/PAR-6/PKC-3 complex is big enough to be able to sense flow, as its mass (123 kDa total) is smaller than that of each PAR-3 monomer (149 kDa). Furthermore, in the *pkc-3(ts)* mutant, in which the CDC-42/PAR-6/PKC-3 complex is stable, we observe no enrichment of the complex in anterior, as would be expected if actomyosin flow could polarise this complex. Therefore there is not enough evidence to support a role for actomyosin

flow in polarising the CDC-42/PAR-6/PKC-3 complex, although the possibility of CDC-42/PAR-6/PKC-3 forming clusters or binding PAR-3 is currently being explored in our research group.

That leaves the other two hypothesis: either the rate at which each mutant binds the membrane is different, or they all bind the membrane at the same rate but get extracted from the membrane at different rates.

If CDC-42(S71)::GFP, CDC-42(S71A)::GFP and CDC-42(S71E)::GFP had different levels of affinity for the membrane, CDC-42(S71A)::GFP would bind the membrane at a higher rate than the wild type form, whereas CDC-42(S71E)::GFP would bind the membrane at a very low rate. Meanwhile in the posterior, CHIN-1 could remove CDC-42 from the membrane by exchanging GTP for GDP. However posterior PARs have only been reported to regulate CDC-42 during maintenance phase, not during establishment phase (Kumfer et al., 2010), and posterior CHIN-1 clusters have only been observed in the posterior membrane during maintenance phase (Kumfer et al., 2010, Sailer et al., 2015).

Moreover, even though this hypothesis could explain the different levels of CDC-42::GFP we observe in anterior membrane for each mutant, it would not be enough to explain the increased expansion of the CDC-42 complex from the PAR-3 complex observed in the anterior domain.

Hence the more simple explanation for the phenotypes we observe is that the rate at which the different CDC-42::GFP mutants get extracted from the membrane is what determines the localisation of CDC-42, rather than the rate at which they get loaded into the membrane. In this case, all CDC-42 mutants would be able to interact with the membrane at similar rates, however in the anterior domain interaction with the PAR-6/PKC-3 heterodimer could stabilise CDC-42(S71)::GFP and CDC-42(S71A)::GFP, whereas CDC-42(S71E)::GPF, which cannot bind PAR-6/PKC-3, would not be stabilised and would be extracted from the membrane at a higher rate. Furthermore, CDC-42(S71A)::GFP could form a more stable interaction with PAR-6/PKC-3, as it cannot be phosphorylated, leading to the bigger expansion from PAR-3 that we observe in this strain.

What does this mean for wild type embryos? In wild type zygotes phosphorylated and un-phosphorylated CDC-42 could both potentially interact with the membrane, but un-phosphorylated CDC-42 would be able to interact with PAR-6/PKC-3 (enriched in the anterior domain thanks to PAR-3), and become stable in the anterior membrane. Once bound to GTP-bound CDC-42, PKC-3 would become active, and could then phosphorylate CDC-42, breaking the interaction between pS71 CDC-42 and PAR-6. PAR-6 and PKC-3 could then be recycled to the cytoplasm, from which they would be able to interact with PAR-3 again, and the interaction of pS71 CDC-42 with the membrane would become unstable, eventually resulting in its release from the membrane.

Further research is still needed to confirm this hypothesis.

3.1. Phosphorylation of S71 affects retraction of PAR-3 and could be affecting actomyosin flow

Another interesting result from the PAR-3 and PKC-3 domain analysis was the change in PAR-3 retraction observed in the phosphomimetic CDC-42(S71E)::GFP, which suggests that CDC-42 phosphorylation could affect actomyosin flow (see **Chapter 6** for further analysis).

CHAPTER 6. pS71 CDC-42 ASSOCIATES WITH THE ACTOMYOSIN NETWORK AND CHANGES THE STRUCTURE OF CORTICAL ACTOMYOSIN

6.1. Introduction

Actomyosin flow was first described as a polarising force in the *C. elegans* zygote during polarity establishment, where it polarises anterior PARs (Munro et al., 2004), but has since been reported to be required for polarisation of the fly neuroblast (Oon and Prehoda, 2019), for compaction of the mouse embryo (Maitre et al., 2015), and for positioning of the cleavage furrow in both fly neuroblast and *C. elegans* embryos (Reymann et al., 2016, Roubinet et al., 2017). All of these are processes in which PAR protein asymmetry is essential (Knoblich, 2008, St Johnston and Ahringer, 2010, Ajduk and Zernicka-Goetz, 2016).

There are tight feedback mechanisms between actomyosin flow and PAR proteins. aPKC has been identified in *C. elegans, Drosophila* amnioserosa cells and mammalian epithelial cell cultures as a regulator of actomyosin activity (Munro, 2006, David et al., 2010, Ishiuchi and Takeichi, 2011, David et al., 2013, Durney et al., 2018). CDC-42 is a well established actomyosin regulator, known to regulate the phosphorylation of Myosin II regulatory light chains (RLC, MLC-4 in *C. elegans*) via its effector kinase MRCK-1 (Unbekandt and Olson, 2014). In *C. elegans*, CDC-42 has been reported to regulate actomyosin via MRCK-1 only during maintenance phase in the *C. elegans* zygote (Kumfer et al., 2010).

However *cdc-42* silencing with RNAi can decrease the posterior ECT-2 clearance that signals initial actomyosin flow start (Motegi and Sugimoto, 2006), suggesting that CDC-42 has a role in actomyosin flow during early polarity establishment. Furthermore, one recent paper using single particle track analysis has also proposed that anterior PAR proteins promote actomyosin flow by stabilising NMY-2 in the anterior domain (as seen with *par-6* RNAi) (Gross et al., 2019): with the rate at which NMY-2 dissociates from the cortex being twice higher in the posterior PAR domain that in the anterior, and the rate that it associates with the cortex being the same in both PAR domains. This dissociation rate is the same both during

establishment, when cortical flow is present, as during maintenance. Whether this is a result of PAR-6 slowing down the dissociation rate of actomyosin, or one of its partner proteins (i.e., PAR-3, PKC-3 or CDC-42), has not been determined yet.

6.1.1.Objectives

In **Chapter 3** we described and compared changes to actomyosin flow, to actomyosin structure and to the time of disassembly of the foci network in *pkc-3(ts)*, *pkc-3* RNAi and *cdc-42* RNAi embryos. Furthermore, in **Chapter 5** we investigated the role of PKC-3 in regulating pS71 CDC-42 phosphorylation, and the effect this phosphorylation could have in anterior PAR organisation. This last chapter explores the question of how CDC-42 phosphorylation could play a role in regulating the actomyosin network.

More specifically, the objectives of the work presented in this chapter were the following:

- To describe the association of pS71 CDC-42 with the actomyosin cytoskeleton.
- To determine if pS71 CDC-42 has a role in regulating the actomyosin cytoskeleton and flow during polarity establishment.
- To investigate the role LET-502 could play in regulating CDC-42 phosphorylation and anterior PARs

6.2. Results

6.2.1.CDC-42 phosphorylation colocalises with actomyosin foci

As described in **Chapter 5**, pS71 CDC-42 forms cortical foci that resemble those of NMY-2. To determine if there could be any association between the two, we first looked at whether there was any colocalisation between the pS71 CDC-42 foci and the actomyosin foci by looking at a strain of *C. elegans* expressing non muscular myosin II (NMY-2) bound to a GFP reporter and staining the embryos with the phosphoantibody against pS71 CDC-42 (**Figure 6.1**). We could not stain for both NMY-2 and pS71 CDC-42 at the same time as both antibodies derive from rabbit.

The immunofluorescent staining showed that NMY-2::GFP colocalises with pS71 significantly more than the control PAR-3 - we selected PAR-3 as a negative control for

colocalisation because it localises in the same area as NMY-2, the anterior domain, but it does not colocalise with NMY-2. The Pearson's correlation coefficient was significantly higher for pS71 than for PAR-3 (Pearson's coefficient (r)=0.56 for pS71 CDC-42, n=11 embryos vs r=0.38 for PAR-3, n=11 embryos, P=0.0002 with an unpaired t-test) (**Figure 6.1 B**), indicating that the pS71 CDC-42 foci colocalise with actomyosin.

This co-localisation is not total, with some NMY-2 foci having much stronger colocalisation with pS71 CDC-42 than others. This could be a result of pS71 foci existing only at a certain stage of the duration of NMY-2 foci (as has been described with GTP-bound-RHO and NMY-2 foci, for example, with GTP-bound-RHO foci slightly preceding NMY-2 foci (Nishikawa et al., 2017)).

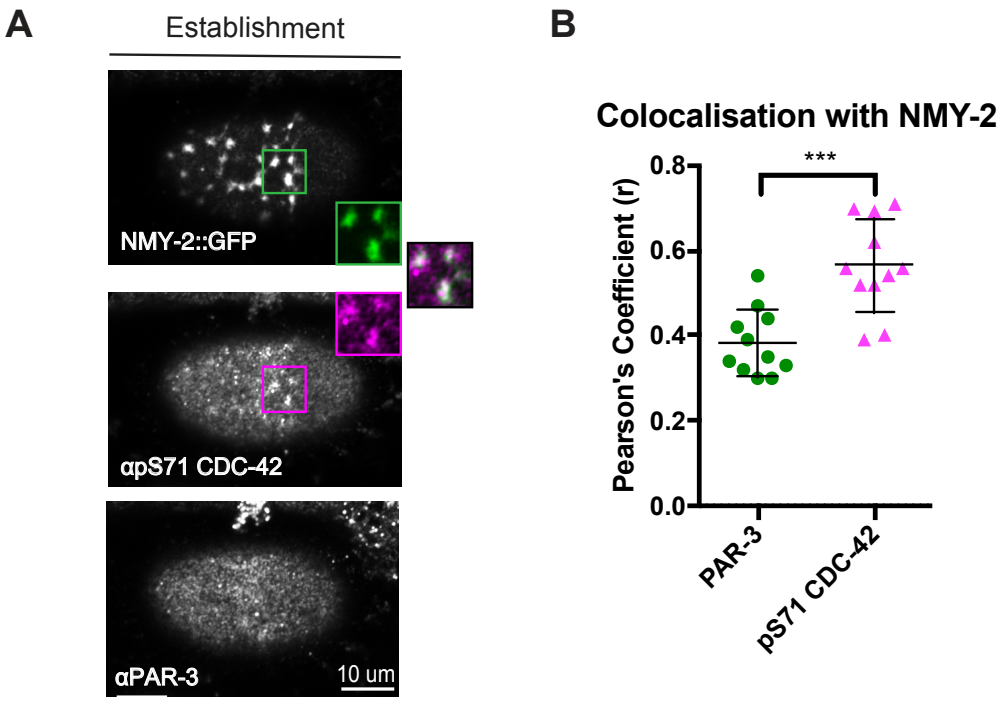

Figure 6.1. Colocalisation of pS71 CDC-42 with NMY-2. A. NMY-2::GFP (JJ1473) embryo during polarity establishment stage, stained for pS71 CDC-42 (Invitrogen, #44214G) and PAR-3 (DSHB, #P4A1), with small selections showing colocalisation of NMY-2::GFP and pS71 in the anterior domain. **B.** Analysis of colocalisation of pS71 CDC-42 and PAR-3 with NMY-2::GFP (n=11 embryos during of polarity establishment stage), as measured with Pearson's coefficient (r). pS71 CDC-42 colocalises with NMY-2::GFP more significantly than PAR-3 (which also localises in the anterior cortex) colocalises with NMY-2 (r=0.38 for PAR-3 vs r=0.56 for pS71). P=0.0002 with a t-test.

6.2.2.pS71 CDC-42 associates with actomyosin

We hypothesised that colocalisation of pS71 CDC-42 foci with NMY-2 foci could be due to two options: either phosphorylated CDC-42 localises to the actomyosin cytoskeleton, or the contraction of the actomyosin cytoskeleton into foci recruits phosphorylated CDC-42 by advection (Saha et al., 2018).

To determine if the colocalisation between pS71 CDC-42 and NMY-2 could be due to a physical interaction between the actomyosin cytoskeleton and pS71 CDC-42, we altered the structure of the actomyosin by affecting both upstream regulators of actomyosin and elements of its structure (**Figures 6.2** and **6.3** for analysis in wild type zygotes, and **Figure 6.4** for analysis in NMY-2::GFP zygotes).

First, we used the *nop-1(it142)* mutant. NOP-1 is a regulator of actin contractility that has no human orthologue, *nop-1(it142)* zygotes have no pseudocleavage (pseudocleavage is the name given to a big contraction event during polarity establishment), decreased contraction and cortical flows (Morton et al., 2012, Tse et al., 2012). The molecular mechanisms that NOP-1 is involved in are unknown, but NOP-1 is believed to be an upstream regulator of RHO during polarity establishment, as the cortical myosin and anillin that are essential for actomyosin flow are absent in *nop-1(it142)* embryos (Morton et al., 2012). We did not observe pS71 CDC-42 foci in any *nop-1(it142)* embryos during establishment stage, suggesting that pS71 CDC-42 foci depend on the actomyosin cytoskeleton (**Figure 6.2 A**).

We then silenced the RHO GEF *ect-2* (therefore decreasing the presence of RHO-GTP). *ect-2* silencing has similar phenotype to the *nop-1* mutants: NMY-2 foci are not formed, and neither are pS71 CDC-42 foci, further confirming that pS71 CDC-42 foci depend on the actomyosin cytoskeleton (**Figure 6.2 A**).

We also analysed pS71 CDC-42 upon *let-502* RNAi. Unlike the *nop-1(it142)* mutation and *ect-2* RNAi, *let-502* RNAi does not result in the complete removal of NMY-2 foci, but in disorganised and weak foci that fail to retract to anterior (**Figure 6.2 B**). In embryos treated with *let-502* RNAi we could not detect pS71 CDC-42 foci (**Figure 6.2 A**), suggesting that LET-502 could play a structural role in the formation of pS71 CDC-42 foci.

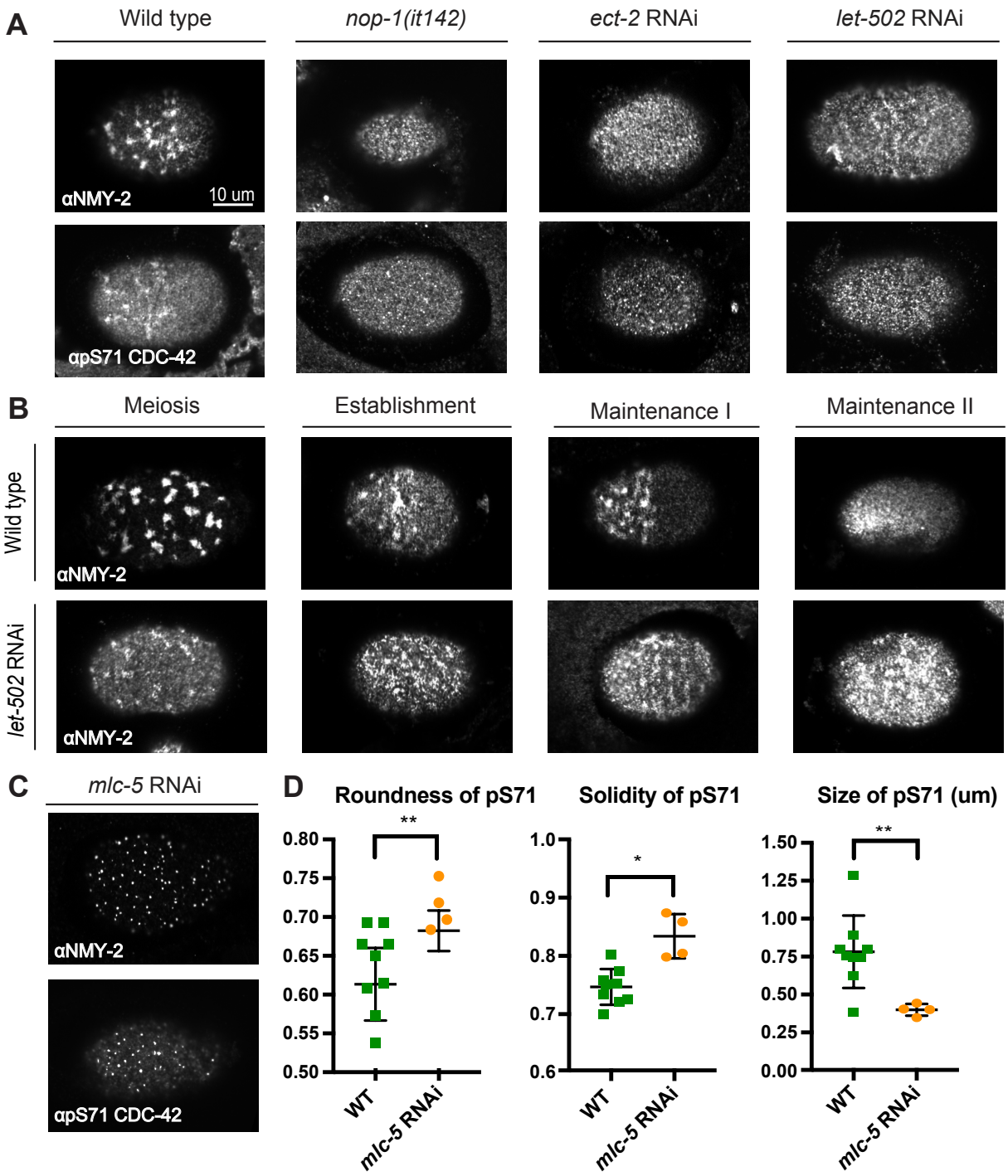

Figure 6.2. Analysis of pS71 CDC-42 association with the actomyosin network. A. Cortical images of pS71 CDC-42 (Invitrogen, #44214G) and NMY-2 staining (Pickel laboratory, #Rb20417) in wild type embryos, *nop-1(it142)* mutants, *ect-2* RNAi and *let-502* RNAi during polarity establishment. pS71 foci are only visible in wild type embryos. NMY-2 foci are visible in wild type embryos, and weakly in embryos treated with RNAi against *let-502*. **B.** Examples of NMY-2 organisation in wild type embryos and embryos treated with *let-502* RNAi throughout the cell cycle, as seen with NMY-2 staining. **C-D**. Silencing the myosin esential chain (*mlc-5*) leads to changes in NMY-2 structure. These changes are mirrored by changes in pS71 CDC-42 punctae, which become more round, solid/compact and smaller.

We also silenced *mlc-5* (**Figure 6.2 C-D**), the orthologue of the essential myosin light chain (ELC). MLC-5 can bind to NMY-2 and the regulatory myosin light chain (MLC-4 in *C. elegans*, or RLC in humans) and is necessary for actomyosin contraction. As previously reported (Fievet et al., 2013), silencing *mlc-5* results in small actomyosin punctae (small and round) that fail to retract effectively to the anterior. We found that when NMY-2 foci were turned into punctae structures by removing *mlc-5* with RNAi, pS71 CDC-42 structure changed as well (with foci becoing smaller, more compact and rounder punctae (**Figure 6.2D**)), indicating that phosphorylated CDC-42 interacts with the actomyosin foci and follows changes in its structure, and that pS71 CDC-42 can be recruited to foci without advection (given the lack of NMY-2 contractility in *mlc-5* knockdown (Fievet et al., 2013).

Finally, we analysed pS71 CDC-42 in the *act-2(ts)* mutant (**Figure 6.3**), which carries a mutation in the serine 14 (S14A) of Actin-2 (Willis et al., 2006). This aminoacid has been linked to the ATP binding and hydrolysing properties of Actin-2 (Sablin et al., 2002, Vorobiev et al., 2003). This mutation results in zygotes that display excessive cortical actomyosin contractility and in which actin forms large and dense patches of actin filaments (Munro et al.,

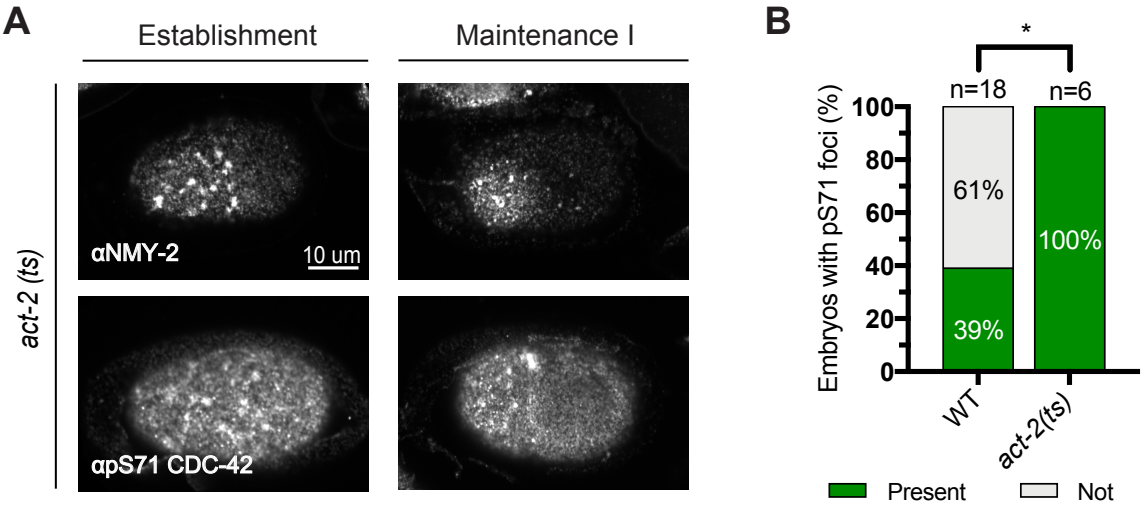

Figure 6.3. Effect of *act-2(ts)* in pS71 CDC-42 foci. A. NMY-2 (Pickel laboratory, #Rb20417) and pS71 (Invitrogen, #44214G) staining in *act-2(ts)* embryos. **B.** Comparison of pS71 CDC-42 presence at Maintenance I stage (when the pronuclei meet) in wild type embryos and embryos of the *act-2(ts)* background. All analysed embryos of the *act-2(ts)* background (n=6) have visible foci during Maintenance I, as opposed to 39% of wild type embryos (n=18). Difference is significant (P=0.0163) with a Fisher's exact test.

2004, Willis et al., 2006). We found that in the *act-2(ts)* mutant, both NMY-2 and pS71 CDC-42 foci were present in all embryos of early polarity maintenance stages (Maintenance I, when the pronuclei meet), whereas in wild type embryos pS71 CDC-42 is only present in 39% of embryos at this stage (P=0.0163 with a Fisher's exact tests). Further showing that pS71 CDC-42 foci depends on the actomyosin network.

In all cases, the structure of the pS71 CDC-42 foci changed in a way that reflected the changes in actomyosin structure and dynamics, indicating that phosphorylated CDC-42 interacts with the actomyosin cytoskeleton. To confirm that the changes observed with those RNAis treatments were truly a reflection of pS71 CDC-42 association with the actomyosin cytoskeleton, we performed the same RNAi silencing experiments in embryos expressing NMY-2::GFP, to analyse NMY-2 and pS71 CDC-42 foci in the same zygote (**Figure 6.4**).

These images confirmed that the pS71 punctae observed upon *mlc-5* RNAi showed very high levels of colocalisation with NMY-2::GFP (**Figure 6.4 A-B**), further proving that changing the structure of the actomyosin cytoskeleton affects the structure of pS71 CDC-42 foci. Furthermore, and as observed in wild type background zygotes, silencing *ect-2* and *let-502* resulted in lack of pS71 CDC-42 punctae (**Figure 6.4 A**). In the case of *ect-2* RNAi, the lack of pS71 CDC-42 foci is probably due to the lack of NMY-2 foci.

In the case of *let-502* RNAi, on the other hand, our results suggest that LET-502 might play a key structural role for pS71 CDC-42 in the actomyosin cytoskeleton. However, and given that *let-502* RNAi disrupts the organisation of NMY-2 foci (**Figure 6.2 B**), we cannot rule out that this disorganisation could lead to the defects we see in pS71 CDC-42 staining.

6.2.3.Phosphorylation of CDC-42 regulates the structure of the actomyosin cytoskeleton

Given that pS71 CDC-42 seemed to be a component of the actomyosin network, and that the CDC-42(S71E)::GFP mutant showed decreased PAR-3 retraction, we analysed the structure of NMY-2 in the CDC-42(S71)::GFP and CDC-42(S71E)::GFP strains, to determine if the phosphorylation of S71 could affect actomyosin structure and flow. Once again, endogenous *cdc-42* was silenced using RNAi against the *3' utr* of the *cdc-42* gene.

Actomyosin organisation, as seen from NMY-2 staining, was not affected in CDC-42(S71)::GFP treated with *3' utr* RNAi, with foci being visible and retracting during polarity establishment (**Figure 6.5**). The phosphomimetic CDC-42(S71E)::GFP, however, showed a significantly different phenotype, with smaller and more compact/solid NMY-2. This foci were reminiscent of the NMY-2 foci visible upon *mlc-5* RNAi, although foci in embryos treated with *mlc-5* RNAi are round (See **Figure 6.2 C-D**), and foci in this phosphomimetic CDC-42(S71E)::GFP strain are not. Suggesting that this phosphorylation site

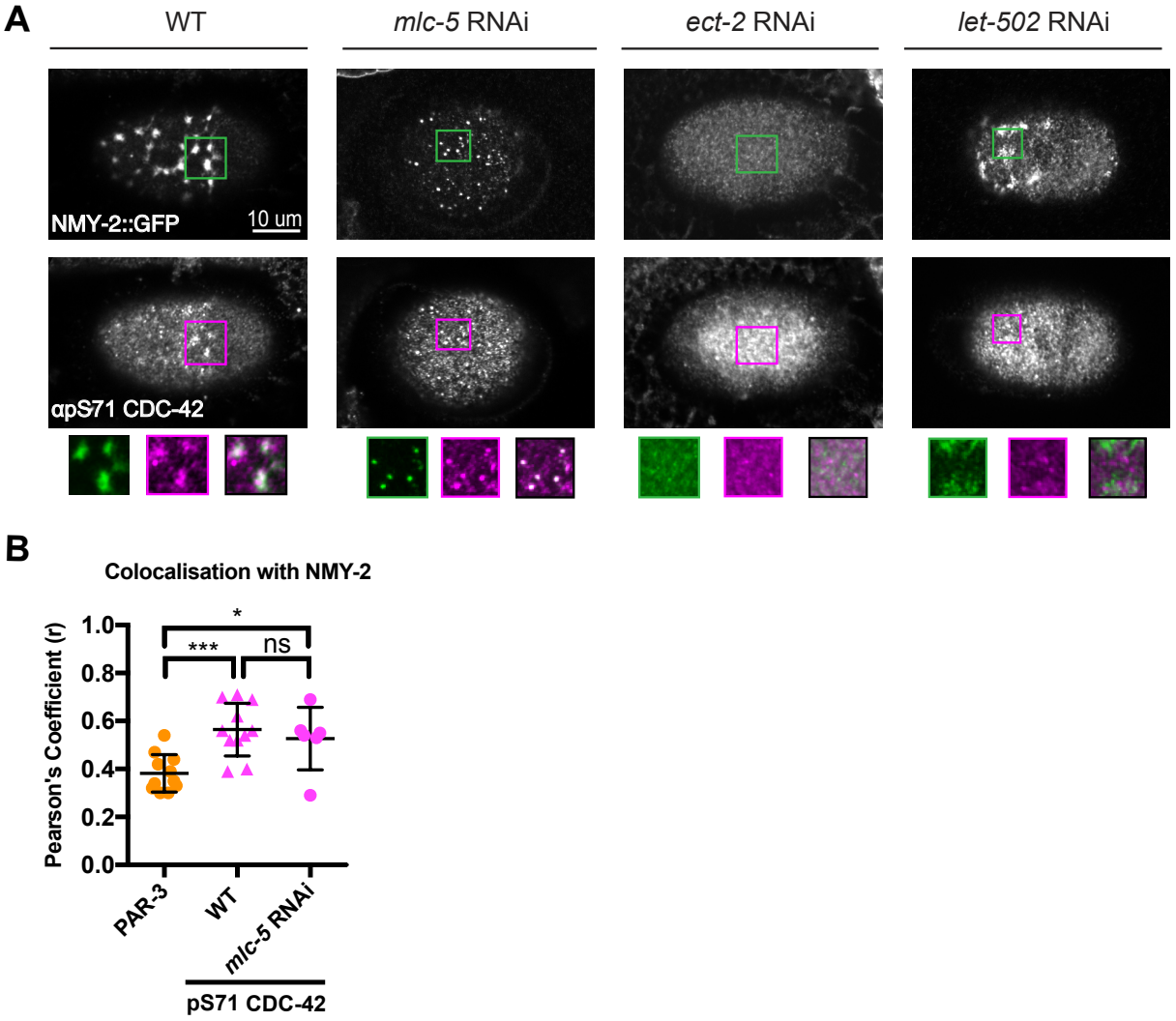

Figure 6.4. Colocalisation analysis of pS71 CDC-42 with actomyosin under different RNAi conditions. A. Cortical images of pS71 CDC-42 (Invitrogen, #44214G) and NMY-2::GFP (JJ1473) in the same embryo, in wild type (NMY-2::GFP) embryos and in embryos of the same strain treated with RNAi against the myosin esential chain (*mlc-5*), the RHO GAP *ect-2* and the RHO kinase *let-502*. **B.** pS71 CDC-42 colocalises with NMY-2::GFP during polarity establishment. Colocalisation of pS71 with NMY2 upon *mlc-5* RNAi is not affected.

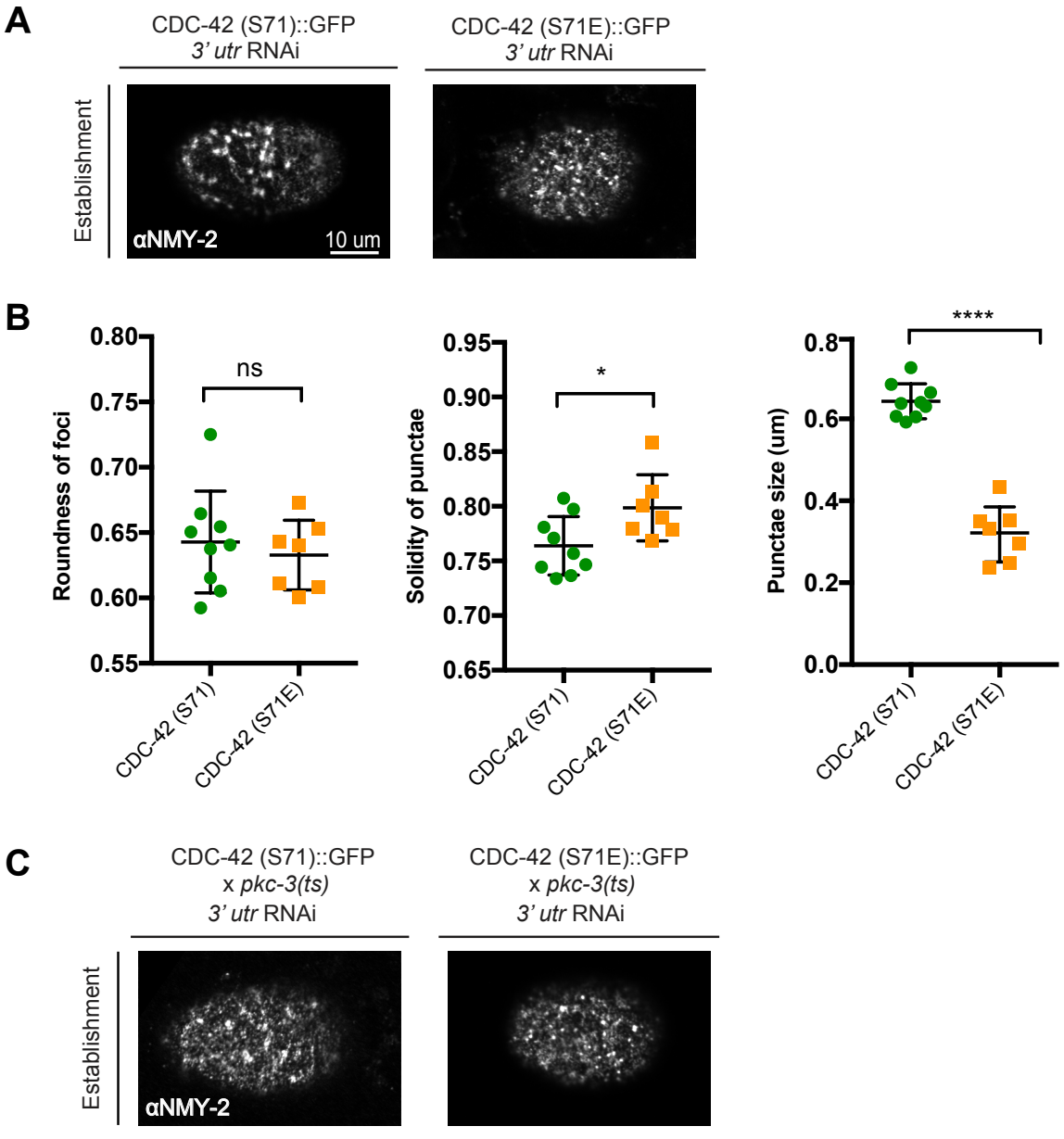

Figure 6.5. Analysis of the effect of CDC-42 S71 mutations on actomyosin structure. A. Immunofluorescent stainings of NMY-2 (Pickel laboratories, #Rb20417) in CDC-42(S71)::GFP and CDC-42(S71E)::GFP strains, endogenous *cdc-42* has been silenced with *3'utr* RNAi . **B.** Analysis of NMY-2 foci structure during establishment in CDC-42(S71):GFP embryos and the phosphomimetic CDC-42(S71E)::GFP embryos, treated with RNAi agains the endogenous *3'utr* of the *cdc-42* gene. The NMY-2 foci look more solid (0.7638 vs 0.7986, with P=0.0336) and smaller (0.6429 vs 0.3215, with P<0.0001). The foci are not significantly different in shape, as measured by roundness (0.6428 vs 0.6328, with P=0.5529). Note that each dot in the graph represents the average value for all the foci of each embryo. Statistical significance determined with t-tests for all three graphs. **C.** Immunofluorescent stainings of NMY-2 in CDC-42(S71)::GFP and CDC-42(S71E)::GFP strains crossed to *pkc-3(ts)*, endogenous *cdc-42* has been silenced with *3'utr* RNAi.

plays a role in regulating the contraction/disassembly cycles of actomyosin foci.

We also analysed NMY-2 structure in the CDC-42(S71)::GFP mutant embryos crossed with *pkc-3(ts)* and in which the endogenous *cdc-42* had been silenced with a *3'utr* RNAi. Even though NMY-2 retained the weak and disorganised aspect characteristic of *pkc-3(ts)* embryos, the CDC-42(S71E)::GFP cross retained the smaller and compact punctae (**Figure 6.5 C**), indicating CDC-42(S71E)::GFP leads to changes in NMY-2 structure regardless of other pathways regulated by PKC-3 activity.

6.2.4.Epistatic analysis of LET-502 and PKC-3

As described in **Section 6.2.2**, we had observed that silencing *let-502* RNAi removed pS71 CDC-42 foci despite the fact that it does not completely remove NMY-2 foci. Given that in every other RNAi condition pS71 seemed to follow NMY-2 structure very closely, we decided to use mutants of the kinases LET-502 and PKC-3 to perform epistatic analysis and increase our understanding of the interactions between LET-502, PKC-3 and pS71 CDC-42 (**Figure 6.6**).

To do this analysis, we used *rga-3/4* RNAi to increase the activity of LET-502, and *chin-1* RNAi to increase the activity of PKC-3 by promoting GTP-bound CDC-42, combined with temperature sensitive strains of each kinase, *pkc-3(ts)* and *let-502(ts)*. The *let-502(ts)* strain carries a missense mutation in an R residue of LET-502's catalytic domain, that results in a strong loss of function phenotype at 25° C (Diogon et al., 2007, Martin et al., 2016), which can be rescued by phosphomimetic mutations of its targets (Shimizu et al. 2018).

If LET-502 were phosphorylating CDC-42, increasing LET-502 activity with *rga-3/4* RNAi in the *pkc-3(ts)* mutant would result in stronger pS71 CDC-42 foci, or a higher number of zygotes presenting foci; and increasing PKC-3 activity with *chin-1* RNAi in the *let-502(ts)* mutant would show no pS71 foci or weaker foci. Whereas if PKC-3 were phosphorylating CDC-42, increasing PKC-3 activity with *chin-1* RNAi in the *let-502(ts)* mutant would show increased levels of phosphorylation whereas increasing LET-502 activity with *rga-3/4* RNAi in the *pkc-3(ts)* mutant would still show no pS71 CDC-42 foci.

To perform this analysis we looked at embryos of both meiosis and establishment stages, as these are the stages in which pS71 is more strongly visible (with 60% of the wild type

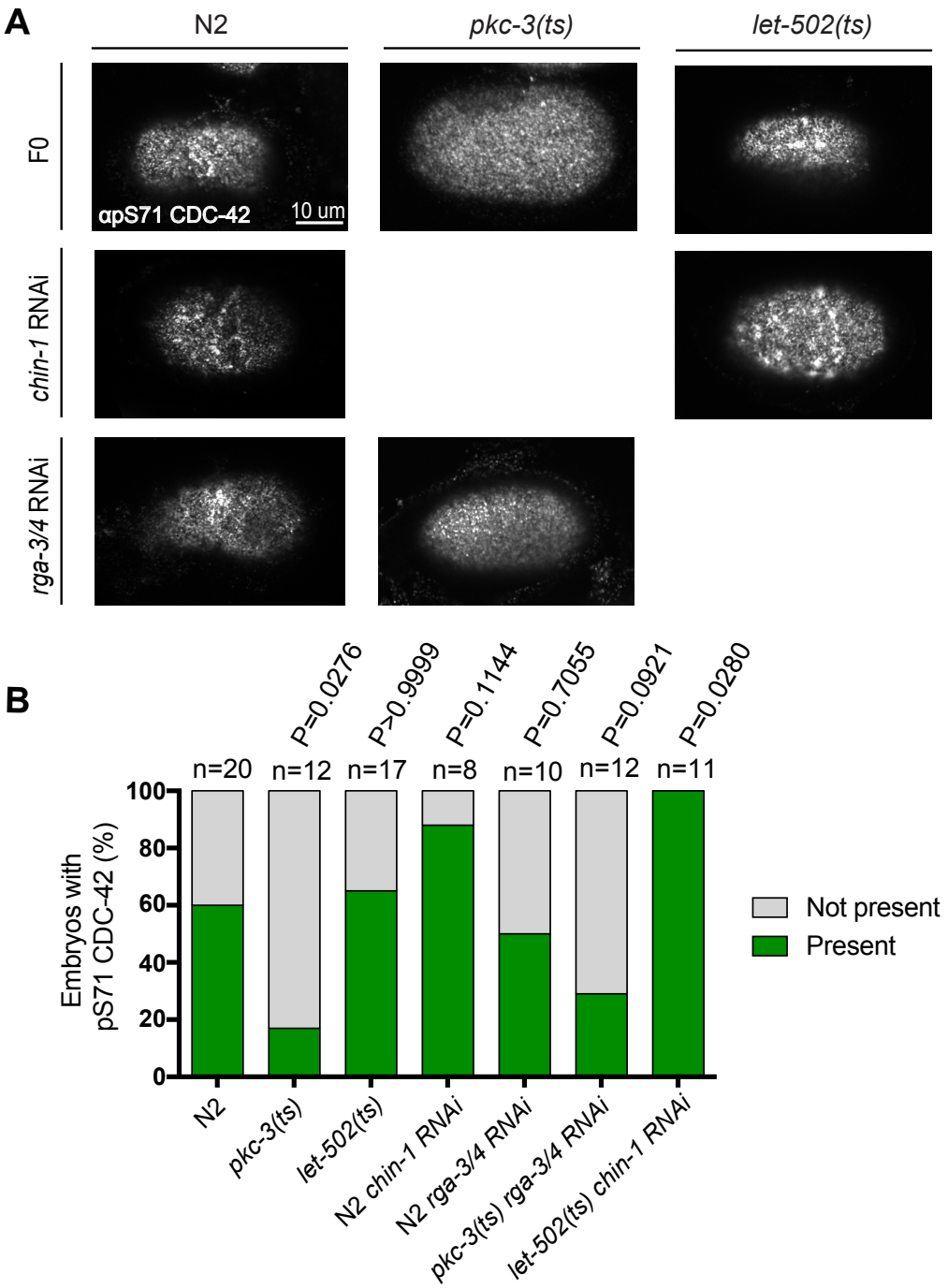

Figure 6.6. Epistatic analysis of the effec of PKC-3 and LET-502 on the phosphorylation of CDC-42 in its S71. A. Epistatic analysis to determine if LET-502 or PKC-3 phosphorylate CDC-42. All images shown are of establishment stage. **B.** During establishment and meiosis stages, 60% of wild type embryos (n=15) showed pS71 CDC-42 foci. This was significantly different to embryos of the *pkc-3(ts)* background (n=6, P=0.0276) and embryos of *let-502(ts)* background treated with *chin-1* RNAi (n=11, P=0.0280). The difference was not significant in *let-502(ts)* embryos (n=17, P<0.9999), or embryos treated with *rga-3/4* RNAi (n=5, P=0.7055). Embryos treated with *chin-1* RNAi (n=8, P=0.1144) and *pkc-3(ts)* treated with *rga-3/4* RNAi (n=12, P=0.0921) had P values that were small, but not significantly different from wild type embryos. All statistical significances checked with Fisher's exact tests.

embryos of this assay presenting pS71 CDC-42). Surprisingly, *let-502(ts)* did not result in any significant difference in pS71 CDC-42 presence (65%, P>0.9999) with a Fisher's exact tests), indicating that the kinase activity of LET-502 is not necessary for pS71 CDC-42 (see **Figure 6.6 B** for n values). Furthermore, increasing LET-502 activity with *rga-3/4* RNAi did not increase the number of embryos presenting pS71 punctae (50%, P=0.7055), further indicating that LET-502 activity does not regulate pS71 CDC-42. Lastly, increasing LET-502 activity with *rga-3/4* RNAi in *pkc-3(ts)* embryos still resulted in a predominately *pkc-3(ts)* phenotype, with only 33% of embryos showing pS71 CDC-42 (although this percentage is not significantly different to wild type embryos, P=0.0921).

On the other hand, lack of PKC-3 activity (*pkc-3(ts)* embryos) did decrease the number of embryos presenting pS71 CDC-42, as presented in the previous chapter (17%, P=0.0276), and increasing PKC-3 activity with *chin-1* RNAi increased the number of embryos presenting pS71 CDC-42 (88%, although the difference is not significant, P=0.1144). Lastly, increasing PKC-3 activity in the absence of active LET-502, by doing *chin-1* RNAi in *let-502(ts)* embryos, resulted in a significant increase in the number of embryos presenting pS71 CDC-42 (100%, P=0.0280). The difference between *chin-1* RNAi and *chin-1* RNAi in *let-502(ts)* was not significant P=0.421). All these results confirm that PKC-3, and not LET-502, phosphorylates CDC-42.

We hypothesised that LET-502 might play a structural role in the actomyosin cytoskeleton, and that presence of LET-502, but not it's kinase activity, were necessary for pS71 CDC-42 foci. To confirm this we imaged pS71 CDC-42 in embryos treated with *let-502* RNAi and embryos of the kinase mutant *let-502(ts)* (**Figure 6.7 A-B**): *let-502* RNAi resulted in a significantly lower number of embryos presenting pS71 foci (17% in *let-502* RNAi vs 86% in wild type embryos, P=0.0054 with a Fisher's exact tests), whereas *let-502(ts)* did not show a significant difference with wild type embryos (92% in *let-502(ts)* vs 86% in wild type embryos, P>0.9999 with a Fisher's exact tests).

We hypothesised that LET-502 played a structural role in the actomyosin cytoskeleton beyond its ability to phosphorylate MLC-4, and that this role was not affected in the temperature sensitive mutant *let-502(ts)*. To confirm if LET-502 could play a structural role key for NMY-2 structure, we stained embryos with a NMY-2 antibody (**Figure 6.7 A** and **C**). Wild

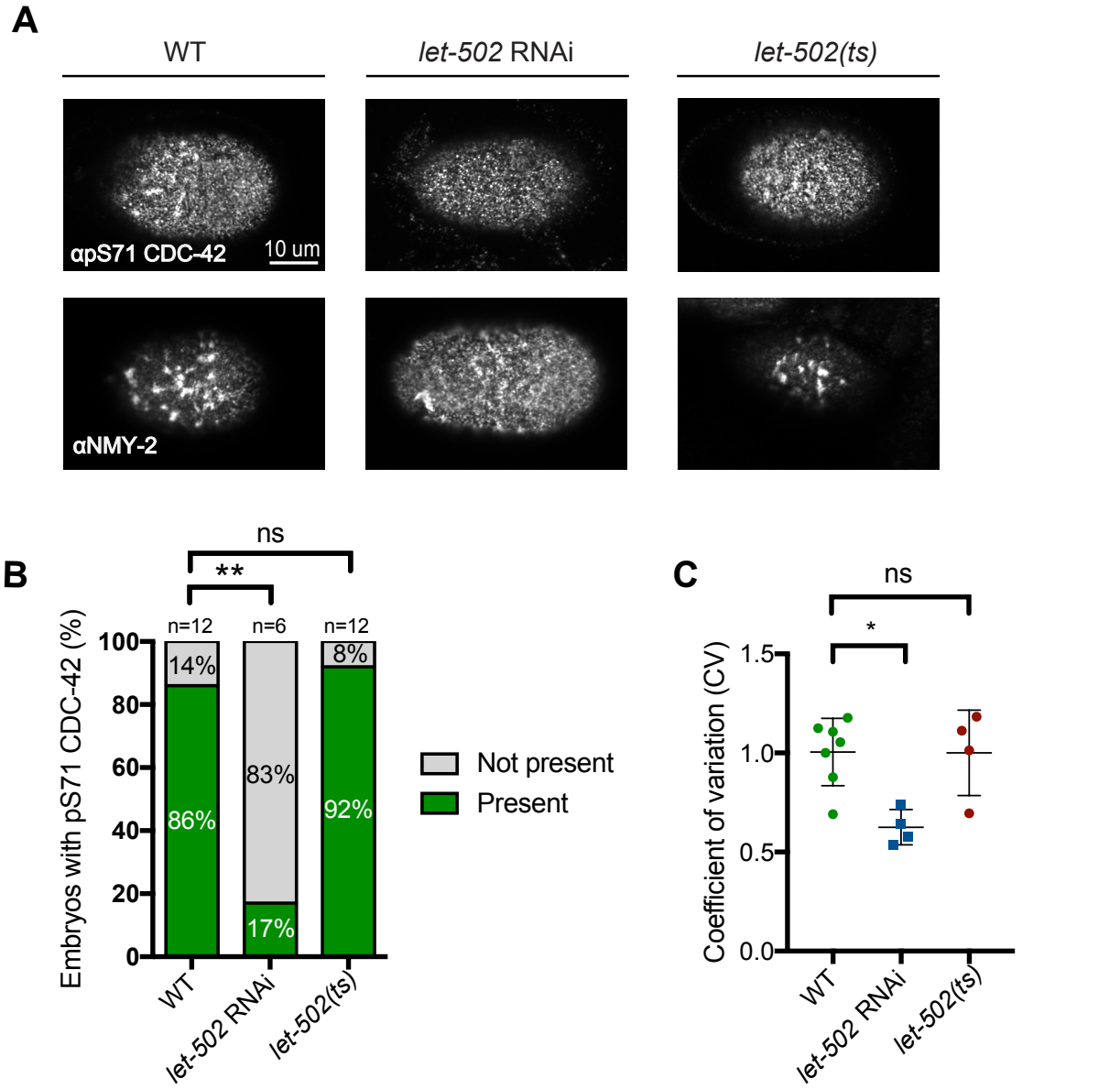

Figure 6.7. Immunofluorescent stainings of pS71 CDC-42 and NMY-2 foci in embryos of *let-502(ts)* strain and embryos treated with *let-502* RNAi. A. Immunofluorescent stainings of pS71 CDC-42 (Invitrogen, #44214G) and NMY-2 (Pickel laboratory, #Rb20417) in embryos during establishment. Images of wild type embryos, embryos treated with *let-502* RNAi and the temperature sensitive kinase mutant *let-502(ts)* at the restrictive temperature. **B.** The percentage of embryos showing pS71 CDC-42 foci during establishment in *let-502* RNAi embryos is significantly smaller than in wild type embryos (P=0.0054, Fisher's exact test). *let-502(ts)* have pS71 CDC-42 foci to a similar rate than the control embryos. **C.** Coefficient of variation of NMY-2 during establishment in wild type embryos, embryos treated with *let-502* RNAi and the temperature sensitive kinase mutant *let-502(ts)*. Values normalised so that wild type CV is 1.00. *let-502* RNAi results in an average CV value of 0.62, significantly lower than wild type (P=0.0381, Kruskal-Wallis test). *let-502(ts)* does not have a significantly different CV value than wild type embryos (CV=1.00, P>0.999, Kruskal-Wallis test).

type embryos and *let-502(ts)* embryos showed very clear and well defined NMY-2 foci during polarity establishment, with no significantly different CV values (P>0.999, Kruskal-Wallis test). In embryos treated with *let-502* RNAi the foci were less clear, and the network seemed disorganised, with a significantly lower CV value than wild type embryos (P=0.0381, Kruskal-Wallis test). These results further suggest that LET-502 plays a structural role in actomyosin organisation beyond its role in phosphorylating MLC-4.

6.2.5.LET-502 regulates aPARs and favours the CDC-42 bound complex

Another result we noticed when analysing *let-502(ts)* embryos and embryos treated with *let-502* RNAi was an apparent change in expansion of PKC-3 from the PAR-3 boundary (**Figure 6.8 A-C**). As mentioned in the introduction, the LET-502 orthologue ROCK has been reported to phosphorylate PAR-3 in four different residues (S827, S829, T833 and S837) in human migrating cells, inhibiting the interaction between PAR-3 and PAR-6/aPKC (Nakayama et al., 2008). In *C. elegans* PKC-3 has been reported to phosphorylate the only two of these residues that are conserved (S827 and S829) *in vitro* (Li et al., 2010a). However our analysis of *pkc-3(ts)* embryos (Rodriguez et al., 2017) suggests that this result may not correspond to what happens *in vivo,* as lack of *pkc-3* activity leads to PKC-3 expansion from PAR-3, instead of to PKC-3 localising with PAR-3.

To determine if LET-502 could be phosphorylating PAR-3 and favouring the CDC-42 complex in the *C. elegans* zygote, as it does in migrating cells, we analysed the localisation of the anterior PAR-3 and PKC-3 by immunofluorescence assays, as proxy for the PAR-3 dependant anterior complex and the CDC-42 dependent anterior complex, respectively (**Figure 6.8 A**). To avoid bias, the results were analysed with a MATLAB script, as described in Rodriguez et al. (2017).

In wild type embryos PAR-3 retracted to 45% of the cell membrane, with PKC-3 expanding a little bit and taking up 51% of the cell (an average expansion of 6% of the cell, significant P=0.0220) (**Figure 6.8 B**). In both *let-502(ts)* and *let-502* RNAi embryos PKC-3 did not expand as much form the PAR-3 complex as it does in wild type: in embryos treated with *let-502* RNAi this difference was less pronounced, with PAR-3 taking up 61% of the cell and

PKC-3 taking up 65% of the cell (an average expansion of 4%, not significant, P=0.4828), and in *let-502(ts)* embryos most embryos did not show any expansion of PKC-3 from the PAR-3 domain (with PAR-3 taking up 52% of the cell and PKC-3 51%, P=0.7175) (**Figure 6.8 B**). The difference in retraction in each embryo can be seen in **Figure 6.8 C**, with the slopes representing expansion of each embryo. Representative examples of each genotype can be seen in **Figure 6.8 A**.

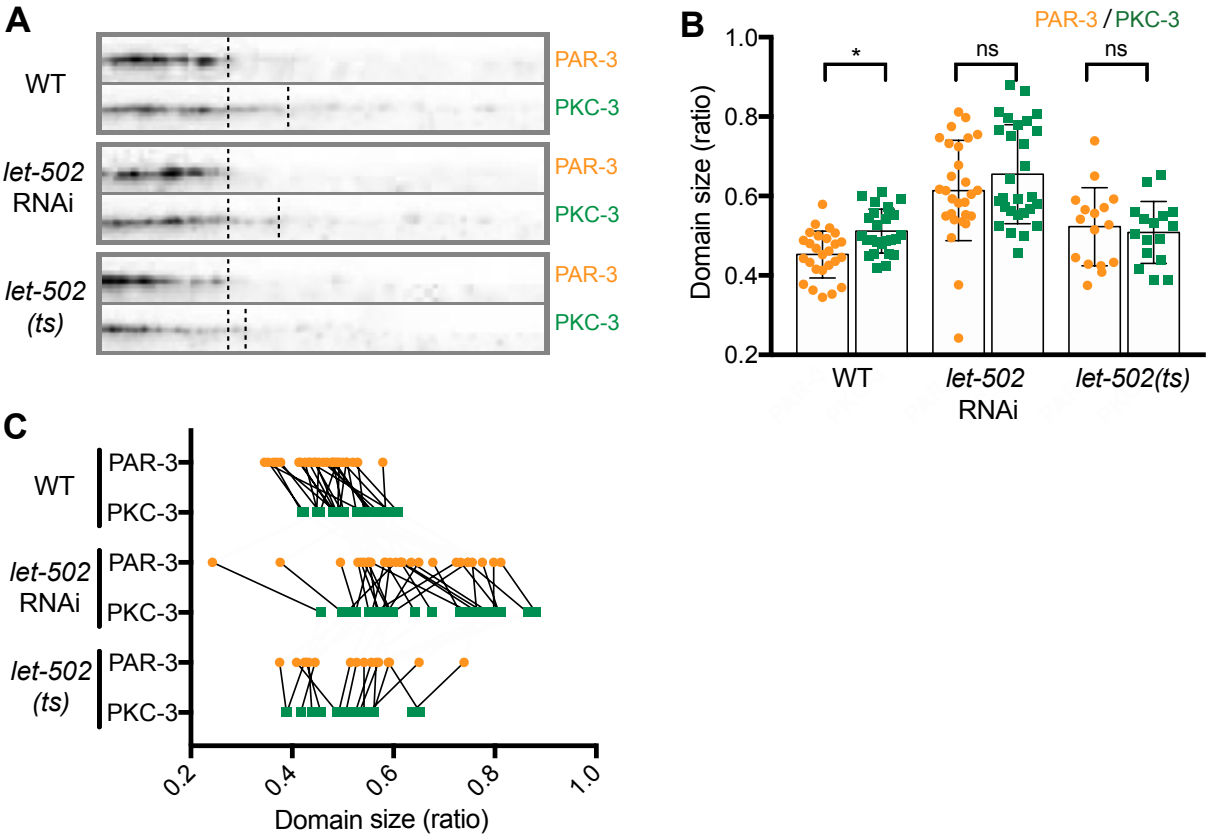

Figure 6.8. Analysis of LET-502 regulation of anterior PARs PAR-3 and PKC-3. A. Close up view of the boundary region showing PAR-3 (DSHB, #P4A1) and PKC-3 (Tabuse et al, 1998) staining for one representative zygote for wild type, *let-502* RNAi and *let-502(ts)* backgrounds. The dashed line represents the limit of the PAR-3 and PKC-3 domains. **B.** Ratio of the embryo cortex with PAR-3 (in red circles) and PKC-3 (in green squares) during polarity maintenance stage. PAR-3 and PKC-3 have a significant difference in their boundaries in wild type embryos (n=26, P=0.022 with a Kruskal Wallis Test), where PAR-3 covers 45% of the embryo and PKC-3 covers 51% of the embryo, but not in *let-502* RNAi (n=28, P=0.483) or *let-502(ts)* embryos (n=16, P=0.718). **C.** Representation of all boundaries between PAR-3 and PKC-3, shown as the domain size of PAR-3 and PKC-3 in each embryo linked with a black line. A vertical line indicates a match between both boundaries, a tilt indicates a difference in PAR-3 and PKC-3 domains. Wild type embryos show a difference (in the form of a tilt) between PAR-3 and PKC-3, indicating an extension of the PKC-3 domain vs the PAR-3 domain. In *let-502* RNAi and *let-502(ts)* embryos this tilt is affected.

These results indicate that, as reported in migrating cells, LET-502 can regulate the interaction between PAR-3 and PAR-6/PKC-3 in the *C. elegans* zygote, as it does in migrating cells (Nakayama et al., 2008). Furthermore, the increased size of the PAR-3 domain observed in *let-502* RNAi (compared to *let-502(ts)* embryos) further indicates that LET-502 plays a structural role in the actomyosin network, beyond its role as a kinase in phosphorylating MLC-4 or other targets.

6.3. Discussion

6.3.1. Phosphorylated CDC-42 associates with the actomyosin cytoskeleton

pS71 CDC-42 foci colocalise with actomyosin foci (**Figure 6.1 B** and **6.4 B**). To understand the association between pS71 CDC-42 and the actomyosin cytoskeleton we affected the structure of the actomyosin cytoskeleton by silencing upstream regulators of actomyosin (such as *nop-1* and *ect-2*) and components of the foci (*mlc-5*) (**Figure 6.2 A, C and D**).

Our results showed that both removing NMY-2 punctae or changing its structure affected the structure of the pS71 CDC-42 foci, and that the enrichment of pS71 CDC-42 in foci was not due to advection into the NMY-2 clusters, as silencing of *mlc-5* with RNAi, which results in small NMY-2 clusters that cannot contract or dissolve, showed perfect colocalisation with pS71 CDC-42 punctae (**Figure 6.2 D**)..

Furthermore, we analysed the hyperactive *act-2(ts)* strain (**Figure 6.3**), in which Actin-2 carries a mutation in the serine 14 (S14A) (Willis et al., 2006), resulting in increased ATP binding and hydrolysis activity (Sablin et al., 2002, Vorobiev et al., 2003). In embryos of this strain NMY-2 foci persist longer in time and are still present in all embryos of the early polarity maintenance stage, and similarly, pS71 CDC-42 foci were also visible in all embryos of polarity maintenance stage of this strain.

These results indicate that increasing actomyosin foci/activity also results in an increase in pS71 CDC-42 colocalisation in this foci. All in all, these results indicate that pS71 CDC-42 depends on the actomyosin cytoskeleton.

Given that the CDC-42 S71E mutation promotes the dissociation of the CDC-42/PAR-3/ aPKC complex (See **Chapter 5**), phosphorylation of CDC-42 could be generating a pool of

CDC-42 that is independent from other anterior PARs and can interact with NMY-2 and regulates its organisation. Interestingly another aPKC substrate, Miranda, has been shown to require aPKC phosphorylation to change localisation and interact with actomyosin in the Drosophila neuroblasts (Hannaford et al., 2018). Our results, together with those reported by Hannaford *et al*.'s suggest that aPKC phosphorylation might be a way of targeting proteins to the actomyosin cytoskeleton.

6.3.2.The structural role of LET-502 is essential for CDC-42 localisation

The only case in which NMY-2 and pS71 CDC-42 structures did not completely match up was that of *let-502* RNAi (**Figure 6.4 A**), in which NMY-2 foci are weak and disorganised, and pS71 CDC-42 foci are gone. This suggested three options: 1) LET-502 could be phosphorylating CDC-42, 2) the role of LET-502 in regulating anterior PARs could affect the presence of the CDC-42/PKC-3 complex, and therefore affect the levels of aPKC and the rate of CDC-42 phosphorylation, or 3) that LET-502 played a structural role in the actomyosin cytoskeleton that was key for CDC-42 foci to form.

To uncover the role of LET-502 in regulating anterior PARs and the pS71 CDC-42 mutation, we employed the temperature sensitive mutant *let-502(ts)* (**Figure 6.6** and **6.7**). This strain carries a missense mutation in an R residue of the catalytic domain (Diogon et al., 2007). Even though this mutation does not completely remove LET-502 activity, it does have strong loss of function phenotype at 25 °C (Martin et al., 2016), and affects LET-502 phosphorylation of downstream targets in the actomyosin network. Phosphomimetic mutations of its target MLC-4 (in T17D and S18D), for example, rescue axon regeneration defects of the *let-502(ts)* mutant (Shimizu et al., 2018)*;* and *let-502(ts)* embryos have been reported to have decreased actomyosin tension on adherent junctions (Vuong-Brender et al., 2018).

Since we did not observe any decreases in pS71 CDC-42 foci presence during establishment in embryos of *let-502(ts)*, we discarded the hypothesis that LET-502 could be phosphorylating the S71 of CDC-42 (**Figure 6.7 B**). This is further supported by our analysis of pS71 CDC-42 foci in embryos treated with *rga-3/4* RNAi: if LET-502 were phosphorylating CDC-42, we would expect to see an increase in the presence of pS71 CDC-42 foci in embryos treated with

rga-3/4 RNAi, however, we did not observe any changes in pS71 CDC-42 foci presence in this RNAi treatment (**Figure 6.6 B**).

Furthermore, since we found that in both *let-502(ts)* and *let-502* RNAi embryos the PAR-3/ PAR-6/PKC-3 complex is favoured against the CDC-42/PAR-6/PKC-3 complex (**Figure 6.8 A-C**), we discarded the hypothesis that LET-502 could be favouring aPKC activity by favouring the CDC-42/PAR-6/PKC-3 complex.

The difference in NMY-2 structure in *let-502* RNAi and *let-502(ts)*, combined with the fact that *let-502* RNAi also results in less PAR-3 retraction than *let-502(ts)*, indicates that removing LET-502, affects both the structure of actomyosin and actomyosin flow, far more than removing the kinase activity of LET-502 does, and pointing to a structural role for the protein LET-502 in actomyosin organisation.

6.3.3.Phosphorylation cycles of CDC-42 regulate actomyosin structure

The phosphomimetic CDC-42(S71E)::GFP strain showed defects in NMY-2 structure (**Figure 6.5**), with smaller and more compact/dense foci that did not retract, indicating that CDC-42 phosphorylation could play a key role in NMY-2 foci dynamics. This phenotype was reminiscent of the one observed upon *mlc-5* RNAi, although in *mlc-5* RNAi embryos the foci are also completely round and look like punctae. Given that PAR-3 retraction is also affected in this mutant (See **Chapter 5**), these results suggest that CDC-42(S71E)::GFP embryos have highly decreased actomyosin flow.

It would be interesting to analyse the phenotype of NMY-2 *in vivo* in lines expressing the CDC-42 S71 mutation, for further analysis of their effect in actomyosin dynamics, and to determine if the small/compact foci observed in the S71E mutant are due to lack of correct foci formation or a result of collapsed NMY-2 foci that fail to resolve. This kind of experiment would allow to determine, for example, if the lower dissociation of NMY-2 observed in the anterior cortex upon *par-6* RNAi is a result of changes in CDC-42's phosphorylation state (Gross et al., 2019).

CHAPTER 7. DISCUSSION AND FUTURE WORK

7.1. PAR dynamics and interactions: conserved mechanisms?

Cell polarity is an intrinsic characteristic of many cell types, and is required for the correct development and function of most animals and plants (Goldstein et al., 2007). Cell polarity can be triggered as a response to external or internal cues, which result in the asymmetric distribution of patterning proteins within the cell (Cowan and Hyman, 2004; Roth and Lynch, 2009; Yi et al. 2013a). Some of this patterning proteins, known as the PAR proteins, are not only highly conserved, but also implicated in the patterning processes of most polarised animal cells (Goldstein et al., 2007; Knobich et al., 2010): from the establishment of the anterior/posterior domains in the *C. Elegans* zygote, to the front/rear domains of migrating cells, or the apical/lateral domains of apical cells.

One of the key characteristics of PAR proteins is their adaptability and versatility: they can form different complexes, which allows them to respond to different cues, and generate different outputs (Lang et al., 2017; Peglion et al., 2019; Gubieda et al., 2020). Despite being able to form organise complexes and respond to different inputs, many of the mechanisms that govern PAR polarity are conserved. For example, both in the *C. elegans* zygote, in epithelial cells and in *Drosphila* neuroblasts, PAR-3 can act as a 'landmark' and recruit other PAR proteins (Rodriguez et al., 2017; Lang et al., 2017).

The ability of PAR proteins to 'divide' their labour, with some complexes sensing the location and other complexes generating outputs, also seems to be a conserved mechanism. For example, in the worm embryo the anterior heterodimer PAR-6/PKC-3 can be found in two complexes: a PAR-3 complex that senses actomyosin flow, and a CDC-42 complex that has signalling activity (Rodriguez et al., 2017; Dickinson et al., 2017, Wang et al., 2017). Similarly, in fly neuroblasts Pins can bind competively to either Inscuteable or Mud, leading to a complex that can 'sense' its localisation, and another complex that is 'functional' (Culurgioni et al., 2011).

Lastly, interactions with other components of the cell also seem to be conserved: actomyosin contraction, for example, is key for the localisation of PAR-3 in the *C. elegans* embryo, but

also to the recruitment of the PAR-3 homologue Bazooka to the apical domain of *Drosophila* amnioserosa cells (Franke et al., 2005).

Most of the research on how the role of actomyosin contraction in polarising PAR proteins have been performed in the *C. elegans* zygote (Munro et al., 2004, Goehring et al., 2011b, Dickinson et al., 2017, Rodriguez et al., 2017, Wang et al., 2017), and so the process is relatively well understood (see Gubieda et al., 2020 for a review), however very little is known about how anterior PARs regulate the polarising flow. The results presented in this thesis have increased our understanding of this aspect of cell polarity.

7.2. PKC-3 and CDC-42 play distinct roles in regulating actomyosin flow and the organisation of the actomyosin network

Very little is known about how anterior PARs regulate actomyosin flow, despite several papers pointing to feedback mechanisms between the two: Motegi et al. (2006), for example, reported that silencing *cdc-42* results in lack of clearing of ECT-2 (the RHO GEF) from posterior at the very early stages of polarisation; Gross et al. (2019) reported that silencing *par-6* result in lower dissociation of NMY-2 in the anterior cortex; and our research group has also reported lower PAR-3 retraction and flow in the *pkc-3(ts)* kinase mutant (Rodriguez et al., 2017).

The tight link between CDC-42 and PKC-3 (with CDC-42 regulating the location and activity of PKC-3, and PKC-3 potentially also regulating the location of CDC-42) makes it difficult to isolate the role of each one of these proteins in regulating actomyosin processes such as flow or foci structure (**Figures 3.1** and **3.3**), since these processes are affected in *pkc-3(ts)* embryos, embryos treated with *pkc-3* and *cdc-42* RNAi, and embryos of the CDC-42(S71E)::GFP strain. However the data presented in this thesis shows that CDC-42 and PKC-3 play some distinct roles in regulating actomyosin flow and the organisation of the actomyosin network: CDC-42, for example, regulates the time of disassembly of the actomyosin network (**Figure 3.4**); while PKC-3 plays a role in regulating the RHO/LET-502 pathway (**Figure 4.2**) (See **Figure 7.1** for a working model of the results presented in this thesis).

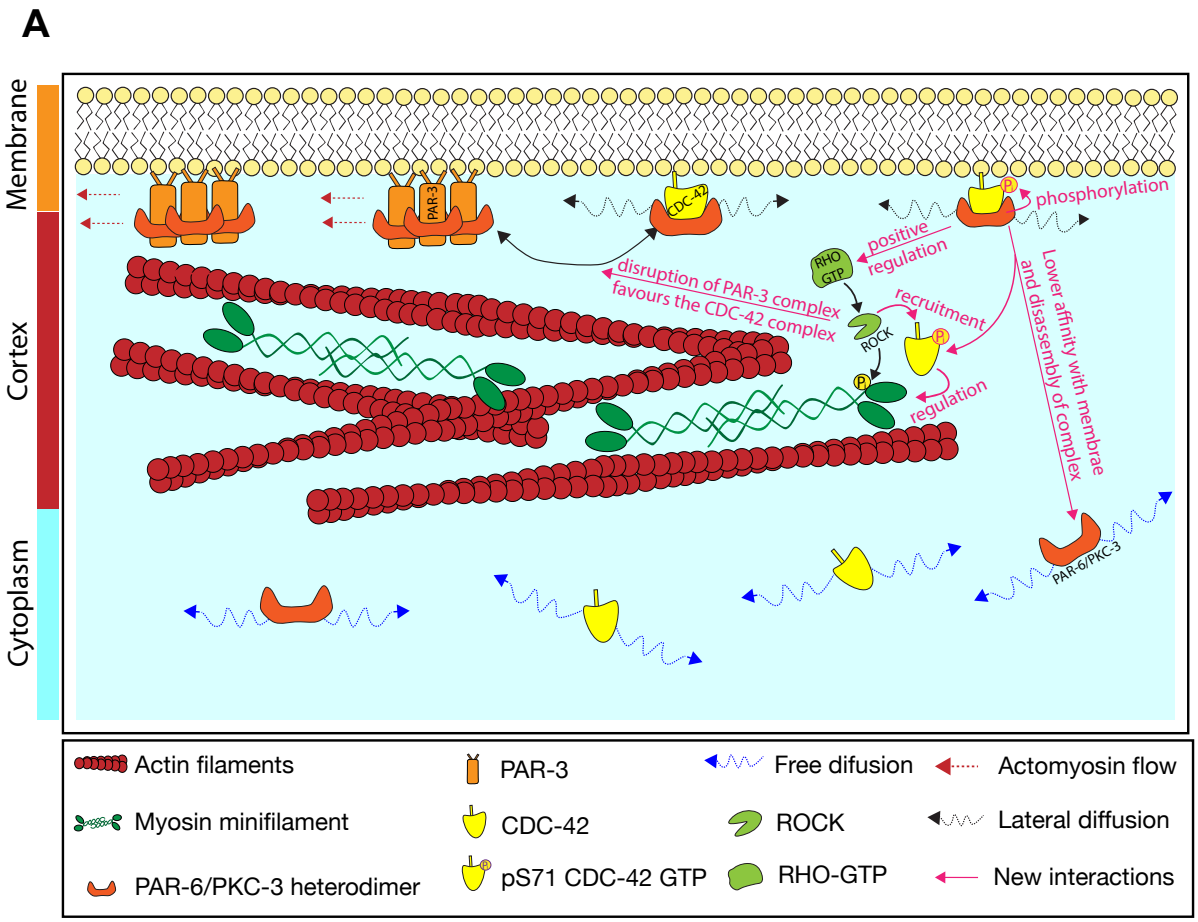

Figure 7.1 Working model. A. The interactions studied and described in this thesis are shown in pink. In the anterior domain the PAR-6/PKC-3 heterodimer can be found in two complexes: a PAR-3 dependent complex that forms oligomers and follows actomyosin flow, and a CDC-42 dependent complex that can diffuse laterally in the membrane. Actomyosin organisatoin and flow is regulated by the RHO/ROCK pathway, and we have found that the ROCK kinase can disrupt the PAR-3 dependent complex, favouring the CDC-42 dependent complex. In the CDC-42 dependent complex PKC-3 is active and can phosphorylate its downstream targets. The kinase activity of PKC-3 is required both for the correct regulation of the RHO/ROCK pathway and for phosphoryation of the serine 71 of CDC-42. Phosphorylation of CDC-42 in its S71 decreases its affinity with the membrane and results in the dissasembly of the CDC-42/PAR-6/PKC-3 complex. Phosphorylated and GTP bound CDC-42 is recruited in foci in a ROCK-dependent way. Phosphorylated CDC-42 seem to estabilise actomyosin foci, regulating foci dynamics and in turn actomyosin flow.

It has been harder to isolate the role of CDC-42 and PKC-3 in other actomyosin processes, such as in NMY-2 foci structure (**Figure 3.3 B**), where we observed visible defects in all conditions (*pkc-3(ts)*, *pkc-3* RNAi, *cdc-42* RNAi as well as in the CDC-42(S71E)::GFP mutant); or the decrease in PAR-3 retraction (also visible in all of the aforementioned conditions) (**Figure 3.2 B**). The presence of these defects in all the aforementioned conditions suggests that these defects are caused by different pathways each involving CDC-42 and/or PKC-3, or that CDC-42 and PKC-3 could be acting together (for example, via PKC-3 phosphorylation of CDC-42). Further study of pS71 CDC-42's role in the regulation of the actomyosin network and flow might clarify some of these questions in the future.

7.3. PKC-3 activates the RHO/LET-502 pathway

aPKC has previously been identified as an inhibitor of the RHO/ROCK pathway. In epithelial adherents junctions, for example, aPKC can phosphorylate ROCK (orthologue of LET-502 in mammalian cells) and inhibit its activation of Myosin II, thus protecting the epithelial apical domains from excessive constriction (Ishiuchi and Takeichi, 2011). Similar results have been reported in tubulogenesis of the *Drosophila* salivary glands, where an anistropically distributed Crumbs can recruit aPKC and in turn negatively regulate Myosin II and prevent the formation of actin cables in the areas of where Crumbs/aPKC are localised (Roper, 2012). And aPKC has also been reported to recruit Smurf1 to cellular protrusions to degrade RhoA and prevent RhoA signalling (Wang et al., 2003)

Even though the results we present in this thesis are preliminary, as we do not know how PKC-3 could be affecting RHO organisation, this is the first report of PKC-3 as an activator of the RHO/LET-502 pathway. How could PKC-3 regulate RHO activity? Regulation of small GTPases is complex, with several GAPs and GEFs regulating their activity, and many more proteins regulating the interaction between the small GTPase and its GAPs/GEFs (Marjoram et al., 2014, Choi et al., 2020).

In the discussion of **Chapter 4** we suggest a few pathways in which aPKC could be involved, such as direct phosphorylation of the GTPAse RHO in S188, or phosphorylation of its GAP in

an integrin dependent pathway (Arthur et al., 2000, Marjoram et al., 2014, Choi et al., 2020). These are good candidates for future studies.

7.4. LET-502 regulates anterior PAR distribution

Another unexpected result was the identification of LET-502 as a regulator of anterior PAR complexes, with both *let-502* RNAi and *let-502(ts)* inhibiting the formation of the CDC-42/ PAR-6/PKC-3 complex (**Figure 6.8**).

There are two conflicting papers in this regard: on one side, ROCK has been reported to phosphorylate the S827, S829, T833 and S837 of PAR-3 in migrating cells (Nakayama et al., 2008), and phosphomimetic mutations of these sites have been reported to inhibit the interaction between PAR-3 and PAR-6/aPKC (Nakayama et al., 2008). On the other hand, in *C. elegans* PKC-3 has been reported to phosphorylate the two conserved sites (the S827 and S829 homologues, S863 and S865 in *C. elegans*) of purified PAR-3 in *in vitro* kinase assays (Li et al., 2010a); and Li et al. (2010a) report that an alanine mutation PAR-3(S863A) results in a strong PAR-3 domain while the glutamic acid mutation PAR-3(S863E) results in weaker PAR-3. Therefore even though both papers agree that phosphorylation of PAR-3 in these sites results in a disruption of the PAR-3/PAR-6/CDC-42 complex, the question remains on whether PKC-3 or LET-502 are responsible for this phosphorylation.

Our results suggest that LET-502 activity, and not PKC-3 activity, can disrupt the PAR-3/ PAR-6/PKC-3 complex and favour the CDC-42/PAR-6/PKC-3 complex (**Figure 6.8**), and thus support that the interaction reported by Nakayama et al. (2008) is conserved in the *C. elegans* zygote. Furthermore, our analysis of the *pkc-3(ts)* strain indicates that PKC-3 activity is not required for the formation of the CDC-42/PAR-6/PKC-3 complex, as the CDC-42/ PAR-6/PKC-3 complex is clearly present in this strain (**Figure 3.2 A**) (Rodriguez et al., 2017).

One likely explanation as to why Li et al. (2010a) report PKC-3 as the kinase in charge of this phosphorylation is a lack of specificity for purified PKC-3 in *in vitro* assays. However, and given the interactions between PKC-3 and LET-502 that we have reported in this thesis (with

PKC-3 being required for correct function of the RHO/LET-502 pathway), further study would be required to confirm the role of LET-502 in regulating anterior PAR organisation.

7.5. PKC-3 dependent phosphorylation of CDC-42 in S71 regulates its activity and interaction with PKC-3

Another novel result presented in this thesis is PKC-3 phosphorylation of CDC-42 on its S71 (**Chapters 5** and **6**). This phosphorylation site has been reported as a substrate for another kinase, AKT, before (Kwon et al., 2000). However our results clearly support PKC-3, and not AKT, as the kinase required for this phosphorylation in the *C. elegans* zygote.

A long debate regarding phosphorylation of S71 in CDC-42 and RAC-1 is whether this phosphorylation affects their GTPase activity and GTP binding ability, or not. Previous studies have shown mixed results in this regard: Kwon et al. (2000) showed that alanine mutations in the S71 of Rac1(S71A) decrease the GTP binding ability and GTPase activity of purified human Rac1 *in vitro*; Shoentaube et al. (2009) showed that phosphomimetic Rac1(S71E) and Cdc42(S71E) have less affinity for GTP in vitro; while Schwarz et al. (2012) reported that Cdc42(S71E) has the same GTP binding affinity as wild type Cdc42.

Our system makes this question hard to answer *in vivo*, as increasing or decreasing CDC-42 activity would also increase or decrease PKC-3 activity (and therefore, pS71 CDC-42 phosphorylation). However our analysis of the active CDC-42 reporter GFP::GBPwsp-1 (**Figure 5.11**) suggests that the pS71 foci we observe during establishment correspond to active GTP-bound CDC-42. Although we still have no answer as to whether phosphorylation of CDC-42 in S71 alters the levels of GTP binding, this could be analysed in the future by generating lines expressing both the active CDC-42 sensor and the S71 CDC-42 mutations.

Another long debate regarding this phosphorylation site is whether the presence of the phosphorylation can inhibit interactions with binding partners: Schoentaube et al. (2009) reported that phosphomimetic Rac1(S71E) and Cdc42(S71E) mutations inhibited binding to Sra-1, N-WASP, and PAK in pull-downs from epithelial cell cultures, but did not affect interaction with IQGAP1/2/3 or MRCK; whereas Schwarz et al. (2012) reported that the

Rac1(S71E) and Cdc42(S71E) mutations could bind IQGAP1/2, MRCK, and PAK's protein binding domain (PDB) in pull-downs from epithelial cell cultures, but could not bind not the full length PAK.

To answer this question we used a GFP binding nano-body carrying a lipid binding domain (PH domain) that can functionalise the nano-body by tethering it to the membrane (Rodriguez et al., 2017, Aguilar et al., 2019), which allowed us to look into the interaction of GFP reporters of CDC-42 with PKC-3 *in vivo* and at the cell stage of interest (**Figure 5.10 A-B**). Our results clearly show that the phosphomimetic CDC-42(S71E)::GFP cannot bind PKC-3 (via PAR-6), as wild type CDC-42(S71)::GFP can, in the *C. elegans* zygote. This is an interesting result, as it means that PKC-3 phosphorylation of CDC-42 could be releasing CDC-42 from its interaction with anterior PARs, and therefore freeing it to interact with other downstream effectors (**Figure 7.1**).

One of the limitation of our research, is its reliance on the pS71 CDC-42 antibody. Our Western Blot analysis suggests that the anti-pS71 CDC-42 antibody cannot identify pS71, as it was unable to recognise any specific band (**Figure 5.2 A**). However this could be due to CDC-42 being denatured in our protein extracts, or due to a very low presence of phosphorylated CDC-42 is in embryonic protein extracts. Our immunofluorescence analysis, on the other hand, strongly supports the pS71 CDC-42 antibody: as the cortical foci structures it detects are gone in embryos expressing CDC-42(S71A)::GFP (**Figure 5.3 A**). However, we cannot rule out the possibility that the alanine mutation of CDC-42 could inhibit the recruitment of a protein to the actomyosin network with a similar structure to CDC-42 (and therefore a potential target for the pS71 antibody).

Therefore, some further experiments would be required to ensure that the anti-pS71 CDC-42 antibody can detect phosphorylated CDC-42, and not a similar protein that requires phosphorylated CDC-42. Some of this experiments could include a native Western Blot, or further analysis of the active CDC-42 reporter GFP::GBPwsp-1 (**Figure 5.11**), which presents foci structures that reemble those observed for pS71 CDC-42. Furthermore, even though some preliminary analysis of other small GTPases (the *rac-1* orthologue *ced-10*) suggests that the

pS71 CDC-42 cortical structures are specific for CDC-42, further analysis whould be carried out with the small GTPase RHO-1, which has a similar domain to CDC-42 and is also known to play a role in regulating actomyosin structure. However this analysis will be complicated, as affecting RHO-1 activity or expression would also affect the actomyosin structure, which is required for pS71 foci to form.

7.6. PKC-3 phosphorylation of CDC-42 in S71 regulates its location

Besides changing its interaction with anterior PARs, we have also shown that phosphorylation of this serine changes the location of CDC-42, decreasing its association with the anterior membrane (**Figure 5.5 C**) and enriching it in actomyosin foci (**Figures 6.1** to **6.4**).

Interestingly, Hannaford et al. (2018) presented a similar mechanism of action for aPKC and Miranda in *Drosophila* neuroblast: Miranda localises uniformly across the cortex during interphase in the fly neuroblast, and is then cleared from the apical membrane during prophase by aPKC phosphorylation in its S96. After nuclear envelope breakdown, Miranda reappears asymmetrically in the basal domain, thanks to its interaction with the actomyosin cytoskeleton (although the phosphorylation state of Miranda at this stage is unclear) (Hannaford et al., 2018).

The results we present in this thesis, together with those of Hannaford et al. (2018) suggest that aPKC mediated displacement of its substrates from the membrane to allow for their interaction with the actomyosin cytoskeleton might be a conserved mechanism of action. However the mechanisms by which PKC-3 phosphorylation decreases CDC-42 levels in the anterior membrane in the *C. elegans* zygote might be different to how aPKC removes Miranda from the apical domain in neuroblasts.

aPKC phosphorylates Miranda in a BH motif (short, highly charged domain), inhibiting its ability to bind phospholipids (Bailey and Prehoda, 2015). CDC-42, however, does not have a BH domain, and phosphomimetic CDC-42(S71E)::GFP can still interact with the membrane (albeit weakly). We propose that the ability of CDC-42(S71)::GFP and CDC-42(S71A)::GFP to interact with other aPARs stabilises CDC-42 in the membrane and decreases the rate at which it is extracted from the membrane. This way, in wild type embryos CDC-42 would get

stabilised in the anterior membrane thanks to its interaction with PAR-6/PKC-3, and PKC-3 phosphorylation would promote the disassembly of the CDC-42/PAR-6/PKC-3 complex, generating a pool of phosphorylated CDC-42 and recycling PAR-6 and PKC-3 (perhaps as a heterodimer) into the cytoplasm (See **Chapter 5** for a more in depth discussion of how phosphorylation could regulate CDC-42 localisation).

A similar mechanism has been proposed in budding yeast, as the rate at which inactive GDP-bound Cdc42 can be extracted from the membrane is higher than the rate at which active Cdc42 is extracted rom the membrane (Woods et al., 2016), and the ability of GTP-bound CDC-42 to bind effectors has been hypothesised to be the reason for the lower the mobility of these complexes (Woods and Lew, 2019).

7.7. CDC-42 phosphorylation cycles are essential for actomyosin organisation and retraction

As above mentioned, a few papers have hinted at anterior PARs as regulators of the actomyosin cytoskeleton. Motegi et al. (2006), for example, reported that silencing *cdc-42* results in lack of clearing of ECT-2 (the RHO GEF) from posterior at the very early stages of polarisation; Gross et al. (2019) have reported that silencing *par-6* result in lower dissociation of NMY-2 in the anterior cortex; and some preliminary data from our collaborator S. Naganathan shows that silencing *cdc-42* leads to more pulsatile flow (personal communication).

The results presented in this thesis point to pS71 CDC-42 as a key regulator of actomyosin, as the phosphomimetic CDC-42(S71E)::GFP completely changes the structure of the actomyosin foci, stops actomyosin from retracting to the anterior, and decreases flow-dependent PAR-3 retraction. How does CDC-42(S71E)::GFP achieve this effect? Actomyosin foci are constantly forming and dissociating (**Figure 1.2**). As described in the introduction, when actomyosin foci form, activators and inhibitors get enriched into the foci by advection and eventually the accumulation of inhibitors (such as RGA-3/4) results in the dissociation of the foci (Michaux et al., 2018). Our results suggest that CDC-42(S71E)::GFP blocks this process, perhaps by not allowing the foci to dissociate. It's a similar effect to that observed for *mlc-5* RNAi (**Figure 6.2**), in which foci lose the ability to go though the contraction/dissociation

cycles and appear as 'collapsed' small circular punctae. Perhaps it is to be expected then, that loss of *cdc-42* and *pkc-3* results in the opposite phenotype, with foci that appear less organised and less contracted (**Figure 3.3**). This could also explain the defective actomyosin flow we have reported (**Figure 3.1**), with any imbalance in foci dynamics (either collapsed or expanded) leading to defective flows.

How could CDC-42 phosphorylation be involved in this process? One theory is that stabilisation of NMY-2 at the anterior might be mediated by pS71 CDC-42, generated by PAR-6/aPKC. This would also explain the high cortical dissociation rate of NMY-2 in anterior observed in embryos treated with *par-6* RNAi by Gross et al. (2019), and the preliminary results from our collaborator S. Naganathan showing that silencing *cdc-42* leads to more pulsatile flow (personal communication). However analysis of the CDC-42 S71 mutations *in vivo* with a fluorescent NMY-2 reporter will need to be done to increase our understanding of how CDC-42 affects actomyosin dynamics.

CHAPTER 8. REFERENCES

Aceto, D., Beers, M. and Kemphues, K. J. (2006) 'Interaction of PAR-6 with CDC-42 is required for maintenance but not establishment of PAR asymmetry in C. elegans', *Dev Biol,* 299(2), pp. 386-97.

Afshar, K., Werner, M. E., Tse, Y. C., Glotzer, M. and Gonczy, P. (2010) 'Regulation of cortical contractility and spindle positioning by the protein phosphatase 6 PPH-6 in one-cell stage C. elegans embryos', *Development,* 137(2), pp. 237-47.

Aguilar, G., Matsuda, S., Vigano, M. A. and Affolter, M. (2019) 'Using Nanobodies to Study Protein Function in Developing Organisms', *Antibodies (Basel),* 8(1).

Ajduk, A. and Zernicka-Goetz, M. (2016) 'Polarity and cell division orientation in the cleavage embryo: from worm to human', *Mol Hum Reprod,* 22(10), pp. 691-703.

Alvarado, J., Sheinman, M., Sharma, A., MacKintosh, F. C. and Koenderink, G. H. (2013) 'Molecular motors robustly drive active gels to a critically connected state', *Nature Physics,* 9, pp. 591.

Amano, M., Ito, M., Kimura, K., Fukata, Y., Chihara, K., Nakano, T., Matsuura, Y. and Kaibuchi, K. (1996) 'Phosphorylation and activation of myosin by Rho-associated kinase (Rho-kinase)', *J Biol Chem,* 271(34), pp. 20246-9.

Armenti, S. T. and Nance, J. (2012) 'Adherens junctions in C. elegans embryonic morphogenesis', *Subcell Biochem,* 60, pp. 279-99.

Arthur, W. T., Petch, L. A. and Burridge, K. (2000) 'Integrin engagement suppresses RhoA activity via a c-Src-dependent mechanism', *Curr Biol,* 10(12), pp. 719-22.

Atwood, S. X., Chabu, C., Penkert, R. R., Doe, C. Q. and Prehoda, K. E. (2007) 'Cdc42 acts downstream of Bazooka to regulate neuroblast polarity through Par-6 aPKC', *J Cell Sci,* 120(Pt 18), pp. 3200-6.

Bailey, M. J. and Prehoda, K. E. (2015) 'Establishment of Par-Polarized Cortical Domains via Phosphoregulated Membrane Motifs', *Dev Cell,* 35(2), pp. 199-210.

Barros, C. S., Phelps, C. B. and Brand, A. H. (2003) 'Drosophila nonmuscle myosin II promotes the asymmetric segregation of cell fate determinants by cortical exclusion rather than active transport', *Dev Cell,* 5(6), pp. 829-40.

Beatty, A., Morton, D. G. and Kemphues, K. (2013) 'PAR-2, LGL-1 and the CDC-42 GAP CHIN-1 act in distinct pathways to maintain polarity in the C. elegans embryo', *Development,* 140(9), pp. 2005-14.

Beers, M. and Kemphues, K. (2006) 'Depletion of the co-chaperone CDC-37 reveals two modes of PAR-6 cortical association in C. elegans embryos', *Development,* 133(19), pp. 3745-54.

Bendezú, F. O., Vincenzetti, V., Vavylonis, D., Wyss, R., Vogel, H. and Martin, S. G. (2015) 'Spontaneous Cdc42 Polarization Independent of GDI-Mediated Extraction and Actin-Based Trafficking', *PLOS Biology,* 13(4), pp. e1002097.

Benton, R. and St Johnston, D. (2003) 'Drosophila PAR-1 and 14-3-3 inhibit Bazooka/PAR-3 to establish complementary cortical domains in polarized cells', *Cell,* 115(6), pp. 691-704.

Bergstralh, D. T., Haack, T. and St Johnston, D. (2013) 'Epithelial polarity and spindle orientation: intersecting pathways', *Philos Trans R Soc Lond B Biol Sci,* 368(1629), pp. 20130291.

Betschinger, J., Mechtler, K. and Knoblich, J. A. (2003) 'The Par complex directs asymmetric cell division by phosphorylating the cytoskeletal protein Lgl', *Nature,* 422(6929), pp. 326-30.

Brenner, S. (1974) 'The genetics of Caenorhabditis elegans', *Genetics,* 77(1), pp. 71-94.

Bulgakova, N. A., Grigoriev, I., Yap, A. S., Akhmanova, A. and Brown, N. H. (2013) 'Dynamic microtubules produce an asymmetric E-cadherin-Bazooka complex to maintain segment boundaries', *J Cell Biol,* 201(6), pp. 887-901.

Caviston, J. P., Longtine, M., Pringle, J. R. and Bi, E. (2003) 'The role of Cdc42p GTPase-activating proteins in assembly of the septin ring in yeast', *Mol Biol Cell,* 14(10), pp. 4051-66.

Chapa-Y-Lazo, B., Hamanaka, M., Wray, A., Balasubramanian, M. K. and Mishima, M. (2020) 'Polar relaxation by dynein-mediated removal of cortical myosin II', *J Cell Biol,* 219(e201903080).

Chen, J., Sayadian, A. C., Lowe, N., Lovegrove, H. E. and St Johnston, D. (2018) 'An alternative mode of epithelial polarity in the Drosophila midgut', *PLoS Biol,* 16(10), pp. e3000041.

Chiou, J. G., Balasubramanian, M. K. and Lew, D. J. (2017) 'Cell Polarity in Yeast', *Annu Rev Cell Dev Biol,* 33, pp. 77-101.

Choi, E. K., Kim, J. G., Kim, H. J., Cho, J. Y., Jeong, H., Park, Y., Islam, R., Cap, C. K. and Park, J. B. (2020) 'Regulation of RhoA GTPase and novel target proteins for ROCK', *Small GTPases,* 11(2), pp. 95-102.

Colombo, K., Grill, S. W., Kimple, R. J., Willard, F. S., Siderovski, D. P. and Gonczy, P. (2003) 'Translation of polarity cues into asymmetric spindle positioning in Caenorhabditis elegans embryos', *Science,* 300(5627), pp. 1957-61.

Consortium, C. e. S. (1998) 'Genome sequence of the nematode C. elegans: a platform for investigating biology', *Science,* 282(5396), pp. 2012-8.

Coravos, J. S. and Martin, A. C. (2016) 'Apical Sarcomere-like Actomyosin Contracts Nonmuscle Drosophila Epithelial Cells', *Dev Cell,* 39(3), pp. 346-358.

Cotteret, S. and Chernoff, J. (2002) 'The evolutionary history of effectors downstream of Cdc42 and Rac', *Genome Biol,* 3(2), pp. REVIEWS0002.

Cowan, C. R. and Hyman, A. A. (2004) 'Centrosomes direct cell polarity independently of microtubule assembly in C. elegans embryos', *Nature,* 431(7004), pp. 92-6.

Culurgioni, S., Alfieri, A., Pendolino, V., Laddomada, F. and Mapelli, M. (2011) 'Inscuteable and NuMA proteins bind competitively to Leu-Gly-Asn repeat-enriched protein (LGN) during asymmetric cell divisions', *Proc Natl Acad Sci U S A,* 108(52), pp. 20998-1003.

Culurgioni, S., Mari, S., Bonetti, P., Gallini, S., Bonetto, G., Brennich, M., Round, A., Nicassio, F. and Mapelli, M. (2018) 'Insc:LGN tetramers promote asymmetric divisions of mammary stem cells', *Nat Commun,* 9(1), pp. 1025.

D'Avino, P. P., Giansanti, M. G. and Petronczki, M. (2015) 'Cytokinesis in animal cells', *Cold Spring Harb Perspect Biol,* 7(4), pp. a015834.

D'Avino, P. P., Savoian, M. S., Capalbo, L. and Glover, D. M. (2006) 'RacGAP50C is sufficient to signal cleavage furrow formation during cytokinesis', *J Cell Sci,* 119(Pt 21), pp. 4402-8.

David, D. J., Wang, Q., Feng, J. J. and Harris, T. J. (2013) 'Bazooka inhibits aPKC to limit antagonism of actomyosin networks during amnioserosa apical constriction', *Development,* 140(23), pp. 4719-29.

David, D. J. V., Tishkina, A. and Harris, T. J. C. (2010) 'The PAR complex regulates pulsed actomyosin contractions during amnioserosa apical constriction in Drosophila', *Development,* 137(10), pp. 1645-1655.

De Simone, A., Nedelec, F. and Gonczy, P. (2016) 'Dynein Transmits Polarized Actomyosin Cortical Flows to Promote Centrosome Separation', *Cell Rep,* 14(9), pp. 2250-2262.

Descovich, C. P., Cortes, D. B., Ryan, S., Nash, J., Zhang, L., Maddox, P. S., Nedelec, F. and Maddox, A. S. (2018) 'Cross-linkers both drive and brake cytoskeletal remodeling and furrowing in cytokinesis', *Mol Biol Cell,* 29(5), pp. 622-631.

Devenport, D. (2014) 'The cell biology of planar cell polarity', *J Cell Biol,* 207(2), pp. 171-9.

Dickinson, D. J., Schwager, F., Pintard, L., Gotta, M. and Goldstein, B. 2016. Single-cell biochemistry reveals a cell cycle-regulated mechanism that couples PAR complex movement to polarizing cortical flows.

Dickinson, D. J., Schwager, F., Pintard, L., Gotta, M. and Goldstein, B. (2017) 'A Single-Cell Biochemistry Approach Reveals PAR Complex Dynamics during Cell Polarization', *Dev Cell,* 42(4), pp. 416-434 e11.

Ding, W. Y., Ong, H. T., Hara, Y., Wongsantichon, J., Toyama, Y., Robinson, R. C., Nedelec, F. and Zaidel-Bar, R. (2017) 'Plastin increases cortical connectivity to facilitate robust polarization and timely cytokinesis', *J Cell Biol,* 216(5), pp. 1371-1386.

Diogon, M., Wissler, F., Quintin, S., Nagamatsu, Y., Sookhareea, S., Landmann, F., Hutter, H., Vitale, N. and Labouesse, M. (2007) 'The RhoGAP RGA-2 and LET-502/ROCK achieve a balance of actomyosin-dependent forces in C. elegans epidermis to control morphogenesis', *Development,* 134(13), pp. 2469-79.

Dong, W., Lu, J., Zhang, X., Wu, Y., Lettieri, K., Hammond, G. R. and Hong, Y. (2019) 'A Polybasic Domain in aPKC Mediates Par-6-Dependent Control of Plasma Membrane Targeting and Kinase Activity'.

Durney, C. H., Harris, T. J. C. and Feng, J. J. (2018) 'Dynamics of PAR Proteins Explain the Oscillation and Ratcheting Mechanisms in Dorsal Closure', *Biophysical Journal,* 115(11), pp. 2230-2241.

Dworkin, J. (2009) 'Cellular polarity in prokaryotic organisms', *Cold Spring Harb Perspect Biol,* 1(6).

Dyer, J. M., Savage, N. S., Jin, M., Zyla, T. R., Elston, T. C. and Lew, D. J. (2013) 'Tracking shallow chemical gradients by actin-driven wandering of the polarization site', *Curr Biol,* 23(1), pp. 32-41.

Elsum, I., Yates, L., Humbert, P. O. and Richardson, H. E. (2012) 'The Scribble-Dlg-Lgl polarity module in development and cancer: from flies to man', *Essays Biochem,* 53, pp. 141-68.

Erickson, J. W., Zhang, C., Kahn, R. A., Evans, T. and Cerione, R. A. (1996) 'Mammalian Cdc42 is a brefeldin A-sensitive component of the Golgi apparatus', *J Biol Chem,* 271(43), pp. 26850-4.

Etemad-Moghadam, B., Guo, S. and Kemphues, K. J. (1995) 'Asymmetrically distributed PAR-3 protein contributes to cell polarity and spindle alignment in early C. elegans embryos', *Cell,* 83(5), pp. 743-52.

Etienne-Manneville, S. (2004) 'Cdc42--the centre of polarity', *J Cell Sci,* 117(Pt 8), pp. 1291-300.

Ferreira, T., Prudencio, P. and Martinho, R. G. (2014) 'Drosophila protein kinase N (Pkn) is a negative regulator of actin-myosin activity during oogenesis', *Dev Biol,* 394(2), pp. 277-91.

Fievet, B. T., Rodriguez, J., Naganathan, S., Lee, C., Zeiser, E., Ishidate, T., Shirayama, M., Grill, S. and Ahringer, J. (2013) 'Systematic genetic interaction screens uncover cell polarity regulators and functional redundancy', *Nat Cell Biol,* 15(1), pp. 103-12.

Fire, A., Albertson, D., Harrison, S. W. and Moerman, D. G. (1991) 'Production of antisense RNA leads to effective and specific inhibition of gene expression in C. elegans muscle', *Development,* 113(2), pp. 503-14.

Flynn, J. R. and McNally, F. J. (2017) 'A casein kinase 1 prevents expulsion of the oocyte meiotic spindle into a polar body by regulating cortical contractility', *Mol Biol Cell,* 28(18), pp. 2410-2419.

Frokjaer-Jensen, C., Davis, M. W., Ailion, M. and Jorgensen, E. M. (2012) 'Improved Mos1-mediated transgenesis in C. elegans', *Nat Methods,* 9(2), pp. 117-8.

Fuerstenberg, S., Peng, C. Y., Alvarez-Ortiz, P., Hor, T. and Doe, C. Q. (1998) 'Identification of Miranda protein domains regulating asymmetric cortical localization, cargo binding, and cortical release', *Mol Cell Neurosci,* 12(6), pp. 325-39.

Galli, M., Munoz, J., Portegijs, V., Boxem, M., Grill, S. W., Heck, A. J. and van den Heuvel, S. (2011) 'aPKC phosphorylates NuMA-related LIN-5 to position the mitotic spindle during asymmetric division', *Nat Cell Biol,* 13(9), pp. 1132-8.

Gandalovicova, A., Vomastek, T., Rosel, D. and Brabek, J. (2016) 'Cell polarity signaling in the plasticity of cancer cell invasiveness', *Oncotarget,* 7(18), pp. 25022-49.

Georgiou, M., Marinari, E., Burden, J. and Baum, B. (2008) 'Cdc42, Par6, and aPKC regulate Arp2/3-mediated endocytosis to control local adherens junction stability', *Curr Biol,* 18(21), pp. 1631-8.

Gnad, F., Ren, S., Cox, J., Olsen, J. V., Macek, B., Oroshi, M. and Mann, M. (2007) 'PHOSIDA (phosphorylation site database): management, structural and evolutionary investigation, and prediction of phosphosites', *Genome Biol,* 8(11), pp. R250.

Goehring, N. W., Hoege, C., Grill, S. W. and Hyman, A. A. (2011a) 'PAR proteins diffuse freely across the anterior-posterior boundary in polarized C. elegans embryos', *J Cell Biol,* 193(3), pp. 583-94.

Goehring, N. W., Trong, P. K., Bois, J. S., Chowdhury, D., Nicola, E. M., Hyman, A. A. and Grill, S. W. (2011b) 'Polarization of PAR proteins by advective triggering of a pattern-forming system', *Science,* 334(6059), pp. 1137-41.

Goldstein, B. and Macara, I. G. (2007) 'The PAR proteins: fundamental players in animal cell polarization', *Dev Cell,* 13(5), pp. 609-22.

Golub, O., Wee, B., Newman, R. A., Paterson, N. M. and Prehoda, K. E. (2017) 'Activation of Discs large by aPKC aligns the mitotic spindle to the polarity axis during asymmetric cell division', *Elife,* 6.

Göransson, O., Deak, M., Wullschleger, S., Morrice, N. A., Prescott, A. R. and Alessi, D. R. (2006) 'Regulation of the polarity kinases PAR-1/MARK by 14-3-3 interaction and phosphorylation', *J Cell Sci,* 119(Pt 19), pp. 4059-70.

Gotta, M., Abraham, M. C. and Ahringer, J. (2001) 'CDC-42 controls early cell polarity and spindle orientation in C. elegans', *Curr Biol,* 11(7), pp. 482-8.

Graybill, C., Wee, B., Atwood, S. X. and Prehoda, K. E. (2012) 'Partitioning-defective protein 6 (Par-6) activates atypical protein kinase C (aPKC) by pseudosubstrate displacement', *J Biol Chem,* 287(25), pp. 21003-11.

Griffin, E. E., Odde, D. J. and Seydoux, G. (2011) 'Regulation of the MEX-5 gradient by a spatially segregated kinase/phosphatase cycle', *Cell,* 146(6), pp. 955-68.

Grishok, A. (2005) 'RNAi mechanisms in Caenorhabditis elegans', *FEBS Lett,* 579(26), pp. 5932-9.

Gross, P., Kumar, K. V., Goehring, N. W., Bois, J. S., Hoege, C., Jülicher, F. and Grill, S. W. (2019) 'Guiding self-organized pattern formation in cell polarity establishment', *Nature Physics,* 15(3), pp. 293-300.

Gubieda, A. G., Packer, J. R., Squires, I., Martin, J. and Rodriguez, J. (2020) 'Going with the flow: insights from Caenorhabditis elegans zygote polarization', *Philosophical Transactions of The Royal Society B,* 375(1809).

Hannaford, M., Loyer, N., Tonelli, F., Zoltner, M. and Januschke, J. (2019) 'A chemical-genetics approach to study the role of atypical Protein Kinase C in Drosophila', *Development,* 146(2).

Hannaford, M. R., Ramat, A., Loyer, N. and Januschke, J. (2018) 'aPKC-mediated displacement and actomyosin-mediated retention polarize Miranda in Drosophila neuroblasts', *Elife,* 7.

Hao, Y., Boyd, L. and Seydoux, G. (2006) 'Stabilization of cell polarity by the C. elegans RING protein PAR-2', *Dev Cell,* 2006.

Harris, T. J. and Peifer, M. (2005) 'The positioning and segregation of apical cues during epithelial polarity establishment in Drosophila', *J Cell Biol,* 170(5), pp. 813-23.

Hegemann, B., Unger, M., Lee, S. S., Stoffel-Studer, I., van den Heuvel, J., Pelet, S., Koeppl, H. and Peter, M. (2015) 'A Cellular System for Spatial Signal Decoding in Chemical Gradients', *Dev Cell,* 35(4), pp. 458-70.

Hirata, J., Nakagoshi, H., Nabeshima, Y. and Matsuzaki, F. (1995) 'Asymmetric segregation of the homeodomain protein Prospero during Drosophila development', *Nature,* 377(6550), pp. 627-30.

Hobert, O. (2013) 'The neuronal genome of Caenorhabditis elegans', *WormBook*, pp. 1-106.

Hoege, C. and Hyman, A. A. (2013) 'Principles of PAR polarity in Caenorhabditis elegans embryos', *Nat Rev Mol Cell Biol,* 14, pp. 315-322.

Hong, Y. (2018) 'aPKC: the Kinase that Phosphoryates Cell Polarity', *F1000Res,* 7(903).

Irazoqui, J. E. and Lew, D. J. (2004) 'Polarity establishment in yeast', *J Cell Sci,* 117(Pt 11), pp. 2169-71.

Ishiuchi, T. and Takeichi, M. (2011) 'Willin and Par3 cooperatively regulate epithelial apical constriction through aPKC-mediated ROCK phosphorylation', *Nat Cell Biol,* 13(7), pp. 860-6.

Iwase, M., Luo, J., Nagaraj, S., Longtine, M., Kim, H. B., Haarer, B. K., Caruso, C., Tong, Z., Pringle, J. R. and Bi, E. (2006) 'Role of a Cdc42p effector pathway in recruitment of the yeast septins to the presumptive bud site', *Mol Biol Cell,* 17(3), pp. 1110-25.

Jaffe, A. B. and Hall, A. (2005) 'Rho GTPases: biochemistry and biology', *Annu Rev Cell Dev Biol,* 21, pp. 247-69.

Jenkins, N., Saam, J. R. and Mango, S. E. (2006) 'CYK-4/GAP provides a localized cue to initiate anteroposterior polarity upon fertilization', *Science,* 313(5791), pp. 1298-1301.

Jiang, H., Guo, W., Liang, X. and Rao, Y. (2005) 'Both the establishment and the maintenance of neuronal polarity require active mechanisms: critical roles of GSK-3beta and its upstream regulators', *Cell,* 120(1), pp. 123-35.

Jiang, T., McKinley, R. F., McGill, M. A., Angers, S. and Harris, T. J. (2015) 'A Par-1-Par-3-Centrosome Cell Polarity Pathway and Its Tuning for Isotropic Cell Adhesion', *Curr Biol,* 25(20), pp. 2701-8.

Joberty, G., Petersen, C., Gao, L. and Macara, I. G. (2000) 'The cell-polarity protein Par6 links Par3 and atypical protein kinase C to Cdc42', *Nat Cell Biol,* 2(8), pp. 531-9.

Johnson, D. I. and Pringle, J. R. (1990) 'Molecular characterization of CDC42, a Saccharomyces cerevisiae gene involved in the development of cell polarity', *J Cell Biol,* 111(1), pp. 143-52.

Johnson, J. M., Jin, M. and Lew, D. J. (2011) 'Symmetry breaking and the establishment of cell polarity in budding yeast', *Curr Opin Genet Dev,* 21(6), pp. 740-6.

Kalmes, A., Merdes, G., Neumann, B., Strand, D. and Mechler, B. M. (1996) 'A serine-kinase associated with the p127-l(2)gl tumour suppressor of Drosophila may regulate the binding of p127 to nonmuscle myosin II heavy chain and the attachment of p127 to the plasma membrane', *J Cell Sci,* 109 (Pt 6), pp. 1359-68.

Kamijo, K., Ohara, N., Abe, M., Uchimura, T., Hosoya, H., Lee, J. S. and Miki, T. (2006) 'Dissecting the role of Rho-mediated signaling in contractile ring formation', *Mol Biol Cell,* 17(1), pp. 43-55.

Kapoor, S. and Kotak, S. (2019) 'Centrosome Aurora A regulates RhoGEF ECT-2 localisation and ensures a single PAR-2 polarity axis in C. elegans embryos', *Development*.

Kay, A. J. and Hunter, C. P. (2001) 'CDC-42 regulates PAR protein localization and function to control cellular and embryonic polarity in C-elegans', *Current Biology,* 11(7), pp. 474-481.

Kemphues, K. J., Priess, J. R., Morton, D. G. and Cheng, N. S. (1988) 'Identification of genes required for cytoplasmic localization in early C. elegans embryos', *Cell,* 52(3), pp. 311-20.

Khaliullin, R. N., Green, R. A., Shi, L. Z., Gomez Cavazos, J. S., Berns, M. W., Desai, A. and Oegema, K. (2018) 'A positive feedback based mechanism for constriction rate acceleratoin during cytokinesis in Caenorhabditis elegans', *Elife,* 7(e36073).

Klinkert, K., Levernier, N., Gross, P., Gentili, C., von Tobel, L., Pierron, M., Busso, C., Herrman, S., Grill, S. W., Kruse, K. and Gonczy, P. (2019) 'Aurora A depletion reveals centrosome-independent polarization mechanism in Caenorhabditis elegans', *Elife,* 8.

Knoblich, J. A. (2001) 'Asymmetric cell division during animal development', *Nat Rev Mol Cell Biol,* 2(1), pp. 11-20.

Knoblich, J. A. (2008) 'Mechanisms of asymmetric stem cell division', *Cell,* 132(4), pp. 583-97.

Knoblich, J. A. (2010) 'Asymmetric cell division: recent developments and their implications for tumour biology', *Nature Reviews Molecular Cell Biology,* 11, pp. 849-860.

Knoblich, J. A., Jan, L. Y. and Jan, Y. N. (1995) 'Asymmetric segregation of Numb and Prospero during cell division', *Nature,* 377(6550), pp. 624-7.

Knoblich, J. A., Jan, L. Y. and Jan, Y. N. (1997) 'The N terminus of the Drosophila Numb protein directs membrane association and actin-dependent asymmetric localization', *Proc Natl Acad Sci U S A,* 94(24), pp. 13005-10.

Koenderink, G. H. and Paluch, E. K. (2018) 'Architecture shapes contractility in actomyosin networks', *Curr Opin Cell Biol,* 50, pp. 79-85.

Kotak, S., Busso, C. and Gonczy, P. (2014) 'NuMA interacts with phosphoinositides and links the mitotic spindle with the plasma membrane', *EMBO J,* 33(16), pp. 1815-30.

Kraut, R. and Campos-Ortega, J. A. (1996) 'inscuteable, a neural precursor gene of Drosophila, encodes a candidate for a cytoskeleton adaptor protein', *Dev Biol,* 174(1), pp. 65-81.

Kraut, R., Chia, W., Jan, L. Y., Jan, Y. N. and Knoblich, J. A. (1996) 'Role of inscuteable in orienting asymmetric cell divisions in Drosophila', *Nature,* 383(6595), pp. 50-5.

Kumfer, K. T., Cook, S. J., Squirrell, J. M., Eliceiri, K. W., Peel, N., O'Connell, K. F. and White, J. G. (2010) 'CGEF-1 and CHIN-1 regulate CDC-42 activity during asymmetric division in the Caenorhabditis elegans embryo', *Mol Biol Cell,* 21(2), pp. 266-77.

Kwon, T., Kwon, D. Y., Chun, J., Kim, J. H. and Kang, S. S. (2000) 'Akt protein kinase inhibits Rac1-GTP binding through phosphorylation at serine 71 of Rac1', *J Biol Chem,* 275(1), pp. 423-8.

Lang, P., Gesbert, F., Delespine-Carmagnat, M., Stancou, R., Pouchelet, M. and Bertoglio, J. (1996) 'Protein kinase A phosphorylation of RhoA mediates the morphological and functional effects of cyclic AMP in cytotoxic lymphocytes', *EMBO J,* 15(3), pp. 510-9.

Layton, A. T., Savage, N. S., Howell, A. S., Carroll, S. Y., Drubin, D. G. and Lew, D. J. (2011) 'Modeling vesicle traffic reveals unexpected consequences for Cdc42p-mediated polarity establishment', *Curr Biol,* 21(3), pp. 184-94.

Leibfried, A., Fricke, R., Morgan, M. J., Bogdan, S. and Bellaiche, Y. (2008) 'Drosophila Cip4 and WASp define a branch of the Cdc42-Par6-aPKC pathway regulating E-cadherin endocytosis', *Curr Biol,* 18(21), pp. 1639-48.

Levayer, R. and Lecuit, T. (2012) 'Biomechanical regulation of contractility: spatial control and dynamics', *Trends Cell Biol,* 22(2), pp. 61-81.

Li, B., Kim, H., Beers, M. and Kemphues, K. (2010a) 'Different domains of C. elegans PAR-3 are required at different times in development', *Dev Biol,* 344(2), pp. 745-57.

Li, J., Kim, H., Aceto, D. G., Hung, J., Aono, S. and Kemphues, K. J. (2010b) 'Binding to PKC-3, but not to PAR-3 or to a conventional PDZ domain ligand, is required for PAR-6 function in C. elegans', *Dev Biol,* 340(1), pp. 88-98.

Liu, J., Maduzia, L. L., Shirayama, M. and Mello, C. C. (2010) 'NMY-2 maintains cellular asymmetry and cell boundaries, and promotes a SRC-dependent asymmetric cell division', *Dev Biol,* 339(2), pp. 366-73.

Loyer, N. and Januschke, J. (2018) 'The last-born daughter cell contributes to division orientation of Drosophila larval neuroblasts', *Nature Communications,* 9(1), pp. 3745.

Loyer, N. and Januschke, J. (2020) 'Where does asymmetry come from? Illustrating principles of polarity and asymmetry establishment in Drosophila neuroblasts', *Curr Opin Cell Biol,* 62, pp. 70-77.

Mack, N. A. and Georgiou, M. (2014) 'The interdependence of the Rho GTPases and apicobasal cell polarity', *Small GTPases,* 5(2), pp. 10.

Mack, N. A., Porter, A. P., Whalley, H. J., Schwarz, J. P., Jones, R. C., Khaja, A. S., Bjartell, A., Anderson, K. I. and Malliri, A. (2012) 'beta2-syntrophin and Par-3 promote an apicobasal Rac activity gradient at cell-cell junctions by differentially regulating Tiam1 activity', *Nat Cell Biol,* 14(11), pp. 1169-80.

Maitre, J. L., Niwayama, R., Turlier, H., Nedelec, F. and Hiiragi, T. (2015) 'Pulsatile cell-autonomous contractility drives compaction in the mouse embryo', *Nat Cell Biol,* 17(7), pp. 849-55.

Marjoram, R. J., Lessey, E. C. and Burridge, K. (2014) 'Regulation of RhoA activity by adhesion molecules and mechanotransduction', *Curr Mol Med,* 14(2), pp. 199-208.

Martin, A. C., Kaschube, M. and Wieschaus, E. F. (2009) 'Pulsed contractions of an actin-myosin network drive apical constriction', *Nature,* 457, pp. 495-499.

Martin, E., Ouellette, M. H. and Jenna, S. (2016) 'Rac1/RhoA antagonism defines cell-to-cell heterogeneity during epidermal morphogenesis in nematodes', *J Cell Biol,* 215(4), pp. 483-498.

Martin-Belmonte, F., Gassama, A., Datta, A., Yu, W., Rescher, U., Gerke, V. and Mostov, K. (2007) 'PTEN-mediated apical segregation of phosphoinositides controls epithelial morphogenesis through Cdc42', *Cell,* 128(2), pp. 383-97.

Mason, F. M., Xie, S., Vasquez, C. G., Tworoger, M. and Martin, A. C. (2016) 'RhoA GTPase inhibition organizes contraction during epithelial morphogenesis', *J Cell Biol,* 214(5), pp. 603-17.

Maupas, E. (1900) 'Modes et formes de reproduction des nématodes.', *Arch. Zool. Exp. Gen.,* (8), pp. 463-624.

Mayer, M., Depken, M., Bois, J. S., Julicher, F. and Grill, S. W. (2010) 'Anisotropies in cortical tension reveal the physical basis of polarizing cortical flows', *Nature,* 467(7315), pp. 617-21.

Mazel, T. (2017) 'Crosstalk of cell polarity signaling pathways', *Protoplasma,* 254(3), pp. 1241-1258.

McGee, A. W., Dakoji, S. R., Olsen, O., Bredt, D. S., Lim, W. A. and Prehoda, K. E. (2001) 'Structure of the SH3-guanylate kinase module from PSD-95 suggests a mechanism for regulated assembly of MAGUK scaffolding proteins', *Mol Cell,* 8(6), pp. 1291-301.

Meister, G. and Tuschl, T. (2004) 'Mechanisms of gene silencing by double-stranded RNA', *Nature,* 431(7006), pp. 343-9.

Menon, V. V., Soumya, S. S., Agarwal, A., Naganathan, S. R., Inamdar, M. M. and Sain, A. (2017) 'Asymmetric flows in the intercellular membrane during cytokinesis', *Biophys J,* 113, pp. 2787-2795.

Michaux, J. B., Robin, F. B., McFadden, W. M. and Munro, E. M. (2018) 'Excitable RhoA dynamics drive pulsed contractions in the early C. elegans embryo', *J Cell Biol,* 217(12), pp. 4230-4252.

Milburn, M. V., Tong, L., deVos, A. M., Brünger, A., Yamaizumi, Z., Nishimura, S. and Kim, S. H. (1990) 'Molecular switch for signal transduction: structural differences between active and inactive forms of protooncogenic ras proteins.', *Science.,* 247(4945), pp. 939-45.

Miller, A. L. and Bement, W. M. (2009) 'Regulation of cytokinesis by Rho GTPase flux', *Nat Cell Biol,* 11(1), pp. 71-7.

Misteli, T. (2001) 'The concept of self-organization in cellular architecture', *J Cell Biol,* 155(2), pp. 181-5.

Møller, L. L. V., Klip, A. and Sylow, L. (2019) 'Rho GTPases-Emerging Regulators of Glucose Homeostasis and Metabolic Health', *Cells,* 8(5).

Moon, W. and Matsuzaki, F. (2013) 'Aurora A kinase negatively regulates Rho-kinase by phosphorylation in vivo', *Biochem Biophys Res Commun,* 435(4), pp. 610-5.

Moran, K. D. and Lew, D. J. (2020) 'How Diffusion Impacts Cortical Protein Distribution in Yeasts', *Cells,* 9(5).

Morton, D. G., Hoose, W. A. and Kemphues, K. J. (2012) 'A genome-wide RNAi screen for enhancers of par mutants reveals new contributors to early embryonic polarity in Caenorhabditis elegans', *Genetics,* 192(3), pp. 929-42.

Motegi, F. and Sugimoto, A. (2006) 'Sequential functioning of the ECT-2 RhoGEF, RHO-1 and CDC-42 establishes cell polarity in Caenorhabditis elegans embryos', *Nat Cell Biol,* 8(9), pp. 978-85.

Motegi, F., Zonies, S., Hao, Y., Cuenca, A. A., Griffin, E. and Seydoux, G. (2011) 'Microtubules induce self-organization of polarized PAR domains in Caenorhabditis elegans zygotes.', *Nature cell biology,* 13, pp. 1361-7.

Muller, H. A. (2000) 'Genetic control of epithelial cell polarity: lessons from Drosophila', *Dev Dyn,* 218(1), pp. 52-67.

Munjal, A., Philippe, J. M., Munro, E. and Lecuit, T. (2015) 'A self-organized biochemical network drives shape changes during tissue morphogenesis', *Nature,* 524, pp. 351-355.

Munro, E., Nance, J. and Priess, J. R. (2004) 'Cortical flows powered by asymmetrical contraction transport PAR proteins to establish and maintain anterior-posterior polarity in the early C. elegans embryo', *Dev Cell,* 7(3), pp. 413-24.

Munro, E. M. (2006) 'PAR proteins and the cytoskeleton: a marriage of equals', *Curr Opin Cell Biol,* 18(1), pp. 86-94.

Naganathan, S. R., Furthauer, S., Nishikawa, M., Julicher, F. and Grill, S. W. (2014) 'Active torque generation by the actomyosin cell cortex drives left-right symmetry breaking', *Elife,* 3, pp. e04165.

Naganathan, S. R., Furthauer, S., Rodriguez, J., Fievet, B. T., Julicher, F., Ahringer, J., Cannistraci, C. V. and Grill, S. W. (2018) 'Morphogenetic degeneracies in the actomyosin cortex', *Elife,* 7.

Nakayama, M., Goto, T. M., Sugimoto, M., Nishimura, T., Shinagawa, T., Ohno, S., Amano, M. and Kaibuchi, K. (2008) 'Rho-kinase phosphorylates PAR-3 and disrupts PAR complex formation', *Dev Cell,* 14(2), pp. 205-15.

Nipper, R. W., Siller, K. H., Smith, N. R., Doe, C. Q. and Prehoda, K. E. (2007) 'Galphai generates multiple Pins activation states to link cortical polarity and spindle orientation in Drosophila neuroblasts', *Proc Natl Acad Sci U S A,* 104(36), pp. 14306-11.

Nishikawa, M., Naganathan, S. R., Julicher, F. and Grill, S. W. (2017) 'Controlling contractile instabilities in the actomyosin cortex', *Elife,* 6.

Nishimura, Y. and Yonemura, S. (2006) 'Centralspindln regulates ECT2 and RhoA accumulation at the equatorial cortex during cytokinesis', *J Cell Sci,* 119, pp. 104-114.

Noatynska, A., Panbianco, C. and Gotta, M. (2010) 'Bora acts with Polo-like kinase 1 to regulate PAR polarity and cell cycle progression', *Development,* 137, pp. 3315-3325.

Nunes de Almeida, F., Walther, R. F., Pressé, M. T., Vlassaks, E. and Pichaud, F. (2019) 'Cdc42 defines apical identity and regulates epithelial morphogenesis by promoting apical recruitment of Par6-aPKC and Crumbs', *Development,* 146(15), pp. dev175497.

Oon, C. H. and Prehoda, K. E. (2019) 'Asymmetric recruitment and actin-dependent cortical flows drive the neuroblast polarity cycle', *Elife,* 8.

Ozdamar, B., Bose, R., Barrios-Rodiles, M., Wang, H. R., Zhang, Y. and Wrana, J. L. (2005) 'Regulation of the polarity protein Par6 by TGFbeta receptors controls epithelial cell plasticity', *Science,* 307(5715), pp. 1603-9.

Padmanabhan, A., Ong, H. T. and Zaidel-Bar, R. (2017) 'Non-junctional E-Cadherin Clusters Regulate the Actomyosin Cortex in the C. elegans Zygote', *Curr Biol,* 27(1), pp. 103-112.

Panbianco, C., Weinkove, D., Zanin, E., Jones, D., Divecha, N., Gotta, M. and Ahringer, J. (2008) 'A casein kinase 1 and PAR proteins regulate asymmetry of a PIP(2) synthesis enzyme for asymmetric spindle positioning', *Dev Cell,* 15(2), pp. 198-208.

Park, H. O. and Bi, E. (2007) 'Central roles of small GTPases in the development of cell polarity in yeast and beyond', *Microbiol Mol Biol Rev,* 71(1), pp. 48-96.

Parmentier, M. L., Woods, D., Greig, S., Phan, P. G., Radovic, A., Bryant, P. and O'Kane, C. J. (2000) 'Rapsynoid/partner of inscuteable controls asymmetric division of larval neuroblasts in Drosophila', *J Neurosci,* 20(14), pp. RC84.

Phillips, M. J., Calero, G., Chan, B., Ramachandran, S. and Cerione, R. A. (2008) 'Effector proteins exert an important influence on the signaling-active state of the small GTPase Cdc42', *J Biol Chem,* 283(20), pp. 14153-64.

Pichaud, F., Walther, R. F. and Nunes de Almeida, F. (2019) 'Regulation of Cdc42 and its effectors in epithelial morphogenesis', *J Cell Sci,* 132(10).

Piekny, A. J., Werner, M. and Glotzer, M. (2005) 'Cytokinesis: welcome to the Rho zone', *Trends Cell Biol,* 15, pp. 651-658.

Plant, P. J., Fawcett, J. P., Lin, D. C., Holdorf, A. D., Binns, K., Kulkarni, S. and Pawson, T. (2003) 'A polarity complex of mPar-6 and atypical PKC binds, phosphorylates and regulates mammalian Lgl', *Nat Cell Biol,* 5(4), pp. 301-8.

Ramanujam, R., Han, Z., Zhang, Z., Kanchanawong, P. and Motegi, F. (2018) 'Establishment of the PAR-1 cortical gradient by the aPKC-PRBH circuit', *Nat Chem Biol,* 14(10), pp. 917-927.

Reich, J. D., Hubatsch, L., Illukkumbura, R., Peglion, F., Bland, T., Hirani, N. and Goehring, N. W. (2019) 'Regulated Activation of the PAR Polarity Network Ensures a Timely and Specific Response to Spatial Cues', *Curr Biol,* 29(12), pp. 1911-1923 e5.

Reymann, A. C., Staniscia, F., Erzberger, A., Salbreux, G. and Grill, S. W. (2016) 'Cortical flow aligns actin filaments to form a furrow', *Elife,* 5.

Rhyu, M. S., Jan, L. Y. and Jan, Y. N. (1994) 'Asymmetric distribution of numb protein during division of the sensory organ precursor cell confers distinct fates to daughter cells', *Cell,* 76(3), pp. 477-91.

Roberts, P. J., Mitin, N., Keller, P. J., Chenette, E. J., Madigan, J. P., Currin, R. O., Cox, A. D., Wilson, O., Kirschmeier, P. and Der, C. J. (2008) 'Rho Family GTPase modification and dependence on CAAX motif-signaled posttranslational modification', *J Biol Chem,* 283(37), pp. 25150-63.

Robin, F. B., McFadden, W. M., Yao, B. and Munro, E. M. (2014) 'Single-molecule analysis of cell surface dynamics in Caenorhabditis elegans embryos', *Nat Methods,* 11(6), pp. 677-82.

Rodriguez, J., Peglion, F., Martin, J., Hubatsch, L., Reich, J., Hirani, N., Gubieda, A. G., Roffey, J., Fernandes, A. R., St Johnston, D., Ahringer, J. and Goehring, N. W. (2017) 'aPKC Cycles between Functionally Distinct PAR Protein Assemblies to Drive Cell Polarity', *Dev Cell,* 42(4), pp. 400-415 e9.

Rodriguez-Boulan, E. and Macara, I. G. (2014) 'Organization and execution of the epithelial polarity programme', *Nat Rev Mol Cell Biol,* 15(4), pp. 225-42.

Rohatgi, R., Ho, H. Y. and Kirschner, M. W. (2000) 'Mechanism of N-WASP activation by CDC42 and phosphatidylinositol 4, 5-bisphosphate', *J Cell Biol,* 150(6), pp. 1299-310.

Roper, K. (2012) 'Anisotropy of Crumbs and aPKC drives myosin cable assembly during tube formation', *Dev Cell,* 23(5), pp. 939-53.

Roth, S. and Lynch, J. A. (2009) 'Symmetry breaking during Drosophila oogenesis', *Cold Spring Harb Perspect Biol,* 1(2), pp. a001891.

Roubinet, C., Tsankova, A., Pham, T. T., Monnard, A., Caussinus, E., Affolter, M. and Cabernard, C. (2017) 'Spatio-temporally separated cortical flows and spindle geometry establish physical asymmetry in fly neural stem cells', *Nature Communications,* 8(1), pp. 1383.

Sablin, E. P., Dawson, J. F., VanLoock, M. S., Spudich, J. A., Egelman, E. H. and Fletterick, R. J. (2002) 'How does ATP hydrolysis control actin's associations?', *Proc Natl Acad Sci U S A,* 99(17), pp. 10945-7.

Saha, S., Nagy, T. L. and Weiner, O. D. (2018) 'Joining forces: crosstalk between biochemical signalling and physical forces orchestrates cellular polarity and dynamics', *Philos Trans R Soc Lond B Biol Sci,* 373(1747).

Sailer, A., Anneken, A., Li, Y., Lee, S. and Munro, E. (2015) 'Dynamic Opposition of Clustered Proteins Stabilizes Cortical Polarity in the C. elegans Zygote', *Dev Cell,* 35(1), pp. 131-42.

Sander, E. E., ten Klooster, J. P., van Delft, S., van der Kammen, R. A. and Collard, J. G. (1999) 'Rac Downregulates Rho Activity: Reciprocal Balance between Both Gtpases Determines Cellular Morphology and Migratory Behavior', *Journal of Cell Biology,* 147(5), pp. 1009-1022.

Schaefer, M., Petronczki, M., Dorner, D., Forte, M. and Knoblich, J. A. (2001) 'Heterotrimeric G proteins direct two modes of asymmetric cell division in the Drosophila nervous system', *Cell,* 107(2), pp. 183-94.

Schaefer, M., Shevchenko, A., Shevchenko, A. and Knoblich, J. A. (2000) 'A protein complex containing Inscuteable and the Galpha-binding protein Pins orients asymmetric cell divisions in Drosophila', *Curr Biol,* 10(7), pp. 353-62.

Schindelin, J., Arganda-Carreras, I., Frise, E., Kaynig, V., Longair, M., Pietzsch, T., Preibisch, S., Rueden, C., Saalfeld, S., Schmid, B., Tinevez, J. Y., White, D. J., Hartenstein, V., Eliceiri, K., Tomancak, P. and Cardona, A. (2012) 'Fiji: an open-source platform for biological-image analysis', *Nat Methods,* 9(7), pp. 676-82.

Schmutz, C., Stevens, J. and Spang, A. (2007) 'Functions of the novel RhoGAP proteins RGA-3 and RGA-4 in the germ line and in the early embryo of C. elegans', *Development,* 134(19), pp. 3495-505.

Schober, M., Schaefer, M. and Knoblich, J. A. (1999) 'Bazooka recruits Inscuteable to orient asymmetric cell divisions in Drosophila neuroblasts', *Nature,* 402(6761), pp. 548-51.

Schoentaube, J., Olling, A., Tatge, H., Just, I. and Gerhard, R. (2009) 'Serine-71 phosphorylation of Rac1/Cdc42 diminishes the pathogenic effect of Clostridium difficile toxin A', *Cell Microbiol,* 11(12), pp. 1816-26.

Scholze, M. J., Barbieux, K. S., De Simone, A., Boumasmoud, M., Suess, C. C. N., Wang, R. and Gonczy, P. (2018) 'PI(4,5)P2 forms dynamic cortical structures and directs actin distribution as well as polarity in Caenorhabditis elegans embryos', *Development,* 145(11).

Schonegg, S., Constantinescu, A. T., Hoege, C. and Hyman, A. A. (2007) 'The Rho GTPase-activating proteins RGA-3 and RGA-4 are required to set the initial size of PAR domains in Caenorhabditis elegans one-cell embryos', *Proc Natl Acad Sci U S A,* 104(38), pp. 14976-81.

Schonegg, S. and Hyman, A. A. (2006) 'CDC-42 and RHO-1 coordinate acto-myosin contractility and PAR protein localization during polarity establishment in C. elegans embryos', *Development,* 133(18), pp. 3507-16.

Schuldt, A. J., Adams, J. H., Davidson, C. M., Micklem, D. R., Haseloff, J., St Johnston, D. and Brand, A. H. (1998) 'Miranda mediates asymmetric protein and RNA localization in the developing nervous system', *Genes Dev,* 12(12), pp. 1847-57.

Schumacher, J. M., Ashcroft, N., Donovan, P. J. and Golden, A. (1998) 'A highly conserved centrosomal kinase, AIR-1, is required for accurate cell cycle progression and segregation of developmental factors in Caenorhabditis elegans embryos.', *Development,* 125, pp. 4391-4401.

Schwarz, J., Proff, J., Havemeier, A., Ladwein, M., Rottner, K., Barlag, B., Pich, A., Tatge, H., Just, I. and Gerhard, R. (2012) 'Serine-71 phosphorylation of Rac1 modulates downstream signaling', *PLoS One,* 7(9), pp. e44358.

Seydoux, G. (2018) 'The P granules of C. elegans: a genetic model for the study of RNA-protein condensates', *J Mol Biol,* 430, pp. 4702-4710.

Shan, Z., Tu, Y., Yang, Y., Liu, Z., Zeng, M., Xu, H., Long, J., Zhang, M., Cai, Y. and Wen, W. (2018) 'Basal condensation of Numb and Pon complex via phase transition during Drosophila neuroblast asymmetric division', *Nat Commun,* 9(1), pp. 737.

Shaye, D. D. and Greenwald, I. (2011) 'OrthoList: a compendium of C. elegans genes with human orthologs', *PLoS One,* 6(5), pp. e20085.

Shen, C. P., Jan, L. Y. and Jan, Y. N. (1997) 'Miranda is required for the asymmetric localization of Prospero during mitosis in Drosophila', *Cell,* 90(3), pp. 449-58.

Shimizu, T., Pastuhov, S. I., Hanafusa, H., Matsumoto, K. and Hisamoto, N. (2018) 'The C. elegans BRCA2-ALP/Enigma Complex Regulates Axon Regeneration via a Rho GTPase-ROCK-MLC Phosphorylation Pathway', *Cell Rep,* 24(7), pp. 1880-1889.

Siegrist, S. E. and Doe, C. Q. (2006) 'Extrinsic cues orient the cell division axis in Drosophila embryonic neuroblasts', *Development,* 133(3), pp. 529-536.

Siller, K. H., Cabernard, C. and Doe, C. Q. (2006) 'The NuMA-related Mud protein binds Pins and regulates spindle orientation in Drosophila neuroblasts', *Nat Cell Biol,* 8(6), pp. 594-600.

Singhvi, A., Teuliere, J., Talavera, K., Cordes, S., Ou, G., Vale, R. D., Prasad, B. C., Clark, S. G. and Garriga, G. (2011) 'The Arf GAP CNT-2 regulates the apoptotic fate in C. elegans asymmetric neuroblast divisions', *Curr Biol,* 21(11), pp. 948-54.

Small, L. E. and Dawes, A. T. (2017) 'PAR proteins regulate maintenance-phase myosin dynamics during Caenorhabditis elegans zygote polarization', *Mol Biol Cell,* 28(16), pp. 2220-2231.

Smith, C. A., Lau, K. M., Rahmani, Z., Dho, S. E., Brothers, G., She, Y. M., Berry, D. M., Bonneil, E., Thibault, P., Schweisguth, F., Le Borgne, R. and McGlade, C. J. (2007) 'aPKC-mediated phosphorylation regulates asymmetric membrane localization of the cell fate determinant Numb', *EMBO J,* 26(2), pp. 468-80.

Solon, J., Kaya-Çopur, A., Colombelli, J. and Brunner, D. (2009) 'Pulsed forces timed by a ratchet-like mechanism drive directed tissue movement during dorsal closure.', *Cell,* 137, pp. 1331-1342.

Sonal, Ganzinger, K. A., Vogel, S. K., Mucksch, J., Blumhardt, P. and Schwille, P. (2018) 'Myosin-II activity generates a dynamic steady state with continuous actin turnover in a minimal actin cortex', *J Cell Sci,* 132(4).

Soriano, E. V., Ivanova, M. E., Fletcher, G., Riou, P., Knowles, P. P., Barnouin, K., Purkiss, A., Kostelecky, B., Saiu, P., Linch, M., Elbediwy, A., Kjaer, S., O'Reilly, N., Snijders, A. P., Parker, P. J., Thompson, B. J. and McDonald, N. Q. (2016) 'aPKC Inhibition by Par3 CR3 Flanking Regions Controls Substrate Access and Underpins Apical-Junctional Polarization', *Dev Cell,* 38(4), pp. 384-98.

Sprang, S. R. (2016) 'Invited review: Activation of G proteins by GTP and the mechanism of Galpha-catalyzed GTP hydrolysis', *Biopolymers,* 105(8), pp. 449-62.

St Johnston, D. and Ahringer, J. (2010) 'Cell polarity in eggs and epithelia: parallels and diversity', *Cell,* 141(5), pp. 757-74.

Steinberg, S. F. (2008) 'Structural basis of protein kinase C isoform function', *Physiol Rev,* 88(4), pp. 1341-78.

Strand, D., Jakobs, R., Merdes, G., Neumann, B., Kalmes, A., Heid, H. W., Husmann, I. and Mechler, B. M. (1994) 'The Drosophila lethal(2)giant larvae tumor suppressor protein forms homo-oligomers and is associated with nonmuscle myosin II heavy chain', *J Cell Biol,* 127(5), pp. 1361-73.

Suzuki, A., Hirata, M., Kamimura, K., Maniwa, R., Yamanaka, T., Mizuno, K., Kishikawa, M., Hirose, H., Amano, Y., Izumi, N., Miwa, Y. and Ohno, S. (2004) 'aPKC acts upstream of PAR-1b in both the establishment and maintenance of mammalian epithelial polarity', *Curr Biol,* 14(16), pp. 1425-35.

Thielicke, W. (2014) 'The Flapping Flight of Birds - Analysis and Application. Phd thesis, Rijksuniversiteit Groningen'.

Thielicke, W. and Stamhuis, E. J. (2014) 'PIVlab – Towards User-friendly, Affordable and Accurate Digital Particle Image Velocimetry in MATLAB.', *Journal of Open Research Software,* 2(1), pp. e30.

Tong, J., Li, L., Ballermann, B. and Wang, Z. (2016) 'Phosphorylation and Activation of RhoA by ERK in Response to Epidermal Growth Factor Stimulation', *PLoS One,* 11(1), pp. e0147103.

Tsankova, A., Pham, T. T., Garcia, D. S., Otte, F. and Cabernard, C. (2017) 'Cell Polarity Regulates Biased Myosin Activity and Dynamics during Asymmetric Cell Division via Drosophila Rho Kinase and Protein Kinase N', *Dev Cell,* 42(2), pp. 143-155 e5.

Tse, Y. C., Werner, M., Longhini, K. M., Labbe, J. C., Goldstein, B. and Glotzer, M. (2012) 'RhoA activation during polarization and cytokinesis of the early Caenorhabditis elegans embryo is differentially dependent on NOP-1 and CYK-4', *Mol Biol Cell,* 23(20), pp. 4020-31.

Unbekandt, M. and Olson, M. F. (2014) 'The actin-myosin regulatory MRCK kinases: regulation, biological functions and associations with human cancer', *J Mol Med (Berl),* 92(3), pp. 217-25.

Vasquez, C. G., Tworoger, M. and Martin, A. C. (2014) 'Dynamic myosin phosphorylation regulates contractile pulses and tissue integrity during epithelial morphogenesis', *J Cell Biol,* 206, pp. 435-450.

Venkateswarlu, K., Brandom, K. G. and Yun, H. (2007) 'PI-3-kinase-dependent membrane recruitment of centaurin-alpha2 is essential for its effect on ARF6-mediated actin cytoskeleton reorganisation', *J Cell Sci,* 120(Pt 5), pp. 792-801.

Verma, V., Mogilner, A. and Maresca, T. J. (2019) 'Classical and emerging regulatory mechanisms of cytokinesis in animal cells', *Biology,* 8(55).

Visco, I., Hoege, C., Hyman, A. A. and Schwille, P. (2016) 'In vitro Reconstitution of a Membrane Switch Mechanism for the Polarity Protein LGL', *J Mol Biol,* 428(24 Pt A), pp. 4828-4842.

von Stein, W., Ramrath, A., Grimm, A., Muller-Borg, M. and Wodarz, A. (2005) 'Direct association of Bazooka/PAR-3 with the lipid phosphatase PTEN reveals a link between the PAR/aPKC complex and phosphoinositide signaling', *Development,* 132(7), pp. 1675-86.

Vorobiev, S., Strokopytov, B., Drubin, D. G., Frieden, C., Ono, S., Condeelis, J., Rubenstein, P. A. and Almo, S. C. (2003) 'The structure of nonvertebrate actin: implications for the ATP hydrolytic mechanism', *Proc Natl Acad Sci U S A,* 100(10), pp. 5760-5.

Vuong-Brender, T. T. K., Boutillon, A., Rodriguez, D., Lavilley, V. and Labouesse, M. (2018) 'HMP-1/α-catenin promotes junctional mechanical integrity during morphogenesis', *PLoS One,* 13(2), pp. e0193279.

Wang, C., Xu, H., Lin, S., Deng, W., Zhou, J., Zhang, Y., Shi, Y., Peng, D. and Xue, Y. (2020) 'GPS 5.0: An Update on the Prediction of Kinase-specific Phosphorylation Sites in Proteins', *Genomics Proteomics Bioinformatics*.

Wang, H. R., Zhang, Y., Ozdamar, B., Ogunjimi, A. A., Alexandrova, E., Thomsen, G. H. and Wrana, J. L. (2003) 'Regulation of cell polarity and protrusion formation by targeting RhoA for degradation', *Science,* 302(5651), pp. 1775-9.

Wang, J. and Seydoux, G. (2013) 'Germ cell specification', *Adv Exp Med Biol,* 757, pp. 17-39.

Wang, S. C., Low, T. Y. F., Nishimura, Y., Gole, L., Yu, W. and Motegi, F. (2017) 'Cortical forces and CDC-42 control clustering of PAR proteins for Caenorhabditis elegans embryonic polarization', *Nat Cell Biol,* 19(8), pp. 988-995.

White, J. G. and Borisy, G. G. (1983) 'On the mechanisms of cytokinesis in animal cells', *J Theor Biol,* 101, pp. 289-316.

Whitney, D. S., Peterson, F. C., Kittell, A. W., Egner, J. M., Prehoda, K. E. and Volkman, B. F. (2016a) 'Binding of Crumbs to the Par-6 CRIB-PDZ Module Is Regulated by Cdc42', *Biochemistry,* 55(10), pp. 1455-61.

Whitney, D. S., Peterson, F. C., Kittell, A. W., Egner, J. M., Prehoda, K. E. and Volkman, B. F. (2016b) 'Correction to Binding of Crumbs to the Par-6 CRIB-PDZ Module Is Regulated by Cdc42', *Biochemistry,* 55(13), pp. 2063.

Willis, J. H., Munro, E., Lyczak, R. and Bowerman, B. (2006) 'Conditional dominant mutations in the Caenorhabditis elegans gene act-2 identify cytoplasmic and muscle roles for a redundant actin isoform', *Mol Biol Cell,* 17(3), pp. 1051-64.

Wilson, R. C. and Doudna, J. A. (2013) 'Molecular mechanisms of RNA interference', *Annu Rev Biophys,* 42, pp. 217-39.

Wirtz-Peitz, F., Nishimura, T. and Knoblich, J. A. (2008) 'Linking cell cycle to asymmetric division: Aurora-A phosphorylates the Par complex to regulate Numb localization', *Cell,* 135(1), pp. 161-73.

Witte, K., Strickland, D. and Glotzer, M. (2017) 'Cell cycle entry triggers a switch between two modes of Cdc42 activation during yeast polarization', *Elife,* 6.

Wolfe, B. A., Takaki, T., Petronczki, M. and Glotzer, M. (2009) 'Polo-like kinase 1 directs assembly of the HsCyk-4 RhoGAP/Ect2 RhoGEF complex to initiate cleavage furrow formation', *PLoS Biol,* 7(5), pp. e1000110.

Woods, B., Lai, H., Wu, C.-F., Zyla, Trevin R., Savage, Natasha S. and Lew, Daniel J. (2016) 'Parallel Actin-Independent Recycling Pathways Polarize Cdc42 in Budding Yeast', *Current Biology,* 26(16), pp. 2114-2126.

Woods, B. and Lew, D. J. (2019) 'Polarity establishment by Cdc42: Key roles for positive feedback and differential mobility', *Small GTPases,* 10(2), pp. 130-137.

Woods, D. F., Hough, C., Peel, D., Callaini, G. and Bryant, P. J. (1996) 'Dlg protein is required for junction structure, cell polarity, and proliferation control in Drosophila epithelia', *J Cell Biol,* 134(6), pp. 1469-82.

Wright, A. J. and Hunter, C. P. (2003) 'Mutations in a beta-tubulin disrupt spindle orientation and microtubule dynamics in the early Caenorhabditis elegans embryo.', *Molecular biology of the cell,* 14, pp. 4512-4525.

Wu, C. F., Chiou, J. G., Minakova, M., Woods, B., Tsygankov, D., Zyla, T. R., Savage, N. S., Elston, T. C. and Lew, D. J. (2015a) 'Role of competition between polarity sites in establishing a unique front', *Elife,* 4.

Wu, Y., Kanchanawong, P. and Zaidel-Bar, R. (2015b) 'Actin-delimited adhesion-independent clustering of E-cadherin forms the nanoscale building blocks of adherens junctions', *Dev Cell,* 32(2), pp. 139-54.

Yamamoto-Hino, M. and Goto, S. (2013) 'In Vivo RNAi-Based Screens: Studies in Model Organisms', *Genes (Basel),* 4(4), pp. 646-65.

Yamanaka, T., Horikoshi, Y., Sugiyama, Y., Ishiyama, C., Suzuki, A., Hirose, T., Iwamatsu, A., Shinohara, A. and Ohno, S. (2003) 'Mammalian Lgl forms a protein complex with PAR-6

and aPKC independently of PAR-3 to regulate epithelial cell polarity', *Curr Biol,* 13(9), pp. 734-43.

Yamanaka, T., Horikoshi, Y., Suzuki, A., Sugiyama, Y., Kitamura, K., Maniwa, R., Nagai, Y., Yamashita, A., Hirose, T., Ishikawa, H. and Ohno, S. (2001) 'PAR-6 regulates aPKC activity in a novel way and mediates cell-cell contact-induced formation of the epithelial junctional complex', *Genes Cells,* 6(8), pp. 721-31.

Ye, M., Shima, F., Muraoka, S., Liao, J., Okamoto, H., Yamamoto, M., Tamura, A., Yagi, N., Ueki, T. and Kataoka, T. (2005) 'Crystal structure of M-Ras reveals a GTP-bound "off" state conformation of Ras family small GTPases', *J Biol Chem,* 280(35), pp. 31267-75.

Yeaman, C., Grindstaff, K. K. and Nelson, W. J. (1999) 'New perspectives on mechanisms involved in generating epithelial cell polarity', *Physiol Rev,* 79(1), pp. 73-98.

Yi, K., Rubinstein, B. and Li, R. (2013a) 'Symmetry breaking and polarity establishment during mouse oocyte maturation', *Philos Trans R Soc Lond B Biol Sci,* 368(1629), pp. 20130002.

Yi, K., Rubinstein, B., Unruh, J. R., Guo, F., Slaughter, B. D. and Li, R. (2013b) 'Sequential actin-based pushing forces drive meiosis I chromosome migration and symmetry breaking in oocytes', *J Cell Biol,* 200(5), pp. 567-76.

Yoshiura, S., Ohta, N. and Matsuzaki, F. (2012) 'Tre1 GPCR signaling orients stem cell divisions in the Drosophila central nervous system', *Dev Cell,* 22(1), pp. 79-91.

Yu, F., Morin, X., Cai, Y., Yang, X. and Chia, W. (2000) 'Analysis of partner of inscuteable, a novel player of Drosophila asymmetric divisions, reveals two distinct steps in inscuteable apical localization', *Cell,* 100(4), pp. 399-409.

Zaidel-Bar, R., Zhenhuan, G. and Luxenburg, C. (2015) 'The contractome--a systems view of actomyosin contractility in non-muscle cells', *J Cell Sci,* 128(12), pp. 2209-17.

Zhang, D. and Glotzer, M. (2015) 'The RhoGAP activity of CYK-4/MgcRacGAP functions non-canonically by promoting RhoA activation during cytokinesis', *Elife,* 4.

Zhang, H., Neimanis, S., Lopez-Garcia, L. A., Arencibia, J. M., Amon, S., Stroba, A., Zeuzem, S., Proschak, E., Stark, H., Bauer, A. F., Busschots, K., Jørgensen, T. J., Engel, M., Schulze, J. O. and Biondi, R. M. (2014) 'Molecular mechanism of regulation of the atypical

protein kinase C by N-terminal domains and an allosteric small compound', *Chem Biol,* 21(6), pp. 754-65.

Zhang, X., Hashemi, S. S., Yousefi, M., Gao, C., Sheng, J., Ni, J., Wang, W., Mason, J. and Man, Y. G. (2009) 'Atypical E-cadherin expression in cell clusters overlying focally disrupted mammary myoepithelial cell layers: implications for tumor cell motility and invasion', *Pathol Res Pract,* 205(6), pp. 375-85.

Zhang, X., Ma, C., Miller, A. L., Katbi, H. A., Bement, W. M. and Liu, X. J. (2008) 'Polar body emission requires a RhoA contractile ring and Cdc42-mediated membrane protrusion', *Dev Cell,* 15(3), pp. 386-400.

Zhao, P., Teng, X., Tantirimudalige, S. N., Nishikawa, M., Wohland, T., Toyama, Y. and Motegi, F. (2019) 'Aurora-A Breaks Symmetry in Contractile Actomyosin Networks Independently of Its Role in Centrosome Maturation', *Dev Cell,* 49(4), pp. 651-653.

Zhuravlev, Y., Hirsch, S. M., Jordan, S. N., Dumont, J., Shirasu-Hiza, M. and Canman, J. C. (2017) 'CYK-4 regulates Rac, but not Rho, during cytokinesis', *Mol Biol Cell,* 28(9), pp. 1258-1270.

Ziman, M., O'Brien, J. M., Ouellette, L. A., Church, W. R. and Johnson, D. I. (1991) 'Mutational analysis of CDC42Sc, a Saccharomyces cerevisiae gene that encodes a putative GTP-binding protein involved in the control of cell polarity', *Mol Cell Biol,* 11(7), pp. 3537-44.

Zonies, S., Motegi, F., Hao, Y. and Seydoux, G. (2010) 'Symmetry breaking and polarization of the C. elegans zygote by the polarity protein PAR-2', *Development,* 137(10), pp. 1669-77.

Zou, Y., Shao, Z., Peng, J., Li, F., Gong, D., Wang, C., Zuo, X., Zhang, Z., Wu, J., Shi, Y. and Gong, Q. (2014) 'Crystal structure of triple-BRCT-domain of ECT2 and insights into the binding characteristics to CYK-4', *FEBS Lett,* 588(17), pp. 2911-20.

APPENDICES

The following appendices have been included:

- Appendix I: Supplemetary figures with DAPI stainings of embryos shown througout the thesis.
- Appendix II: article and review published during this thesis.

The following articles have been included in this appendix:

Rodriguez J*, Peglion F*, Martin J, Hubatsch L, Reich J, Hirani N, **Gubieda AG**, Roffey J, Fernandes AR, St Johnston D, Ahringer J, Goehring NW. (August 2017) aPKC Cycles between Functionally Distinct PAR Protein Assemblies to Drive Cell Polarity. *Dev Cell.*

Gubieda AG*, Parker J*, Squire I, Martin J, Rodriguez J. (August 2020) Going with the flow: insights from *Caenorhabditis elegans* zygote polarisation. *Philos Trans R Soc B.*

Appendix I: Supplementary Figures of Embryo Staging

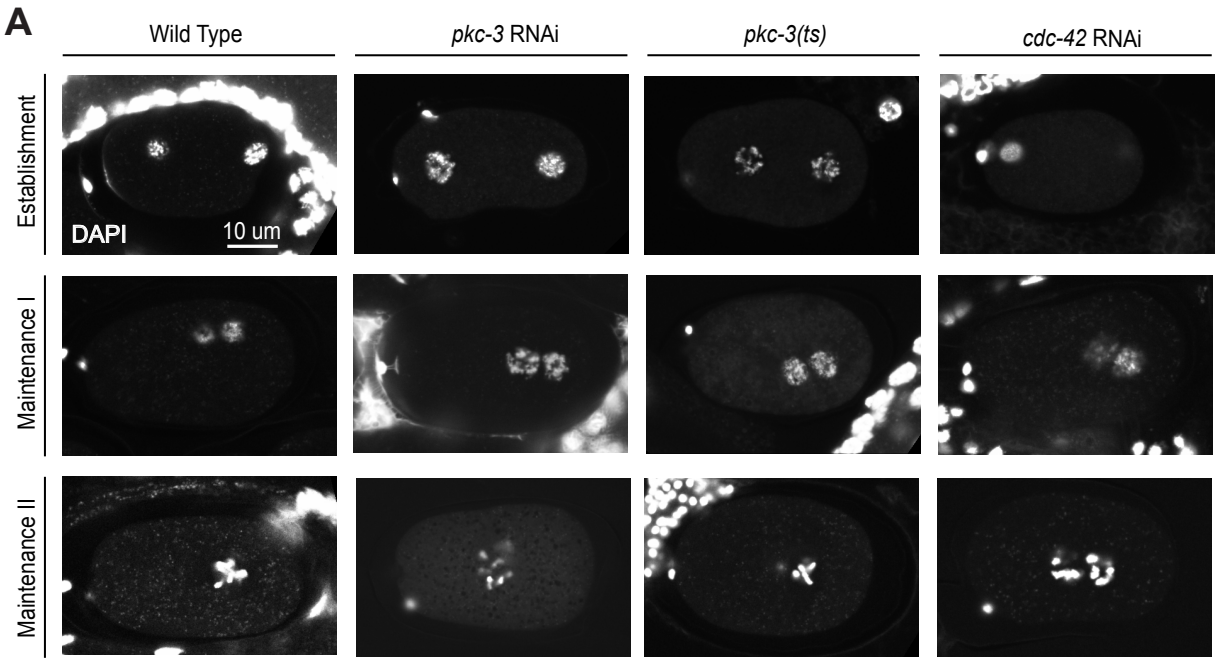

Figure S1. A. Midplane images of DNA (DAPI) in embryos shown in **Chapter 3, Figure 3.4.**

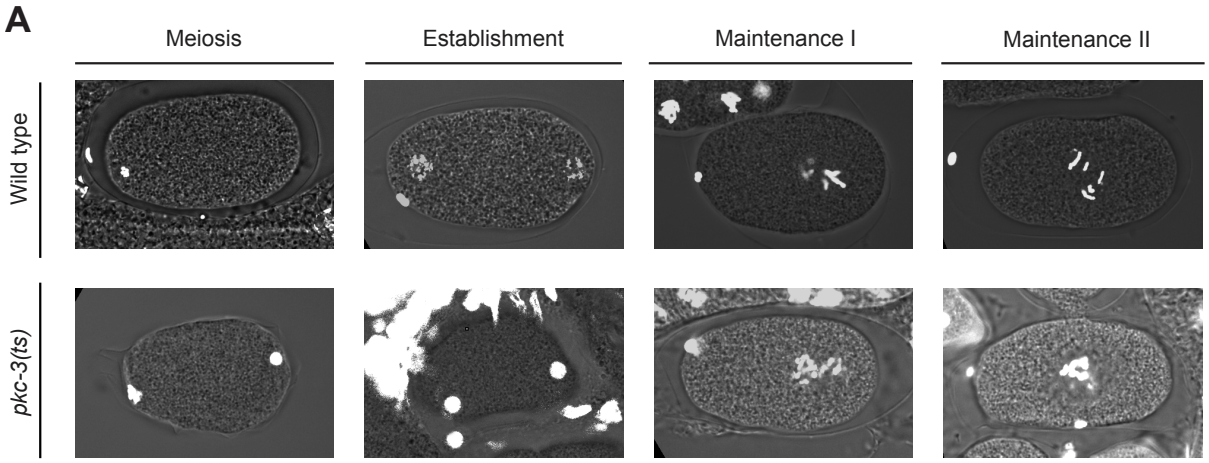

Figure S2. A. Midplane images of DNA (DAPI staining) and transmited light in embryos shown in **Chapter 5, Figure 5.2.**

Appendix II: Published Articles

CellPress

Developmental Cell
Article

aPKC Cycles between Functionally Distinct PAR Protein Assemblies to Drive Cell Polarity

Josana Rodriguez,[1,2,6,7,*] Florent Peglion,[3,6] Jack Martin,[1] Lars Hubatsch,[3] Jacob Reich,[3] Nisha Hirani,[3] Alicia G. Gubieda,[1] Jon Roffey,[4] Artur Ribeiro Fernandes,[2] Daniel St Johnston,[2] Julie Ahringer,[2] and Nathan W. Goehring[3,5,*]

[1]Institute for Cell and Molecular Biosciences, Newcastle University, Newcastle upon Tyne NE2 4HH, UK
[2]Wellcome Trust/Cancer Research UK Gurdon Institute, Cambridge CB2 1QN, UK
[3]The Francis Crick Institute, London NW1 1AT, UK
[4]Cancer Research Technology, Wolfson Institute for Biomedical Research, London WC1E 6BT, UK
[5]Medical Research Council Laboratory for Molecular Cell Biology, University College London, London WC1E 6BT, UK
[6]These authors contributed equally
[7]Lead Contact
*Correspondence: josana.rodriguez@ncl.ac.uk (J.R.), nate.goehring@crick.ac.uk (N.W.G.)
http://dx.doi.org/10.1016/j.devcel.2017.07.007

SUMMARY

The conserved polarity effector proteins PAR-3, PAR-6, CDC-42, and atypical protein kinase C (aPKC) form a core unit of the PAR protein network, which plays a central role in polarizing a broad range of animal cell types. To functionally polarize cells, these proteins must activate aPKC within a spatially defined membrane domain on one side of the cell in response to symmetry-breaking cues. Using the *Caenorhabditis elegans* zygote as a model, we find that the localization and activation of aPKC involve distinct, specialized aPKC-containing assemblies: a PAR-3-dependent assembly that responds to polarity cues and promotes efficient segregation of aPKC toward the anterior but holds aPKC in an inactive state, and a CDC-42-dependent assembly in which aPKC is active but poorly segregated. Cycling of aPKC between these distinct functional assemblies, which appears to depend on aPKC activity, effectively links cue-sensing and effector roles within the PAR network to ensure robust establishment of polarity.

INTRODUCTION

A crucial step in the polarization of metazoan cells is the localization of conserved sets of polarity effectors, known as the partitioning-defective or PAR proteins, to discrete membrane-associated cortical domains. Regulation of PAR protein distribution is essential for the localized activation of signaling pathways that coordinate many aspects of embryonic development, including asymmetric cell division, epithelial organization, and embryo axis establishment (Goldstein and Macara, 2007; St Johnston and Ahringer, 2010). Although the precise details vary between systems, in most cases the conserved PDZ domain proteins PAR-3 and PAR-6, the small guanosine triphosphatase (GTPase) CDC-42 and atypical protein kinase C (aPKC) act together to establish polarity on one side of the cell and drive asymmetry of a range of downstream pathways (reviewed in Goehring, 2014; McCaffrey and Macara, 2012; Suzuki et al., 2004; Ziomek et al., 1982).

In *Caenorhabditis elegans*, PAR-3, PAR-6, CDC-42, and the aPKC ortholog, PKC-3, play an essential role in polarizing the one-cell embryo or zygote by defining an anterior domain and hence are referred to as anterior PARs or aPARs (Figures 1A–1C). An opposing set of posterior PARs or pPARs, consisting of PAR-1, PAR-2, LGL-1, and the CDC-42 GAP, CHIN-1, form a complementary domain at the posterior. Together, aPARs and pPARs define the anterior-posterior axis of the zygote and orchestrate an asymmetric division that restricts germline determinants to the posterior daughter cell (Beatty et al., 2010; Boyd et al., 1996; Etemad-Moghadam et al., 1995; Gotta et al., 2001; Guo and Kemphues, 1995; Hoege et al., 2010; Kay and Hunter, 2001; Kumfer et al., 2010; Tabuse et al., 1998; Watts et al., 1996).

Polarization is triggered by the sperm-donated centrosome via two semi-redundant pathways (Figures 1A and 1B). First, the centrosome induces actomyosin cortical flow away from the newly defined posterior pole, which transports membrane-associated aPAR proteins into the anterior (Cheeks et al., 2004; Goehring et al., 2011b; Mayer et al., 2010; Munro et al., 2004). Second, centrosomal microtubules promote local loading of PAR-2 in the posterior. PAR-2 then recruits PAR-1, which drives posterior exclusion of aPARs through phosphorylation of PAR-3 (Boyd et al., 1996; Hao et al., 2006; Motegi et al., 2011). Following this "establishment phase," the zygote enters a "maintenance phase" during which mutual antagonism between anterior and posterior PARs ensures their continued asymmetric localizations (Boyd et al., 1996; Cuenca et al., 2003; Etemad-Moghadam et al., 1995; Guo and Kemphues, 1995; Tabuse et al., 1998; Watts et al., 1996).

Anterior PAR protein function is mediated through the kinase activity of PKC-3, which can phosphorylate PAR-1, PAR-2, and LGL-1 and drive their dissociation from the membrane (Beatty et al., 2010; Hao et al., 2006; Hoege et al., 2010; Hurov et al., 2004; Motegi et al., 2011). PAR-3, PAR-6, and CDC-42 are all required for proper PKC-3 membrane localization (Gotta et al.,

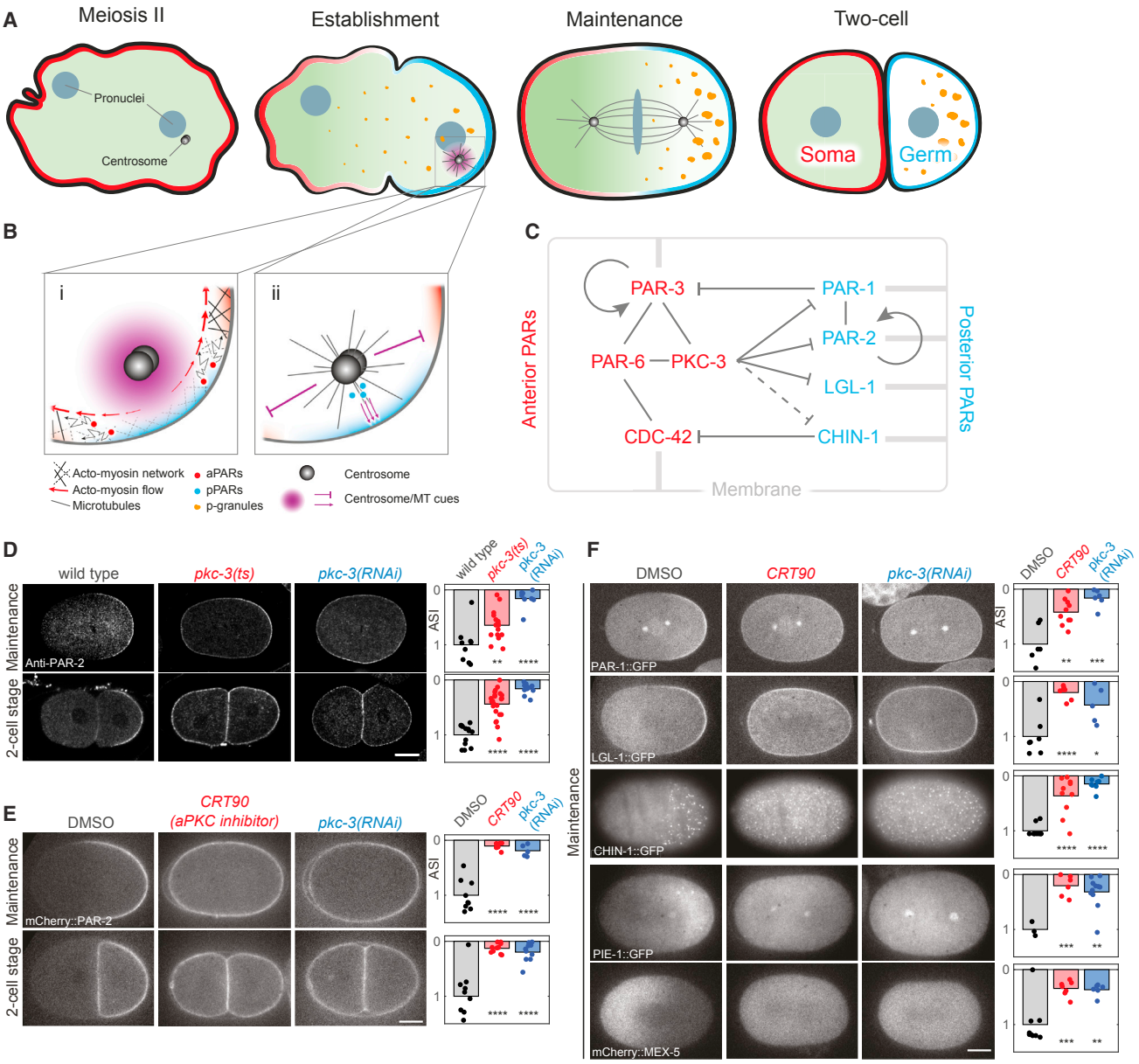

Figure 1. PKC-3 Kinase Inhibition Leads to Symmetric Division and Loss of Asymmetry of Downstream Polarity Markers

(A–C) Model for symmetry breaking by the PAR system in *C. elegans*. aPARs (red) initially occupy the membrane and pPARs (blue) are cytoplasmic (A, Meiosis II). A cue (purple) from the centrosome pair (black spheres) segregates aPARs into the anterior and promotes formation of a posterior PAR domain at the opposite pole (A, Establishment). PAR domains are then stable until cytokinesis (A, Maintenance) and drive polarization of cytoplasmic factors such as MEX-5/6 (green) and P granules (orange), which ensure the daughter cells acquire distinct fates (A, Two-cell). (B) Symmetry breaking can occur in two ways: (i) segregation of aPARs by cortical actomyosin flow (advection); and (ii) posterior PAR-2 loading. (C) A complex network of physical and regulatory interactions links the PAR proteins. Membrane binding (gray lines), physical interactions (black lines), as well as positive (→) and negative (⊥) feedback, are shown. Where links are indirect or unknown, dashed lines are used. Both CDC-42 and PAR-3 are required for stable membrane association of PAR-6/PKC-3. PAR-6 and PKC-3 depend on each other for membrane association. PAR-2, LGL-1, and presumably CHIN-1, are able to load onto the membrane independently. PAR-1 also binds membrane but requires PAR-2 to reach maximal concentrations. PKC-3 phosphorylates PAR-1, PAR-2, and LGL-1 and displaces them from the membrane. Exclusion of CHIN-1 from the anterior is dependent on PKC-3, but whether it is a direct target of PKC-3 is unknown. Together, PAR-1, via phosphorylation of PAR-3, and CHIN-1, by suppressing activated CDC-42, prevent invasion of the posterior domain by aPARs. PAR-3 and PAR-2 have been proposed to undergo oligomerization, which is thought to enhance their membrane association (noted by circular arrows). See recent reviews (Goehring, 2014; Hoege and Hyman, 2013; Motegi and Seydoux, 2013) for more information.

(D) Midsection confocal images of fixed zygotes stained for PAR-2 at polarity maintenance and two-cell stage comparing wild-type, *pkc-3*(*ts*), and *pkc-3*(*RNAi*) conditions.

(E) Midsection fluorescent images of mCherry:PAR-2-expressing zygotes at maintenance and two-cell stage in DMSO (control), CRT90-treated, and *pkc-3*(*RNAi*).

(legend continued on next page)

2001; Kay and Hunter, 2001; Schonegg and Hyman, 2006; Tabuse et al., 1998). Consequently, loss of any of these four proteins results in identical zygote polarity phenotypes: posterior PAR proteins are found uniformly on the embryo membrane and the first cell division is symmetric, leading to cell fate defects and embryo lethality (Etemad-Moghadam et al., 1995; Kay and Hunter, 2001; Tabuse et al., 1998; Watts et al., 1996).

This similarity of aPAR mutant phenotypes, their co-segregation within the anterior domain, and their ability to interact with one another in a wide range of systems (Izumi et al., 1998; Joberty et al., 2000; Lin et al., 2000; Qiu et al., 2000) has led to consideration of an effective aPAR unit comprising PAR-3, PAR-6, PKC-3, and CDC-42. However, work across a range of cell types suggests that such minimalism belies significant complexity in the regulation of aPAR localization and function, which we are only beginning to decipher.

For example, in epithelia, PAR-3 and aPKC localize to distinct regions of the apical domain: PAR-3 is primarily junctional, while PAR-6 and aPKC are more apical and, together with CDC-42 and Crumbs, exclude PAR-1 and LGL from the apical domain (Betschinger et al., 2003; Harris and Peifer, 2005; Morais-De-Sa et al., 2010; Yamanaka et al., 2006; Yamanaka et al., 2003).

In the *C. elegans* zygote, two modes of aPAR membrane association have been proposed: one associated with PAR-3 and independent of CDC-42, and one dependent on CDC-42 but not associated with PAR-3. Supporting this hypothesis, PAR-6 and PKC-3 only partially co-localize with PAR-3 in wild-type embryos, but co-localize strongly when CDC-42 is depleted (Beers and Kemphues, 2006; Hung and Kemphues, 1999; Tabuse et al., 1998). However, it remains unclear whether these observations reflect the existence of discrete functional modules and, if so, what their respective functions are.

A primary role of the aPAR network is to restrict PKC-3 kinase activity to the anterior domain. However, because localization, function, and regulation of PKC-3 are tightly coupled, parsing their individual contributions is difficult using traditional RNAi and knockout studies. Consequently, despite the central role of PKC-3 in polarity, we lack insight into how the individual contributions by PAR-3, PAR-6, CDC-42, and PKC-3 itself combine to ensure PKC-3 is activated only within the anterior domain. To address these questions, we require tools to independently modulate the localization and function of aPAR proteins.

Here we describe methods to independently manipulate PKC-3 activity and localization, which we use to investigate how PKC-3 kinase activity regulates organization of the aPAR network, and how PKC-3 activity is modulated by other network members. We find that localized PKC-3 kinase activity is linked to dynamic cycling of PAR-6/PKC-3 between two functionally distinct aPAR assemblies: (1) a PAR-3-dependent assembly that is associated with clusters and efficiently responds to polarizing cues, but in which PKC-3 activity is inhibited, and (2) a more diffuse CDC-42-dependent assembly that is less able to respond to polarizing cues but contains active PKC-3 and is responsible for posterior PAR protein exclusion. We propose that the dynamic exchange of PAR-6/PKC-3 between these two assemblies allows the PAR network to efficiently translate symmetry-breaking cues into an asymmetric homogeneous domain of PKC-3 activity.

RESULTS

Acute Inhibition of PKC-3 Function Leads to Loss of Asymmetric Division

We took two approaches to inhibit PKC-3 kinase activity. First, we examined a previously identified temperature-sensitive allele of *pkc-3*, *ne4246* (Fievet et al., 2012), which alters a conserved Asp residue (D386V) close to the active site. Strains carrying *pkc-3*(*ne4246*) are subsequently referred to as *pkc-3*(*ts*). Consistent with loss of PKC-3 function, in *pkc-3*(*ts*) zygotes at the restrictive temperature (25°C), PAR-2 is not restricted to the posterior membrane and is partitioned symmetrically into the two blastomeres at the first cell division (Figure 1D). Loss of asymmetry was quantified by the asymmetry index (ASI) (see STAR Methods), which measures the asymmetry of a feature, e.g., PAR-2 membrane intensity, relative to wild-type on a scale from zero (no asymmetry) to 1 (normal asymmetry) (Figure 1D and Movie S1). Results below and in Figure S1 indicate that loss of asymmetry in *pkc-3*(*ts*) zygotes is due to loss of PKC-3 activity rather than degradation.

In parallel, we examined PKC-3 inhibitors in permeable, *perm-1*(*RNAi*) embryos (Carvalho et al., 2011) to identify compounds that yielded a PKC-3 deficient polarity phenotype. One compound, CRT0103390 (CRT90), a derivative of CRT0066854 (Figures S2A–S2C) (Kjær et al., 2013; Dorsey et al., 2013) resulted in embryos that progressed normally through the cell cycle but showed loss of PAR-2 asymmetry and divided symmetrically (Figure 1E and Movie S1). CRT90 embryos exhibited other common phenotypes associated with *pkc-3*(*RNAi*) and *pkc-3*(*ts*), including simultaneous division of the two daughter cells and ectopic spindle rotation in the anterior daughter cell, leading to a chain-like arrangement of cells in the 4-cell embryo (data not shown). As expected for an inhibitor of PKC-3 activity, CRT90 treatment caused loss of asymmetry in other posterior PAR proteins (PAR-1, LGL-1, and CHIN-1) as well as the loss of cytoplasmic asymmetry in the cell fate determinants PIE-1 and MEX-5 (Figure 1F).

PKC-3 Inhibition Yields Distinct Phenotypes from PKC-3 Depletion

We next investigated the distributions of the anterior PAR proteins when PKC-3 activity was inhibited, and compared these to those observed when PKC-3 was depleted by RNAi. Normally, PAR-3, PAR-6, and PKC-3 are efficiently segregated into the anterior during the polarity establishment phase and remain asymmetric until cytokinesis (Figures 1A and 2A–2F) (Cuenca et al., 2003). When PKC-3 is depleted by RNAi of *pkc-3*, PAR-6 fails to localize to the membrane (Figure 2A) (Hung and

(F) Midsection (PAR-1, LGL-1, PIE-1, MEX-5) or cortical (CHIN-1) fluorescent images of maintenance-phase zygotes expressing markers to various downstream polarity markers in DMSO (control), CRT90-treated, and *pkc-3*(*RNAi*). Asymmetry in (D) to (F) is quantified by the asymmetry index, with one being normal asymmetry and zero, no asymmetry (ASI, normalized to DMSO/WT controls).
*p < 0.05, **p < 0.01, ***p < 0.001, ****p < 0.0001. Scale bars, 10 μm. See also Figures S1 and S2; Movie S1.

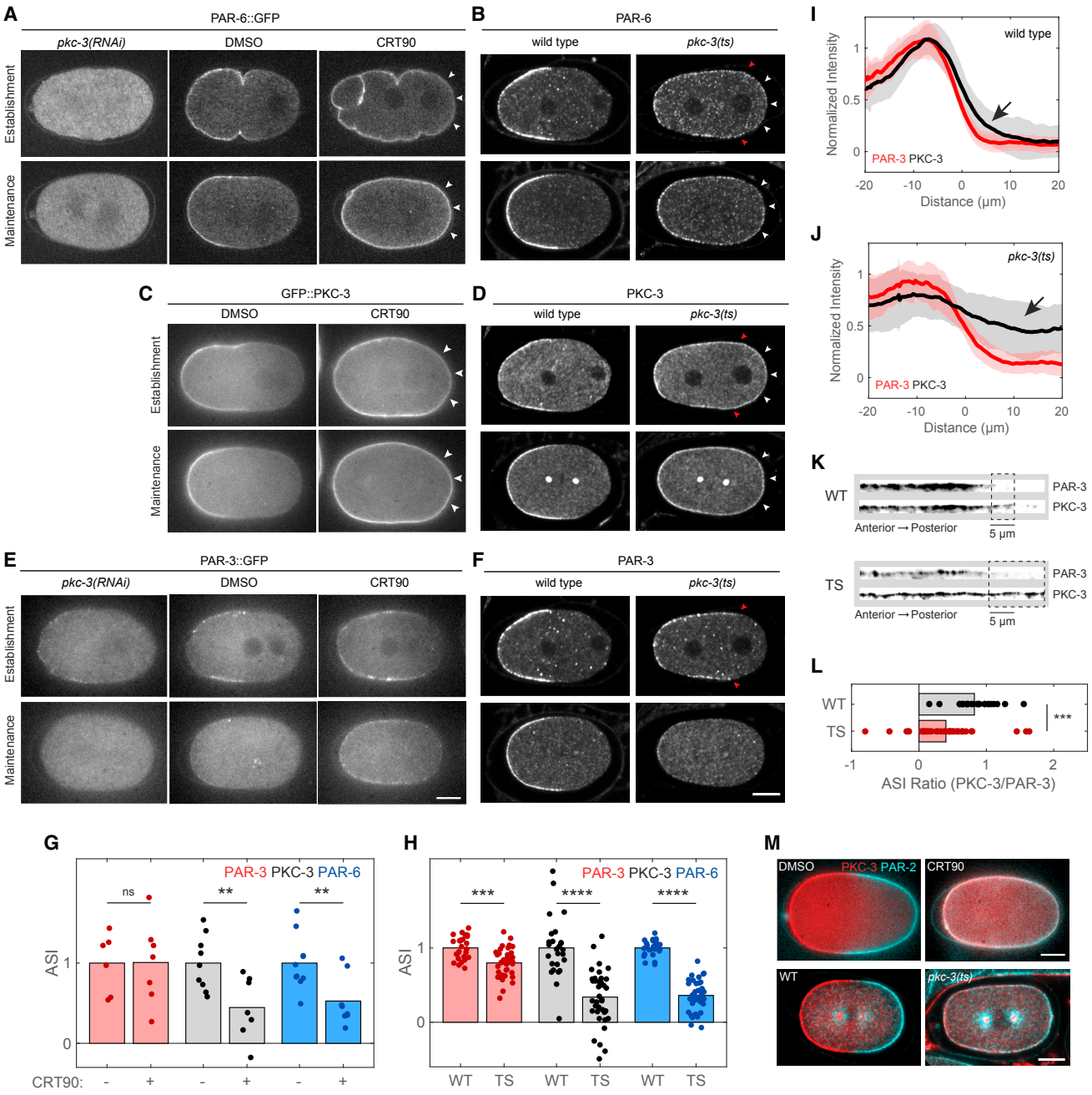

Figure 2. Membrane Localization of PAR-6/PKC-3 Is Decoupled from PAR-3 when PKC-3 Is Inactive

(A–F) Representative midsection confocal images of live and fixed zygotes at establishment and maintenance phase comparing control (DMSO, wild-type), *pkc-3(RNAi)*, and PKC-3-inhibited (CRT90, *pkc-3(ts)*) conditions. PAR-6 (A and B) and PKC-3 (C and D) show loss of asymmetric membrane staining in PKC-3-inhibited zygotes at both establishment and maintenance phase (posterior localization indicated by white arrowheads). In *pkc-3(RNAi)*, PAR-6 is absent from the membrane at all times. PAR-3 (E and F) still polarizes in PKC-3-inhibited zygotes, but becomes weaker and less asymmetric during maintenance phase. Note that (B), (D), and (F) show the same wild-type and TS zygotes with the PAR-3 boundary position in TS indicated (red arrowheads) to allow comparison: PAR-6 and PKC-3 are clearly visible at the posterior membrane (white arrowheads), while PAR-3 is undetectable, as in wild-type. Bright foci in (D) are non-specific centrosome staining.

(G and H) Normalized ASI measurements for late establishment phase datasets represented in (A) to (F). ASI is normalized to control (wild-type [WT] or DMSO) for each protein.

(I and J) Anterior to posterior membrane distributions of PAR-3 (red) and PKC-3 (black) in wild-type (I) and *pkc-3(ts)* (J) embryos. Arrows highlight the posterior extension of PKC-3 relative to PAR-3. Mean ± SD is shown.

(legend continued on next page)

Kemphues, 1999). By contrast, PAR-3 remains membrane associated and segregates into the anterior, but this population is generally reduced compared to wild-type and is lost as the cell proceeds through mitosis (Figure 2E) (Tabuse et al., 1998).

Unlike *pkc-3*(*RNAi*), when PKC-3 is inhibited by the D386V mutation or CRT90, PAR-6 and PKC-3 remain membrane associated, fail to segregate efficiently to the anterior, and a significant pool of both proteins remains localized at the posterior pole resulting in a loss of asymmetry relative to controls (Figures 2A–2D, 2G, and 2H; Movie S2). In contrast to PAR-6 and PKC-3, PAR-3 still segregates into the anterior during the establishment phase in PKC-3-inhibited zygotes (Figures 2E and 2F, Establishment). The domain is typically somewhat enlarged relative to wild-type zygotes, but PAR-3 asymmetry remains high and PAR-3 is absent from the posterior pole (Figures 2G and 2H). Following the establishment phase, PAR-3 levels at the membrane decline and become more symmetric (Figures 2E and 2F, Maintenance).

The distinct response of PAR-3 versus PAR-6 and PKC-3 is particularly clear in the quantification of dual-labeled fixed zygotes. In wild-type zygotes, the boundaries of the PAR-3 and PKC-3 domains are positioned similarly at the center of the zygote, although the PKC-3 domain extends a few microns further into the posterior (Figures 2I and 2K, WT). By contrast, in PKC-3-inhibited embryos, PKC-3 extends significantly further into the posterior compared with PAR-3, a condition we refer to as ''decoupled'' (Figures 2J–2L, TS). Consistent with this decoupling, upon PKC-3-inhibition we observe a decrease in co-localization between PAR-3 and PAR-6 at the membrane/cortex, even in the anterior domain where these PAR proteins overlap (Figure S3). Thus, we conclude that PKC-3 is required for the normally tight coupling between PAR-6/PKC-3 and PAR-3 during symmetry breaking.

These results point to an unappreciated complexity in the assembly and regulation of the PAR proteins at the cell membrane:

First, the loss of membrane-associated PAR-6 in PKC-3-depleted zygotes, but not in PKC-3-inhibited zygotes (Figure 2A), shows that disruption of PKC-3 activity or the resulting invasion of pPARs into the anterior (Figures 1D–1F) do not account for loss of PAR-6 membrane association. Rather, there appears to be a requirement for PKC-3 protein itself to target and stabilize PAR-6 at the membrane. Consistent with this interpretation, mutations in *par-2* and *par-1* fail to rescue PAR-6 membrane localization in *pkc-3*(*RNAi*) zygotes (Figure S4).

Second, in PKC-3-inhibited zygotes, anterior and posterior PAR protein distributions on the membrane overlap (Figure 2M). Posterior PAR proteins are thought to directly antagonize the ability of anterior PAR proteins to associate with the membrane, yet in these zygotes aPARs appear resistant to pPAR antagonism. PKC-3 inhibition could conceivably affect the activity of posterior PARs. However, we found that PAR-1 kinase activity, as measured by MEX-5 mobility (Griffin et al., 2011), appears normal in PKC-3-inhibited zygotes (Figures S2D–S2F). Thus, PKC-3 activity appears necessary to render anterior PARs sensitive to the antagonistic effects of posterior PARs, challenging the simple paradigm of mutual antagonism, which would predict pPAR dominance.

Finally, decoupling of PAR-6/PKC-3 from PAR-3 localization in PKC-3-inhibited zygotes during symmetry breaking suggests that PKC-3 drives formation of distinct PAR complexes or assemblies during polarity establishment in the *C. elegans* zygote. Contrary to what has been observed in *Drosophila* epithelia, where aPKC activity promotes decoupling of PAR-3 from PAR-6/aPKC and their targeting to distinct sites (Morais-De-Sa et al., 2010), here we observe the opposite: PKC-3 kinase activity is implicated in coupling the behaviors of PAR-3 and PAR-6/PKC-3, allowing their coordinated segregation during symmetry breaking.

PKC-3 Inhibition Promotes PAR-3-Independent Formation of CDC-42-Dependent PAR-6/PKC-3 Assemblies

If PKC-3 inhibition favors formation or trapping of a distinct functional assembly, we reasoned that it might affect the normal dependencies of PAR-6 and PKC-3 on PAR-3 and CDC-42. PKC-3 and PAR-6 normally require both PAR-3 and CDC-42 to localize stably to the membrane (Beers and Kemphues, 2006; Sailer et al., 2015). The dependency on PAR-3 is stronger: PKC-3 and PAR-6 fail to localize to the membrane in PAR-3-depleted zygotes (*par-3*(*RNAi*) in Figures 3A–3F) (Tabuse et al., 1998). By contrast, in CDC-42-depleted zygotes, PKC-3 and PAR-6 initially localize to the membrane and segregate to the anterior, but their membrane localization is gradually lost during the maintenance phase, becoming weaker and more uniform as zygotes approach cytokinesis (*cdc-42*(*RNAi*) Figures 3A–3F and Movie S4)(Beers and Kemphues, 2006; Gotta et al., 2001; Motegi and Sugimoto, 2006; Sailer et al., 2015; Schonegg and Hyman, 2006). Importantly, depletion of PAR-1 or PAR-2, which invade the anterior in the absence of PAR-3 or CDC-42 (Etemad-Moghadam et al., 1995; Gotta et al., 2001; Kay and Hunter, 2001; Schonegg and Hyman, 2006), fails to rescue PAR-6 membrane localization in these conditions (Figure S4). Thus, both PAR-3 and CDC-42 are directly required to promote membrane association of PAR-6 and PKC-3.

We find that under conditions of PKC-3 inhibition (D386V or CRT90), PKC-3 and PAR-6 no longer depend on PAR-3 to localize to the membrane (Figures 3A–3F and S5A; Movies S3 and S4). The degree of localization varies between the two methods of PKC-3 inhibition, possibly reflecting differences in the mechanism or timing/kinetics of kinase inhibition. By contrast, CDC-42 is still required for PKC-3 and PAR-6 membrane localization in PKC-3-inhibited zygotes (Figures 3A–3F, S5A, and S5B; Movie S4), indicating that CDC-42 is still required for PAR-6/PKC-3 membrane targeting even when PKC-3 is inhibited. Consistent with previous work showing that

(K) Close-up view of the boundary region showing PAR-3 (top) and PKC-3 (bottom) for one representative zygote for wild-type (WT) and *pkc-3*(*ts*) backgrounds as indicated. Dashed rectangular selection denotes regions where PKC-3 is present in absence of PAR-3.

(L) PKC-3 to PAR-3 ASI ratio for wild-type (WT) and *pkc-3*(*ts*).

(M) Dual labeling of PAR-2 and PKC-3 in live, CRT90-treated zygotes (top) and fixed, *pkc-3*(*ts*) embryos (bottom) reveal overlap of aPAR and pPAR proteins.

**p < 0.01, ***p < 0.001, ****p < 0.0001. ns, not significant. Scale bars, 10 μm. See also Figures S3 and S4; Movie S2.

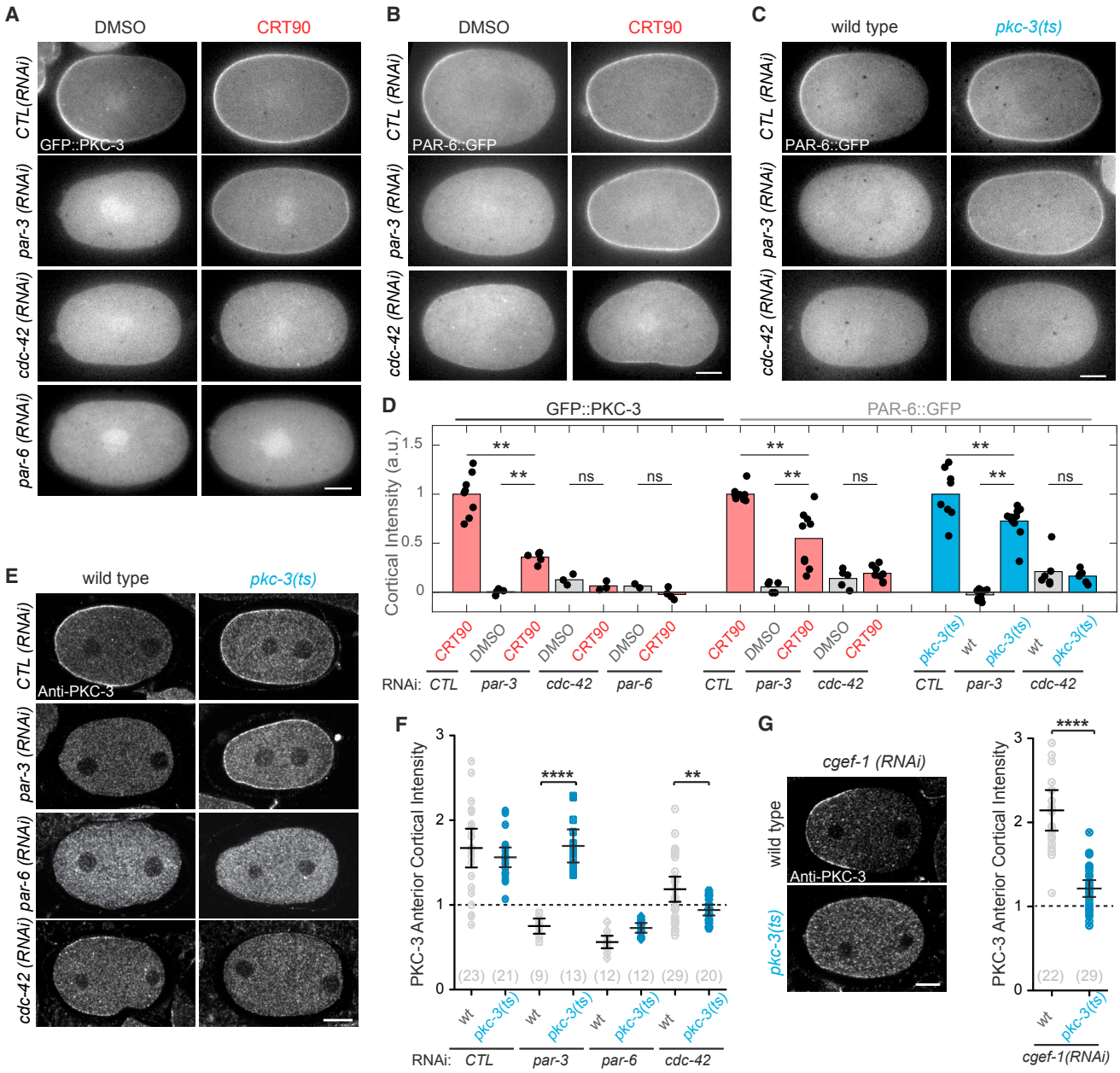

Figure 3. PKC-3 Inhibition Promotes PAR-3-Independent Formation of CDC-42-Dependent PAR-6/PKC-3 Assemblies

(A–C) Representative midsection confocal images of live embryos at maintenance phase showing GFP::PKC-3 (A) or PAR-6::GFP (B and C) of DMSO, CRT90-treated, and *pkc-3*(*ts*) zygotes subject to RNAi as indicated.

(D) Quantification of rescue for datasets represented in (A) to (C), normalized to membrane signal in control RNAi and CRT90-treated/*pkc-3*(*ts*) zygotes for each dataset.

(E) Representative midsection confocal images of wild-type and *pkc-3*(*ts*) zygotes during polarity establishment subject to RNAi as indicated and immunostained for PKC-3.

(F) Quantification of rescue as measured by anterior domain cortical intensity of PKC-3 for datasets represented in (E). For each zygote, anterior PKC-3 cortical intensity is divided by cytoplasmic intensity. Values greater than 1 indicate presence at the membrane. Mean ± 95% confidence interval (CI) (N) is shown. See STAR Methods for further details.

(G) Representative midsection confocal images during polarity establishment of wild-type and *pkc-3*(*ts*) embryos upon *cgef-1*(*RNAi*), stained for PKC-3. Scatterplot representing the anterior domain cortical intensity of PKC-3 as in (F) in *cgef-1*(*RNAi*) and *pkc-3*(*ts*);*cgef-1*(*RNAi*). Mean ± 95% CI (N) is shown.

**p < 0.01, ****p < 0.0001. ns, not significant. Scale bars, 10 μm. See also Figure S5; Movies S3 and S4.

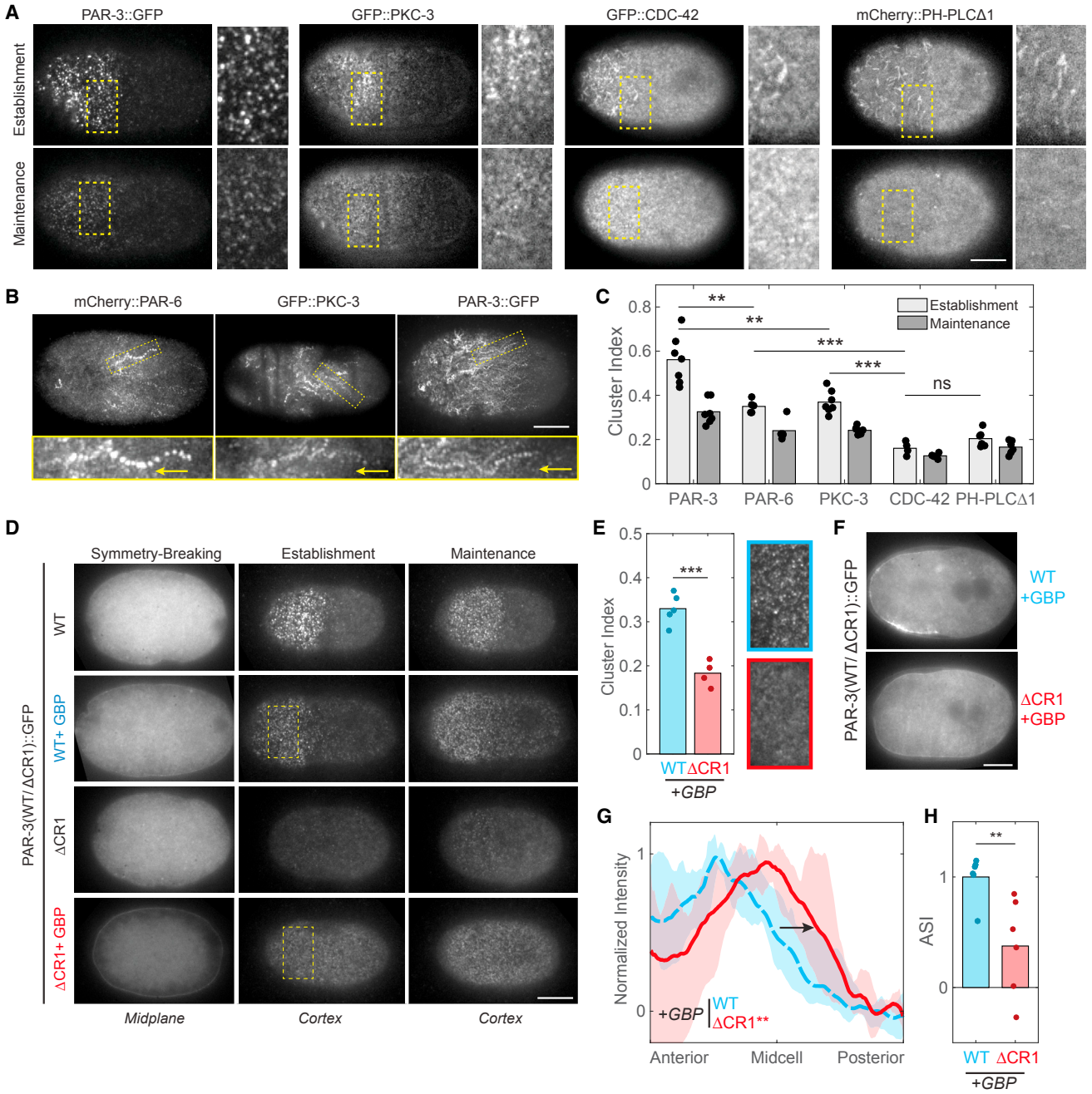

Figure 4. Segregation of Anterior PAR Proteins Involves Cortical Clusters

(A) Representative cortical images of PAR-3, PKC-3, CDC-42, and PH-PLCΔ1 in late-establishment and maintenance-phase zygotes along with zoom of inset region (yellow box).

(B) Time-averaged cortical images spanning 180 s reveal anterior-directed tracks of cortical clusters of PAR-3, PAR-6, and PKC-3. Insets highlight the motion (arrows) of a representative single cluster in the image above.

(C) Cluster index for the full dataset in (A) and PAR-6::GFP (images not shown). Significance between establishment and maintenance: $p < 0.01$ for PAR-3, PAR-6, and PKC-3.

(D) Representative midsection or cortical images of PAR-3::GFP (WT) or PAR-3ΔCR1::GFP (ΔCR1) with and without co-expression of the membrane tether PH::GBP (±GBP) shown at symmetry-breaking, establishment, or maintenance phase. Note enhancement of membrane signal visible in GBP-expressing zygotes viewed in midsection and lack of bright clusters of PAR-3ΔCR1::GFP viewed at the cortex.

(E) Cluster index for WT and ΔCR1 in the presence of the PH-GBP membrane tether (+GBP) along with magnification of insets (yellow dashed-line rectangles in D) indicated to highlight the difference in clustering.

(F) Representative midplane images of WT and ΔCR1 subject to GBP-membrane targeting showing defective segregation of ΔCR1. Images shown are from late-establishment phase.

(legend continued on next page)

PAR-6/aPKC are typically associated with an active, guanosine triphosphate (GTP)-bound form of CDC-42 (Atwood et al., 2007; Gotta et al., 2001; Joberty et al., 2000; Lin et al., 2000; Qiu et al., 2000), we found that decreasing CDC-42/GTP by depletion of the CDC-42 GEF, CGEF-1, reduces membrane association of PAR-6/PKC-3 in *pkc-3*(*ts*) embryos compared with wild-type, while leaving PAR-3 levels unchanged (Figures 3G and S5A–S5E). Finally, PKC-3 remains dependent on PAR-6 in PKC-3-inhibited embryos, consistent with PAR-6 being required to mediate the interactions of the PAR-6/PKC-3 heterodimer with PAR-3 and/or CDC-42 (Figures 3A and 3D–3F; Movie S4) (Joberty et al., 2000; Qiu et al., 2000), as well as our general findings that PKC-3 and PAR-6 respond similarly in all assays described.

Thus, inhibition of PKC-3 activity allows PKC-3 to bypass its normal requirement on PAR-3 to load onto the membrane and form stable membrane-associated CDC-42/GTP-dependent complexes. We postulate that it is this dependency on PAR-3, enforced by PKC-3 kinase activity, that ensures the coupled distributions of PKC-3 and PAR-3 in the embryo.

Segregation of Anterior PAR Proteins Is Associated with PAR-3-Dependent Clustering at the Membrane

So far, we have shown that inhibition of PKC-3 kinase activity promotes CDC-42-dependent assemblies, and in so doing prevents PKC-3 and PAR-6 from segregating efficiently with PAR-3 into the anterior during symmetry breaking. Previous work has shown that the efficient segregation of anterior PAR proteins is due to advective transport by anteriorly-directed actomyosin cortical flow (Cheeks et al., 2004; Goehring et al., 2011b; Munro et al., 2004). Because PAR-3 continues to be segregated efficiently in PKC-3-inhibited zygotes, we reasoned that PKC-3 inhibition may selectively alter the molecular organization of PAR-6 and PKC-3 at the membrane relative to PAR-3, which would be consistent with the observed shift toward CDC-42-dependent PKC-3 assemblies.

To investigate these possibilities, we imaged PAR-3, PAR-6, and PKC-3 at the membrane using variable-angle epifluorescence microscopy (VAEM or pseudo-TIRF) (Konopka and Bednarek, 2008). All three proteins exhibit a distinct clustered appearance during the polarity establishment phase, consistent with reports of non-homogenous distributions of PAR proteins at the membrane (Figures 4A and 5A, Establishment) (Munro et al., 2004; Robin et al., 2014; Sailer et al., 2015). Similar to previous analysis of PAR-6 (Munro et al., 2004), we find that clusters of PAR-6, PAR-3, and PKC-3 move in a highly directional manner in the direction of cortical flow, coinciding with increasing overall asymmetry (Figure 4B and Movie S5). While aPAR clusters have been noted (Hung and Kemphues, 1999; Munro et al., 2004; Sailer et al., 2015), the relationship between clustered and non-clustered PAR proteins and their ability to segregate in response to flow has not been explored.

To test whether clustering is a key driver of aPAR segregation, we examined whether PAR-3 transport depends on its ability to cluster. PAR-3 contains a conserved CR1 oligomerization domain, which is required for membrane binding and is targeted by PAR-1 kinase to induce displacement form the membrane (Benton and St Johnston, 2003; Feng et al., 2007; Li et al., 2010; Mizuno et al., 2003). We reasoned that this domain would be required for clustering; however, because mutations in the CR1 domain disrupt membrane binding (Figure 4D, WT versus ΔCR1), assessing clustering and segregation of a PAR-3ΔCR1 mutant requires an alternative mode of membrane targeting. We restored membrane localization of GFP:PAR-3ΔCR1 using a membrane-tethered anti-GFP nanobody (PH-GBP) and compared this with the behavior of GFP:PAR-3 (wild-type) that was also tethered to the membrane via PH-GBP. Targeting both wild-type and ΔCR1 to the membrane with PH-GBP reduces potential confounding effects of PAR-1-induced membrane displacement in the posterior. Thus, differences in segregation in PAR-3ΔCR1 relative to wild-type should be due to changes in clustering rather than differential sensitivity to PAR-1.

Consistent with oligomerization being required for clustering, membrane-tethered PAR-3ΔCR1 exhibited more diffuse membrane localization compared with wild-type controls (Figures 4D and 4E, WT + GBP versus ΔCR1 + GBP). PAR-3ΔCR1 also showed reductions in both segregation into the anterior and overall asymmetry (Figures 4F–4H and Movie S5). Thus, the ability of the CR1 domain to drive formation of membrane-associated PAR-3 clusters ensures that PAR-3 is efficiently transported by cortical flows in addition to its known role in promoting membrane association.

Balance between PAR-3 and CDC-42 Assemblies Tunes Cortical Organization and Sensitivity to Cortical Flow

The correlation between lack of PAR-3 clustering and defects in advective transport prompted us to examine the organization of anterior PAR proteins at the membrane in more detail. Although PAR-6 and PKC-3 exhibit a distinct clustered appearance similar to PAR-3 during polarity establishment, clusters are less pronounced and accompanied by a background of a more diffuse population (Figures 4A, 4C, and 5A). By contrast, CDC-42 exhibits a more uniform signal overall that resembles typical membrane markers, such as the PIP_2 (phosphatidylinositol-4,5-bisphosphate) probe PH-PLCΔ1 (Figures 4A and 4C). Membrane markers do exhibit enriched signals in membrane folds and protrusions, which are also enriched in the anterior, but these signals are clearly distinguishable from clusters.

With the transition into maintenance phase, clusters of PAR-6 and PKC-3 become less prominent and a diffuse population dominates. This change coincides temporally with a decrease in the prominence of PAR-3 clusters and an overall reduction in PAR-3 membrane localization (Figures 4A and 4C) as well as an increase in anterior CDC-42 activity (Figures S5C–S5E) (Kumfer et al., 2010). We therefore speculated that the mix of diffuse and clustered PAR-6/PKC-3 observed during establishment phase may reflect the distinct CDC-42- and PAR-3-dependent assemblies that we describe above. Consequently,

(G) Membrane intensity profiles for the full dataset represented in (F), showing average (solid line) and full range of data (shaded). Arrow highlights posterior expansion of the PAR-3 domain boundary.

(H) ASI quantification of membrane intensity profiles in (G) showing significant reduction in asymmetry in the ΔCR1 mutant.

**$p < 0.01$, ***$p < 0.001$. ns, not significant. Scale bars, 10 μm. See also Movie S5.

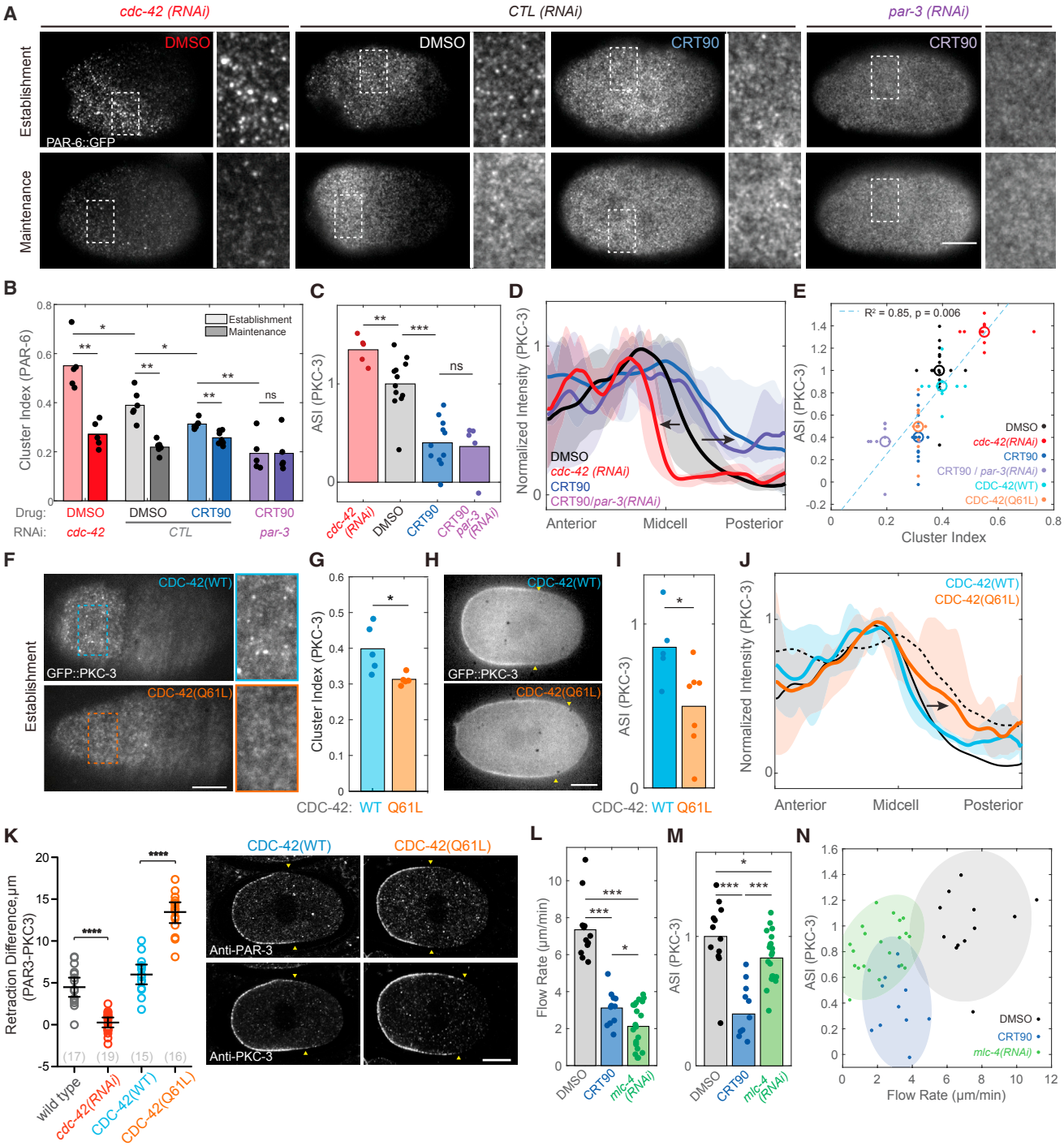

Figure 5. Regulation of PKC-3/PAR-6 Cluster Association by PAR-3/CDC-42 Balance Tunes Responsiveness to Cortical Flows

(A) Representative cortical images of PAR-6::GFP at late-establishment and maintenance-phase embryos for indicated conditions, shown along with a zoom of inset region (white boxes).

(B) Cluster index measurements of full dataset reveal a gradient of cluster association across conditions. Note that clustering decreases when embryos enter maintenance phase, except for CRT90/*par-3*(*RNAi*) embryos, which show minimal clustering even in establishment phase.

(C) ASI measurements of midsection images taken at late-establishment phase for a similar set of embryos as in (A) and (B), but expressing GFP::PKC-3, show a similar trend.

(D) Profiles of membrane signal for zygotes in (C) showing average (solid line) and full range of data (shaded) reveal shift of the PKC-3 domain boundary (arrows) toward the anterior in *cdc-42*(*RNAi*) embryos and toward the posterior in CRT90-treated zygotes, resulting in significantly ($p < 0.01$) smaller and larger domain sizes, respectively.

(legend continued on next page)

cell-cycle-dependent changes in the balance between assembly types could effectively tune the system to promote efficient transport of aPAR species during the polarity establishment phase.

To test this hypothesis, we altered the balance between CDC-42- and PAR-3-dependent assemblies and monitored the corresponding changes in (1) organization at the membrane, and (2) segregation efficiency. In general, we find a striking correlation between quantitative measures of cortical clustering and overall asymmetry.

Depletion of CDC-42 is known to increase co-localization of PAR-6 with PAR-3 during polarity establishment (Beers and Kemphues, 2006). We find that this also increases overall clustering of PAR-6 (Figures 5A and 5B). Examination of PKC-3 distributions clearly reveals enhanced segregation, with increased ASI (Figure 5C) and a visibly steeper domain boundary that is shifted toward the anterior (Figure 5D), resulting in a smaller anterior domain (*$p < 0.01$). Consistent with these data, we also observe a tighter coupling between the PAR-3 and PKC-3 domain boundaries in dual-labeled fixed zygotes (Figure 5K).

In contrast to CDC-42 depletion, inhibition of PKC-3 using CRT90, which favors CDC-42-dependent assemblies, shows reduced clustering of PAR-6, which could be reduced further by also depleting PAR-3 (Figures 5A and 5B). Under these conditions that favor CDC-42-dependent assemblies and reduced clustering, PKC-3 segregated less efficiently than DMSO controls, exhibited a reduced ASI, and failed to be fully excluded from the posterior (Figures 5C and 5D). To confirm that this reduction in clustering and segregation is due to favoring CDC-42-dependent assemblies, we examined the effect of expressing CDC-42 (Q61L), which stabilizes the active GTP-bound form of CDC-42 (Aceto et al., 2006; Ziman et al., 1991). Unlike PKC-3 inhibition, CDC-42 (Q61L) does not efficiently bypass the normal dependence of PKC-3 on PAR-3 (Figures S5F–S5J). This suggests that inhibition of PKC-3 favors CDC-42-associated assemblies via a mechanism distinct from stabilizing the GTP-bound form of CDC-42. However, similar to what we see when PKC-3 is inhibited, expression of CDC-42 (Q61L) reduced clustering and resulted in less efficient segregation of PKC-3 (Figures 5F–5K). Thus, regardless of the mechanism by which we alter the balance between PAR-3- and CDC-42-dependent assemblies, we achieve similar effects on clustering and segregation. This is particularly striking when we plot mean cluster index versus asymmetry across all conditions at establishment phase (Figure 5E).

Because PAR proteins are known to regulate actomyosin dynamics (Cheeks et al., 2004; Munro et al., 2004), and changes in flow velocities could, in principle, affect advective transport (Goehring et al., 2011b), we wanted to confirm that clustering rather than potential changes in flow velocity were the cause of reduced segregation efficiency. Measurements of flow rates from yolk granule motion in differential interference contrast (DIC) images allowed us to test the relationship between cortical flow rates and asymmetry in individual zygotes. Consistent with anterior PARs promoting their own segregation via stimulation of cortical flows, we find that PKC-3 inhibition results in a reduction of flow rates from approximately 6–10 μm/min in controls to approximately 2–5 μm/min in CRT90-treated embryos (Figure 5L). To test whether alterations in flow velocities could account for the observed segregation defects, we performed a partial depletion of MLC-4 to generate embryos with flow velocities of a similar range as observed in PKC-3-inhibited embryos (Figure 5L). Despite a similar range of flow velocities, MLC-4-depleted zygotes show a minimal reduction in asymmetry versus controls (Figures 5M and S6A). Plotting flow velocity versus ASI reveals a weak decline in ASI as flow rates are reduced (Figure 5N). By contrast, CRT90-treated embryos show a lower ASI across the full range of observed flow rates (~2–5 μm/min, Figures 5N and S6A). Finally, to test whether restoring flows could rescue efficient segregation of PKC-3, we used RNAi to target the RhoGAPs, RGA-3/4, which results in excess actomyosin contractility and increased cortical flow rates (Fievet et al., 2012; Schonegg et al., 2007). Despite fully rescuing the moderate reduction in asymmetry of PAR-3 observed in *pkc-3*(*ts*) embryos to levels indistinguishable from wild-type, RGA-3/4 depletion failed to restore asymmetry of PKC-3 (Figures S6B and S6C).

Together these data suggest that it is the failure of PKC-3 to associate with clusters rather than changes in flow rates that are the dominant factor in the decoupling between the localization of PAR-3 and PAR-6/PKC-3 observed in PKC-3-inhibited embryos. In fact, the resilience of PKC-3 asymmetry in embryos partially depleted of MLC-4 suggests that there is a relatively low threshold velocity required for efficient segregation of aPAR proteins by cortical flow, provided aPARs are able to associate normally into clusters.

We therefore conclude that although both PAR-3 and CDC-42 are critical for normal PAR-6/PKC-3 localization at the membrane in wild-type embryos, they drive formation of distinct aPAR assemblies, with distinct physical properties and

(E) Combining clustering data from pseudo-TIRF imaging in (A) and (B) and (F) and (G) with ASI measurements of a complete GFP::PKC-3 dataset for late-establishment phase across all conditions allows us to plot cluster index versus ASI for the mean of each condition, revealing a strong correlation (linear regression: $R^2 = 0.85$, $p < 0.01$).

(F–I) Representative cortical images (F, full zygote and inset zoom), cluster index (G), representative midsection images (H), and ASI (I) for late-establishment phase zygotes expressing GFP::PKC-3 in combination with either CDC-42(WT) or CDC-42 (Q61L). Yellow arrowheads in (H) highlight PKC-3 domain boundaries.

(J) Profiles of membrane signal for zygotes in (I) showing average (solid line) and full range of data (shaded) highlight the posterior shift (black arrow) of the PKC-3 boundary in Q61L-expressing zygotes ($p < 0.05$). Profiles for wild-type (solid black line) and CRT90-treated (dashed line) from (D) shown for comparison.

(K) Quantification of the difference in boundary position between PAR-3 and PKC-3 in dual-labeled fixed zygotes for indicated conditions. Mean ± 95% CI (N) is shown. Positive values indicate reduced PKC-3 segregation relative to PAR-3. Representative images of PAR-3 and PKC-3 in zygotes overexpressing CDC-42(WT) of CDC-42 (Q61L). Yellow arrowheads indicate the posterior boundary of the PAR-3 or PKC-3 domains.

(L and M) Comparison of cortical flow velocities (L) and PKC-3 asymmetry (M, ASI) for DMSO, CRT90, or *mlc-4*(*RNAi*) embryos taken at late-establishment phase.

(N) A plot of PKC-3 ASI versus cortical flow rates for individual zygotes treated with DMSO, CRT90, or *mlc-4*(*RNAi*). Data points for individual embryos are shown with a 90% confidence boundary (shaded region).

*$p < 0.05$, **$p < 0.01$, ***$p < 0.001$, ****$p < 0.0001$. ns, not significant. Scale bars, 10 μm. See also Figure S6.

responsiveness to cortical flow: PAR-3-dependent assemblies exhibit pronounced clustering, at least during the establishment phase, and are efficiently segregated by cortical flow. By contrast, CDC-42-dependent assemblies are more diffuse, likely reflecting enhanced diffusional mobility, and are inefficiently segregated by flow. Importantly, the balance between these two species appears to be subject to cell-cycle-dependent regulation to ensure maximal clustering and transport during the period of peak actomyosin cortical flows.

A PKC-3 Membrane-Targeting Assay Reveals Opposing Roles for PAR-3 and CDC-42 in Regulating PKC-3 Activity

We next sought to explore whether there were other functional differences in these two types of assemblies. Specifically, we wondered whether PAR-3 and CDC-42 may have distinct regulatory effects on PKC-3 activity *in vivo*, which is difficult to analyze given their roles in PKC-3 membrane loading. While CDC-42 is generally thought to play an activating role (Atwood et al., 2007; Gotta et al., 2001; Joberty et al., 2000; Lin et al., 2000; Qiu et al., 2000), the roles for PAR-3 and PAR-6 are less clear and may vary in different contexts (Achilleos et al., 2010; Atwood et al., 2007; David et al., 2013; Graybill et al., 2012; Lin et al., 2000; McCaffrey and Macara, 2009; Wirtz-Peitz et al., 2008).

To directly assess whether PKC-3 activity differs in PAR-3-associated and CDC-42-associated assemblies *in vivo*, we targeted PKC-3 to the membrane by fusing it to the C1B domain of human PKCα, which can be induced to bind the membrane by the addition of phorbol ester (Figure 6A) (Lekomtsev et al., 2012). This bypasses the membrane-binding requirement of PKC-3 on PAR-3, PAR-6, and CDC-42, allowing us to test their contribution to PKC-3 activity by monitoring membrane removal of the PKC-3 target, PAR-2.

In the absence of phorbol ester, C1B-PKC-3 mirrors endogenous PKC-3 localization and is anteriorly enriched, with PAR-2 restricted to the posterior as in wild-type (Figure 6B, No PMA). Upon addition of 100 μM phorbol 12-myristate 13-acetate (PMA), C1B-PKC-3 is recruited uniformly to the membrane and the PAR-2 domain shrinks, consistent with an increase in posterior PKC-3 activity (Figure 6B, +PMA; Figure 6C; Movie S6). The reduction in PAR-2 domain size is not seen in the absence of PMA, when targeting the C1B domain alone to the membrane, or if we inhibit PKC-3 with CRT90 (Figures 6B and 6D). The failure to completely remove PAR-2 in polarized zygotes is not simply due to PAR-2 being concentrated in a domain, because ectopic PAR-2 domains that form in meiotic arrest mutants, e.g., *mei-1* and *emb-27* (Wallenfang and Seydoux, 2000), are rapidly cleared (Figure S7).

In *par-3*, *par-6*, or *cdc-42*(*RNAi*) zygotes, both endogenous PKC-3 and the C1B-PKC-3 fusion are cytoplasmic in the absence of PMA, allowing PAR-2 to localize uniformly to the membrane (Figures 6E and 6F). In *par-6* and *cdc-42*(*RNAi*) zygotes, membrane targeting of C1B-PKC-3 (+PMA) has no effect on PAR-2 distribution: it remains uniformly enriched at the membrane with no difference compared with controls in which C1B alone is targeted to the membrane (Figures 6E and 6F; Movie S7). Thus, both PAR-6 and CDC-42 are required for PKC-3 activity *in vivo*.

By contrast, membrane targeting of C1B-PKC-3 in *par-3*(*RNAi*) zygotes induces rapid loss of PAR-2 from the membrane, with near complete removal within minutes (Figures 6E and 6F; Movie S7). The displacement of PAR-2 is stronger than in wild-type zygotes, suggesting that PAR-3 normally acts to inhibit or suppress PKC-3 activity (Figure 6B, +PMA). Thus PAR-3 has two roles *in vivo*: it promotes PKC-3 membrane targeting while at the same time limiting its activation, reconciling *in vivo* reports whereby PAR-3 positively regulates PAR polarity (Achilleos et al., 2010; McCaffrey and Macara, 2009) with data indicating that PAR-3 can inhibit PKC-3 activity *in vitro* (Graybill et al., 2012; Lin et al., 2000; Soriano et al., 2016).

DISCUSSION

Taken together, our data suggest that efficient polarization requires PKC-3 to cycle between functionally specialized modules of the anterior PAR network: a PAR-3-dependent module that segregates in response to symmetry-breaking signals, but which is inactive, and a CDC-42-dependent module that uses spatial information provided by PAR-3 to create an anterior domain of PKC-3 activity on the membrane (Figure 7).

In previous work, we showed that the diffusion and membrane dissociation rates of aPARs were in principle sufficient to explain segregation in response to flows (Goehring et al., 2011b). Here we show that segregation of aPARs is directly linked to PAR-3-dependent clustering. Clustering reduces the effective diffusion of membrane-associated aPARs, which should favor advective transport. Alternatively, the sheer size of clusters may allow them to sense flow that would not affect individual proteins, possibly by allowing them to extend into the cortical actomyosin layer. Regardless of the physical mechanism, as we show here, clustering drives robust segregation of PAR-3 by cortical flow. This fact, coupled with PAR-3 exclusion from the posterior by PAR-1-dependent phosphorylation (Motegi et al., 2011), supports a model in which PAR-3 is responsible for sensing asymmetry-generating cues. Importantly, once it is asymmetric, PAR-3 provides a landmark for polarized loading of PAR-6/PKC-3, explaining recent observations that PAR-6 loads preferentially in the anterior of polarized embryos (Sailer et al., 2015).

Because our *in vivo* PKC-3 activity assay indicates that PKC-3 activity is suppressed within PAR-3-dependent assemblies, PAR-6/PKC-3 molecules must be converted into an activated CDC-42-dependent species, a state that we show is non-clustered and diffusive. Whereas this diffusive behavior of CDC-42-assemblies is a disadvantage for transport by cortical flow, it is an advantage for creating a uniform, wider-range field of PKC-3 activity that can efficiently exclude pPARs. If the same complexes had to respond to flow and exclude pPARs, there would be a trade-off between efficiency of transport by flow and uniformity of pPAR inhibition at the anterior.

For this field of activated CDC-42-dependent PKC-3 assemblies to remain coupled to the spatial information provided by PAR-3, two conditions must be satisfied. First, PKC-3 membrane localization must be dependent on PAR-3, and second, diffusion of CDC-42-associated PKC-3 away from loading sites must be limited, with PKC-3 ultimately being released back into the cytoplasm, where it again becomes dependent on PAR-3. This turnover restricts the effective distance these

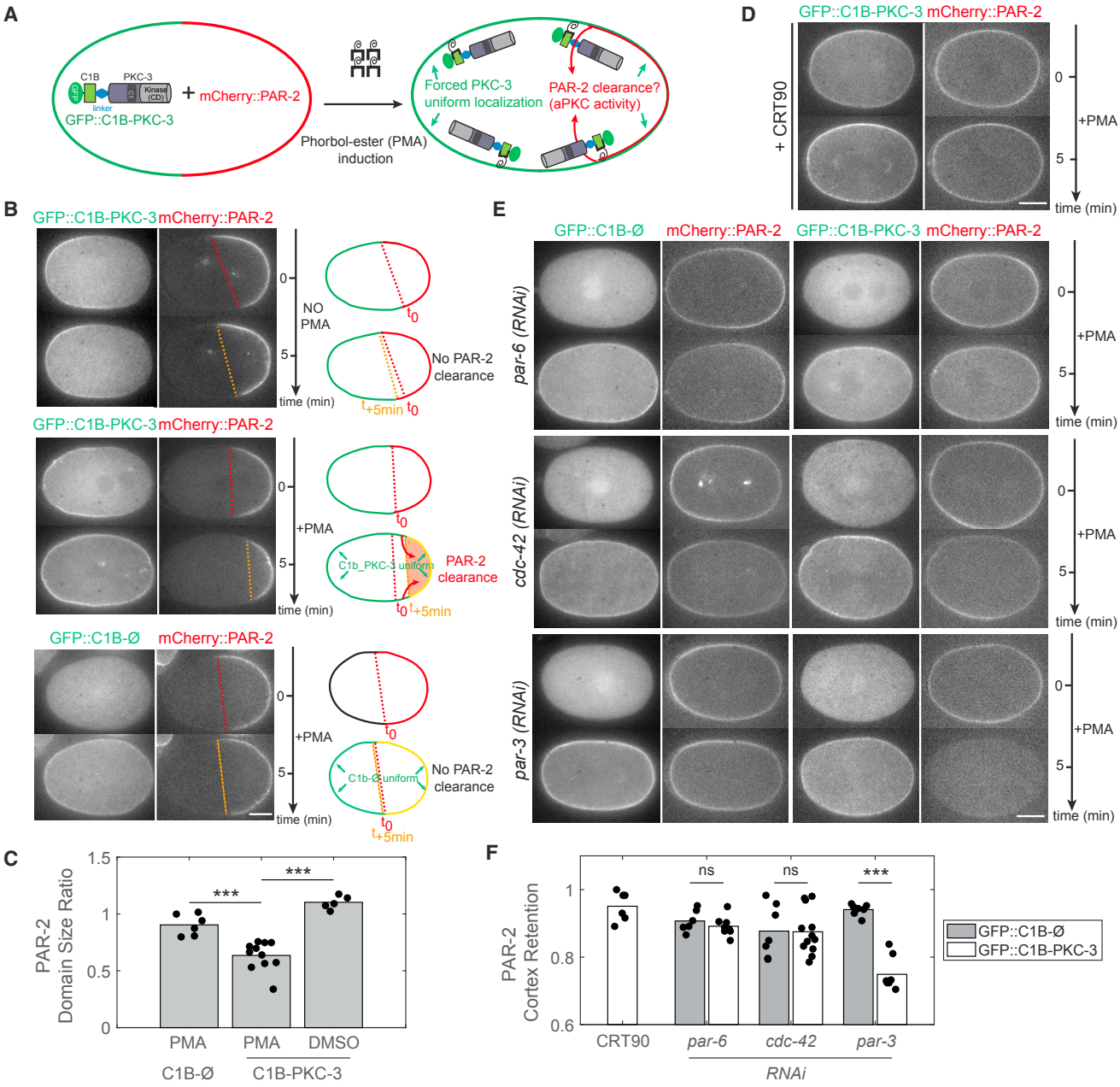

Figure 6. PAR-3 and CDC-42 Have Opposing Regulatory Roles in an *In Vivo* PKC-3 Activity Assay

(A) C1B targeting strategy for inducing PKC-3 membrane loading by PMA. PKC-3 kinase activity is monitored by following loss of PAR-2 from the membrane.

(B) Zygotes expressing GFP::C1B alone (GFP::C1B-Ø) or GFP::C1B-PKC-3 along with mCherry::PAR-2 were subject to the indicated treatment. Note that uniform membrane targeting of C1B-PKC-3 leads to reduction of PAR-2 domain size, whereas omitting PMA or expressing C1B alone has no effect. Right: cartoon representation of results.

(C) Quantification of PAR-2 domain size ratio for embryos shown in (B).

(D) PAR-2 retention in GFP::C1B-PKC-3 expressing zygotes treated with PMA and CRT90 confirms that induced PAR-2 loss is dependent on PKC-3 kinase activity.

(E) Zygotes expressing mCherry::PAR-2 with GFP::C1B-Ø or GFP::C1B-PKC-3 subject to *par-6*, *cdc-42*, or *par-3*(*RNAi*) before and 5 min after PMA addition.

(F) Quantification of PAR-2 cortex retention comparing GFP::C1B-PKC-3 and GFP::C1B-Ø zygotes after treatment with PMA as in (E).

Representative midsection confocal images are shown in (B), (D), and (E) before and 5 min after PMA/DMSO addition. ***$p < 0.001$. ns, not significant. Scale bars, 10 μm. See also Figure S7; Movies S6 and S7.

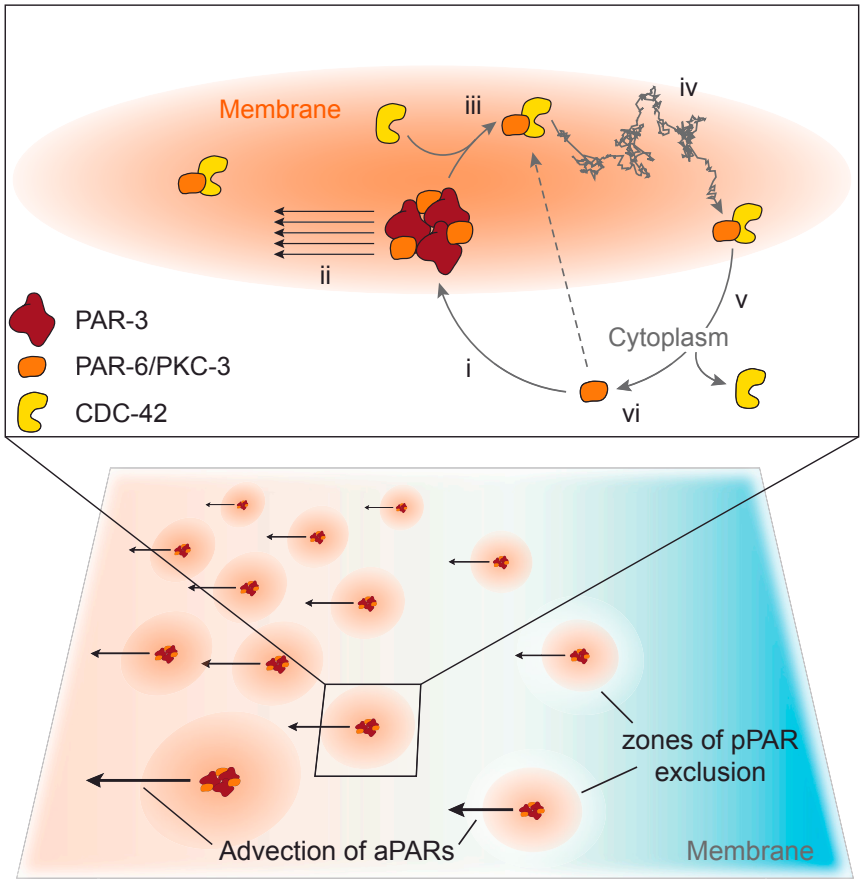

Figure 7. Polarization through Coupling of PAR-3- and CDC-42-Dependent aPAR Assemblies

(i) PKC-3 kinase activity ensures that PKC-3 loads via a PAR-3 intermediate, in which PKC-3 activity is suppressed. This dependence on PAR-3 can be bypassed upon inhibition of PKC-3 (dashed arrow). (ii) Clustering of membrane-associated PAR-3 allows it to be segregated by cortical flow into the anterior, carrying along associated PKC-3 molecules and generating asymmetric sites for further PKC-3 loading. (iii) PKC-3 activation requires conversion into a CDC-42-associated assembly, which relieves inhibition of PKC-3 by PAR-3. (iv) The CDC-42-dependent module is freely diffusible on the membrane and locally excludes pPARs. (v) Dissociation of CDC-42-dependent assemblies limits the spread of active PKC-3 at the membrane from the PAR-3 recruiting site. (vi) PKC-3 returns to the cytoplasm where it must load again via PAR-3.

complexes can diffuse from their initial sites of formation, defining an effective "sphere of influence" around PAR-3 loading sites. Together, these requirements result in a cycle of localized membrane loading, activation, and release (Figure 7).

Our data suggest that the first of these requirements, PAR-3-dependent loading, is dependent on the kinase activity of PKC-3 itself, although the precise mechanism is unclear. Given the limited ability of CDC-42 (Q61L) to rescue PKC-3 membrane localization in PAR-3-depleted embryos, PKC-3 is likely to act at the step of CDC-42 complex generation, either inhibiting its own association with CDC-42, and/or destabilizing nascent CDC-42/PAR-6/PKC-3 assemblies. We speculate that it could be the very act of inhibiting PKC-3 through which PAR-3 promotes generation of stable CDC-42-dependent assemblies, but further work will be required to reveal the details of this molecular handover. Because the inhibitory role of PAR-3 appears to be broadly conserved (David et al., 2013; Graybill et al., 2012; Lin et al., 2000; McCaffrey et al., 2012; Soriano et al., 2016), this apparent paradoxical role of PAR-3 in promoting formation of membrane-associated aPKC complexes, yet also suppressing PKC-3 activity, may be a general feature of aPKC regulation.

How diffusion of CDC-42-associated PKC-3 is limited also remains unclear. Measurements elsewhere suggest that the distance these activated assemblies travel is on the order of 5–10 μm (Goehring et al., 2011a; Robin et al., 2014), consistent with the PKC-3 gradient extending further into the posterior than PAR-3 during the establishment phase even in wild-type embryos (see Figure 2I). Because CDC-42 assemblies appear to be resistant to removal by posterior PAR proteins (Figure 2M), including the CDC-42 GAP CHIN-1, it seems likely that it is not preferential removal of these complexes in the posterior by pPARs, but rather the intrinsic lifetime of CDC-42-dependent PKC-3 assemblies that limits their diffusion into the posterior. This is compatible with a model in which aPKC undergoes asymmetric membrane loading but symmetric dissociation (Robin et al., 2014).

By loading PKC-3 via what we presume is an inhibited PAR-3-associated state, which must then be activated, PKC-3 localization and activation are segregated into distinct modules of the PAR network, which can be regulated independently. This division of labor may be critical for PAR proteins, which operate across diverse contexts, where the polarity cues, substrates, scales, and even the concentrations of PAR molecules themselves may vary substantially. Even within the *C. elegans* zygote, the mechanisms of PAR segregation vary. During polarity establishment, when cortical flow is the major cue for anterior PAR segregation, PAR-3 clustering is prominent (Cheeks et al., 2004; Goehring et al., 2011b; Munro et al., 2004). As the system enters the maintenance phase, flow ceases and continued aPAR segregation becomes dependent on the activity of PAR-1 and CHIN-1 (Beatty et al., 2013; Guo and Kemphues, 1995; Kumfer et al., 2010; Sailer et al., 2015). Notably, clustering appears to be reduced during this phase, which Dickinson et al. (2017) show is dependent on PLK-1. This change in PAR molecular organization potentially reflects the shift in the spatial signals to which the PAR network must respond. At the same time, despite these changes, PKC-3 activity must remain efficient at displacing pPARs from the anterior domain, highlighting the adaptability of the PAR network.

In summary, here we have identified a critical role for the separation of signal-receiving and signal-transducing functions between modules of the aPAR network that are distinct, but

coupled via dynamic exchange of the shared signaling component, PKC-3. We suggest that functional specialization of coupled modules resolves potential molecular constraints between components that must be sensitive to polarity cues and those that must propagate the signals. It further allows the system to independently modulate responsiveness to cues as well as the extent and strength of the output signal. The adaptability of such a paradigm suggests it is likely to be a common strategy in patterning systems.

STAR★METHODS

Detailed methods are provided in the online version of this paper and include the following:

- KEY RESOURCES TABLE
- CONTACT FOR REAGENT AND RESOURCE SHARING
- EXPERIMENTAL MODEL AND SUBJECT DETAILS
  - *C. elegans* Strains and Maintenance
  - *C. elegans* Transgenic Animals
  - Cell Lines
  - Bacterial Strains
- METHOD DETAILS
  - *C. elegans* - RNAi Culture Conditions
  - *C. elegans* Embryos – Western Blots
  - *C. elegans* Zygotes – Drug Treatment
  - *C. elegans* Zygotes - Immunofluorescence
  - *C. elegans zygotes* - Live Imaging
  - *In vitro* PKC Enzyme Assays
  - Cellular Biochemical Assay
  - Kinase Selectivity
- QUANTIFICATION AND STATISTICAL ANALYSIS
  - Image Analysis - General
  - Image Analysis - Asymmetry Index (ASI)
  - Image Analysis – Cluster Index
  - Image Analysis – CHIN-1 Foci
  - Image Analysis – MEX-5 Mobility
  - Image Analysis - Colocalization
  - Image Analysis – Flow Speeds
  - Image Analysis – Anterior Cortical Intensity (Immunofluorescence)
  - Image Analysis – Anterior PAR Retraction (Immunofluorescence)
  - Image Analysis – Intensity Profile Extraction
  - Image Analysis – PAR-3 versus PKC-3 Cortical Profile Comparison (Immunofluorescence)
  - Image Analysis – Domain Size/Segregation Efficiency
  - Image Analysis – Total Membrane Signal Change
  - Statistics
  - Data and Software Availability

SUPPLEMENTAL INFORMATION

Supplemental Information includes seven figures and seven movies and can be found with this article online at http://dx.doi.org/10.1016/j.devcel.2017.07.007.

AUTHOR CONTRIBUTIONS

Conceptualization, J. Rodriguez, F.P., and N.W.G.; Methodology, J. Rodriguez, F.P., J.M., L.H., J. Reich, N.H. and N.W.G.; Investigation, J. Rodriguez, F.P., J.M., L.H., N.H, A.G.G., A.R.F., and N.W.G.; Resources, J. Roffey; Writing – Original Draft, J. Rodriguez, F.P., and N.W.G.; Writing – Review & Editing, J. Rodriguez, F.P., D.StJ., J.A., and N.W.G.; Funding Acquisition, J. Rodriguez, D.StJ., J.A., and N.W.G.; Supervision, J. Rodriguez, D.StJ., J.A., and N.W.G. To satisfy Cell Press guidelines, one corresponding author was chosen at random to serve as Lead Contact, although both will be maintaining the reagents.

ACKNOWLEDGMENTS

The authors wish to thank Nic Tapon, Elizabeth Veal, Jonathan Higgins and members of the N.W.G. and J. Rodriguez laboratories for critical comments, Neil McDonald for helpful discussions, Ken Kemphues for his generosity in providing unpublished strains and PKC-3 antibody, Monica Gotta for providing PAR-6 antibody, and Dan Dickinson for sharing results prior to publication. This work was supported by a Faculty Fellowship from Newcastle University and a Royal Society Research Grant (RG2015R2 to J. Rodriguez), a BBSRC PhD fellowship (J.M.), a PhD fellowship from Newcastle University (A.G.G.), Wellcome Trust Senior and Principal Research Fellowships (054523, to J.A.; 080007, to D.StJ.), a University of Cambridge Studentship via the Wellcome Trust PhD Program in Developmental Biology (A.R.F.), and the Francis Crick Institute (N.W.G.), which receives its core funding from Cancer Research UK (FC001086), the UK Medical Research Council (FC001086), and the Wellcome Trust (FC001086). N.W.G. and J. Rodriguez are members of the GENiE network supported by COST Action BM1408 and EMBO. Some strains were provided by the CGC, which is funded by NIH Office of Research Infrastructure Programs (P40 OD010440). The P4A1 monoclonal antibody developed by J. Priess was obtained from the Developmental Studies Hybridoma Bank developed under the auspices of the NICHD and maintained by The University of Iowa, Department of Biology, Iowa City, IA 52242. J. Roffey is an employee of Cancer Research Technology Ltd. (CRT), a company registered in England and Wales under number 1626049 with registered office at Angel Building, 407 St John Street London, EC1V 4AD, England. CRT is wholly owned by Cancer Research UK (a charity and company registered in England and Wales with registered charity number 1089464 and registered company number 4325234).

Received: November 17, 2016
Revised: June 19, 2017
Accepted: July 10, 2017
Published: August 3, 2017

REFERENCES

Aceto, D., Beers, M., and Kemphues, K.J. (2006). Interaction of PAR-6 with CDC-42 is required for maintenance but not establishment of PAR asymmetry in *C. elegans*. Dev. Biol. *299*, 386–397.

Achilleos, A., Wehman, A.M., and Nance, J. (2010). PAR-3 mediates the initial clustering and apical localization of junction and polarity proteins during *C. elegans* intestinal epithelial cell polarization. Development *137*, 1833–1842.

Andrews, R., and Ahringer, J. (2007). Asymmetry of early endosome distribution in *C. elegans* embryos. PLoS One *2*, e493.

Atwood, S.X., Chabu, C., Penkert, R.R., Doe, C.Q., and Prehoda, K.E. (2007). Cdc42 acts downstream of Bazooka to regulate neuroblast polarity through Par-6 aPKC. J. Cell Sci. *120*, 3200–3206.

Audhya, A., Hyndman, F., McLeod, I.X., Maddox, A.S., Yates, J.R., Desai, A., and Oegema, K. (2005). A complex containing the Sm protein CAR-1 and the RNA helicase CGH-1 is required for embryonic cytokinesis in *Caenorhabditis elegans*. J. Cell Biol. *171*, 267–279.

Beatty, A., Morton, D., and Kemphues, K. (2010). The *C. elegans* homolog of *Drosophila* Lethal giant larvae functions redundantly with PAR-2 to maintain polarity in the early embryo. Development *137*, 3995–4004.

Beatty, A., Morton, D.G., and Kemphues, K. (2013). PAR-2, LGL-1 and the CDC-42 GAP CHIN-1 act in distinct pathways to maintain polarity in the *C. elegans* embryo. Development *140*, 2005–2014.

Beers, M., and Kemphues, K. (2006). Depletion of the co-chaperone CDC-37 reveals two modes of PAR-6 cortical association in *C. elegans* embryos. Development *133*, 3745–3754.

Benton, R., and St Johnston, D. (2003). A conserved oligomerization domain in *Drosophila* bazooka/PAR-3 is important for apical localization and epithelial polarity. Curr. Biol. *13*, 1330–1334.

Betschinger, J., Mechtler, K., and Knoblich, J.A. (2003). The Par complex directs asymmetric cell division by phosphorylating the cytoskeletal protein Lgl. Nature *422*, 326–330.

Boyd, L., Guo, S., Levitan, D., Stinchcomb, D.T., and Kemphues, K.J. (1996). PAR-2 is asymmetrically distributed and promotes association of P granules and PAR-1 with the cortex in *C. elegans* embryos. Development *122*, 3075–3084.

Brenner, S. (1974). The genetics of *Caenorhabditis elegans*. Genetics *77*, 71–94.

Carvalho, A., Olson, S.K., Gutierrez, E., Zhang, K., Noble, L.B., Zanin, E., Desai, A., Groisman, A., and Oegema, K. (2011). Acute drug treatment in the early *C. elegans* embryo. PLoS One *6*, e24656.

Caussinus, E., Kanca, O., and Affolter, M. (2011). Fluorescent fusion protein knockout mediated by anti-GFP nanobody. Nat. Struct. Mol. Biol. *19*, 117–121.

Cheeks, R.J., Canman, J.C., Gabriel, W.N., Meyer, N., Strome, S., and Goldstein, B. (2004). *C. elegans* PAR proteins function by mobilizing and stabilizing asymmetrically localized protein complexes. Curr. Biol. *14*, 851–862.

Cuenca, A.A., Schetter, A., Aceto, D., Kemphues, K., and Seydoux, G. (2003). Polarization of the *C. elegans* zygote proceeds via distinct establishment and maintenance phases. Development *130*, 1255–1265.

David, D.J.V., Wang, Q., Feng, J.J., and Harris, T.J.C. (2013). Bazooka inhibits aPKC to limit antagonism of actomyosin networks during amnioserosa apical constriction. Development *140*, 4719–4729.

Dickinson, D.J., Ward, J.D., Reiner, D.J., and Goldstein, B. (2013). Engineering the *Caenorhabditis elegans* genome using Cas9-triggered homologous recombination. Nat. Methods *10*, 1028–1034.

Dickinson, D.J., Schwager, F., Pintard, L., Gotta, M., and Goldstein, B. (2017). Dev. Cell *42*, this issue, in press.

Dong, Y., Bogdanova, A., Habermann, B., Zachariae, W., and Ahringer, J. (2007). Identification of the *C. elegans* anaphase promoting complex subunit Cdc26 by phenotypic profiling and functional rescue in yeast. BMC Dev. Biol. *7*, 19.

Dorsey, B.D., Learn, K.S., Morris, E.L., Ott, G.R., Roffey, J.R., Soudy, C.N., and Wagner, J.C. (2013). Thienopyrimidine inhibitors of atypical protein kinase C. Patent WO 2013078126 A1, filed 19 November, 2012.

Edgar, L.G., and Goldstein, B. (2012). Culture and manipulation of embryonic cells. Methods Cell Biol. *107*, 151–175.

Etemad-Moghadam, B., Guo, S., and Kemphues, K.J. (1995). Asymmetrically distributed PAR-3 protein contributes to cell polarity and spindle alignment in early *C. elegans* embryos. Cell *83*, 743–752.

Feng, W., Wu, H., Chan, L.-N., and Zhang, M. (2007). The Par-3 NTD adopts a PB1-like structure required for Par-3 oligomerization and membrane localization. EMBO J. *26*, 2786–2796.

Fievet, B.T., Rodriguez, J., Naganathan, S., Lee, C., Zeiser, E., Ishidate, T., Shirayama, M., Grill, S.W., and Ahringer, J. (2012). Systematic genetic interaction screens uncover cell polarity regulators and functional redundancy. Nat. Cell Biol. *15*, 103–112.

Goehring, N.W. (2014). PAR polarity: from complexity to design principles. Exp. Cell Res. *328*, 258–266.

Goehring, N.W., Hoege, C., Grill, S.W., and Hyman, A.A. (2011a). PAR proteins diffuse freely across the anterior-posterior boundary in polarized *C. elegans* embryos. J. Cell Biol. *193*, 583–594.

Goehring, N.W., Trong, P.K., Bois, J.S., Chowdhury, D., Nicola, E.M., Hyman, A.A., and Grill, S.W. (2011b). Polarization of PAR proteins by advective triggering of a pattern-forming system. Science *334*, 1137–1141.

Goldstein, B., and Macara, I.G. (2007). The PAR proteins: fundamental players in animal cell polarization. Dev. Cell *13*, 609–622.

Gotta, M., Abraham, M.C., and Ahringer, J. (2001). CDC-42 controls early cell polarity and spindle orientation in *C. elegans*. Curr. Biol. *11*, 482–488.

Graybill, C., Wee, B., Atwood, S.X., and Prehoda, K.E. (2012). Partitioning-defective protein 6 (Par-6) activates atypical protein kinase C (aPKC) by pseudosubstrate displacement. J. Biol. Chem. *287*, 21003–21011.

Griffin, E.E., Odde, D.J., and Seydoux, G. (2011). Regulation of the MEX-5 gradient by a spatially segregated kinase/phosphatase cycle. Cell *146*, 955–968.

Guo, S., and Kemphues, K.J. (1995). par-1, a gene required for establishing polarity in *C. elegans* embryos, encodes a putative Ser/Thr kinase that is asymmetrically distributed. Cell *81*, 611–620.

Hao, Y., Boyd, L., and Seydoux, G. (2006). Stabilization of cell polarity by the *C. elegans* RING protein PAR-2. Dev. Cell *10*, 199–208.

Harris, T.J.C., and Peifer, M. (2005). The positioning and segregation of apical cues during epithelial polarity establishment in Drosophila. J. Cell Biol. *170*, 813–823.

Hoege, C., Constantinescu, A.-T., Schwager, A., Goehring, N.W., Kumar, P., and Hyman, A.A. (2010). LGL can partition the cortex of one-cell *Caenorhabditis elegans* embryos into two domains. Curr. Biol. *20*, 1296–1303.

Hoege, C., and Hyman, A.A. (2013). Principles of PAR polarity in *Caenorhabditis elegans* embryos. Nat. Rev. Mol. Cell Biol. *14*, 315–322.

Hung, T.J., and Kemphues, K.J. (1999). PAR-6 is a conserved PDZ domain-containing protein that colocalizes with PAR-3 in *Caenorhabditis elegans* embryos. Development *126*, 127–135.

Hurov, J.B., Watkins, J.L., and Piwnica-Worms, H. (2004). Atypical PKC phosphorylates PAR-1 kinases to regulate localization and activity. Curr. Biol. *14*, 736–741.

Izumi, Y., Hirose, T., Tamai, Y., Hirai, S., Nagashima, Y., Fujimoto, T., Tabuse, Y., Kemphues, K.J., and Ohno, S. (1998). An atypical PKC directly associates and colocalizes at the epithelial tight junction with ASIP, a mammalian homologue of *Caenorhabditis elegans* polarity protein PAR-3. J. Cell Biol. *143*, 95–106.

Joberty, G., Petersen, C., Gao, L., and Macara, I.G. (2000). The cell-polarity protein Par6 links Par3 and atypical protein kinase C to Cdc42. Nat. Cell Biol. *2*, 531–539.

Kachur, T.M., Audhya, A., and Pilgrim, D.B. (2008). UNC-45 is required for NMY-2 contractile function in early embryonic polarity establishment and germline cellularization in *C. elegans*. Dev. Biol. *314*, 287–299.

Kamath, R.S., Fraser, A.G., Dong, Y., Poulin, G., Durbin, R., Gotta, M., Kanapin, A., Le Bot, N., Moreno, S., Sohrmann, M., et al. (2003). Systematic functional analysis of the *Caenorhabditis elegans* genome using RNAi. Nature *421*, 231–237.

Kay, A.J., and Hunter, C.P. (2001). CDC-42 regulates PAR protein localization and function to control cellular and embryonic polarity in *C. elegans*. Curr. Biol. *11*, 474–481.

Kjær, S., Linch, M., Purkiss, A., Kostelecky, B., Knowles, P.P., Rosse, C., Riou, P., Soudy, C., Kaye, S., Patel, B., et al. (2013). Adenosine-binding motif mimicry and cellular effects of a thieno[2,3-d]pyrimidine-based chemical inhibitor of atypical protein kinase C isoenzymes. Biochem. J. *451*, 329–342.

Konopka, C.A., and Bednarek, S.Y. (2008). Variable-angle epifluorescence microscopy: a new way to look at protein dynamics in the plant cell cortex. Plant J. *53*, 186–196.

Kumfer, K.T., Cook, S.J., Squirrell, J.M., Eliceiri, K.W., Peel, N., O'Connell, K.F., and White, J.G. (2010). CGEF-1 and CHIN-1 regulate CDC-42 activity during asymmetric division in the *Caenorhabditis elegans* embryo. Mol. Biol. Cell *21*, 266–277.

Lekomtsev, S., Su, K.-C., Pye, V.E., Blight, K., Sundaramoorthy, S., Takaki, T., Collinson, L.M., Cherepanov, P., Divecha, N., and Petronczki, M. (2012). Centralspindlin links the mitotic spindle to the plasma membrane during cytokinesis. Nature *492*, 276–279.

Li, B., Kim, H., Beers, M., and Kemphues, K. (2010). Different domains of *C. elegans* PAR-3 are required at different times in development. Dev. Biol. *344*, 745–757.

Li, Q., Lau, A., Morris, T.J., Guo, L., Fordyce, C.B., and Stanley, E.F. (2004). A syntaxin 1, Gα(o), and N-type calcium channel complex at a presynaptic nerve terminal: analysis by quantitative immunocolocalization. J. Neurosci. *24*, 4070–4081.

Lin, D., Edwards, A.S., Fawcett, J.P., Mbamalu, G., Scott, J.D., and Pawson, T. (2000). A mammalian PAR-3-PAR-6 complex implicated in Cdc42/Rac1 and aPKC signalling and cell polarity. Nat. Cell Biol. *2*, 540–547.

Mayer, M., Depken, M., Bois, J.S., Jülicher, F., and Grill, S.W. (2010). Anisotropies in cortical tension reveal the physical basis of polarizing cortical flows. Nature *467*, 617–621.

McCaffrey, L.M., and Macara, I.G. (2012). Signaling pathways in cell polarity. Cold Spring Harb. Perspect. Biol. *4*.

McCaffrey, L.M., and Macara, I.G. (2009). The Par3/aPKC interaction is essential for end bud remodeling and progenitor differentiation during mammary gland morphogenesis. Genes Dev. *23*, 1450–1460.

McCaffrey, L.M., Montalbano, J., Mihai, C., and Macara, I.G. (2012). Loss of the Par3 polarity protein promotes breast tumorigenesis and metastasis. Cancer Cell *22*, 601–614.

Mizuno, K., Suzuki, A., Hirose, T., Kitamura, K., Kutsuzawa, K., Futaki, M., Amano, Y., and Ohno, S. (2003). Self-association of PAR-3-mediated by the conserved N-terminal domain contributes to the development of epithelial tight junctions. J. Biol. Chem. *278*, 31240–31250.

Morais-De-Sa, E., Mirouse, V., and St Johnston, D. (2010). aPKC phosphorylation of Bazooka defines the apical/lateral border in *Drosophila* epithelial cells. Cell *141*, 509–523.

Motegi, F., and Seydoux, G. (2013). The PAR network: redundancy and robustness in a symmetry-breaking system. Philos. Trans. R. Soc. Lond. B Biol. Sci. *368*, 20130010.

Motegi, F., and Sugimoto, A. (2006). Sequential functioning of the ECT-2 RhoGEF, RHO-1 and CDC-42 establishes cell polarity in *Caenorhabditis elegans* embryos. Nat. Cell Biol. *8*, 978–985.

Motegi, F., Zonies, S., Hao, Y., Cuenca, A.A., Griffin, E.E., and Seydoux, G. (2011). Microtubules induce self-organization of polarized PAR domains in *Caenorhabditis elegans* zygotes. Nat. Cell Biol. *13*, 1361–1367.

Munro, E., Nance, J., and Priess, J.R. (2004). Cortical flows powered by asymmetrical contraction transport PAR proteins to establish and maintain anterior-posterior polarity in the early *C. elegans* embryo. Dev. Cell *7*, 413–424.

Neukomm, L.J., Zeng, S., Frei, A.P., Huegli, P.A., and Hengartner, M.O. (2014). Small GTPase CDC-42 promotes apoptotic cell corpse clearance in response to PAT-2 and CED-1 in *C. elegans*. Cell Death Differ. *21*, 845–853.

Pelletier, V., Gal, N., Fournier, P., and Kilfoil, M.L. (2009). Microrheology of microtubule solutions and actin-microtubule composite networks. Phys. Rev. Lett. *102*, 188303.

Praitis, V., Casey, E., Collar, D., and Austin, J. (2001). Creation of low-copy integrated transgenic lines in *Caenorhabditis elegans*. Genetics *157*, 1217–1226.

Qiu, R.G., Abo, A., and Steven Martin, G. (2000). A human homolog of the *C. elegans* polarity determinant Par-6 links Rac and Cdc42 to PKCzeta signaling and cell transformation. Curr. Biol. *10*, 697–707.

Redemann, S., Pecreaux, J., Goehring, N.W., Khairy, K., Stelzer, E.H.K., Hyman, A.A., and Howard, J. (2010). Membrane invaginations reveal cortical sites that pull on mitotic spindles in one-cell *C. elegans* embryos. PLoS One *5*, e12301.

Redemann, S., Schloissnig, S., Ernst, S., Pozniakowsky, A., Ayloo, S., Hyman, A.A., and Bringmann, H. (2011). Codon adaptation-based control of protein expression in *C. elegans*. Nat. Methods *8*, 250–252.

Robin, F.B., McFadden, W.M., Yao, B., and Munro, E.M. (2014). Single-molecule analysis of cell surface dynamics in *Caenorhabditis elegans* embryos. Nat. Methods *11*, 677–682.

Sailer, A., Anneken, A., Li, Y., Lee, S., and Munro, E. (2015). Dynamic opposition of clustered proteins stabilizes cortical polarity in the *C. elegans* zygote. Dev. Cell *35*, 131–142.

Schindelin, J., Arganda-Carreras, I., Frise, E., Kaynig, V., Longair, M., Pietzsch, T., Preibisch, S., Rueden, C., Saalfeld, S., Schmid, B., et al. (2012). Fiji: an open-source platform for biological-image analysis. Nat. Methods *9*, 676–682.

Schonegg, S., and Hyman, A.A. (2006). CDC-42 and RHO-1 coordinate actomyosin contractility and PAR protein localization during polarity establishment in *C. elegans* embryos. Development *133*, 3507–3516.

Schonegg, S., Constantinescu, A.T., Hoege, C., and Hyman, A.A. (2007). The Rho GTPase-activating proteins RGA-3 and RGA-4 are required to set the initial size of PAR domains in *Caenorhabditis elegans* one-cell embryos. Proc. Natl. Acad. Sci. USA *104*, 14976–14981.

Seitz, A., and Surrey, T. (2006). Processive movement of single kinesins on crowded microtubules visualized using quantum dots. EMBO J. *25*, 267–277.

Soriano, E.V., Ivanova, M.E., Fletcher, G., Riou, P., Knowles, P.P., Barnouin, K., Purkiss, A., Kostelecky, B., Saiu, P., Linch, M., et al. (2016). aPKC inhibition by Par3 CR3 flanking regions controls substrate access and underpins apical-junctional polarization. Dev. Cell *38*, 384–398.

St Johnston, D., and Ahringer, J. (2010). Cell polarity in eggs and epithelia: parallels and diversity. Cell *141*, 757–774.

Suzuki, A., Hirata, M., Kamimura, K., Maniwa, R., Yamanaka, T., Mizuno, K., Kishikawa, M., Hirose, H., Amano, Y., Izumi, N., et al. (2004). aPKC acts upstream of PAR-1b in both the establishment and maintenance of mammalian epithelial polarity. Curr. Biol. *14*, 1425–1435.

Tabuse, Y., Izumi, Y., Piano, F., Kemphues, K.J., Miwa, J., and Ohno, S. (1998). Atypical protein kinase C cooperates with PAR-3 to establish embryonic polarity in *Caenorhabditis elegans*. Development *125*, 3607–3614.

Wallenfang, M.R., and Seydoux, G. (2000). Polarization of the anterior-posterior axis of *C. elegans* is a microtubule-directed process. Nature *408*, 89–92.

Watts, J.L., Etemad-Moghadam, B., Guo, S., Boyd, L., Draper, B.W., Mello, C.C., Priess, J.R., and Kemphues, K.J. (1996). par-6, a gene involved in the establishment of asymmetry in early *C. elegans* embryos, mediates the asymmetric localization of PAR-3. Development *122*, 3133–3140.

Wirtz-Peitz, F., Nishimura, T., and Knoblich, J.A. (2008). Linking cell cycle to asymmetric division: aurora-A phosphorylates the Par complex to regulate Numb localization. Cell *135*, 161–173.

Yamanaka, T., Horikoshi, Y., Izumi, N., Suzuki, A., Mizuno, K., and Ohno, S. (2006). Lgl mediates apical domain disassembly by suppressing the PAR-3-aPKC-PAR-6 complex to orient apical membrane polarity. J. Cell Sci. *119*, 2107–2118.

Yamanaka, T., Horikoshi, Y., Sugiyama, Y., Ishiyama, C., Suzuki, A., Hirose, T., Iwamatsu, A., Shinohara, A., and Ohno, S. (2003). Mammalian Lgl forms a protein complex with PAR-6 and aPKC independently of PAR-3 to regulate epithelial cell polarity. Curr. Biol. *13*, 734–743.

Ziman, M., O'Brien, J.M., Ouellette, L.A., Church, W.R., and Johnson, D.I. (1991). Mutational analysis of CDC42Sc, a *Saccharomyces cerevisiae* gene that encodes a putative GTP-binding protein involved in the control of cell polarity. Mol. Cell Biol. *11*, 3537–3544.

Ziomek, C.A., Johnson, M.H., and Handyside, A.H. (1982). The developmental potential of mouse 16-cell blastomeres. J. Exp. Zool. *221*, 345–355.

Zipperlen, P., Fraser, A.G., Kamath, R.S., Martinez-Campos, M., and Ahringer, J. (2001). Roles for 147 embryonic lethal genes on *C. elegans* chromosome I identified by RNA interference and video microscopy. EMBO J. *20*, 3984–3992.

STAR★METHODS

KEY RESOURCES TABLE

REAGENT or RESOURCE	SOURCE	IDENTIFIER
Antibodies		
Rabbit Anti-PAR-2	(Dong et al., 2007)	N/A
Rabbit Anti-PAR-6	(Gotta et al., 2001)	N/A
Rat Anti-PKC-3	(Tabuse et al., 1998)	N/A
Mouse Anti-PAR-3	Developmental Studies Hybridoma Bank	P4A1; RRID: AB_528424
Mouse Anti-αTubulin	Sigma	DM1A (T9026); RRID: AB_477593
Rabbit Anti-pLLGL1/2(S650/S654)	Abnova	PAB4657; RRID: AB_1577970
α-rabbit-Alexa488/594/647	Molecular Probes	RRID: AB_2576217 / RRID: AB_2534095 / RRID: AB_2535813
α-mouse-Alexa488/594/647	Molecular Probes	RRID: AB_138404 / RRID: AB_141672 / RRID: AB_141725
α-rat-Alexa488/594/647	Molecular Probes	RRID: AB_141373 / RRID: AB_141374 / RRID: AB_141778
α-mouse-HRP	DAKO	P0447; RRID: AB_2617137
α-rat-HRP	DAKO	P0450; RRID: AB_2630354
Bacterial and Virus Strains		
E. coli: OP50: *E. coli* B, uracil auxotroph	CGC	WB Strain: OP50
E. coli: HT115(DE3): F-, mcrA, mcrB, IN(rrnD-rrnE)1, rnc14::Tn10(DE3 lysogen: lavUV5 promoter-T7 polymerase).	CGC	WB Strain: HT115(DE3)
E. coli : DH5α Electrocompetent cells	Gift from Colin Dolphin	N/A
Chemicals, Peptides, and Recombinant Proteins		
aPKC inhibitor: CRT0103390	Cancer Research Technology LTD	CRT0103390
phorbol 12-myristate 13-acetate (PMA)	Sigma-Aldrich	Cat#P1585-1MG
PKCι-(recombinant human baculovirus-expressed)	EMD Millipore	Cat#14-505
PKCζ-(recombinant active protein, His tagged, Sf21 cells-expressed)	EMD Millipore	Cat#14-525
FAM-PKCε-pseudosubstrate	Molecular Devices	Cat#RP7548
ATP	Sigma-Aldrich	Cat#A7699
Critical Commercial Assays		
IMAP fluorescence polarization progressive binding system	Molecular Devices	#R8127
KINOMEscan	DiscoveRx	N/A
Deposited Data		
CRT0103390 synthesis	Patent	WO/2013/078126
pkc-3(ne4246)	Allele Sequence	*ne4246*
Experimental Models: Cell Lines		
HEK-293	Cell Production, Cancer Research UK (CRUK)	HEK-293
Experimental Models: Organisms/Strains		
C. elegans: N2 (Bristol)	CGC	WB Strain: N2
C. elegans: HT1593: *unc-119(ed3) III.*	CGC	WB Strain: HT1593
C. elegans: DR466: *him-5(e1490) V.*	CGC	WB Strain: DR466
C. elegans: DP38: unc-119(ed3) *III*; *daf-?.*	CGC	WB Strain: DP38
C. elegans: JA1643*[gfp::wsp-1; pkc-3 (ts)]*: *ojIs40 [Ppie-1::gfp::GBDwsp-1 + unc-119(+)];pkc-3(ne4246)II*	this paper	JA1643

(*Continued on next page*)

Continued

REAGENT or RESOURCE	SOURCE	IDENTIFIER
C. elegans: JA1644[*gfp*::*cdc-42*; *pkc-3*(*ts*)]: *unc-119*(*ed3*) *III*; *tjIs6* [*Ppie-1*::*gfp*::*cdc-42* + *unc-119*(+)]; *pkc-3*(*ne4246*)*II.*	this paper	JA1644
C. elegans: JH2802[*Dendra2*::*MEX-5*]: *unc-119*(*ed3*) *III*; *axIs1950*[*mex-5p*:: *Dendra2*::*TEV*::*S-peptide*::*mex-5RR*:: *mex-5 3'UTR* + *unc-119*(+)]	CGC	WB Strain: JH2802
C. elegans: *JH2840*[*mCherry*::*mex-5*]: *axIs???* [*nmy-2p*::*pgl-1*::*GFP*::*patr-1*:: *nmy-2 3'UTR*]. *axIs1731* [*pie-1p*:: *mCherry*::*mex-5*::*pie-1 3'UTR* + *unc-119*(+)]	CGC	WB Strain: JH2840
C. elegans: *KK1063*[*lgl-1*::*gfp*]: *it256* [*lgl-1*::*gfp* + *unc-119*(+)]; *unc-119*(*ed4*) *III*; *lgl-1*(*tm2616*) *X*	(Beatty et al., 2010)	WB Strain: KK1063
C. elegans: *KK114*[*par-2*(*ts*)]: *daf-7*(*e1372*) *par-2*(*it5*) *III*	CGC	WB Strain: KK114
C. elegans: *KK1216*[*par-3*::*gfp*]: *par-3*(*it298* [*par-3*::*gfp*]) *III*	Ken Kemphues / CGC	WB Strain: KK1216
C. elegans: *KK1228*[*gfp*::*pkc-3*]: *pkc-3*(*it309* [*gfp*::*pkc-3*]) *II*	Liam Coyne Ken Kemphues / CGC	WB Strain: KK1228
C. elegans: *KK1248*[*par-6*::*gfp*]: *par-6*(*it310*[*par-6*::*gfp*]) *I*	Anushae Syed Ken Kemphues / CGC	WB Strain: KK1248
C. elegans: *KK1262*[*par-1*::*gfp*]: *par-1* (*it324*[*par-1*::*gfp*::*par-1 exon 11a*])	Diane Morton / CGC	WB Strain: KK1262
C. elegans: *KK822*[*par-1*(*ts*)]: *par-1*(*zu310*) *V*	CGC	WB Strain: KK822
C. elegans: *KK973*[*par-3*:Δ*cr1*:*gfp*]: *itIs169* [*Ppar-3*::*par-3 CR1* Δ(*69-82*):::*gfp*, *unc-119*(+)]; *unc-119*(*ed4*) *III*	Ken Kemphues	KK973
C. elegans: *NWG0003*[*par-2*(*ts*); *gfp*:: *par-6*]: *daf-7*(*e1372*) *par-2*(*it5*) *III*; *unc-119* (*ed3*) *III*; *ddIs8* [*gfp*::*par-6*(*cDNA*); *unc-119*(+)]	this paper	NWG0003
C. elegans: *NWG0012*[*gfp*::*c1b*]: *unc-119*(*ed3*)*III*; *crkIs4*[*Ppie-1*::*sfgfp*:: *c1b*::*pie-1utr*; *unc-119*(+)]	this paper	NWG0012
C. elegans: *NWG0016*[*gfp*::*c1b*::*pkc-3*]: *unc-119*(*ed3*)*III*; *crkIs10*[*Ppie-1*::*sfgfp*:: *c1b*::*pkc-3*::*pie-1utr*; *unc-119*(+)]	this paper	NWG0016
C. elegans: *NWG0021*[*gfp*::*c1b*::*pkc-3*; *mCherry*::*par-2*]:*unc-119*(*ed3*)*III*; *ddIs31*[*pie-1p*::*mCherry*::*par-2*::*pie-1utr*; *unc-119*(+)]; *crkIs10*[*Ppie-1*::*sfgfp*::*c1b*:: *pkc-3*::*pie-1utr*; *unc-119*(+)]	this paper	NWG0021
C. elegans: *NWG0022*[*gfp*::*c1b*;*mCherry*:: *par-2*]: *unc-119*(*ed3*)*III*; *ddIs31*[*pie-1p*:: *mCherry*::*par-2*::*pie-1utr*; *unc-119*(+)]; *crkIs4*[*Ppie-1*::*sfgfp*::*c1b*::*pie-1utr*; *unc-119*(+)]	this paper	NWG0022
C. elegans: *NWG0026*[*par-6*::*gfp*; *mCherry*:: *par-2*]: *par-6*(*it310*[*par-6*::*gfp*]) *I*;*unc-119* (*ed3*)*III*; *ddIs31*[*pie-1p*::*mCherry*::*par-2*; *unc-119*(+)]	this paper	NWG0026
C. elegans: *NWG0027*[*gfp*::*pkc-3*; *mCherry*:: *par-2*]: *pkc-3*(*it309* [*gfp*::*pkc-3*]) *II*;*unc-119*(*ed3*)*III*; *ddIs31*[*pie-1p*::*mCherry*::*par-2*; *unc-119*(+)]	this paper	NWG0027

(*Continued on next page*)

Continued

REAGENT or RESOURCE	SOURCE	IDENTIFIER
C. elegans: *NWG0028[par-3::gfp; mCherry::par-6]*: *par-3(it298 [par-3::gfp]) III;unc-119(ed3)III;ddIs26 [mCherry::T26E3.3;unc-199(+)]*	this paper	NWG0028
C. elegans: *NWG0039[par-1(ts); par-6::gfp]*: *par-1(zu310) V*; *par-6(it310[par-6::gfp]) I.*	this paper	NWG0039
C. elegans: *NWG0047[PH-GBP]*: *unc-119(ed3) III*; *crkEx1[pNG19*: *mex-5p::PH(PLC1Δ1)::GBP::mKate::nmy-2UTR + unc-119(+)]*; *him-5 (e1490) V.*	this paper	NWG0047
C. elegans: *NWG0053[par-6::gfp;pkc-3(ts)]*: *par-6(it310[par-6::gfp]) I*; *pkc-3(ne4246)II*	this paper	NWG0053
C. elegans: *OD70[mCherry::PH-PLCΔ1]*: *unc-119(ed3) III*; *ltIs44[pie-1p-mCherry::PH(PLC1Δ1) +unc-119(+)] V*	(Kachur et al., 2008)	WB Strain: OD70
C. elegans: *SA131[gfp::cdc-42]*: *unc-119(ed3)III*; *tjIs 6[Ppie-1::gfp::cdc-42+unc-119(+)]*	(Motegi and Sugimoto, 2006)	WB Strain: SA131
C. elegans: *TH129[gfp::par-2]*: *unc-119 (ed3)III;ddIs25[GFP::F58B6.3;unc-119(+)]*;	(Schonegg et al., 2007)	TH129
C. elegans: *TH159[mCherry-cdc-42]*: unc-119(ed3)III; ddIs46[WRM0625bA11 GLCherry::cdc-42; Cbr-unc-119(+)]	Tony Hyman	TH159
C. elegans: *TH209[mCherry::par-2]*: *unc-119(ed3)III*; *ddIs31[pie-1p::mCherry::par-2*; *unc-119(+)]*	(Schonegg et al., 2007)	TH209
C. elegans: *TY3558[gfp::his-11*; *b-tubulin::gfp]*: *ruIs[pie-1::GFPhis-11] III*; *ojIs1 [β-tubulin::GFP]*	CGC	WB Strain: TY3558
C. elegans: *UE37[pie-1::gfp]*: *axEx73 [pie-1p::pie-1::GFP + rol-6(su1006) + N2 genomic DNA]*; *tubulin mCherry*	Carrie Cowan	UE37
C. elegans: *WH423[mCherry::cdc-42(Q61L)]*: *Ppie-1::mcherry::cdc-42(Q61L)*	(Kumfer et al., 2010)	WH423
C. elegans: *WH497[gfp::chin-1]*: *ojIs69 [pie-1::mGFP::chin-1 + unc-119(+)]*	CGC	WB Strain: WH497
C. elegans: *WH517[gfp::wsp-1]*: *ojIs40 [Ppie-1::gfp::GBDwsp-1 + unc-119(+)]*	CGC	WB Strain: WH517
C. elegans: *WM150[pkc-3(ts)]*: *pkc-3(ne4246) II*	(Fievet et al., 2012)	WM150
C. elegans: *WS5018[gfp::cdc-42]*: *cdc-42(gk388)*; *opIs295 [cdc-42p::gfp::cdc-42(genomic)::cdc-42 3'UTR + unc-119(+)] II.*	(Neukomm et al., 2014)	WB Strain: WS5018
Oligonucleotides		
pkc-3(genomic) fwd:CCCACTAGTATGTCG TCTCCGACAT (SpeI)	IDT DNA	N/A
pkc-3(genomic) rev:CCCAGGCCTTCAGAC TGAATCTTCC (StuI)	IDT DNA	N/A
PH-GBP gBlock: fwd: TTCCGTTTTCTCATTGTATTCTCTC	IDT DNA	N/A
PH-GBP gBlock: rev: ATGATGCCGGCTTAGCTAGC	IDT DNA	N/A
Site-directed mutagenesis (PAM site) in pNG0018, fwd: GTCTGTTTCGTAACTGTCTTCTGTATAACT	IDT DNA	N/A

(*Continued on next page*)

Continued

REAGENT or RESOURCE	SOURCE	IDENTIFIER
Site-directed mutagenesis (PAM site) in pNG0018, fwd: TGATATCGAAACAAACACTG	IDT DNA	N/A
ctl (RNAi): fwd: ATCGATAAGCTTTGTATCCTCTTG	IDT DNA	N/A
ctl (RNAi): rev: ACCGGCGGATCCTTAAATACGG	IDT DNA	N/A
Recombinant DNA		
Fosmid: WRM069dD11	Source BioScience	WB Clone: WRM069dD11
Plasmid: L4440	Addgene	plasmid#1654
Plasmid: pUC57-C1B(codon-optimized)	GenScript	N/A
Plasmid: pTH699	Gift from Tony Hyman	N/A
Plasmid: pC1B-Ø	This paper	N/A
Plasmid: pC1B-pkc-3	This paper	N/A
Plasmid: CmKate2 MosSci vector	Gift from Tony Hyman	N/A
Plasmid: pNG0018	This paper	N/A
Plasmid: pNG0019	This paper	N/A
Ahringer Feeding RNAi: *cdc-42*	Source BioScience	WB Clone: sjj_R07G3.1
Ahringer Feeding RNAi: emb-27	Source BioScience	WB Clone: sjj_F10B5.6
Ahringer Feeding RNAi: *par-3*	Source BioScience	WB Clone: sjj_F54E7.3
Ahringer Feeding RNAi: *par-6*	Source BioScience	WB Clone: sjj_T26E3.3
Ahringer Feeding RNAi: *pkc-3*	Source BioScience	WB Clone: sjj_F09E5.1
Ahringer Feeding RNAi: *perm-1*	Source BioScience	WB Clone: sjj_T01H3.4
Ahringer Feeding RNAi: *rga-3*	Source BioScience	WB Clone: sjj_K09H11.3
Ahringer Feeding RNAi: *cgef-1*	Source BioScience	WB Clone: sjj_C14A11.3
Feeding RNAi: *mlc-4*	(Redemann et al., 2010)	N/A
Feeding RNAi: control(ctl)	This paper	N/A
PH-GBP gBlock (sequence on request)	IDT DNA	N/A
ctl (RNAi): gBlock (sequence on request)	IDT DNA	N/A
Software and Algorithms		
Matlab	Mathworks	R2016a
Kilfoil Feature Tracking (feature2D.m)	http://people.umass.edu/kilfoil/downloads.html	N/A
Fiji (ImageJ)	https://fiji.sc/#	N/A
ActivityBase	IDBS	N/A

CONTACT FOR REAGENT AND RESOURCE SHARING

Requests for resources and reagents should be directed to and will be fulfilled by the Lead Contact, Josana Rodriguez (josana.rodriguez@ncl.ac.uk). CRT0103390 may be obtained through an MTA from Cancer Research Technology (jroffey@cancertechnology.com).

EXPERIMENTAL MODEL AND SUBJECT DETAILS

C. elegans Strains and Maintenance

C. elegans strains were maintained on nematode growth media (NGM) under standard conditions (Brenner, 1974) at 16°C or 20°C unless otherwise indicated. Strains listed in the Key Resources Table. Note analysis of zygotes precludes determination of animal sex.

C. elegans Transgenic Animals

Following the scheme of (Lekomtsev et al., 2012), a codon-optimized (Redemann et al., 2011) sequence encoding the C1B domain from human PKCα (GenScript) was inserted into pTH699 via BamHI and SmaI to generate a *sfgfp::c1b* fusion under control of the *pie-1* promoter and -3' UTR (pC1B-Ø). Genomic *pkc-3* was amplified from fosmid WRM069dD11 (Source BioScience, WB Clone: WRM069dD11) using the following primers (fwd:cccactagtatgtcgtctccgacat; rev:cccaggccttcagactgaatcttcc) and inserted into

(pC1B-Ø) using SpeI and StuI to generate pC1B-pkc-3. Both plasmids were introduced by biolistic bombardment into HT1593 worms (Praitis et al., 2001), yielding NWG0012 and NWG0016.

The membrane-tethered GFP-binding protein (PH-GBP) was generated by combining amino acids 1-175 corresponding to the PH domain of rat PH-PLCΔ1 (Audhya et al., 2005) and VHH4GFP (Caussinus et al., 2011) coupled by a SGQGGSGGSGGS linker. The resulting sequence was codon-optimized (CAI = 0.49) and a single GFP intron inserted as described (Redemann et al., 2011). A synthetic gBlock (IDT DNA) encoding the PH-GBP was PCR amplified and cloned in frame with a C-terminal codon-optimized mKate2 under the control of the *mex-5* promoter and *nmy-2* 3' UTR in a MosSCI vector containing wild-type *unc-119* obtained from the Hyman Lab. The resulting plasmid (pNG0018) was inserted at the ttTi5605 *mos1* site locus of DP38 worms via CRISPR after mutating the sgRNA/PAM site following the method described (pNG0019) (Dickinson et al., 2013). Modified worms were crossed into DR466 to generate a stable male line expressing PH-GBP (NWG0047). To rescue membrane localization of PAR-3 variants, we crossed NWG0047 with KK1216 (*par-3*::*gfp*) or KK973 (*par-3Δcr1*::*gfp*) lines. We were unable to obtain a stable homozygous line for the endogenously tagged PAR-3::GFP, presumably due to the toxic effects of continuously targeting all PAR-3 to the membrane throughout embryogenesis. Thus, we used F1 progeny heterozygous for PAR-3::GFP for analysis. By contrast, for PAR-3ΔCR1::GFP, which is expressed ectopically from a multi-copy random insertion, we readily obtained animals homozygous for both PAR-3ΔCR1::GFP and PH-GBP, which were used for subsequent analysis. However, no significant difference in the segregation of PAR-3ΔCR1::GFP was seen between heterozygous and homozygous animals.

For analysis of GFP::CDC-42, SA131 was used unless otherwise indicated.

For analysis of the effects of CDC-42(Q61L) on GFP::PKC-3 localization, zygotes were taken from F1 animals resulting from crossing KK1228 with either TH159 or WH423 due to difficulties obtaining stable animals homozygous for both markers.

Cell Lines

HEK-293 are female and were obtained from Cell Production, Cancer Research UK (CRUK) and cultivated in DMEM (Dulbecco's modified Eagle's medium), 10% FBS (fetal bovine serum) and penicillin–streptomycin (Invitrogen) (Kjær et al., 2013).

Bacterial Strains

OP50 bacteria and HT115(DE3) were obtained from CGC. DH5α was obtained from Colin Dolphin. Feeding by RNAi used HT115(DE3) bacteria strains containing a plasmid carrying the indicated RNAi feeding plasmid.

METHOD DETAILS

C. elegans - RNAi Culture Conditions

RNAi by feeding was performed similar to described methods (Kamath et al., 2003). Briefly, HT115(DE3) bacterial feeding clones were inoculated from LB agar plates to LB liquid cultures and grown overnight at 37°C in the presence of 10 μg/ml carbenicillin. Bacterial cultures were induced with 5 mM IPTG at 37° for 4h with agitation before spotting 100 μl of induced bacteria onto 60 mm agar RNAi plates (10 μg/ml carbenicillin, 1 mM IPTG). L4 larva were added to RNAi feeding plates and incubated for 24-72 hr depending on gene and temperature. For temperature sensitive lines, feeding was performed at 15°C for 48-72 hr and shifted to 25°C for 2-5 hr before imaging. For double depletion experiments, L3/L4 larva carrying *par-1*(*zu310*) or *par-2*(*it5*) temperature sensitive mutants were placed on RNAi plates at 15°C for 24 hr before a fraction of those were moved to fresh RNAi expressing plates for 18 to 22 hr at 25°C. Partial RNAi for *mlc-4* was performed for 14-24 hr at 20°C. For partial depletion of *perm-1*, *rga-3/4* or *pkc-3*, bacteria expressing the desired clone were mixed at the indicated ratios with bacteria expressing control RNAi. *par-3*, *par-6*, *cdc-42*, *pkc-3*, *perm-1*, rga-3/4, *cgef-1* and *emb-27* clones are from the Ahringer library (Kamath et al., 2003). *mlc-4* is from Redemann et al., 2010. A control RNAi clone was generated by synthesizing a random 500bp sequence using the Matlab random number generator with no homology to the worm genome, cloned into Bgl-II / HindIII sites of L4440 (Addgene, plasmid#1654), and transformed into HT115 bacteria.

C. elegans Embryos – Western Blots

Embryos were obtained by a standard bleaching protocol and resuspended in NuPAGE LDS sample buffer (Invitrogen) prior to sonication using the Biorupture (Diagenode) for 5 - 30 s on, 30 s off cycles. Samples were heated at 70°C for 10 min before centrifugation at 13.000 rpm for 20 min to obtain cleared supernatant. Samples were run on a 12% NuPAGE gel using MOPS SDS running buffer (Invitrogen) and transferred onto PVDF membrane (Immobilon-P membrane 0.45 um, Millipore). PKC-3 and tubulin was detected using the primary (anti-PKC-3 1:10.000 and anti-tubulin 1:20.000) and secondary antibodies (as recommended by provider) indicated in Key Resources Table and detected via chemiluminescence (ECL prime, GE Healthcare Life Sciences). PKC-3 band intensity was analyzed using the Fiji Gel analysis tool.

C. elegans Zygotes – Drug Treatment

All drug treatment experiments were performed in 10 to 50% *perm-1*(*RNAi*) (Carvalho et al., 2011). Drugs were dissolved in DMSO and used at the following concentrations: phorbol 12-myristate 13-acetate (PMA, Sigma-Aldrich, P1585-1MG), 100 μM; CRT90 (CRT0103390, Cancer Research Technology LTD), 10 μM. When drug treatment alone was required, we obtained zygotes with permeable eggshells by placing L4 animals on a 1:1 mix of bacteria expressing *perm-1*(*RNAi*) and *ctl* (*RNAi*) for 16 to 20 hr at

20°C. When drug treatment was combined with additional RNAi treatment, L4 animals were placed on bacteria expressing *perm-1*(*RNAi*) mixed at a 1:9 ratio with bacteria expressing the desired RNAi (*par-3*, *par-6*, *cdc-42*, *control*) and incubated for 40-48 hr at 20°C.

C. elegans Zygotes - Immunofluorescence

Immunofluorescence was performed as previously described (Andrews and Ahringer, 2007). Briefly, gravid hermaphrodite worms were washed and then transferred to a 7 μl drop of M9 on a 0.1% poly-lysine coated well. Embryos were released using a needle and then covered with a coverslip to compress the embryos. Slides were snap-frozen on dry ice for 30 min after which the coverslip was quickly removed and the slide fixed in methanol at room temperature for 20 min. Samples were washed and re-hydrated with PBS followed by two 10 min washes in PBS+0.2% Tween-20 before proceeding with antibody incubations, DAPI staining and mounting in Mowiol (Sigma-Aldrich). All antibodies used in this study are listed in Key Resources Table. Primary antibody dilutions used: anti-PAR-2 1:500, anti-PAR-6 1:10, anti-PKC-3 1:500 and anti-PAR-3 1:50. Secondary antibodies were used as recommended by provider. Confocal images were acquired using Carl Zeiss Axioplan 2, LSM510 Meta confocal equipped with LSM image software and Nikon A1R equipped with Nikon elements software and a 63× objective. Cortical super-resolution images were acquired using the DeltaVision OMX system equipped with SoftWoRx and OMX acquisition software. Secondary processing of images was performed using Photoshop CS5 and Illustrator CS5 (Adobe).

C. elegans zygotes - Live Imaging

Embryos were dissected in 2-4 μl of M9 buffer (22 mM KH_2PO_4, 42 mM $NaHPO_4$, 86 mM NaCl and 1 mM $MgSO_4$) on a coverslip and mounted under 2% agarose pads (Zipperlen et al., 2001) or dissected in Shelton's Growth Medium (Edgar and Goldstein, 2012) and mounted with 16-21 μm polystyrene beads between a slide and coverslip and sealed with VALAP (Goehring et al., 2011a). 16-18 μm beads were used for cortex imaging to maximize imaging surface. In all other cases, 21 μm beads were used to minimize compression effects on development. For CRT90 experiments, embryos were dissected in the presence of 10 μM CRT90. For C1B targeting experiments, two sides of the coverslip were left unsealed to create a flow chamber (Goehring et al., 2011a) and PMA washed in at the indicated times.

To maximize viability, embryos were typically imaged at 20-22°C, except for temperature sensitive alleles, which were imaged at the indicated temperatures using an objective temperature control collar (Bioptechs / Linkam, PE94). For consistency, establishment phase embryos were taken at pronuclear meeting, and maintenance phase was defined as the interval from nuclear envelope breakdown to metaphase.

Cortex images were captured with a 100x 1.49 NA TIRF objective on a Nikon TiE (Nikon) equipped with an iLas2 TIRF unit (Roper), 488 or 561 fiber coupled diode lasers (Obis), and an Evolve Delta camera (Photometrics). Midplane imaging was performed on Carl Zeiss Axioplan 2, LSM510 Meta confocal or a Nikon TiE with 63x or 100x objectives, further equipped with either a Spectra-X LED light source (wide-field) or a custom X-Light V1 spinning disk system (CrestOptics, S.p.A.) with 50μm slits, 488, 561 fiber-coupled diode lasers (Obis) and either a CoolSnap HQ or Evolve Delta (Photometrics). Imaging systems were run using Metamorph (Molecular Devices) and configured by Cairn Research (Kent, UK).

In vitro PKC Enzyme Assays

The ability of compounds to inhibit the kinase activity of recombinant human baculovirus-expressed full-length PKCι was measured using the IMAP fluorescence polarization (FP) progressive binding system (Molecular Devices #R8127, Sunnyvale, CA) in 384-well black, non-binding, flat-bottom assay plates (Corning #3575, Corning, NY). The assay mixture (final volume = 10 μL) contained 20 mM Tris-HCL (pH 7.5), 150 μM ATP, 10 mM MgCl2, 0.01% Triton X-100, 250 μM EGTA, 1 mM DTT, 15 pM PKCι (EMD Millipore #14-505, Billerica, MA), 100 nM FAM-PKCε-pseudosubstrate (Molecular Devices #RP7548), 0.1% DMSO and various concentrations of test compound. Compound dilutions (prepared in 100% DMSO) were added to the assay plate at 100 nL using the BioMek NX pin tool (Beckman Coulter, Indianapolis, IN). Enzyme reactions were initiated by the addition of ATP (Sigma- Aldrich #A7699, St. Louis, MO), followed by incubation of the plates for 1 hour in a 25°C incubator. A 20 μL aliquot of IMAP detection reagent (1:400 in 85% 1X Binding Buffer A and 15% 1X Binding Buffer B) was added to each well followed by a 2-hour incubation at 25°C. Fluorescence polarization was then measured using the PerkinElmer Envision 2102 multi-label plate reader (PerkinElmer, Waltham, MA) using the FP dual mirror, FP480 excitation filter and P-pol 535 and S-pol 535 emission filters. Data analysis was performed using ActivityBase (IDBS, Guilford, UK). IC_{50} values were calculated by plotting percent inhibition versus log10 of the concentration of compound and fitting to the 4-parameter logistic model (top and bottom constrained to 100 and 0, respectively) in XLFit 4 (IDBS).

The PKCζ kinase assay was performed using the IMAP FP progressive binding system as described above for PKCι but with some modifications. The concentration of PKCζ (recombinant active protein, His tagged, expressed in Sf21 cells, Millipore, 14-525) was 10pM, while the substrate concentrations were 100 nM and 40 μM for the FAM-PKCε-pseudosubstrate (Molecular Devices #RP7548) and ATP, respectively.

Cellular Biochemical Assay

HEK-293 cells were transfected in a 10 cm dish as per the manufacturer's instructions (Corning). After 16 hr, the cells were trypsinized and seeded into a 96-well plate at 1.5×10^4 cells/well and medium was replenished. After a further 24 hr, the medium was replaced by new medium and a range of CRT0103390 inhibitor concentrations. After 1 hr of inhibitor treatment, lysates were prepared using

ice-cold Tris lysis buffer [150 mM NaCl, 20 mM Tris (pH 7.5), 1 mM EGTA, 1 mM EDTA and 1% Triton X-100]. Lysates were transferred on to an anti-FLAG-coated ELISA plate (Sigma) and incubated for 2 hr with gentle shaking, followed by an automated wash step (Tecan plate washer) with wash buffer [50 mM Tris (pH 7.5), 0.15 M NaCl and 0.02% Tween 20]. The immunocomplexed protein was incubated with anti-pLLGL1/2 (S650/S654) primary antibody overnight at 4°C, followed by an automated wash and then addition of HRP-conjugated secondary antibody. After a further wash, 3,3',5,5'-tetramethylbenzidine (Sigma) was added according to the manufacturer's instructions and attenuance was read at 450 nm using an Ascent plate reader (Thermo Labsystems).

Kinase Selectivity

CRT0103390 was profiled using the KINOMEscan *in vitro* competition binding screening platform at DiscoveRx against a panel of 442 mutant and non-mutant kinases at a test concentration of 1 μM. Selectivity scores were calculated as the number of non-mutant kinases with % activity relative to control < 20/number of non-mutant kinases tested. CRT0103390 demonstrated a high degree of selectivity in this panel, with an S(80) of 0.09.

QUANTIFICATION AND STATISTICAL ANALYSIS

Image Analysis - General

All image analysis was performed in Fiji (ImageJ)(Schindelin et al., 2012) and Matlab (Mathworks).

Image Analysis - Asymmetry Index (ASI)

The asymmetry index (ASI) of a feature is defined by:

$$\frac{A-P}{2(A+P)}$$

where A and P define the anterior and posterior signal, respectively. Raw ASI values are normalized to the mean ASI observed in respective controls, such that a value of 1 indicates wild-type asymmetry and zero indicates complete loss of asymmetry. Anterior and posterior signals are defined depending on the condition examined and include cross-sectional area (AB vs P1 asymmetry), fluorescence intensity on the two cell halves for the membrane (midsection PAR analysis) or cytoplasm (MEX-5, PIE-1), or cluster number (CHIN-1).

Image Analysis – Cluster Index

The Cluster Index is defined as the variance in cortical intensity within the anterior domain. It was calculated in Matlab across user specified ROIs that were subject to background subtraction and normalization to mean intensity before analysis.

Image Analysis – CHIN-1 Foci

CHIN-1 foci were identified using the feature2D.m script, part of the feature detection and particle tracking package from the Kilfoil Lab (Pelletier et al., 2009). Embryos were automatically detected and partitioned into 3 domains (Anterior, Middle, Posterior) and normalized anterior vs posterior particle densities used for ASI calculation.

Image Analysis – MEX-5 Mobility

For MEX-5 mobility, five pre-bleach frames were captured by spinning disk confocal microscopy. A central 20-pixel wide stripe was then bleached along the AP axis using a 473 diode laser (Obis) and recovery was monitored every 2 s. Because MEX-5 is uniform in the quantified conditions, fluorescence was monitored within a central 20 x 100-pixel box.

Image Analysis - Colocalization

Colocalization analysis of PAR-6 and PAR-3 was performed in ROIs at the anterior cortex of establishment phase zygotes (wild-type n=8 and *pkc-3*(*ts*) n=9). Costes' Mask and intensity correlation quotient (Li et al., 2004) were obtained using JaCOP plug-in in Fiji.

Image Analysis – Flow Speeds

Anterior-directed cortical flow speed during establishment phase was measured using midplane, brightfield images acquired every second until late establishment phase at which point we switched to fluorescent imaging to obtain suitable images for measuring PAR asymmetry. Using the Kymograph Plugin in Fiji (Seitz and Surrey, 2006), we generated kymographs for individual embryos by tracing a segmented line along the cortex starting at the origin of flow. A minimum of 10 yolk granule trajectories, each spanning approximately 200s were selected for a minimum of 5 embryos per condition. The cortical flow velocity was defined as the total distance over time calculated from a line connecting the start and end positions of the granule on the kymograph. Measurement of cortical flow in wild-type embryos expressing GFP fusions to PAR-3, PKC-3 or CDC-42 yielded a velocity of 7.1+/-1.4 μm/min (n=22), consistent with previously published values (7.66+/-1.0 μm/min, n=6)(Munro et al., 2004).

Image Analysis – Anterior Cortical Intensity (Immunofluorescence)

Anterior cortical intensity of each PAR protein is the mean greyscale value of a line 2 pixels wide (in each corresponding fluorescent channel) covering the PAR-3 cortical domain of the zygote. The cortical intensity value is then normalized by dividing it by the mean greyscale value of a nearby cytoplasmic region to correct for embryo IF staining variability. In *par-3*(*RNAi*) zygotes, we cannot distinguish anterior from posterior cortex and the entire cortex of zygotes is analyzed. Each experimental condition was analyzed in three independent experiments.

Image Analysis – Anterior PAR Retraction (Immunofluorescence)

The posterior boundary of anterior PARs in fixed, midsection fluorescent images is defined at the intersection between the equatorial zygote line (longest line linking the zygotes' poles) and the line that links the cortical ends (top and bottom) of the PAR protein analyzed. Retraction is the distance between this posterior boundary and the posterior pole of the zygote. Retraction difference is defined as the difference in retraction distance between PAR-3 and PKC-3. Data were collected from three independent experiments.

Image Analysis – Intensity Profile Extraction

In general, to assess PAR signal from midsection images, a 60-pixel wide stripe encompassing the cell membrane was extracted and straightened to generate a profile for each embryo for further analysis.

For spatial analysis (ASI, profile plots, domain size, segregation efficiency), the top 4 central pixels corresponding to the membrane were taken at each x-position and averaged to the given local membrane signal. Background and cytoplasmic signal were calculated locally from inner and outer edges of this stripe, allowing normalization for variation in signal between conditions. Briefly, background was subtracted and then membrane divided by cytoplasmic intensity.

Image Analysis – PAR-3 versus PKC-3 Cortical Profile Comparison (Immunofluorescence)

To quantitatively compare PAR cortical profiles in multi-labelled fixed embryos, two identical profiles along the cortex were extracted in each channel as above. Each set of profiles was split in half to generate two boundary regions. After normalization to maximum and minimum values, profiles were registered using the inflection point, c, based on fitting each PAR-3 profile using the following function:

$$I(x) = a + \frac{b}{2}(erf(mx - c))$$

where erf is the error function, c is the domain boundary position, m the boundary slope and a and b allow for scaling and displacement on the y-axis.

Image Analysis – Domain Size/Segregation Efficiency

To extract domain size data (PAR-2 domain size change, segregation efficiency) from single channel images, cortical fluorescence profiles were normalized to total embryo perimeter length and aligned to the center of posterior PAR domain determined by fitting the profile to the following function:

$$I(x) = a \pm \frac{b}{2}(erf(mx - c_1) - erf(mx - c_2))$$

with the center of the posterior domain specified by:

$$\frac{c_2 - c_1}{2}$$

posterior domain size given by:

$$\frac{c_2 - c_1}{L}$$

and anterior domain size given by:

$$1 - \frac{c_2 - c_1}{L}$$

where L is the length of the profile.

PAR-2 domain size change for each embryo was calculated as the ratio of domain size taken from images before and 5 min after PMA addition. Segregation efficiency into the anterior was scored by relative anterior domain size, with smaller anterior domains defined as more efficient segregation.

Image Analysis – Total Membrane Signal Change

To estimate total membrane signal in PAR-6 and PKC-3 rescue experiments straightened profiles were projected in x to give a cross-section profile spanning background, crossing the membrane and into the cytoplasm for the full circumference. Cross-section profiles were then normalized with background = 0 and cytoplasm = 1. To get the most accurate estimate of isolated membrane signal,

we generated a mean cross-section for embryos with no detectable membrane signal from *par-3* and *par-6* RNAi embryos to define the shape of the outside to inside fluorescence step. The shape of this curve was extremely consistent allowing a mean profile to be generated, which could then be subtracted from individual embryo cross-section profiles with the sum of the difference taken as membrane signal.

For PAR-2 retention in C1B-induced PKC-3 membrane-targeting experiments, a cytoplasm-normalized 4-pixel wide stripe encompassing the cell membrane was taken from images before and 5 min after PMA addition to generate profiles. PAR-2 retention was defined as the ratio of total membrane signal before and after PMA addition.

Statistics

For all assays, significance was assessed using an unpaired, two-tail Student's T test unless otherwise noted with the following criteria: *p<0.05, **p<0.01, ***p<0.001, ****p<0.0001. Data are presented as mean values plus all data points or mean ± 95% confidence interval (CI), in which case (N) is indicated.

Data and Software Availability

Sequence data for *pkc-3(ne4246)* has been submitted to Wormbase (WB Gene: *pkc-3*).

PHILOSOPHICAL TRANSACTIONS B

royalsocietypublishing.org/journal/rstb

Review

Cite this article: Gubieda AG, Packer JR, Squires I, Martin J, Rodriguez J. 2020 Going with the flow: insights from *Caenorhabditis elegans* zygote polarization. *Phil. Trans. R. Soc. B* **375**: 20190555.
http://dx.doi.org/10.1098/rstb.2019.0555

Accepted: 9 July 2020

One contribution of 15 to a discussion meeting issue 'Contemporary morphogenesis'.

Subject Areas:
biophysics, cellular biology, developmental biology, molecular biology

Keywords:
actomyosin flow, cytoplasmic streaming, cell polarity, PAR patterning, asymmetric cell division, mechanochemical feedback

Author for correspondence:
Josana Rodriguez
e-mail: josana.rodriguez@ncl.ac.uk

†These authors contributed equally to the study.

THE ROYAL SOCIETY PUBLISHING

Going with the flow: insights from *Caenorhabditis elegans* zygote polarization

Alicia G. Gubieda†, John R. Packer†, Iolo Squires, Jack Martin and Josana Rodriguez

Biosciences Institute, Newcastle University, Newcastle upon Tyne NE2 4HH, UK

JRP, 0000-0003-1170-8445; JR, 0000-0001-8800-1283

Cell polarity is the asymmetric distribution of cellular components along a defined axis. Polarity relies on complex signalling networks between conserved patterning proteins, including the PAR (*par*titioning defective) proteins, which become segregated in response to upstream symmetry breaking cues. Although the mechanisms that drive the asymmetric localization of these proteins are dependent upon cell type and context, in many cases the regulation of actomyosin cytoskeleton dynamics is central to the transport, recruitment and/or stabilization of these polarity effectors into defined subcellular domains. The transport or advection of PAR proteins by an actomyosin flow was first observed in the *Caenorhabditis elegans* zygote more than a decade ago. Since then a multifaceted approach, using molecular methods, high-throughput screens, and biophysical and computational models, has revealed further aspects of this flow and how polarity regulators respond to and modulate it. Here, we review recent findings on the interplay between actomyosin flow and the PAR patterning networks in the polarization of the *C. elegans* zygote. We also discuss how these discoveries and developed methods are shaping our understanding of other flow-dependent polarizing systems.

This article is part of a discussion meeting issue 'Contemporary morphogenesis'.

1. Introduction

Most metazoan cells are polarized along a defined axis, presenting molecular and structural asymmetries that are key to their function. Cell polarity can be triggered in response to a wide variety of cell-intrinsic or extrinsic cues that lead to different cellular responses, such as activation of signalling cascades, changes in membrane composition and cytoskeletal rearrangements. Through these processes, polarity cues promote the asymmetric cortical distribution of patterning proteins, the localization of which also depends on complex signalling networks, typically involving cooperative and mutually antagonistic interactions among these patterning proteins (figure 1*a*). From their established localizations, these proteins ultimately define distinct subcellular domains by controlling the activity of downstream targets that deliver the polarized phenotype. The coordination of these polarization events permits a multitude of higher biological outcomes ranging from cell fate determination and differentiation to tissue patterning and morphogenesis [1,2]. Among the polarity effectors, the *par*titioning defective (or PAR) proteins constitute a highly conserved network that includes the scaffolding proteins, Par3 and Par6, the small GTPase Cdc42 and the atypical protein kinase aPKC. PARs were initially identified in screens for mutations affecting the asymmetric cell division of the one-cell embryo (zygote) of the nematode *Caenorhabditis elegans* [3–5]; since then they have been implicated in patterning distinct regions in most polarized cells. For example, the same set of PARs defines the 'anterior' domain not only in the *C. elegans* zygote (figure 1*a*,*f*) but also

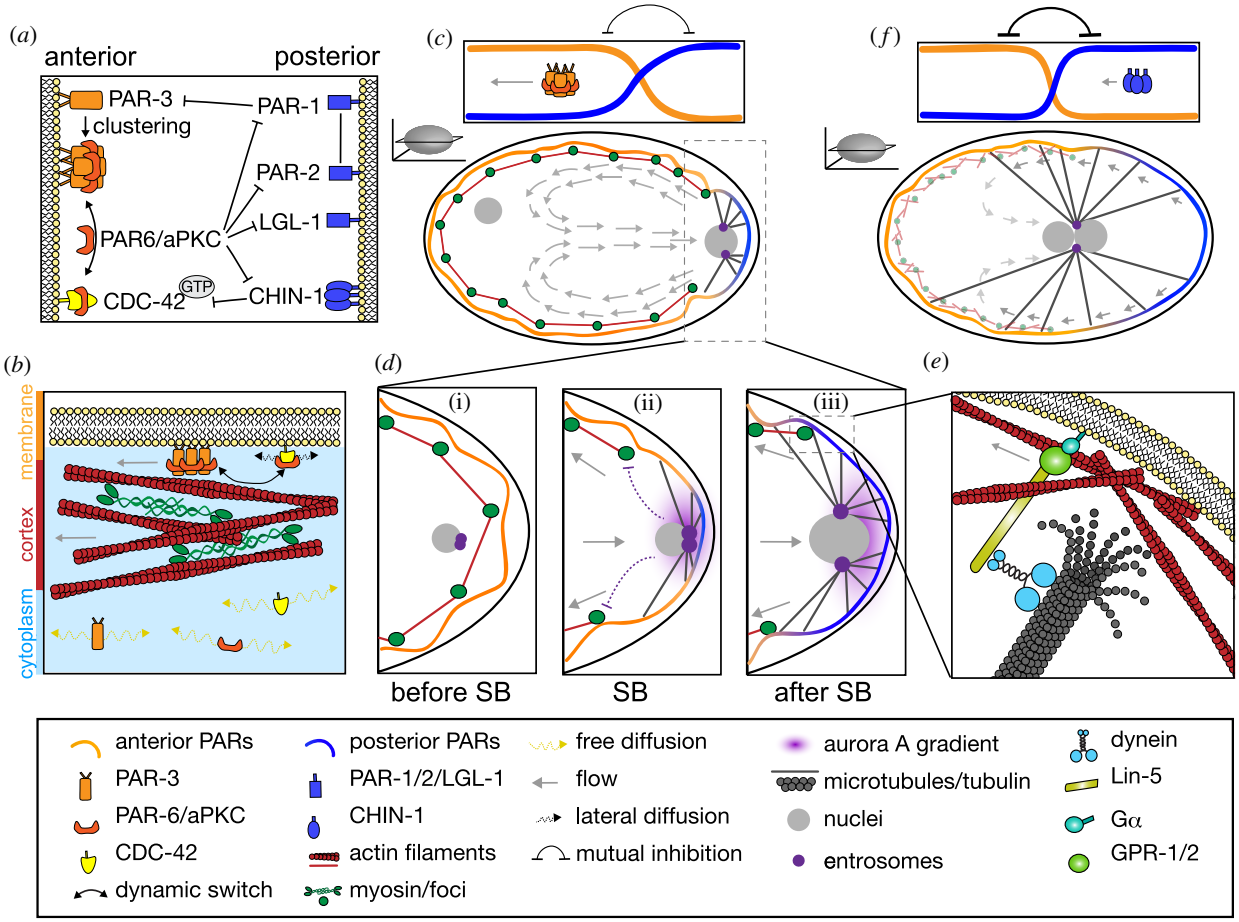

Figure 1. PAR patterning depends on actomyosin flow in the *C. elegans* zygote. (*a*) PAR protein network in the *C. elegans* zygote. In the anterior domain, CDC-42 and PAR-3 are required for stable membrane association of the PAR-6/aPKC heterodimer. PAR-3 can form clusters that recruit PAR-6/aPKC, which can switch between PAR-3- and CDC-42-dependent states. At the posterior, the accumulation of PAR-3 clusters is inhibited by PAR-1, which is stabilized at the posterior domain through PAR-2-binding. PAR-1, PAR-2 and the other posterior PAR, LGL-1, can be phosphorylated by aPKC and displaced from the membrane. Exclusion of the CDC-42-GAP CHIN-1 clusters from the anterior is dependent on aPKC, but whether it is a direct target of aPKC is unknown. In return, CHIN-1 at the posterior inactivates CDC-42. (*b*) The actomyosin cortex is a thin meshwork below the membrane that flows towards the zygote anterior during polarity establishment. At the membrane, PAR-6/aPKC follows advective actomyosin flow when bound to PAR-3 clusters (diffusion coefficient: D_c approx. 0.001 µm^2 s^{-1}). In association with CDC-42, PAR-6/aPKC diffuses freely in the plane of the membrane (lateral diffusion: D_c approx. 0.1 µm^2 s^{-1}). PAR proteins at the membrane exchange with a cytoplasmic pool, where they can freely diffuse with high mobility dissipating any source of asymmetry in the cytoplasm (D_c approx. 1 µm^2 s^{-1}). (*c*) Midplane view of the zygote during polarity establishment or symmetry breaking (SB), with the initiation of cortical actomyosin and concomitant cytoplasmic flow (zygote's length approx. 45 µm). The inset graph shows anterior (orange) and posterior (blue) PAR cortical levels (*y*-axis) along the length of the zygote (*x*-axis). The PARs exclude each other from their respective membrane domains. During polarity establishment, the boundary of anterior and posterior PARs shifts with the anterior-directed cortical flow (approx. 7 µm min^{-1}), which transports PAR-6/aPKC in cluster with PAR-3. (*d*) Temporal snapshots during SB: (i) after fertilization, aPARs initially occupy the entire membrane, while pPARs are mostly cytoplasmic. The sperm-derived centrosomes (purple spheres) are positioned close to the cortex at the future posterior pole. (ii) A diffusive cue of Aurora A from the centrosomes inhibits actomyosin contractility in the posterior pole, resulting in a cortical flow towards the anterior domain. Microtubules emanating from the centrosomes are thought to aid the deposition of PAR-2 at the membrane. (iii) The actomyosin flow also generates a cytosolic backflow, which contributes to placing the posterior male pronucleus (PN) closer to the membrane. This holds the cue in place to promote further cortical flow and, synergizing with cortically-attached microtubules, facilitates the separation of the centrosomes around the male PN. (*e*) In the cortex, the microtubules associate with the Gα/GPR-1/2/LIN-5 complex via dynein and are pulled towards the anterior thanks to the actomyosin flow. This coupling of microtubules to flow and the positioning of the male PN within the zygote posterior pole drives the separation of the centrosomes. (*f*) Midplane view of the embryo during polarity maintenance phase. The male and female pronuclei meet, and the actomyosin network disassembles. aPAR and pPARs each occupy 50% of the embryo cortex and exclude each other from the membrane. In the posterior, CHIN-1 clusters follow the weaker actomyosin flow (approx. 2 µm^2 s^{-1}) towards the anterior where they disassemble, presumably owing to aPKC activity.

in *Drosophila melanogaster* (*Drosophila* from here onwards) oocytes, the 'front' in migrating cells, and the 'apical' domain in epithelial cells and mouse oocyte blastomeres [6–8]. The adaptability of this core PAR module resides in its dynamism. Variant combinations of PAR components and/or modulation by other cell type-specific patterning regulators allow these core polarity effectors to respond to different cues and mediate distinct polarity outputs [9,10].

The asymmetric localization of polarity effectors is produced by a variety of different mechanisms. In some instances, their polarization does not depend on a symmetry breaking cue. In budding yeast, a positive feedback loop, whereby active Cdc42 GTPase at the membrane promotes the recruitment of its own activator (the guanine nucleotide exchange factor, Cdc24), leads to several clusters of Cdc42-GTP (active, GTP-bound). The later specification of a

unique cluster does not seem to rely on a prior polarity cue but on a competition event where the largest cluster becomes the bud by outcompeting the others in the recruitment of polarity factors from the cytoplasm [11].

Conversely, PAR polarity is generally driven by directional cues. For example, PARs can be assembled at a specific site in response to the activation of a signalling cascade. In migrating cells, integrin signalling leads to the local activation of Cdc42 and subsequent enlisting of the aPKC–Par6–Par3 complex to the leading edge of the cell [12]. Similarly, in epithelial cells, PTEN phosphatase activation leads to PIP_2 (phosphatidylinositol-4,5-bisphosphate) enrichment and consequent recruitment of Cdc42, aPKC and Par6 at the developing apical domain [13]. Other means to dock PARs to specific cellular domains involve rearrangements in the cytoskeleton. Par-1 kinase is trapped at the *Drosophila* oocyte posterior in an actin-dependent manner [14], and Par3 is thought to be recruited to the apical domain of outer cells in the eight-cell stage mouse embryo by an apical contractile actomyosin network [15].

The enrichment of PARs to specific cellular domains can also be attained by their active directional transport via motor proteins walking on polarized cytoskeleton structures, such as the localization of Bazooka (Baz, *Drosophila* Par3 homologue) to epithelial adheren junctions by the microtubule (MT) minus-end-directed motor dynein [16] or the transport of Cdc42-enriched vacuoles to the nascent apical domain of endothelial cells during tubule formation [17,18]. Indirect transport or advection that does not involve direct contact of PARs with the underlying cytoskeleton has also been reported. In this review, we will focus on this alternative means of generating PAR asymmetry, which typically involves cortical actomyosin reorganization and bulk cytosolic movements, referred to as cytoplasmic flow or streaming.

Cytoplasmic flows are present in many cell types and occur by a variety of mechanisms, including cell shape changes, osmotic gradients and most frequently by cytoskeletal dynamics at the cell cortex [19–21]. These cytoskeletal dynamics entail the motor-dependent transport of organelles/vesicles along tracks and the long-range movement of cytoskeletal networks, typically of the actomyosin network underlying the membrane (actomyosin cortex) [20]. These movements are transmitted to the cortical cytosol that permeates the cytoskeletal structures, powering bulk movements of the cytoplasm [22]. Cytoplasmic flow was first observed in Characean algae [23] and is a common feature of large eukaryotic cells (greater than 100 µm) such as plant cells [24] and oocytes [21,25,26]. In this context, streaming of the cytoplasm is proposed to aid the transport of metabolites, proteins and other cellular components over distances that would be impossible by simple diffusion, at required timescales [20,27].

However, over the past decade, there has been an appreciation that flow can lead to the generation of organelle and molecular asymmetries within cells [21]. For example, the posterior localization of *oskar* mRNA, key to the patterning of the *Drosophila* oocyte, is achieved by the combined action of directional transport and advection. Kinesin 1-dependent transport on a weakly polarized MT network [28,29] together with cytoplasmic streaming, which promotes the encounter and trapping of cytoplasmic *oskar* mRNAs by the posterior actomyosin cortex [26,30], drive *oskar* mRNA posterior localization. This cytoplasmic streaming is generated by kinesins and their cargoes dragging the cytoplasm as they walk on cortical MTs attached by their minus-end to the cortex, ultimately leading to the coupling of MT movement and the formation of MT parallel arrays responsible for the long-range cytoplasmic flow [26,31]. A similar mechanism of MT-dependent cytoplasmic streaming exists in the *C. elegans* zygote, but here the alignment of MTs relies on the endoplasmic reticulum [32–34]. This meiotic cytoplasmic streaming (MeiCS) influences the position of the sperm-derived pronucleus (PN) and associated centrosomes (PN/centrosome complex), which will determine the antero-posterior axis (AP axis) of the *C. elegans* embryo [35–38].

In many cases, however, flows are driven by the activity of the actomyosin cortex. Retrograde actin flow in migrating cells is involved in cell movement and leads to the asymmetric accumulation of myosin and polarity regulators along the migration axis [39–45]. The asymmetric position of the meiotic spindle in the mouse oocyte and the male PN in the *C. elegans* zygote (this occurs at a later stage than MeiCS) depends on reverse-fountain-like cytoplasmic streaming. These bulk movements of cytosol arise from the dynamics of the actin cortex underlying the membrane, which lead to a cortical cytoplasmic flow followed by a countercurrent central flow that pushes these nuclear structures close to the cortical site from where the flow originated (figure 1*c*,*d*, shown for *C. elegans*) [46–50]. Different actomyosin dynamics are responsible for the above-indicated flows; in the mouse oocyte, it is the actin treadmilling along the inner cell surface, in the *C. elegans* zygote it is the contractility of the actomyosin network and in migrating cells it appears that a combination of both may drive cytoplasmic flow (figure 2*a*,*b*, shown for *C. elegans*). In *C. elegans* zygote asymmetric division, the described cortical cytoplasmic flow also establishes the AP axis of the embryo by driving the anterior localization of PAR-3, PAR-6, aPKC and CDC-42 (Par3, Par6, aPKC and Cdc42 *C. elegans* homologues, also referred to as anterior PARs or aPARs) by advection [36,37,51–57] (figure 1*b*,*c*) . This is arguably one of the best-studied systems, where a comprehensive description of the interplay between flow and PAR polarity has emerged.

Caenorhabditis elegans cytoplasmic flow was first observed in 1960 by Nigon *et al*. [58]. Contractions in the *C. elegans* zygote produced movements in the cytoplasm that appeared necessary to mediate the asymmetric cell division of the zygote. Further investigation revealed that the actomyosin cortex became asymmetric during this first cell division [59–61] and that the observed cytoplasmic flow could be a product of this reorganization of cortical actomyosin [35,60]. Cortical and central cytoplasmic flow speeds were first directly measured by Hird & White, who also proposed that these movements may arise as a result of a gradient of cortical tension within the actomyosin cortex [35,62]. With the advent of live-cell imaging and GFP reporters, Munro and co-workers supported this hypothesis and revealed the cytoskeletal dynamics responsible for the cortical cytoplasmic flow [36,37]. Since its initial description, we have come a long way in our understanding of the biophysical and molecular properties of this actomyosin-dependent cortical flow. Here, we will review the most current work in the *C. elegans* zygote.

Advection of PAR proteins by an actomyosin-dependent cytoplasmic flow (figure 1*b*) was first observed by Munro and co-workers in the *C. elegans* zygote [36,37]. Since initial observation, the establishment of PAR polarity by flow has been proposed in other systems. These include the fly

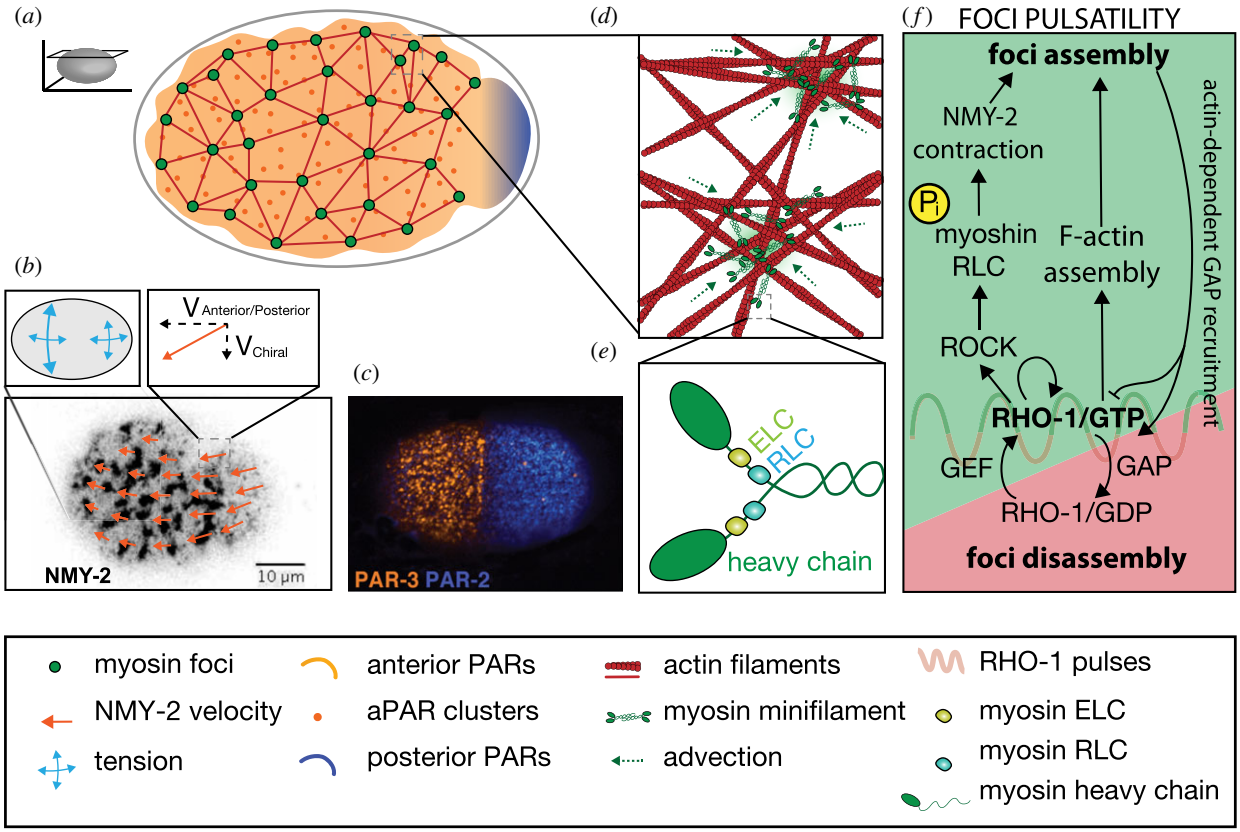

Figure 2. Regulation of actomyosin-dependent flow. (*a*) Cortical view of the embryo just after symmetry breaking. The actomyosin network (actin filaments and NMY-2 foci) retracts towards the anterior domain and carries clusters of anterior PARs (orange dots) with it. This retraction to anterior allows posterior PARs (in blue) to load to the posterior domain. (*b*) Actomyosin flow is associated with anisotropies in cortical tension, which is higher orthogonal to the AP axis in anterior (blue arrows). NMY-2 foci move towards the anterior, along the AP axis (*x*-axis), but also present chiral displacement—a directional component orthogonal to the AP axis (*y*-axis). (*c*) Cortical image of PAR-3 and PAR-2, showing PAR-3 clusters retracted. (*d*) Myosin contraction can result in the accumulation of components in the actomyosion foci via local recruitment or advective flow (green arrows). (*e*) Non-muscle myosin II is composed of two heavy chains (NMY-2 in *C. elegans*), two essential light chains (ELC, MLC-5 in *C. elegans*) and two regulatory light chains (RLC, MLC-4 in *C. elegans*). (*f*) The small GTPase RHO-1 is the main regulator of actomyosin contractility during polarity establishment. RHO-1 can cycle between its active (RHO-1/GTP) and inactive (RHO-1/GDP) states through the action of GAPs (RGA-3/4) and GEFs (ECT-2). In addition, RHO-1 can promote its own activity by an unknown mechanism (looped arrow). RHO-1/GTP can activate its downstream kinase ROCK, which phosphorylates the myosin RLC, increasing its motor activity and promoting the formation of myosin minifilaments, all leading to actomyosin contraction. In addition, RHO-1 can promote F-actin assembly, possibly via formin (CYK-1). These parallel outputs of RHO-1 lead to foci assembly. During foci assembly, enrichment of actin can lead to a delayed recruitment of RGA-3/4 causing foci disassembly, from where the cycle can start again. Therefore, pulses in RHO-1 activity coordinate the cyclical assembly and disassembly of NMY-2 foci.

neuroblast, where it aids the generation of an apical cap of aPKC and Bazooka [63–65], and in mammalian epithelia, where actomyosin contractility promotes apical localization of aPKC–Par6 [66]. In these systems, PARs could couple to the actomyosin flow by advection, as described in *C. elegans*, given that they are embedded in the cytosol influenced by the motion of the contractile actomyosin cortex [10,21,67] (figure 1*b*, shown for the *C. elegans* zygote). Here, we will review the molecular mechanisms underlying PAR advection by flow as they have been the subject of recent work in *C. elegans*.

The possibility that the PARs could, in turn, affect actomyosin network organization and dynamics was discussed from their very discovery in *C. elegans* [3,68]. It has subsequently become apparent that, as PARs are asymmetrically localized in response to actomyosin dynamics, these polarity effectors can, in turn, modulate properties of the cytoskeleton. For example, in *Drosophila* amnioserosa cells, Bazooka and Par-6/aPKC are recruited to the apical domain by a highly contractile medioapical actomyosin network, where they concomitantly regulate actomyosin contractility leading to dorsal closure [69–73]. A similar positive feedback loop exists in the *C. elegans* zygote, whereby anterior PARs become asymmetrically localized through the actomyosin flow that they promote [9,67,74,75].

Recent publications have greatly enhanced our understanding of the interplay that exists between cortical actomyosin flow and patterning mechanisms in the *C. elegans* zygote. In §2, we give an overview of the polarization of the zygote, indicating stages and factors that are critical in the creation of PAR-based asymmetry. In §3, we focus upon aspects of cortical flow generation and regulation. We discuss the identification of regulators of emergent physical behaviours of the actomyosin cortex and the origins and biological relevance of one of these physical behaviours, pulsatility. Section 4 reviews the molecular and physical properties membrane PAR proteins must exhibit to be transported by flow, and the positive feedback PARs have on the flow that transports them. In §5, we discuss the generation of cytoplasmic asymmetries for which the original dogma of flow as the source of these asymmetries has been replaced by reaction–diffusion and phase separation models. In §6, we review the contribution of flow to other key aspects of *C. elegans* zygote asymmetric cell division, in particular centrosome separation leading to a bipolar spindle, and

polarity domain correction during cytokinesis. Given the prevalence of actomyosin flow in the polarization of cells, throughout the review we indicate how research in the *C. elegans* zygote compares with or can inform studies in other systems.

2. Overview of *Caenorhabditis elegans* zygote polarization

PAR-dependent patterning of the one-cell embryo of *C. elegans* defines the AP axis and drives its asymmetric division, critical for the initiation of distinct cell lineages. Prior to polarization, a highly contractile cortex, involving a dynamic network of actin filaments and non-muscle myosin II foci, occupies the entire zygote [35–37,59–61]. Upon fertilization and completion of maternal meiosis, the sperm-donated centrosome induces a local inhibition of actomyosin contractility at the posterior pole of the zygote. This leads to flow of the actomyosin network towards the anterior, leaving a smoothened posterior cortex (akin to placing an elastic band under tension and then cutting one end) [35–37,76,77] (figures 1*c*,*d*(ii) and 2*a*,*b*). As a result of this actomyosin retraction, cytoplasmic flow is generated; an anterior-directed cortical flow, which subsequently produces countercurrent posterior-directed central flow owing to the fluid-like properties of the cytoplasm and geometry of the zygote [35–37,78] (figure 1*c*, zygote). Posterior-directed cytoplasmic flow and centrosomal MT asters synergize to position the PN/centrosome complex close to the cortex at the posterior pole, ensuring robust polarization of the zygote [37,46,48,78–82] (figure 1*d*(ii)). This initiates a mechanochemical-positive feedback loop whereby the signal emanating from the centrosomes promotes actomyosin flow, which maintains centrosome–cortex proximity and strengthens the polarity signal [37,46,48,49,79,82–88].

The anterior-directed cortical flow also transports membrane-associated PAR-3, PAR-6, aPKC and CDC-42 into the anterior [36,37,51–57] (figures 1*b*,*c* and 2*a*–*c*). aPARs stimulate cortical contractility, further promoting flow and, hence, their own asymmetric localization [36,37,52,54,55,82,89–93]. In this establishment phase of polarity, actomyosin contractility is primarily dependent on the small GTPase RhoA homologue, RHO-1 [77,94,95], the activity of which is regulated by the GEF ECT-2 (guanine nucleotide exchange factor) [77,90–92] and the GAPs (GTPase-activating proteins), RGA-3 and RGA-4 [94–97] (figure 2*f*). The precise molecular mechanism(s) of how PARs regulate actomyosin flow are still under investigation; however, aPARs have been described to stabilize myosin II at the anterior domain [82] and might regulate RHO-1 via the TAO kinase KIN-18 [98].

Concomitantly to the anterior PAR protein transport, PAR-2, PAR-1 and LGL-1 load to the posterior membrane domain (hence also referred to as posterior PARs or pPARs) (figures 1*c* and 2*a*,*c*). Their loading is reported to be aided by MT asters from the centrosome that protect PAR-2 from aPKC-mediated membrane expulsion [99] (figure 1*d*(ii)). Anterior and posterior PAR domains are further established through kinase-dependent mutual antagonism. The posterior PARs can be phosphorylated by aPKC, which drives their dissociation from the membrane [93,99–103], and similarly, the PAR-1 kinase, recruited by membrane-associated PAR-2, removes cortical aPARs via phosphorylation of PAR-3 [99,101,104] (figure 1*a*). Following this 'establishment phase' of polarity, the zygote enters a 'maintenance phase' during which large-scale flow ceases and control of actomyosin contractility switches to CDC-42 [90,91]. This small GTPase moves to the anterior alongside the other aPARs and is inhibited at the posterior by its cognate GAP, CHIN-1. In the absence of high-speed flow, mutual antagonism between anterior and posterior PARs plays a major role in ensuring opposing gradients of aPARs and pPARs at the membrane [9,37,51,52,54,89,93,99,101,102,105] (figure 1*a*,*f*).

Cortical flow and asymmetrically localized PARs drive downstream events, such as the segregation of cytoplasmic cell fate determinants and mitotic spindle organization and positioning [67,106]. All of this will lead to an essential asymmetric division that generates two daughter cells, the somatic AB cell and the germline P1 precursor [107] (figure 4).

3. The anterior-directed cortical flow that polarizes the *Caenorhabditis elegans* zygote

The transport of PAR proteins by an actomyosin-directed cortical flow was first described in the *C. elegans* zygote by Munro and co-workers in 2004 [36,37,51] (figures 1*b*,*c* and 2*a*–*c*). In this seminal work, the authors found that the high contractility of the actomyosin cortex, leading to strong membrane ruffling (including a pseudocleavage furrow) and the generation of flow, is dependent on the motor ability of non-muscle myosin II (*C. elegans* non-muscle myosin heavy chain, NMY-2), with cortical flow being abrogated upon depletion of the regulatory myosin light chain (RLC, MLC-4 in *C. elegans*) (figure 2*a*,*d*,*e*). The authors also supported a previous hypothesis, indicating that the cortex is under tension [19,35,62], as they observed that contractions between neighbouring NMY-2 foci were mechanically coupled. In this scenario, after fertilization, the local reduction of NMY-2 foci at the posterior pole would produce an imbalance in cortical tension and cause the actomyosin network to retract towards the opposite pole [35,37]. The actomyosin flow presented as a collective movement of actin filaments and NMY-2 foci towards the anterior of the zygote, with foci speed of approximately 7 µm min^{-1} (figure 2*a*,*b*). Since initial description, cortical flow in the zygote has been extensively studied and we now know that flow is indeed associated with anisotropies in cortical tension in the anterior domain, where tension is higher orthogonal to the AP axis [76] (figure 2*b*, blue arrows). In addition, the gradient in actomyosin contractility, caused by the reduction of NMY-2 at the posterior, supports a long-range flow thanks to the viscosity of the cortex, which presents fluid-like properties constantly contracting, rearranging and turning over (hydrodynamic properties). These physical qualities allow the force of a single contraction to influence the network over a significant distance (approx. 14 µm) within the zygote (total length approx. 45 µm) [76]. Flow also presents an orthogonal component to the AP axis, leading to chiral counter-rotatory flow (figure 2*b*) that reflects the molecular torque properties of actomyosin (counter-rotation of cross-linked actin filaments). There is no role described for this chiral flow in the zygote; however, similar chiral flows drive embryo left–right asymmetry at a later stage (four- to six-cell stage) [108,109]. Another emergent large-scale mechanical property of this actomyosin flow is its pulsatile nature, which might emerge from the regular cyclic assembly and disassembly

of NMY-2 foci during flow. This property has been the focus of recent studies reviewed here [94,95].

From a molecular point of view, the organization and contractility of the actomyosin cortex is known to be regulated by the small GTPases RHO-1 in polarity establishment [77,94,95] and CDC-42 in maintenance, although a role in establishment has also been reported [37,52,90,91]. These GTPases cycle between active GTP-bound and inactive GDP-bound states, modulated by their GEFs and GAPs [52,77,90–92,94–97]. The GTP-bound state of the RHO-1 homologue, RhoA, is known to exert its effects through the recruitment and/or activation of formins, anillin and Rho-associated protein kinase (ROCK) [110,111]. Active ROCK stimulates myosin II motor activity and facilitates minifilament assembly and activity by phosphorylating the myosin regulatory light chain and inhibiting myosin phosphatase [112] (figure 2*f*). In the *C. elegans* zygote, depletion of the ROCK homologue, LET-502, leads to defects in actomyosin organization and flow [94]. During maintenance, CDC-42-dependent activation of non-muscle myosin II is driven by the kinase MRCK-1 (myotonic dystrophy-related CDC-42-binding kinase homologue) [52,54]. In addition, several actin-binding proteins (ABPs) have been implicated in the organization of this cortex [113], including F-actin-polymerizing (profilin PFN-1, formin CYK-1, ARX-2/3) [114–116], -cross-linking (anillin, ANI-1/2) [117–119] and -bundling (plastin, PLST-1) [120,121] proteins.

Here, we will review recent studies that have begun to illuminate how known and newly identified regulators contribute to large-scale biophysical properties of the actomyosin flow, showing a molecular degeneracy where multiple molecular activities modulate each property [120,122]. Therefore, the gradient of actomyosin contractility responsible for this patterning flow could be shaped by various factors, making it difficult to identify the polarity cue(s) that trigger this cortical flow. Recent publications debate the exact molecular nature of the polarity cue and mechanisms underlying the polarization of the zygote.

(a) Aurora A regulates actomyosin flow and ensures a monopolar antero-posterior axis

For over 20 years, evidence has supported that the sperm-derived centrosomes produce a cue that inhibits local contractility of the actomyosin cortex at the presumptive posterior pole, leading to the actomyosin flow that polarizes the zygote [36,37,46,48,51,79,123] (figure 1*d*(ii)). However, the nature of this polarity cue has remained elusive until recently [83,84,88] in part owing to polarity being dependent on centrosomal maturation [124–129] and on MTs organized by the centrosomes [46,48,80,92,99,130,131]. *Caenorhabditis elegans* zygote polarization also relies on several feedback loops, so it is difficult to pin-point where the polarity cue is acting. For example, both sets of PARs mutually antagonize each other to occupy and define their respective domains [9,67,74] (figure 1*a*,*c*), and the anterior PARs promote the actomyosin flow that transports them [9,67,74,75] (figures 1*c* and 2*a*).

Recent theory observations indicate that, in the early zygote, polarization feedback loops remain subcritical to avoid spontaneous pattern formation [82]. Hence, the system will only polarize in response to a guidance cue that will strongly promote instability in the patterning feedback loops. For example, the symmetry breaking cue initiates a flow that is stronger than required to transport the aPARs to an opposing domain from which they can stably antagonize their posterior counterparts [82]. In agreement with a strong guidance cue being needed to start PAR asymmetry, it has been observed that centrosomes can signal from a distance (greater than 10 µm), but polarization is faster and more robust if centrosomes are closer to the cell cortex [48,85–87] (figure 1*d*(ii)). This led to the idea of a diffusive polarization cue that emanates from the centrosomes and promotes the downregulation of NMY-2 at the posterior pole, initiating the contractile imbalance that will drive flow and subsequent asymmetric localization of PARs.

Recent publications have reactivated discussion on the cue's definitive molecular nature and function, each proposing that the Aurora A kinase homologue, AIR-1, ensures a monopolar AP axis independent of its role in both centrosome maturation and MT organization [83,84,88,132].

The kinase's spatio-temporal regulation appears to be tightly controlled before and during zygote polarization. Prior to symmetry breaking, AIR-1 is associated with MTs at the cortex and diffusely distributed in the cytoplasm [83], from where it suppresses cortical actomyosin contractility globally [83,88]. AIR-1 is subsequently recruited to the pericentriolar material, where it is required for full MT organizing activity of centrosomes [83,125,133,134] and for zygote polarity (figure 1*d*(ii)). From this location, it is proposed that AIR-1 forms a diffusive gradient reaching the posterior pole of the zygote, where it robustly targets polarization via local inhibition of actomyosin contractility and/or loading of PAR-2 to the membrane [83,84,88] (figure 1*d*(ii)). During polarity maintenance, AIR-1 becomes cytoplasmic once more and aids global disassembly of the actomyosin network, suppressing later centrosome-independent polarization mechanisms [84]. Interestingly, for all these functions, AIR-1 localization to MTs is not required, unlike at a later stage of mitosis where TPXL-1 recruits AIR-1 to astral MTs, from where the kinase inhibits polar actomyosin contractility [135].

Intriguingly, knockdown of *air-1* does not lead to loss of polarity as would be expected from the symmetry breaking cue. Instead, it causes a previously reported bipolar phenotype, where PAR-2 is aberrantly localized at both poles of the zygote [129,133], and weak cortical flows are directed towards the embryo centre from the poles [83]. This bipolar phenotype could derive from events in the oocyte, before fertilization has even occurred. During ovulation, AIR-1 and PLK-1 (Polo-like kinase) prevent premature polarization, by regulating the timing of aPAR membrane loading [132]. This is presumably due to PAR-3 phosphorylation by PLK-1, which could prevent PAR-3 membrane loading, as observed at a later stage in the zygote [55]. Binding of PAR-3 to the oocyte membrane therefore initiates a PAR maturation cycle that takes 20–30 min to complete [132]. Upon maturation, the PAR system becomes sensitive to symmetry breaking cues, which, in wild-type embryos, permits a timely response to the correct guidance cue of the posterior centrosomes. The removal of AIR-1 or PLK-1 causes the PAR system to mature early and become sensitive to spontaneous, cryptic or maternal symmetry breaking cues, producing the reverse and bipolar phenotypes observed in AIR-1 depletion [83,84,88,132].

The penetrance of the PAR-2 bipolar phenotype versus a complete reverse polarity, where PAR-2 is only in the anterior pole, varies between each study (bipolarity favoured in [83,88,132], whereas reverse polarity in [84]), possibly owing to different knockdown strengths or reporter strains used, leading to some discrepancies. The reverse anterior polarity

observed by Zhao *et al*., upon *air-1* RNAi, led the authors to further support the requirement of centrosomal AIR-1 to mediate local inhibition of actomyosin contractility at the posterior pole of the zygote [84]. Upon AIR-1 depletion, Klinkert *et al*. mostly observed bipolar recruitment of PAR-2 that does not require cortical flow or MTs [83]. In addition, PAR-2 always associates with the membrane at the poles, independent of where the centrosomes contact the cortex, possibly owing to increased membrane curvature permitting geometry-dependent PAR-2 recruitment/stabilization (as observed in zygotes grown in micro-patterns [83]). The authors postulate that the cortical and cytoplasmic pools of AIR-1, prior to the kinase's recruitment to the centrosome, protect the zygote from spontaneous symmetry breaking through PAR-2 membrane recruitment at high-curvature sites [83]. This is different from what was proposed by Kapoor & Kotak [88], who observed that PAR-2 bipolarity depends on actomyosin contractility, and hence postulated that AIR-1 global suppression of actomyosin contractility prevents early ectopic polarization (anterior PAR-2 localization) by flow.

The multipolarity observed in AIR-1 loss of function is reminiscent of the capacity of certain cells to spontaneously polarize in random orientations in the absence of tight regulation from a specific guidance cue(s) [136]. Overall, AIR-1 could protect the zygote from inappropriate symmetry breaking by promoting the subcritical state of polarization feedback loops proposed by Gross *et al.* [82]. Furthermore, by supporting symmetry breaking in response to the sperm centrosome, AIR-1 helps establish the correct monopolar axis. These studies and the molecular degeneracy of the actomyosin cortex [120,122] (discussed below) indicate that the polarization of the zygote most likely relies on the timely and spatial coordination of multiple molecular processes. This is further exemplified by a recent finding from De Henau *et al*. [137], who have reported a novel mechanism/requirement for symmetry breaking. Here, high levels of H_2O_2, released from a polarized mitochondrial network, can drive posteriorization of the zygote. All the above indicate that a single guidance cue being responsible for the polarization of the zygote is unlikely; instead, several cues may regulate the different molecular functions required for timely symmetry breaking, as indicated in these AIR-1 studies.

It is still unclear how AIR-1 exerts its regulatory capacity. Given the tight feedback loops that exist between PARs and the actomyosin cytoskeleton in the polarization of the zygote [9,67,74,75], it is currently hard to determine if AIR-1 is directly targeting PARs (for example, by influencing aPAR membrane loading) or cortical contractility, or both. AIR-1 phosphorylates PARs and actomyosin regulators in other systems. In *Drosophila*, Aurora A inhibits ROCK [138], activates the aPAR complex by phosphorylation of Par-6 at a conserved Aurora site [139], and releases Lgl from the membrane through phosphorylation [140,141]. It would therefore be interesting to determine whether Aurora A plays a universal role in controlling the timing of response of the PAR network and/or influencing the anisotropies in cortical tension to ensure monopolarity in other systems.

(b) Large-scale actomyosin behaviours can be attained by modulating diverse molecular functions

Over a hundred proteins are proposed to modulate cortical dynamics in other systems [142,143], yet for most it is unknown how they influence large-scale biophysical properties of actomyosin flow. Recently, unbiased methods have been used to assign known and novel cortical regulators to these properties of flow in the *C. elegans* zygote [120,122]. Candidates were selected from high-throughput genetic screens where knockdown altered the dynamic properties of the actomyosin cortex [120,122]. This identified enhancers and suppressors of NMY-2, LET-502 (ROCK), MEL-11 (myosin phosphatase) and ACT-2 (actin) function [120]. Sixty-five putative regulators were found, among them genes encoding known actomyosin modulators (e.g. myosin chaperone UNC-45, WASP-interacting protein WIP-1 and myosin light chain MLC-5) and ABPs (plastin PLST-1, ezrin ERM-1) from other systems, indicating that the identified proteins are valid candidates for cortical regulation. Eleven selected hits were studied in more detail to assess their involvement in actomyosin organization and dynamics. Flow velocities (both along the AP axis—AP flow, and orthogonal to the AP axis—chiral flow, figure 2*b*), flow pulsatility, hydrodynamic length (as a proxy of cortex viscosity) and density/size of NMY-2 foci in the zygote were measured following knockdown. This analysis was done in parallel with 33 ABPs [120,122].

Altogether, this implicated 14 new regulators (eight identified in these screens) of cortical actomyosin dynamics during AP axis establishment. These proteins clustered into functional groups, each containing effectors modulating diverse molecular mechanisms [122]. For example, chiral counter-rotatory flow (figure 2*b*) was found to be regulated by two upstream regulators of RHO-1 (the GAP, RGA-3, and the casein kinase 1, CSNK-1) and two ABPs, an actin membrane cross-linker (annexin, NEX-1) and an inhibitor of myosin ATPase activity (calponin, CPN-1). This suggests that this diverse set of proteins regulates the molecular torque properties of actomyosin, leading to cell-scale changes where the cortex of the zygote twists along the AP axis [108]. As another example, pulsatility of cortical flow is modulated by regulators of actin filament turnover, such as F-actin-polymerizing (PFN-1, CYK-1 and ARX-2), -severing (UNC-60 and FLI-1) and -capping (CAP-1) proteins. This requirement of cortical turnover for pulsation is also supported in more detailed studies [94,95], reviewed in the later section on pulsatility. For the zygote to have such a diverse set of proteins, each with distinct molecular functions, regulating the same large-scale physical property (degenerate functioning) is extremely advantageous, as it provides robustness to the underlying morphogenetic process.

Recent single gene studies of actomyosin regulators identified in these screens [120,122] have subsequently deepened understanding of cortical regulatory processes. The cross-linker PLST-1, which regulates AP flow velocity, has been proposed to increase the connectivity of the actomyosin network facilitating coordinated and persistent cortical flow [121]. Optimal levels of cross-linkers might provide the correct connectivity to propagate tension and allow long-range flow [121,143]. A similar effect has been described during cytokinesis, where above or below optimal levels of anillin and NMY-2 can be detrimental to ring closure [144]. Another AP flow velocity regulator, the septin UNC-59, is asymmetrically localized in the zygote (downstream of PAR signalling) and can also regulate cytokinesis [145,146]. The chiral flow regulator casein kinase, CSNK-1, is also necessary for NMY-2 foci disassembly in meiosis through inhibition of the RHO-1 pathway [147] and for the

rotational cortical flow required for cytokinesis under mechanical stress [148].

Unbiased screens combined with detailed phenotypic analyses of actomyosin dynamics have proved to be a successful strategy to identify proteins underlying long-range flow and properties of the cortex such as pulsatility. The future challenge will be to mechanistically decipher how the combined function of these proteins leads to cellular-scale dynamic behaviours of the cortex, bridging the gap between molecular- and cellular-scale processes. Synthetic biology approaches, studying minimal systems, are beginning to address these challenges [75,149,150]. Approaches using super-resolution imaging in combination with methods that manipulate the function and location of the proteins *in vivo* (i.e. optogenetics, temperature-sensitive mutants and molecule-trapping techniques) will greatly assist progress in this field [151–153].

(c) Organized actomyosin pulsatility leads to an efficient flow

Pulsatility is an intrinsic feature of highly contractile actomyosin networks, documented in a wide variety of developmental processes [37,70,154–159]. In the *C. elegans* zygote, NMY-2 foci pulse with an intensity that increases and decreases cyclically over a period of approximately 30 s [94,95,122]. The network is responsive to these pulses, and flow velocity exhibits temporal fluctuations accordingly [94,122] (figure 2*a*,*d*,*f*). Currently, there are two major streams of thought on how actomyosin pulsatility is achieved in single cells, with RhoA playing a central role in both models [160–162]. However, the proposed requirement of RhoA is different for the two models. In the first, RhoA is recruited by NMY-2 contraction as part of a mechano-chemical feedback, whereas in the second, cyclic activity of RhoA orchestrates the actomyosin pulses [163].

The mechanochemical feedback model is described in *Drosophila* embryonic cells [160,162]. Here, increased apical non-muscle myosin II contractility produces an advective enrichment of both non-muscle myosin II and upstream positive regulators (RhoA pathway), which promote further contraction (figure 2*d*). Parallel accrual of actin filaments and negative regulators of myosin II activity (myosin phosphatase), by the advective flow, decreases contractile ability and thus advection. This delayed negative feedback promotes dissipation of the foci, allowing the cycle to start again.

Contrary to this mechanochemical system that is driven by the stochastic upregulation of myosin II contractility, in the *C. elegans* zygote the cyclical activity of the RhoA homologue, RHO-1, sits upstream and is responsible for the coordination of NMY-2 pulses [94,95] (figure 2*f*). RHO-1 promotes its own activity, leading to a rapid accumulation of active RHO-1 that is necessary for pulsation [95]. These fluctuations in RHO-1 activity temporally precede those of NMY-2 and are not dependent on contractility of the motor protein [94,95]. Furthermore, single-molecule tracking shows that the enrichment of NMY-2 and actin to contractile foci is mediated by the modulation of local assembly/disassembly, with little contribution from advection [95]. The pulse is then terminated through the delayed actin-dependent recruitment of the GAPs, RGA-3 and RGA-4 [95] (figure 2*f*). Interestingly, zygotes with aberrant spatio-temporal oscillation of RHO-1 activity still have anterior-directed cortical flow, yet strong fluctuation and irregular behaviours in the actomyosin disrupt the normal establishment of polarity along the AP axis. Thereby, the pulsatile behaviour of RHO-1 activity acts as a pacemaker of contractile instabilities of the actomyosin cortex, defining the spatio-temporal oscillation pattern of cortical actomyosin foci assembly–disassembly [94,95].

We are beginning to understand the mechanisms underlying this mode of contraction and its biological relevance beyond the context of a single cell [164]. The *Drosophila* embryo represents the best-studied system for tissue-scale pulsatility. In this model, distinct tissue folding events such as dorsal closure [69–73], ventral furrow formation [154,160,165–167] and germband extension [155,162,168,169] all use the pulsatile nature of actoymosin networks to coordinate morphogenesis. For example, in formation of the ventral furrow the combination of pulsatility, which leads to stimulation of contractions in neighbouring cells [165], and a tissue-scale actomyosin contractility gradient [166] facilitates correct tissue folding. It has recently been proposed that actomyosin pulses may also contribute to tissue integrity, accommodating rapid cell and tissue deformations in different systems [159,160,164,170,171]. It would be interesting to determine if RhoA also holds a pacemaker role in other systems and at a tissue scale.

4. PAR protein advection by actomyosin-dependent flow

Cortical actomyosin flow is able to transport certain membrane-bound proteins to the anterior of the *C. elegans* zygote, facilitating their asymmetric distribution (figures 1*c* and 2*a*). Given that not all membrane proteins are segregated by retraction of the actomyosin network, how then do certain proteins couple to flow?

Membrane proteins may be physically bound to the underlying cortex and are then 'dragged' through the membrane. An example of this in *C. elegans* is the E-cadherin homologue HMR-1 [172]. Cadherins are canonically known for their role in cell–cell contacts, yet during polarity establishment HMR-1 forms clusters that are dragged to the anterior domain by actin filaments [37,172]. These clusters decrease actomyosin flow velocity as they create a frictional component, with HMR-1 acting as a 'picket fence' against the movement of the cortex [172].

Anterior PAR proteins, on the other hand, show a similar directed movement yet in the absence of physical interactions with the actomyosin cytoskeleton [36,37,51–57] (figure 1*b*). PAR proteins move freely on the membrane by lateral diffusion (diffusion coefficient, D_c, in the order of 0.1 $\mu m^2\,s^{-1}$) [53,105,173]. Here, they exchange at different rates of binding and unbinding with the cytoplasmic pool, in which their diffusion (random movement) is an order of magnitude faster [36,105,173,174] (figure 1*b*). Once aPARs start to become segregated, there are several mechanisms in place that maintain their asymmetry: the antagonism of pPARs, which begin to accumulate in the posterior membrane as aPARs are cleared [9,67,74] (see §2, figure 1*a*,*c*,*f*), and the spatially differential binding and unbinding rates of PARs from the newly defined anterior and posterior membrane domains [173,174]. For example, PAR-6 is recruited to the membrane approximately seven times faster at the anterior in agreement with the enrichment of several binding partners in this domain, while dissociation rates of PAR-6 are uniform [173]. But

how are aPARs initially segregated? Their movement needs to be somehow coupled to the actomyosin flow triggered by the polarity cue [36,37,53] (figure 1*c*,*d*). The physical mechanism proposed is that shear stress transmits the bulk movement of the actomyosin cortex to the nearby cytoplasm, creating an advective cytoplasmic flow. This is possible given the hydrodynamic properties (liquid-like behaviour, viscosity) of both elements (actomyosin cortex and cytoplasm) [21,22]. PAR proteins attached to the membrane and embedded in this cytoplasm will be advected by this flow (approx. 7 µm min^{-1}) as long as their exchange rate with the cytoplasm and lateral diffusion are slow enough (membrane lifetime approx. 100 s and D_c in the order of 0.001 $\mu m^2 s^{-1}$) [53,173]. In this way, PARs will remain on the membrane long enough to be transported by the flow and their directional movement will surpass their free membrane diffusion, producing their anterior asymmetric localization [21,53]. However, the molecular determinants that allow advection by flow have, until recently, been largely unclear.

(a) PAR proteins sense flow by clustering

Recent work has proposed that the mechanism which allows the anterior scaffolding protein PAR-3 to couple to cortical flow is its ability to form clusters [54–57] (figures 1*b*,*c* and 2*a*,*c*). PAR-3 oligomerization, through its N-terminal CR1 domain, has been reported to mediate PAR-3 membrane localization and clustering in a wide range of polarizing systems [55–57,175–181]. In *C. elegans*, disruption of PAR-3 oligomerization strongly decreases PAR-3 protein levels at the membrane [55–57,178]. Forcing a PAR-3 mutant that cannot oligomerize to the membrane is insufficient to restore PAR-3 asymmetric localization by flow [56]. This indicates that clustering not only stabilizes PAR-3 at the membrane (increased residency time), but also reduces its capability to move freely on the membrane (reduced lateral diffusion). These two outcomes of PAR-3 clustering are in agreement with single particle tracking observations, where larger clusters remain associated with the membrane longer and are more efficiently transported by cortical flow to the anterior of the zygote [55]. PAR-3 clusters have a total diffusive length of less than 3 µm in the plane of the membrane [55] and a low diffusion coefficient of approximately 0.008 $\mu m^2 s^{-1}$ (inferred from subdiffusive PAR-6), which fulfils advection requirements [53,173]. It is not known exactly how clustering stabilizes PAR-3 at the membrane, but we can speculate that the coalescence of multiple membrane-binding domains could synergize to increase avidity for the membrane [182], and in a similar way, multiple membrane contact sites might increase resistance and prevent the lateral diffusion of the cluster. In addition, cluster size alone may also restrict diffusion or alter the ability of clusters to associate with or be corralled by features in the membrane or the cortex. More work is needed to dissect the precise mechanistic basis of flow-sensing by clusters.

PAR-3 clustering also promotes the recruitment of PAR-6, allowing the coupling of the PAR-6/aPKC heterodimer to the advective flow sensed by PAR-3 during establishment [55] (figures 1*b*,*c* and 2*a*). At the membrane, the PAR-6/aPKC heterodimer exists in two states: a clustered state bound to PAR-3 that follows advective flow and a diffuse state that is associated with CDC-42 [54,56,57,173,183] (figure 1*b*). Both of these PAR-6/aPKC membrane states become asymmetrically localized to the anterior of the zygote during polarity establishment. The model proposed for total PAR-6/aPKC to tap into flow is dynamic switching between these two membrane states. Transient interaction between flow-sensitive PAR-3 and flow-insensitive CDC-42 during PAR-6/aPKC transfer may facilitate the asymmetric localization of all parties even though only the PAR-3-associated state can couple to flow [56] (figure 1*b*). In addition, both clustered and diffusive populations are required for correct spatio-temporal regulation of kinase activity. aPKC phosphorylates downstream targets when in complex with PAR-6 and CDC-42 [56,91,183–186]. Therefore, the ability to dynamically transfer between PAR-3 clusters, which sense flow, and the diffusive CDC-42 assembly, which permits kinase activity, produces the anterior enrichment and specific spatial activation of aPKC [56] (figure 1*a*–*c*).

The clustering ability of PAR-3 also exhibits tight spatio-temporal modulation. During polarity establishment increased cortical tension, generated by actomyosin contractility, stimulates PAR-3 oligomerization, therefore promoting PAR-3 advection to the anterior [57]. Furthermore, cluster formation is linked to the cell cycle, as active PLK-1 can phosphorylate PAR-3 at its N-terminus, inhibiting oligomerization. The periodic activity of PLK-1 throughout the cell cycle can therefore regulate membrane loading, clustering and thus advective transport of PAR-3 [55,132]. In establishment, lack of PLK-1 activity allows PAR-3 clustering and hence anterior advection, whereas in mitosis (during polarity maintenance) temporally activated PLK-1 inhibits oligomerization, preventing the disruption of PAR-3 asymmetry by later flows [55].

Posterior PAR proteins also form clusters in the zygote. PAR-2 forms an oligomeric gradient across the AP axis, with larger oligomers (up to tetramers) enriched at the posterior cortex [174]. However, tetrameric PAR-2 stoichiometry is much smaller than the stoichiometry reported for PAR-3 clusters (up to 15mers in establishment) [55]. This could explain why PAR-2 motion at the membrane does not present a directional movement that could alter its asymmetric localization. Instead, cortical PAR-2 asymmetry is mostly mediated by local exchange reactions dependent on aPKC, which promote higher dissociation from the anterior and recruitment at the posterior membrane domains [105,174].

The CDC-42 GAP, CHIN-1[52], forms clusters at the cortex during polarity maintenance phase [54] and is presumed to be restricted to the posterior by aPKC [52,54,56] (figure 1*a*,*f*). CHIN-1 clusters can be tracked on the cortex for longer periods than PAR-3 clusters (greater than 100 s), suggesting that its oligomerization results in very stable association with the membrane [54]. This agrees with the strong coupling observed for CHIN-1 clusters to the weaker anterior-directed flow that occurs in maintenance (approx. 2 µm min^{-1}) compared with establishment (approx. 7 µm min^{-1}). Clusters switch from growth to decay as they approach the anterior domain of the zygote. Here, at a threshold density of PAR-6/aPKC, they uncouple from flow and drop from the membrane [54]. More importantly, modelling supports that anterior PAR-3 and posterior CHIN-1 clusters, when coupled to flow and with a cluster growth ultrasensitive to antagonism by PAR-1 and PAR-6/aPKC, respectively, provide the anterior–posterior cross-inhibitory circuits (figure 1*a*) with bistable dynamics (two stable equilibrium states). This allows robust formation of PAR cortical asymmetries [54] (figure 1*c*,*f*, graphs).

The above are examples of mechanochemical events, where the regulation of protein clustering can determine whether a protein couples to flow. Given the existence of similar cortical flows [63,65,66] and clusters of polarity determinants [181,187–190] in other contexts, the described mechanisms here in *C. elegans* could account for an emerging patterning system, where cells can modulate their polarity programmes through the spatio-temporal regulation of dynamic clusters.

(b) Central cytoplasmic flow can contribute to the generation of PAR asymmetries

Concomitantly to the anterior-directed cortical actomyosin flow, a central cytoplasmic flow arises, both driving recirculation of particles [78,79,81] (figure 1*c*). This central cytoplasmic flow (approx. 5 µm min^{-1}) also depends on the contractility of the cortex. The shear forces generated by NMY-2 at the cortex could be transmitted towards the central cytoplasmic region owing to the hydrodynamic properties of the cytoplasm [78], which behaves as an incompressible fluid; hence, anterior-directed cortical flow in the confines of the zygote leads to a countercurrent posterior-directed central flow [78]. Cytoplasmic flow in the zygote was thought to drive the posterior localization of certain cytoplasmic components [35,36,191,192]. However, as for cortical flow, proteins in the cytoplasm will need to present certain dynamic properties that will grant them sensitivity to cytoplasmic flow (further discussed in §5).

A novel non-invasive technique has permitted the study of cytoplasmic flow alterations, giving opportunity to further explore flow properties and their effects in the zygote. Mittasch *et al*. [81] employed focused-light-induced cytoplasmic streaming (FLUCS), where an infrared laser beam induces temperature-travelling fields in the cytoplasm that can lead to flows [193]. Laser scan patterns permit the modulation of both the speed and direction of the intracellular flows [81]. Surprisingly, increasing cytoplasmic flow speed perpendicular to the posterior PAR-2 domain to twice the velocity observed in wild-type zygotes resulted in a threefold increase of PAR-2 loading at the membrane [81]. Flows could increase the volume of cytoplasm scanned by a domain with docking properties, and in this way increase loading/trapping of a highly diffusive molecule. This scenario has been proposed for the enrichment of mRNA- and RNA-binding proteins at the posterior pole of the *Drosophila* oocyte [30,194,195]. Furthermore, generating clockwise rotational cortical flow, by FLUCS, can rotate both the PAR-2 domain and the actomyosin cortex [81]. The complete reverse polarity of PAR-2 can also be generated, but only if the domain is rotated over 90° past its usual posterior alignment, highlighting the robustness of cortical polarization against abnormal rotational forces. This work has activated research in a previously underappreciated process. However, further studies will need to elucidate the degree of contribution of central cytoplasmic flow to the polarization of the wild-type zygote.

(c) PAR proteins regulate the actomyosin flow that transports them

PAR proteins have been observed to regulate the actomyosin cytoskeleton in varied cellular contexts. For example, Bazooka is required for actin cortex integrity in the *Drosophila* oocyte [196], aPKC promotes RhoA degradation in migrating cells [197] and Par3 suppresses Rac GTPase activity and controls the organization of the actin cytoskeleton to stabilize nascent tight junctions in epithelial cells [198]. In the *C. elegans* zygote, a tight mechanochemical feedback exists between PAR proteins and the actomyosin cortex [9,67,74,75].

Anterior PARs are transported by the cortical flow [36,37,51–57] yet also contribute to the flow by modulation of actomyosin [36,37,52,54,82,89–93]. Depletion of either PAR-3 or CDC-42 severely reduces flow and the clearance of the RHO-1/GEF, ECT-2, from the posterior at symmetry break [37,90]. Here, the observed effects are not due to an expansion of the posterior PAR domain, as simultaneous knockdown of PAR-2 in PAR-3-depleted embryos does not change the PAR-3 phenotype [37]. In agreement with pPARs not having an early effect on flow, zygotes depleted of PAR-2 show a normal ECT-2 clearance from the posterior pole [90].

A recent publication indicates more specifically how anterior PARs can regulate actomyosin flow [82]. FRAP (fluorescence recovery after photobleaching) and fluorescence-based image quantification revealed that the NMY-2 association rate to the cortex is similar in the anterior and posterior PAR domains (anterior $k_{on} = 0.19$ µm s^{-1}, posterior $k_{on} = 0.21$ µm s^{-1}). However, the dissociation rate in the anterior is two times slower than in the posterior (anterior $k_{diss} = 0.072\ s^{-1}$, posterior $k_{diss} = 0.14\ s^{-1}$) [82]. aPARs seem to stabilize cortical NMY-2 and mediate their effect independently of pPARs, as knockdown of *par-6* and *par-2* produces the same dissociation rate as that observed in the wild-type posterior domain.

The posterior PARs, PAR-2 and LGL-1, which show no direct role in early establishment, might prevent the recruitment and/or stabilization of NMY-2 at the posterior cortex during polarity maintenance [37,89,93]. In agreement with this, cortical NMY-2 levels are downregulated in *cdc-42* RNAi-treated zygotes, where PAR-2 becomes strongly localized over the whole cortex [90,91]. However, it is likely that CDC-42 could also be regulating NMY-2 levels/function independently of pPARs, via the kinase MRCK-1, at this later stage of zygote polarization [52,54]. Supporting this idea, loss of posterior PARs leads to ectopic posterior-directed cortical flow during the polarity maintenance phase that can be rescued by inhibiting non-muscle myosin II contractility through depletion of MRCK-1 [37,54,93].

Mechanochemical-positive feedback between PARs and actomyosin has been described in other systems and, as in the zygote, it promotes robustness of the patterning process [69–73]. The identification of the molecular mechanisms involved will greatly impact developmental research, most immediately of polarizing systems where cooperative regulations between flow and cortical polarity are emerging, such as in the *Drosophila* neuroblast [65,199,200].

5. PAR polarity leads to cytoplasmic asymmetries through phase separation and reaction–diffusion mechanisms

Concomitantly to the establishment of the zygote cortical polarization, the asymmetric localization of cytoplasmic determinants contributes to cell fate specification. As described above, the anterior-directed cortical flow is critical for the production of cortical PAR asymmetry and generates a countercurrent

posterior-directed cytoplasmic flow [78,79,81] (figure 1*c*) that was initially thought to drive the posterior localization of certain cytoplasmic components [35,36,191,192]. However, recent studies indicate that gradients of several proteins and RNA/protein assemblies are not reliant on this backflow. Instead, they depend more directly on PAR asymmetry and on intrinsic physical properties of the cytoplasmic proteins themselves, such as their diffusion coefficients or capacity to phase separate from the cytoplasm [192,201–207]. Below we will discuss these mechanisms, focusing on the segregation of germ granules and RNA/protein assemblies in the zygote.

(a) Spatial regulation of phase separation drives P granule asymmetry supporting germline specification

The zygote divides asymmetrically along the AP axis into an anterior daughter cell, which will give rise to the worm's somatic tissues, and a posterior germline blastomere [107]. This cell stems the immortal germ lineage that will generate sperm and oocytes [208]. Embryonic germ cell fate specification is supported by inheritance of germ granules, known as P granules in *C. elegans*, that contain RNA and RNA-binding proteins [209,210]. P granules are non-membrane-bound cellular compartments that share similar properties with the P bodies and stress granules of somatic cells [211]. They were among the first cytoplasmic components described to de-mix from their environment (the cytoplasm) through liquid–liquid phase separation (LLPS) [192,201]. Individual components of P granules can dynamically exchange between condensed (granule) and dilute (cytoplasm) liquid phases. Interestingly, it is through the regulation of P granule condensation/dissolution and not through advective transport by cytoplasmic flow that P granules accumulate at the posterior pole of the zygote after polarity is established [201].

Individual granule components diffuse freely and become incorporated into P granules preferentially at the posterior (figure 3*a*). The separation into the condensed granule phase by LLPS causes the concentration of each individual component to become lower in the surrounding posterior cytoplasm. P granules act as a sink, promoting the posterior-directed flux of P granule constituents from the anterior. Through this AP flux, P granule components continue to condense and become incorporated into growing granules. These larger assemblies diffuse slowly and stabilize at the posterior. This strategy could allow rapid and efficient sorting of complex mixtures in cells without requiring active transport [67,201].

As granule formation reduces the entropy state of the cytoplasm, phase separation is likely driven by energetically favoured interactions between condensate components [214]. Out of the dozens of proteins present in P granules [215], MEG-3, PGL-1, its paralogue PGL-3 and the DDX3 RNA helicase LAF-1 are considered to be the main drivers of phase separation and act as scaffolding proteins [201–203,207,216,217]. All contain RNA-binding and intrinsically disordered domains, a combination of motifs canonically implicated in phase separation of RNA/protein assemblies [214]. By replicating physiological conditions *in vitro*, PGL-3, LAF-1 and MEG-3 were observed to phase separate into droplets. RNA enhances the phase separation of these proteins, both *in vitro* and *in vivo* [202,203,217] (figure 3*a*).

Upstream polarity signalling controls the LLPS of granules by dynamically regulating accessibility of RNAs to the P granule scaffolding proteins [202,203]. The PAR-1 kinase promotes an anteriorly enriched cytoplasmic gradient of the MEX-5 RNA-binding protein that, in turn, enforces P granule asymmetry [192,201,212,218–221] (figure 3*a*,*c*). MEX-5 outcompetes PGL-3 and MEG-3 for RNA-binding *in vitro*, decreasing the ability of the P granule proteins to undergo RNA-stimulated phase separation. *In vivo* experiments and kinetic modelling support that a gradient of MEX-5-dependent RNA competition is responsible for the observed posterior segregation of P granules [202,203] (figure 3*a*,*c*).

Interestingly, despite the similar requirements and regulations for PGL-3 and MEG-3 in P granule formation, they occupy different sites in the condensates. MEG-3 can surround the granule, while the majority of PGL-3 is localized to the interior of the structure (figure 3*a* phase separation inset) [216]. This variant structural distribution of MEG-3 in the P granule reflects a recently identified role. MEG-3 can phase separate into more stable gel-like condensates, which further enhances granule stability at the posterior [207]. The ability of condensates to present subdomains with different properties (liquid phase–dynamic growth versus gel phase–stabilization) that can be subjected to independent regulation highlights further fine-tuning mechanisms that cells can utilize in the spatio-temporal partitioning of proteins.

(b) Spatial regulation of diffusion-state switching produces the gradient of the cell fate determinant MEX-5

P granule asymmetry is reliant upon the inverse gradient of MEX-5 in the *C. elegans* zygote. A recent study on MEX-5 mobility has revealed a physical mechanism that can generate the MEX-5 gradient. Diffusion-state switching can produce intracellular gradients of highly mobile proteins [205], which do not respond to cytoplasmic flow and would typically dissipate any source of asymmetry by rapid diffusion [222]. Tracking of single MEX-5 particles in the cytoplasm identified that the protein exists in two different diffusive states, fast (FD, D_c approx. 5 $\mu m^2 s^{-1}$) and slow (SD, $D_c = 0.1\ \mu m^2 s^{-1}$) [205] (figure 3*b*). These particles show isotropic displacement with no bias towards anterior-directed movement. However, MEX-5 dynamically switches between fast and slow states, with the rate of this switching varying along the AP axis (figure 3*b*). MEX-5 switches more frequently from FD to SD in the anterior (approx. 3.1-fold higher), where it persists in the SD state longer than at the posterior (SD to FD in the zygote posterior is approx. 1.8-fold higher). In addition, mathematical modelling demonstrates that the spatially regulated kinetics of the MEX-5 state switch are optimal for rapid gradient formation and enrichment in the zygote anterior [205].

The origin of the hierarchical cytoplasmic gradients in the *C. elegans* zygote is the effect of the posterior PAR-1 kinase on MEX-5 mobility (figure 3*c*). It has been proposed that PAR-1 phosphorylation promotes MEX-5 release from a slow-diffusing substrate, increasing its mobility in the posterior cytoplasm. Fast-diffusing MEX-5 could then rapidly access the anterior domain, where the action of the PP2A phosphatase would lead to MEX-5 incorporation into a slow diffusion substrate and the stabilization of MEX-5 at the anterior [212,220]. By being able to track individual molecules, it has become

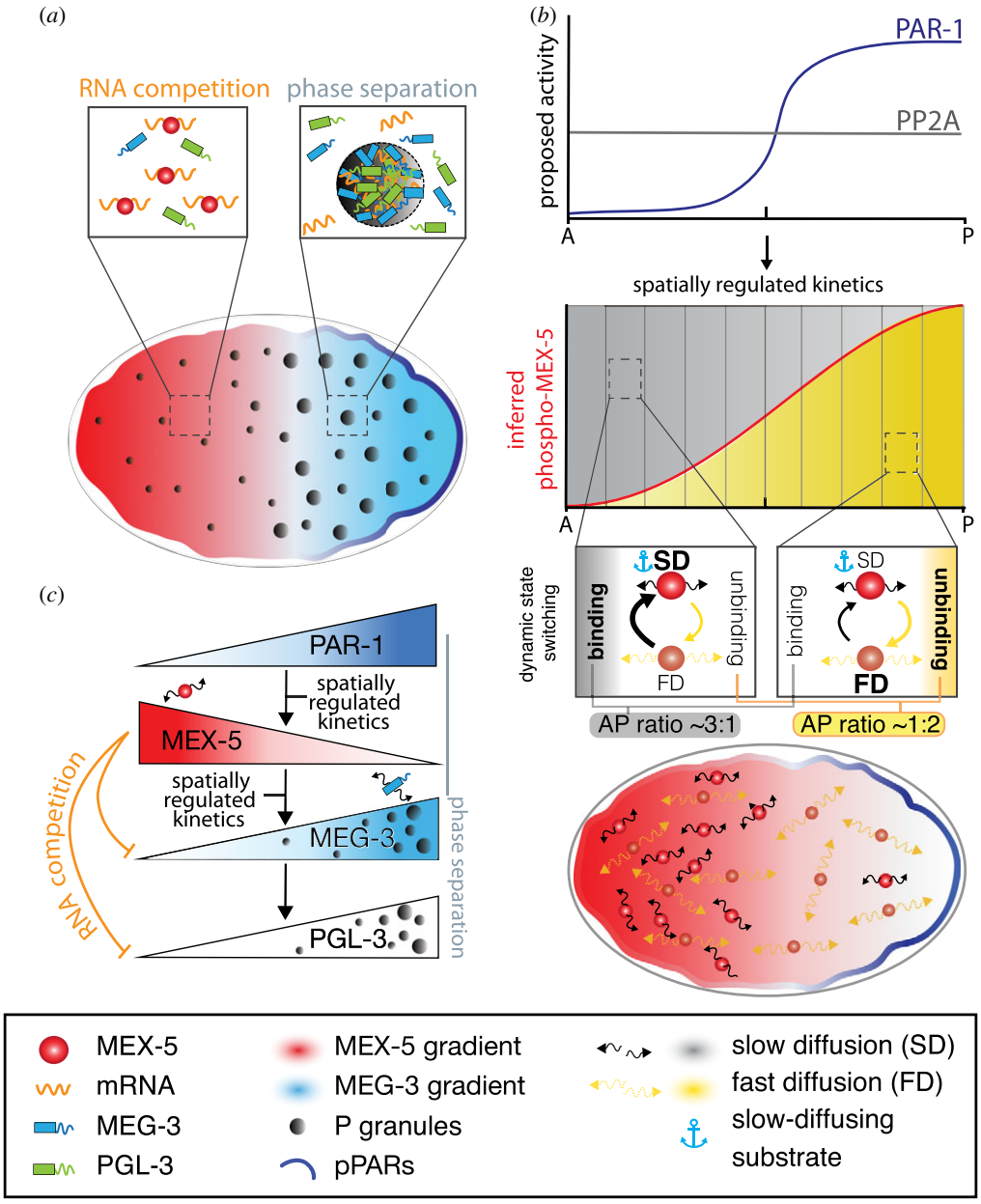

Figure 3. Generation of cytoplasmic cell fate determinant asymmetries. (*a*) In the anterior domain, MEX-5 outcompetes MEG-3 and PGL-3 for RNA-binding, whereas in the posterior, MEG-3 and PGL-3 can bind RNA and undergo phase separation, leading to P granule formation. MEG-3 phase separates into more stable gel-like condensates at the surface of P granules (see phase separation inset); hence, MEG-3 gradient can lead to granule stability at the posterior. (*b*) An inferred posterior-enriched activity gradient of the kinase PAR-1 [212,213] in combination with the opposing PP2A phosphatase (homogeneously distributed) is proposed to generate a phosphorylated MEX-5 gradient that controls MEX-5 kinetics along the AP axis. The protein MEX-5 locally switches between a fast and slow diffusive state (FD D_c approx. 5 $\mu m^2\ s^{-1}$ and SD D_c approx. 0.1 $\mu m^2\ s^{-1}$) through its binding to/dissociation from a slow diffusive substrate (cytoplasmic RNAs). FD to SD is enhanced at the anterior, whereas the opposite switch is promoted at the posterior, leading to the accumulation of SD MEX-5 state at the anterior and hence the formation of the stable protein gradient of MEX-5 in the zygote. (*c*) Hierarchical interactions between PAR-1, MEX-5 and the P granule scaffolding proteins MEG-3, PGL-3. A gradient of PAR-1 activity controls the dynamic switch of MEX-5 between FD and SD states along the AP axis, favouring the accumulation of slow-diffusing MEX-5 state towards the anterior. This MEX-5 protein gradient in turn leads to the formation of an opposite gradient of slow-diffusing MEG-3 by regulating MEG-3's spatial kinetics. Furthermore, MEX-5 outcompetes MEG-3 and PGL-3 for RNA-binding in the anterior, promoting P granule formation at the posterior.

more apparent that the action of posterior-enriched PAR-1 and uniformly distributed PP2A could lead to a gradient of MEX-5 phosphorylation along the AP axis that translates into local differences in the kinetics of binding/dissociation of MEX-5 to/from its slow-diffusing substrate [205] (figure 3*b*). As mentioned above, the frequency at which FD MEX-5 transitions to the SD state is approximately three times higher in the anterior than in the posterior of wild-type embryos. Upon PAR-1 depletion, the rate of fast to slow switching becomes uniform along the AP axis. PAR-1 is therefore postulated to create the MEX-5 gradient by inhibiting the transition from FD to SD [205]. The physical mechanism and nature of the slow-diffusing substrate that leads to the MEX-5 SD state is not clear; however, SD MEX-5 depends on RNA-binding. Therefore, the simplest model is that MEX-5 binding to RNA can slow MEX-5 down [205,212].

Similar studies have characterized the dynamics of fellow RNA-binding proteins, such as POS-1, PIE-1 and MEG-3, which become segregated to the posterior in response to the MEX-5 gradient [203,218,223–225]. MEX-5 gradient locally controls the dynamic switch between fast- and slow-diffusing particles such that the SD state accumulates at the posterior

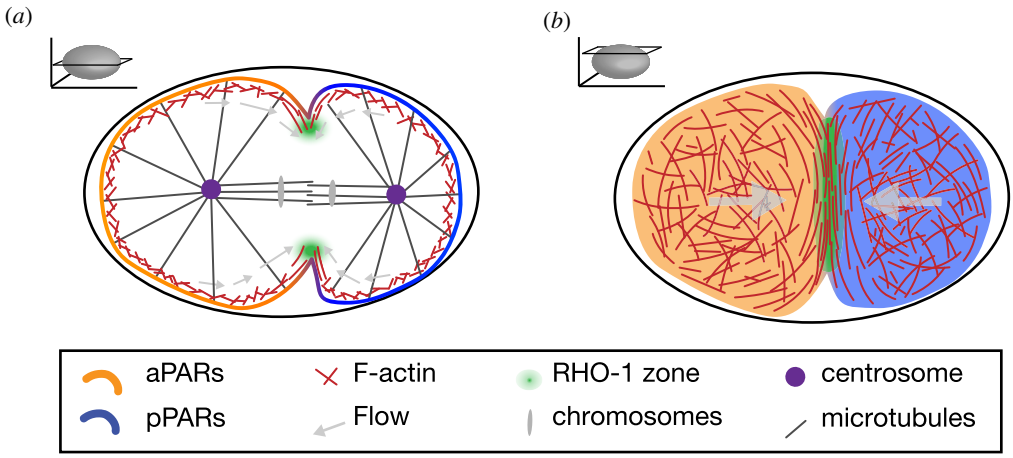

Figure 4. Actomyosin-dependent flows and PAR domains in cytokinesis. (*a*) Midplane view of zygote prior to cytokinesis. Astral microtubules cause a relaxation of polar cortical tension, while equatorial active RHO-1 (*C. elegans* RhoA homologue) increases myosin II activity. Anisotropy in cortical tension produces cortical flows directed towards the equatorial region of the dividing cell. These flows may transport PARs, making the PAR domain boundary match with the position of the cleavage furrow. (*b*) Cortical view of the zygote prior to cytokinesis. The flows initiated have been predicted to aid the equatorial alignment of actin filaments in the RHO-1 zone. However, recent work indicates that actin filament turnover is too fast to support alignment by compressing flows.

[204–206] (figure 3*c*). It is not yet clear how MEX-5 controls these kinetics. MEX-5 can recruit PLK-1, which in turn phosphorylates POS-1, inhibiting its retention in slow-diffusing particles [204]. Also, the POS-1 and PIE-1 switch to the SD state seems to depend on their ability to bind RNA [204]; hence, a MEX-5 RNA competition could be a possible additional mechanism. Whether analogous processes regulate MEG-3 kinetics is not known; however, genetic data support a role for PLK-1 in MEG-3 segregation [206]. In the future, it will be key to determine and characterize the slow-diffusing substrate of these different RNA-binding proteins as similar mechanisms might underlie the asymmetries of RNA and RNA-binding proteins in other cell types.

Overall, the molecular mechanisms responsible for the cytoplasmic asymmetries described here nicely exemplify how modulation in space of association to/dissociation from slow-diffusing structures, either P granules or unknown substrates, can generate patterns of asymmetry. These mechanisms could help overcome the stirring effect that a cytoplasmic 'whirlpool' type of flow might have and ensure stable cytoplasmic gradients within the spatio-temporal scales required (AP axis approx. 45 µm; polarization time approx. 10 min) [205]. In this regard, it would be interesting to determine how robust these patterning mechanisms are to different types of flows (i.e. creating artificial flows by FLUCS [81]).

6. Cortical flow powers other key aspects of the zygote asymmetric division

(a) Forces generated by the anterior-directed actomyosin flow can be used to separate centrosomes

Forces generated between the cortex and astral MTs have been extensively studied during mitotic spindle positioning. Initial work in the *C. elegans* zygote revealed that pulling forces exerted at the cortex on astral MTs are primarily generated by an evolutionarily conserved ternary complex: Gα/GPR/LIN-5 (Gα/LGN/NuMA in mammals) (recently reviewed in Kotak [106]). This complex anchors the dynein motor to the membrane, where it can capture and pull on astral MTs by virtue of its minus-end-directed motility [226–228]. PAR proteins drive the posterior displacement of the mitotic spindle by regulating the activity and localization of this ternary complex, leading to stronger MT pulling forces at the posterior [229–235]. Recently, it has also been proposed that, during polarity establishment, this molecular machinery can transmit the forces generated by the anterior-directed actomyosin flow to the MT asters at the sperm centrosomes [236,237]. The spatial configuration of the duplicated centrosomes positioned between the male PN and the posterior cortex (figure 1*d*(ii)) allows these forces to separate the centrosomes, a pre-requisite to bipolar spindle assembly [237] (figures 1*d*(iii) and 4*a*).

During polarity establishment, cortical depletion of dynein or reduction of actomyosin contractility severely reduces centrosome separation [236]. Given the high degree of movement correlation between flow versus cortical MT anchors (GPR-1/2) and local cortical flow versus the closest centrosome to the flow, the proposed model is that MTs emanating from each of the sperm centrosomes are anchored by dynein, via the Gα/GPR/LIN-5 complex, to the cortical region closest to their position (figure 1*d*(ii,iii),*e*). Given that the anterior-directed flow is induced at either side of the male PN, opposing forces ensure correct centrosome separation. As the actomyosin network retracts, each centrosome is pulled towards the anterior around the male PN, which is simultaneously pushed towards the posterior of the zygote by the concomitant cytoplasmic backflow [236,237] (figure 1*d*(ii,iii)). The interplay of all these forces ensures correct centrosome separation and bipolar spindle assembly prior to the zygote's asymmetric cell division.

The question remains of how the membrane-bound Gα/GPR/LIN-5 complex senses the actomyosin flow. Computational modelling indicates that the motor activity of dynein is not required for the transmission of actomyosin-derived forces, it may simply act as a linker together with the Gα/GPR/LIN-5 complex [236]. GPR-1 particles seem to form small aggregates that persist over time, similar to aPAR clusters, which could be captured by cortical flow [236]. Another

possibility is that complex members could interact with or be regulated by ABPs. For example, in HeLa cells, MISP regulates the cortical distribution of the LIN-5 homologue (NuMA) and the dynein–dynactin complex [238,239], while the membrane–actin linkers ezrin/radixin/moesins can promote the cortical recruitment of GPR/LIN-5 homologues (LGN/NuMA) during metaphase [239,240].

Alternatively, actomyosin has been described to regulate MT dynamics [241], and loss of actomyosin contractility can affect MT pulling forces owing to a softened cortex [242]. Moreover, anisotropic actomyosin contractility, leading to flow, could also support centrosome orientation and spindle positioning independently of the Gα/LGN/NuMA complex, as recently described in *C. elegans*, *Drosophila* and mouse embryos [243,244]. This variant mechanism is dependent upon cell–cell contacts that reduce actomyosin contractility at the contact area. Cell divisions are subsequently oriented relative to cell contacts in the developing embryo [244]. Given that actomyosin contractility/flow affects centrosome separation/orientation in a wide range of biological contexts [108,243–248], it is key to understand how these seemingly divergent processes are coupled.

(b) Crosstalk between cortical flows and PAR proteins during cytokinesis

Once organized and properly positioned, the mitotic spindle separates the duplicated chromosomes, which are then partitioned into each of the daughter cells during cytokinesis. Cell viability depends on the correct position of the cleavage furrow in between the segregating chromosomes. Animal cells have resorted to using the mitotic spindle as a primary source of cleavage positional information. Briefly, a combination of positive and negative regulatory signals from the central spindle and astral MTs promotes the activation of RhoA signalling at the cell equator [249] (figure 4*a*). This leads to the subsequent assembly of an actomyosin-based contractile ring that constricts to divide the cell. In addition, the assembly of the contractile ring can be aided by cortical flows [250,251]. Suppression of cortical contractility at the poles (polar relaxation) by astral MTs and/or equatorial contractility activation has been proposed to lead to cortical flows that move towards the furrow [252–262] (figure 4*a*). The molecular mechanism leading to polar relaxation is still unclear. However, recent work in the *C. elegans* zygote proposes that cortical non-muscle myosin II is removed by dynein-mediated transport on astral MTs [263]. Interestingly, coordination of polar myosin II clearance with the cell cycle could be mediated by AIR-1 signalling. AIR-1 activation and localization to astral MTs via TPXL-1 promotes the removal of contractile ring components at the poles, leading to cortical relaxation [135].

White & Borisy [62] proposed in the early 80s that cortical flows could aid the assembly of the contractile ring, owing to compression of the actomyosin network and alignment of actin filaments at the cell equator (figure 4*b*). Spatio-temporal quantification of compression and filament orientation in the *C. elegans* zygote in combination with theory prediction support that compression by flow can drive ring formation during cytokinesis [264]. Interestingly, it was proposed that this mechanism can lead to actin alignment with minimal contribution from equatorial RHO-1 activity and the corresponding local increase in non-muscle myosin II [264]. This phenomenon is particularly apparent in pseudocleavage formation, which occurs during polarity establishment as a result of anisotropies in cortical tension, in the absence of an active RHO-1 band [37,76,264]. However, an interplay between active ring myosin II and flows has been observed during ring constriction. In the proposed model, ring myosin-mediated compression of the cortical surface at the equator coupled with cortical pole relaxation drives cortical flows. Myosin-driven compression pulls the adjacent cortex into the equatorial RHO-1 active zone, leading to more myosin II recruitment and hence more pull. The model predicts that this positive feedback loop can maintain a high constriction rate during ring closure [262,265]. Contrary to the above-described work, a very recent publication indicates that flows cannot mediate actin filament alignment, owing to the rapid turnover of these filaments. Alternatively, the mechanism proposed is that equatorially aligned filaments serve as templates to guide the growth of new ones [266]. The prevalence of equatorial alignment might be supported by other mechanisms. For example, myosin minfilaments turn over more slowly than single actin filaments [267] and hence may be aligned by flow [148]. Local membrane curvature induced by ring constriction can also promote local filament alignment [268].

In asymmetrically dividing cells, crosstalk between PAR proteins and the division machinery ensures correct segregation of polarity effectors and cell fate determinants into daughter cells. Many studies have focused on the alignment of the mitotic spindle relative to the existing PAR polarity [269,270]. However, spindle-independent mechanisms can also ensure correct positioning of the division plane relative to a polarity axis. In the *C. elegans* zygote, cortical PAR asymmetry promotes cytokinesis by restricting anillin and septin to the anterior cortex. This facilitates F-actin accumulation and ring constriction at the furrow site, in a manner that appears independent of PARs' role in the organization of the mitotic spindle [146]. Instead, PARs, by specifying the localization of these actin cross-linkers, may control ring formation and/or global properties of the cortex that could alter the described cortical flows [262,264]. The non-asymmetrically localized PAR-4 and PAR-5 [271,272] also regulate cytokinetic furrow position by modulating cortical dynamics. The kinase PAR-4 (LKB1 homologue) restricts cortical levels of non-muscle myosin II, inhibiting the formation of an anterior myosin cap that can lead to the anterior displacement of the furrow. PAR-4 and its potential target PIG-1/MELK may synergize with anillin to control furrow position [117,119]. PAR-5 limits RhoA activation by inhibiting cortical localization of centralspindlin complex [273]. Moreover, cortical localization of centralspindlin at the equatorial region is mediated through the local inhibition of PAR-5 by AIR-2/Aurora B [273]. Further demonstration that a polarized actomyosin cortex can drive furrow positioning independently of the spindle occurs in the Q neuroblast lineage of *C. elegans*, where the anterior enrichment of myosin II leads to an asymmetric division even when the cell presents a centred spindle [274]. Surprisingly, this asymmetric enrichment of myosin II is promoted rather than inhibited by the PAR-4 pathway described above [119,274,275]. Spindle-independent furrow positioning cues have also been reported in other cell types [276,277]. In *Drosophila* neuroblasts, a basally polarized cap of myosin II downstream of the LGN/Dlg polarity pathway controls furrow formation [199,276], and in human cell

cultures, perturbation of the cortex at the poles of dividing cells leads to furrow displacement [278].

Processes leading to cell division can also reposition the PAR domain boundary to ensure correct segregation and inheritance of these patterning proteins. In the *C. elegans* zygote, errors in the relative sizes of aPAR and pPAR cortical domains and thus the position of the boundary between them can be corrected during anaphase to match the cleavage furrow [96,279,280]. This polarity domain correction is regulated by Gα, which facilitates cortical flows via astral MT–cortex interactions [255,280–282]. These flows are proposed to transport PARs towards the cleavage furrow [280]. In this context, PARs could be advected by flows, as observed during polarity establishment [36,37,51–57]. In the *Drosophila* neuroblast, a polarity domain correction mechanism, known as telophase rescue, repositions the cortical Gα, LGN, Dlg domain with respect to the spindle orientation. This correction is mediated by the binding of kinesin Khc-73 to the adaptor protein Dlg [283,284]. In agreement with MTs influencing cortical domains in neuroblasts, during interphase, MT–cortex signalling acts as a source of polarity memory, maintaining the constant orientation of cortical polarity and subsequent asymmetric division over successive divisions [285]. In the neuroblast, it is likely that actomyosin-dependent flows influence polarity domain formation [65,200] and correction; however, these flows may not originate from MT–cortex interaction, as in the *C. elegans* zygote, but from the site of contact with its own daughter cell [286].

Studies in the *C. elegans* zygote have greatly advanced our understanding of the signalling pathways that specify the site of cleavage in asymmetrically dividing cells [249]. As summarized here, the process is tightly regulated by crosstalk between cell polarity, spindle positioning and cytokinesis furrow. Moreover, recent research suggests the existence of mechanochemical feedback between cortical polarity and actomyosin flows, similar to that observed in the zygote during polarity establishment [146,280,37,53]. In cytokinesis, PARs can regulate actomyosin cortical dynamics (directly or via the mitotic spindle), possibly influencing the flows that transport them and ensure their correct segregation. In this way, coordination between these processes might lend robustness to patterning of asymmetric divisions [270].

7. Concluding remarks

Actomyosin-dependent cytoplasmic flow has emerged as a mechanism to drive cell patterning in a wide range of organisms, from plants to mammals [21]. Different actomyosin organization/dynamics can transmit forces to the cytoplasm by a variety of mechanisms. These include the treadmilling effect of actin filaments [44,45,47,50], the transport of cargoes along actin bundles [20] and bulk cortical movements or reorganizations, such as those described for the *C. elegans* zygote [37,76]. Polarity effectors can acquire their asymmetric localization through direct contact with cortical constituents such as the actin cytoskeleton, motor proteins or ABPs, or by physical entanglement with the network itself [2,10]. An indirect transport of membrane proteins, through advection, is also observed as a mechanism by which polarity effectors can tap into long-range cytoplasmic flow generated by actomyosin dynamics [20,21].

Patterning by advection relies on the transfer of movement between the actomyosin cortex, permeating cytoplasm and embedded patterning proteins. To operate during restricted time frames and to capture specific proteins, physical and molecular mechanisms regulate the dynamic behaviour of each of the above patterning elements and coordinate their functional coupling. The biophysical basis underlying these processes is an area of active research, where both physical studies and mathematical modelling are greatly aiding our understanding of how cytoskeleton dynamics and cytoplasmic movements are impacting patterning systems [22]. Evolving technologies are supporting investigation of these spatio-temporally-dependent processes *in vivo*, such as in studies examining cortical dynamics upon laser ablation [76], the creation of artificial flows by FLUCS [81], live super-resolution imaging in combination with methods that manipulate protein function and localization [54–57,173,205,266] and synthetic biology approaches, studying minimal systems [75,149,150].

Concerning the molecular mechanisms involved in flow-dependent patterning, a great challenge is to understand how the molecular players contribute to cellular-scale events [143]. For example, how do actomyosin regulators (GTPases, motors, ABP and kinases/phosphatases) influence the dynamic behaviours of the cortex that generate flow? Recent efforts have identified actomyosin regulators involved in the patterning flow of the *C. elegans* zygote. Through high-throughput phenotypic profiling, this work has identified the contribution of regulators to different large-scale biophysical properties of actomyosin flow, indicating that molecular degeneracy (multiple molecular activities that regulate one biophysical property) underlies the actomyosin dynamic behaviours that polarize the zygote [120,122]. While conferring robustness to this patterning system, as loss of a single effector is likely to alter the dynamic behaviour but not to abolish it, this research also leaves open the question of how different molecular functions that influence a large-scale behaviour are spatially and temporally coordinated.

Spatio-temporal coordination of molecular activities could be driven either by a master regulator or through self-organization. We have discussed examples for both scenarios, suggesting that, in principle, a combination of master regulators and self-organizing systems could operate in cells to direct flow-dependent patterning. In the *C. elegans* zygote, Aurora A fulfils the role of a key polarity regulator as it restricts actomyosin contractility, flow and the activation of the patterning PAR network [83,84,88,132]. Whether Aurora A is a master regulator in this regard across polarizing systems remains to be seen. The presence of self-organizing systems, on the other hand, is being increasingly discussed across developmental contexts [287]. Here, we have described self-organizing systems that rely on biochemical networks and mechanochemical feedback loops. These drive pulsatility of the actomyosin cortex, key to the patterning of the *C. elegans* zygote as well as to morphogenetic processes such as those involved in the *Drosophila* embryo and in mammalian blastocyst compaction [70,94,95,154,155,159,165–167,169]. Similar mechanochemical feedbacks may also operate between actomyosin flows and patterning domains in asymmetrically dividing cells to ensure correct segregation and inheritance of polarity effectors and cell fate determinants [65,82,96,117,119,146,199,200, 263,264,273,276,279,280].

Spatio-temporal regulation of protein clustering at the membrane is an emerging mechanism that can regulate the sensitivity of proteins to patterning flows. Clustering of PAR proteins may reduce their diffusion in the plane of the

membrane and their dissociation rates from the membrane, granting PARs the ability to tap into cortical flows [54–57]. In addition, PAR clustering and advection by flow may provide cross-inhibitory PAR networks with bistable dynamics [54]. Clustering is also exploited in a mechanical positive feedback, whereby cortical flows that advect anterior PARs also promote their clustering, further ensuring PAR asymmetric localization in the zygote [57]. Furthermore, Polo-like kinase inhibits PAR clustering, providing a biochemical link between the cell cycle and PAR advection by flow [55,132]. If phase separation is involved in PAR clustering, as suggested by a recent report [288], this could provide another means to regulate PAR advection. Clustering is also observed for other polarity determinants and cytoskeleton regulators [181,187–190], indicating that they might be able to sense flow. We have discussed this possibility in relation to flow-dependent mitotic spindle organization and position [235,237], which is emerging as a means to generate the diversity of division plane orientations needed during embryonic development [243,244].

Cytoplasmic flow also influences the transport of cytoplasmic proteins, allowing rapid polarization of large cells. Flows can increase the exposure of a cytoplasmic factor to a polarized docking site [30] or speed the generation of a stable protein gradient in the cytoplasm [195]. However, this stirring effect of cytoplasmic flow can also be detrimental to patterning maintenance. Here, we have reviewed how phase separation and diffusion-state switching may provide mechanisms by which proteins can become insensitive to flow. P granule posterior localization thus relies upon the spatial control of phase transition to overcome advection by flow. Nevertheless, cytoplasmic streaming might aid this process by ensuring the homogeneous distribution of P granule components [201]. Similarly, patterning of cytoplasmic proteins that diffuse too fast to be advected by flow relies on spatial regulation of their association/dissociation from slow-diffusing structures/anchors [204–207]. The anchoring mechanism is still under study, yet the biophysical implications will no doubt extend to other polarized contexts with observed cytoplasmic asymmetries.

In conclusion, we are experiencing an exponential discovery phase, where the *C. elegans* zygote is helping bridge theory and live observations, yielding insights into the molecular- to cellular-scale processes that create polarity through flow.

Data accessibility. This article has no additional data.

Authors' contribution. A.G.G., J.R.P., I.S., J.M. and J.R. contributed to initial drafts of the text. A.G.G. designed most of the figures. J.R.P. and J.R. delivered the final manuscript.

Competing interests. We declare we have no competing interests.

Funding. This work was supported by BBSRC (grant no. BB/R019436/1, J.R. and J.R.P.), a Newcastle University Faculty Fellowship (J.R.), BBSRC PhD Fellowships (J.M. and I.S.) and a Newcastle University PhD Fellowship (A.G.G.).

Acknowledgements. The authors wish to thank Nate Goehring, Erik Griffin, Tim Davies, Sundar Naganathan and Adam Wollman for helpful comments.

References

1. McCaffrey LM, Macara IG. 2012 Signaling pathways in cell polarity. *Cold Spring Harb. Perspect. Biol.* **4**, a009654. (doi:10.1101/cshperspect.a009654)
2. Campanale JP, Sun TY, Montell DJ. 2017 Development and dynamics of cell polarity at a glance. *J. Cell Sci.* **130**, 1201–1207. (doi:10.1242/jcs.188599)
3. Kemphues KJ, Priess JR, Morton DG, Cheng NS. 1988 Identification of genes required for cytoplasmic localization in early *C. elegans* embryos. *Cell* **52**, 311–320. (doi:10.1016/S0092-8674(88)80024-2)
4. Watts JL, Etemad-Moghadam B, Guo S, Boyd L, Draper BW, Mello CC, Priess JR, Kemphues KJ. 1996 *par-6*, a gene involved in the establishment of asymmetry in early *C. elegans* embryos, mediates the asymmetric localization of PAR-3. *Development* **122**, 3133–3140.
5. Tabuse Y, Izumi Y, Piano F, Kemphues KJ, Miwa J, Ohno S. 1998 Atypical protein kinase C cooperates with PAR-3 to establish embryonic polarity in *Caenorhabditis elegans*. *Development* **125**, 3607–3614.
6. Goldstein B, Macara IG. 2007 The PAR proteins: fundamental players in animal cell polarization. *Dev. Cell* **13**, 609–622. (doi:10.1016/j.devcel.2007.10.007)
7. St Johnston D, Ahringer J. 2010 Cell polarity in eggs and epithelia: parallels and diversity. *Cell* **141**, 757–774. (doi:10.1016/j.cell.2010.05.011)
8. Zhu M, Zernicka-Goetz M. 2020 Building an apical domain in the early mouse embryo: lessons, challenges and perspectives. *Curr. Opin. Cell Biol.* **62**, 144–149. (doi:10.1016/j.ceb.2019.11.005)
9. Lang CF, Munro E. 2017 The PAR proteins: from molecular circuits to dynamic self-stabilizing cell polarity. *Development* **144**, 3405–3416. (doi:10.1242/dev.139063)
10. Peglion F, Goehring NW. 2019 Switching states: dynamic remodelling of polarity complexes as a toolkit for cell polarization. *Curr. Opin. Cell Biol.* **60**, 121–130. (doi:10.1016/j.ceb.2019.05.002)
11. Chiou J, Balasubramanian MK, Lew DJ. 2017 Cell polarity in yeast. *Annu. Rev. Cell Dev. Biol.* **33**, 77–101. (doi:10.1016/0168-9525(94)90036-1)
12. Mayor R, Etienne-Manneville S. 2016 The front and rear of collective cell migration. *Nat. Rev. Mol. Cell Biol.* **17**, 97–109. (doi:10.1038/nrm.2015.14)
13. Martin-Belmonte F, Gassama A, Datta A, Yu W, Rescher U, Gerke V, Mostov K. 2007 PTEN-mediated apical segregation of phosphoinositides controls epithelial morphogenesis through Cdc42. *Cell* **128**, 383–397. (doi:10.1016/j.cell.2006.11.051)
14. Doerflinger H, Benton R, Torres IL, Zwart MF, St Johnston D. 2006 *Drosophila* anterior-posterior polarity requires actin-dependent PAR-1 recruitment to the oocyte posterior. *Curr. Biol.* **16**, 1090–1095. (doi:10.1016/j.cub.2006.04.001)
15. Zhu M, Leung CY, Shahbazi MN, Zernicka-Goetz M. 2017 Actomyosin polarisation through PLC-PKC triggers symmetry breaking of the mouse embryo. *Nat. Commun.* **8**, 921. (doi:10.1038/s41467-017-00977-8)
16. Harris TJC, Peifer M. 2005 The positioning and segregation of apical cues during epithelial polarity establishment in *Drosophila*. *J. Cell Biol.* **170**, 813–823. (doi:10.1083/jcb.200505127)
17. Kim DJ, Martinez-Lemus L, Davis GE. 2013 EB1, p150Glued, and Clasp1 control endothelial tubulogenesis through microtubule assembly, acetylation, and apical polarization. *Blood* **121**, 3521–3530. (doi:10.1054/ijoa.2001.0838)
18. Kamei M, Saunders WB, Bayless KJ, Dye L, Davis GE, Weinstein BM. 2006 Endothelial tubes assemble from intracellular vacuoles *in vivo*. *Nature* **442**, 453–456. (doi:10.1038/nature04923)
19. Bray D, White JG. 1988 Cortical flow in animal cells. *Science* **239**, 883–888. (doi:10.1126/science.3277283)
20. Goldstein RE, van de Meent JW. 2015 A physical perspective on cytoplasmic streaming. *Interface Focus* **5**, 20150030. (doi:10.1098/rsfs.2015.0030)
21. Illukkumbura R, Bland T, Goehring NW. 2019 Patterning and polarization of cells by intracellular flows. *Curr. Opin. Cell Biol.* **62**, 123–134. (doi:10.1016/j.ceb.2019.10.005)
22. Mogilner A, Manhart A. 2018 Intracellular fluid mechanics: coupling cytoplasmic flow with active

cytoskeletal gel. *Annu. Rev. Fluid Mech.* **50**, 347–370. (doi:10.1146/annurev-fluid-010816-060238)

23. Corti B. 1774 *Osservazioni microscopiche sulla tremella e sulla circolazione del fluido in una pianta acquajuola*. Lucca: Giuseppe Rocchi. [In Italian.]
24. Allen NS, Allen RD. 1978 Cytoplasmic streaming in plants. *Annu. Rev. Biophys.* **7**, 497–526. (doi:10.1016/j.ceb.2003.11.009)
25. Yi K, Rubinstein B, Li R. 2013 Symmetry breaking and polarity establishment during mouse oocyte maturation. *Phil. Trans. R. Soc. B* **368**, 20130002. (doi:10.1098/rstb.2013.0002)
26. Quinlan ME. 2016 Cytoplasmic streaming in the *Drosophila* oocyte. *Annu. Rev. Cell Dev. Biol.* **32**, 173–195. (doi:10.1146/annurev-cellbio-111315-125416)
27. Pickard WF. 2003 The role of cytoplasmic streaming in symplastic transport. *Plant Cell Environ.* **26**, 1–15. (doi:10.1046/j.1365-3040.2003.00845.x)
28. Brendza RP, Serbus LR, Duffy JB, Saxton WM. 2000 A function for kinesin I in the posterior transport of *oskar* mRNA and Staufen protein. *Science* **289**, 2120–2122. (doi:10.1126/science.289.5487.2120)
29. Zimyanin VL, Belaya K, Pecreaux J, Gilchrist MJ, Clark A, Davis I, St Johnston D. 2008 In vivo imaging of *oskar* mRNA transport reveals the mechanism of posterior localization. *Cell* **134**, 843–853. (doi:10.1016/j.cell.2008.06.053)
30. Lu W, Lakonishok M, Serpinskaya AS, Kirchenbüechler D, Ling SC, Gelfand VI. 2018 Ooplasmic flow cooperates with transport and anchorage in *Drosophila* oocyte posterior determination. *J. Cell Biol.* **217**, 3497–3511. (doi:10.1083/jcb.201709174)
31. Monteith CE, Brunner ME, Djagaeva I, Bielecki AM, Deutsch JM, Saxton WM. 2016 A mechanism for cytoplasmic streaming: kinesin-driven alignment of microtubules and fast fluid flows. *Biophys. J.* **110**, 2053–2065. (doi:10.1016/j.bpj.2016.03.036)
32. Yang H, McNally K, McNally FJ. 2003 MEI-1/katanin is required for translocation of the meiosis I spindle to the oocyte cortex in *C. elegans*. *Dev. Biol.* **260**, 245–259. (doi:10.1016/S0012-1606(03)00216-1)
33. McNally KL, Martin JL, Ellefson M, McNally FJ. 2010 Kinesin-dependent transport results in polarized migration of the nucleus in oocytes and inward movement of yolk granules in meiotic embryos. *Dev. Biol.* **339**, 126–140. (doi:10.1016/j.ydbio.2009.12.021)
34. Kimura K *et al*. 2017 Endoplasmic-reticulum-mediated microtubule alignment governs cytoplasmic streaming. *Nat. Cell Biol.* **19**, 399–406. (doi:10.1038/ncb3490)
35. Hird SN, White JG. 1993 Cortical and cytoplasmic flow polarity in early embryonic cells of *Caenorhabditis elegans*. *J. Cell Biol.* **121**, 1343–1355. (doi:10.1083/jcb.121.6.1343)
36. Cheeks R, Canman J, Gabriel W, Meyer N, Strome S, Goldstein B. 2004 *C. elegans* PAR proteins function by mobilizing and stabilizing asymmetrically localized protein complexes. *Curr. Biol.* **14**, 851–862. (doi:10.1016/j.cub.2004.05.022)
37. Munro E, Nance J, Priess JR. 2004 Cortical flows powered by asymmetrical contraction transport PAR proteins to establish and maintain anterior-posterior polarity in the early *C. elegans* embryo. *Dev. Cell* **12**, 705–711. (doi:10.1016/j.devcel.2004.08.001)
38. Kimura K, Kimura A. 2020 Cytoplasmic streaming drifts the polarity cue and enables posteriorization of the *Caenorhabditis elegans* zygote at the side opposite of sperm entry. *Mol. Biol. Cell* **31**, 1765–1773. (doi:10.1091/mbc.e20-01-0058)
39. Svitkina TM, Verkhovsky AB, McQuade KM, Borisy GG. 1997 Analysis of the actin–myosin II system in fish epidermal keratocytes: mechanism of cell body translocation. *J. Cell Biol.* **139**, 397–415. (doi:10.1083/jcb.139.2.397)
40. Recho P, Putelat T, Truskinovsky L. 2013 Contraction-driven cell motility. *Phys. Rev. Lett.* **111**, 2–6. (doi:10.1103/PhysRevLett.111.108102)
41. Ruprecht V *et al*. 2015 Cortical contractility triggers a stochastic switch to fast amoeboid cell motility. *Cell* **160**, 673–685. (doi:10.1016/j.cell.2015.01.008)
42. Barnhart E, Lee KC, Allen GM, Theriot JA, Mogilner A. 2015 Balance between cell-substrate adhesion and myosin contraction determines the frequency of motility initiation in fish keratocytes. *Proc. Natl. Acad. Sci. USA* **112**, 5045–5050. (doi:10.1073/pnas.1417257112)
43. Liu YJ, Le Berre M, Lautenschlaeger F, Maiuri P, Callan-Jones A, Heuzé M, Takaki T, Voituriez R, Piel M. 2015 Confinement and low adhesion induce fast amoeboid migration of slow mesenchymal cells. *Cell* **160**, 659–672. (doi:10.1016/j.cell.2015.01.007)
44. Maiuri P *et al*. 2015 Actin flows mediate a universal coupling between cell speed and cell persistence. *Cell* **161**, 374–386. (doi:10.1016/j.cell.2015.01.056)
45. Lavi I, Piel M, Lennon-Duménil AM, Voituriez R, Gov NS. 2016 Deterministic patterns in cell motility. *Nat. Phys.* **12**, 1146–1152. (doi:10.1038/nphys3836)
46. Cowan CR, Cowan AA. 2004 Centrosomes direct cell polarity independently of microtubule assembly in *C. elegans* embryos. *Nature* **431**, 92–96. (doi:10.1038/nature02825)
47. Yi K, Unruh JR, Deng M, Slaughter BD, Rubinstein B, Li R. 2011 Dynamic maintenance of asymmetric meiotic spindle position through Arp2/3-complex-driven cytoplasmic streaming in mouse oocytes. *Nat. Cell Biol.* **13**, 1252–1258. (doi:10.1038/ncb2320)
48. Bienkowska D, Cowan CR. 2012 Centrosomes can initiate a polarity axis from any position within one-cell *C. elegans* embryos. *Curr. Biol.* **22**, 583–589. (doi:10.1016/j.cub.2012.01.064)
49. Saturno DM, Castanzo DT, Williams M, Parikh DA, Jaeger EC, Lyczak R. 2017 Sustained centrosome-cortical contact ensures robust polarization of the one-cell *C. elegans* embryo. *Dev. Biol.* **422**, 135–145. (doi:10.1016/j.ydbio.2016.12.025)
50. Uraji J, Scheffler K, Schuh M. 2018 Functions of actin in mouse oocytes at a glance. *J. Cell Sci.* **131**, jcs218099. (doi:10.1242/jcs.218099)
51. Cuenca AA, Schetter A, Aceto D, Kemphues K, Seydoux G. 2003 Polarization of the *C. elegans* zygote proceeds via distinct establishment and maintenance phases. *Development* **130**, 1255–1265. (doi:10.1242/dev.00284)
52. Kumfer KT, Cook SJ, Squirrell JM, Eliceiri KW, Peel N, O'Connell KF, White JG. 2010 CGEF-1 and CHIN-1 regulate CDC-42 activity during asymmetric division in the *Caenorhabditis elegans* embryo. *Mol. Biol. Cell* **21**, 266–277. (doi:10.1091/mbc.E09)
53. Goehring NW, Trong PK, Bois JS, Chowdhury D, Nicola EM, Hyman AA, Grill SW. 2011 Polarization of PAR proteins by advective triggering of a pattern-forming system. *Science* **334**, 1137–1141. (doi:10.1126/science.1208619)
54. Sailer A, Anneken A, Li Y, Lee S, Munro E. 2015 Dynamic opposition of clustered proteins stabilizes cortical polarity in the *C. elegans* zygote. *Dev. Cell* **35**, 131–142. (doi:10.1016/j.devcel.2015.09.006)
55. Dickinson DJ, Schwager F, Pintard L, Gotta M, Goldstein B. 2017 A single-cell biochemistry approach reveals PAR complex dynamics during cell polarization. *Dev. Cell* **42**, 416–434.e11. (doi:10.1016/j.devcel.2017.07.024)
56. Rodriguez J *et al*. 2017 aPKC cycles between functionally distinct PAR protein assemblies to drive cell polarity. *Dev. Cell* **42**, 400–415.e9. (doi:10.1016/j.devcel.2017.07.007)
57. Wang SC, Low TYF, Nishimura Y, Gole L, Yu W, Motegi F. 2017 Cortical forces and CDC-42 control clustering of PAR proteins for *Caenorhabditis elegans* embryonic polarization. *Nat. Cell Biol.* **19**, 988–995. (doi:10.1038/ncb3577)
58. Nigon V, Guerrier P, Monin H. 1960 L'architecture polaire de l'œuf et les mouvements des constituants cellulaires au cours des premières étapes du développement chez quelques nématodes. *Bull. Biol. Fr. Belg.* **93**, 131–202. [In French.]
59. Strome S. 1986 Fluorescence visualization of the distribution of microfilaments in gonads and early embryos of the nematode *Caenorhabditis elegans*. *J. Cell Biol.* **103**, 2241–2252. (doi:10.1083/jcb.103.6.2241)
60. Guo S, Kemphues KJ. 1996 A non-muscle myosin required for embryonic polarity in *Caenorhabditis elegans*. *Nature* **382**, 455–458. (doi:10.1038/382455a0)
61. Shelton CA, Carter JC, Ellis GC, Bowerman B. 1999 The nonmuscle myosin regulatory light chain gene *mlc-4* is required for cytokinesis, anterior-posterior polarity, and body morphology during *Caenorhabditis elegans* embryogenesis. *J. Cell Biol.* **146**, 439–451. (doi:10.1083/jcb.146.2.439)
62. White JG, Borisy GG. 1983 On the mechanisms of cytokinesis in animal cells. *J. Theor. Biol.* **101**, 289–316. (doi:10.1016/0022-5193(83)90342-9)
63. Roubinet C, Tsankova A, Pham TT, Monnard A, Caussinus E, Affolter M, Cabernard C. 2017 Spatio-temporally separated cortical flows and spindle geometry establish physical asymmetry in fly neural stem cells. *Nat. Commun.* **8**, 1383. (doi:10.1038/s41467-017-01391-w)
64. Hannaford M, Loyer N, Tonelli F, Zoltner M, Januschke J. 2019 A chemical-genetics approach to study the role of atypical protein kinase C in

Drosophila. *Development* **146**, dev170589. (doi:10.1242/dev.170589)

65. Oon CH, Prehoda KE. 2019 Asymmetric recruitment and actin-dependent cortical flows drive the neuroblast polarity cycle. *eLife* **8**, e45815. (doi:10.7554/eLife.45815)
66. Zihni C, Vlassaks E, Terry S, Carlton J, Leung TKC, Olson M, Pichaud F, Balda MS, Matter K. 2017 An apical MRCK-driven morphogenetic pathway controls epithelial polarity. *Nat. Cell Biol.* **19**, 1049–1060. (doi:10.1038/ncb3592)
67. Hoege C, Hyman AA. 2013 Principles of PAR polarity in *Caenorhabditis elegans* embryos. *Nat. Rev. Mol. Cell Biol.* **14**, 315–322. (doi:10.1038/nrm3558)
68. Kirby C, Kusch M, Kemphues K. 1990 Mutations in the *par* genes of *Caenorhabditis elegans* affect cytoplasmic reorganization during the first cell cycle. *Dev. Biol.* **142**, 203–215. (doi:10.1016/0012-1606(90)90164-E)
69. Franke JD, Montague RA, Kiehart DP. 2005 Nonmuscle myosin II generates forces that transmit tension and drive contraction in multiple tissues during dorsal closure. *Curr. Biol.* **15**, 2208–2221. (doi:10.1016/j.cub.2005.11.064)
70. Solon J, Kaya-Çopur A, Colombelli J, Brunner D. 2009 Pulsed forces timed by a ratchet-like mechanism drive directed tissue movement during dorsal closure. *Cell* **137**, 1331–1342. (doi:10.1016/j.cell.2009.03.050)
71. David DJV, Tishkina A, Harris TJC. 2010 The PAR complex regulates pulsed actomyosin contractions during amnioserosa apical constriction in *Drosophila*. *Development* **137**, 1645–1655. (doi:10.1242/dev.044107)
72. David DJV, Wang Q, Feng JJ, Harris TJC. 2013 Bazooka inhibits aPKC to limit antagonism of actomyosin networks during amnioserosa apical constriction. *Development* **140**, 4719–4729. (doi:10.1242/dev.098491)
73. Durney CH, Harris TJC, Feng JJ. 2018 Dynamics of PAR proteins explain the oscillation and ratcheting mechanisms in dorsal closure. *Biophys. J.* **115**, 2230–2241. (doi:10.1016/j.bpj.2018.10.014)
74. Motegi F, Seydoux G. 2013 The PAR network: redundancy and robustness in a symmetry-breaking system. *Phil. Trans. R. Soc. B* **368**, 20130010. (doi:10.1098/rstb.2013.0010)
75. Gross P, Kumar KV, Grill SW. 2017 How active mechanics and regulatory biochemistry combine to form patterns in development. *Annu. Rev. Biophys.* **46**, 337–356. (doi:10.1146/annurev-biophys-070816-033602)
76. Mayer M, Depken M, Bois JS, Jülicher F, Grill SW. 2010 Anisotropies in cortical tension reveal the physical basis of polarizing cortical flows. *Nature* **467**, 617–621. (doi:10.1038/nature09376)
77. Tse YC, Werner M, Longhini KM, Labbe JC, Goldstein B, Glotzer M. 2012 RhoA activation during polarization and cytokinesis of the early *Caenorhabditis elegans* embryo is differentially dependent on NOP-1 and CYK-4. *Mol. Biol. Cell* **23**, 4020–4031. (doi:10.1091/mbc.E12-04-0268)
78. Niwayama R, Shinohara K, Kimura A. 2011 Hydrodynamic property of the cytoplasm is sufficient to mediate cytoplasmic streaming in the *Caenorhabiditis elegans* embryo. *Proc. Natl. Acad. Sci. USA* **108**, 11 900–11 905. (doi:10.1073/PNAS.1101853108)
79. Goldstein B, Hird SN. 1996 Specification of the anteroposterior axis in *Caenorhabditis elegans*. *Development* **122**, 1467–1474.
80. Tsai MC, Ahringer J. 2007 Microtubules are involved in anterior-posterior axis formation in *C. elegans* embryos. *J. Cell Biol.* **179**, 397–402. (doi:10.1083/jcb.200708101)
81. Mittasch M *et al*. 2018 Non-invasive perturbations of intracellular flow reveal physical principles of cell organization. *Nat. Cell Biol.* **20**, 344–351. (doi:10.1038/s41556-017-0032-9)
82. Gross P, Kumar KV, Goehring NW, Bois JS, Hoege C, Jülicher F, Grill SW. 2019 Guiding self-organized pattern formation in cell polarity establishment. *Nat. Phys.* **15**, 293–300. (doi:10.1038/s41567-018-0358-7)
83. Klinkert K *et al*. 2019 Aurora A depletion reveals centrosome-independent polarization mechanism in *Caenorhabditis elegans*. *eLife* **8**, e44552. (doi:10.7554/eLife.44552)
84. Zhao P, Teng X, Tantirimudalige SN, Nishikawa M, Wohland T, Toyama Y, Motegi F. 2019 Aurora-A breaks symmetry in contractile actomyosin networks independently of its role in centrosome maturation. *Dev. Cell* **48**, 631–645.e6. (doi:10.1016/j.devcel.2019.02.012)
85. Lyczak R, Zweier L, Group T, Murrow MA, Synder C, Kulovitz L, Beatty A, Smith K, Bowerman B. 2006 The puromycin-sensitive aminopeptidase PAM-1 is required for meiotic exit and anteroposterior polarity in the one-cell *Caenorhabditis elegans* embryo. *Development* **133**, 4281–4292. (doi:10.1242/dev.02615)
86. Fortin SM, Marshall SL, Jaeger EC, Greene PE, Brady LK, Isaac RE, Schrandt JC, Brooks DR, Lyczak R. 2010 The PAM-1 aminopeptidase regulates centrosome positioning to ensure anterior–posterior axis specification in one-cell *C. elegans* embryos. *Dev. Biol.* **344**, 992–1000. (doi:10.1016/j.ydbio.2010.06.016)
87. McCloskey RJ, Kemphues KJ. 2012 Deubiquitylation machinery is required for embryonic polarity in *Caenorhabditis elegans*. *PLoS Genet.* **8**, e1003092. (doi:10.1371/journal.pgen.1003092)
88. Kapoor S, Kotak S. 2019 Centrosome Aurora A regulates RhoGEF ECT-2 localisation and ensures a single PAR-2 polarity axis in *C. elegans* embryos. *Development* **8**, 55. (doi:10.1242/dev.174565)
89. Beatty A, Morton DG, Kemphues K. 2013 PAR-2, LGL-1 and the CDC-42 GAP CHIN-1 act in distinct pathways to maintain polarity in the *C. elegans* embryo. *Development* **140**, 2005–2014. (doi:10.1242/dev.088310)
90. Motegi F, Sugimoto A. 2006 Sequential functioning of the ECT-2 RhoGEF, RHO-1 and CDC-42 establishes cell polarity in *Caenorhabditis elegans* embryos. *Nat. Cell Biol.* **8**, 978–985. (doi:10.1038/ncb1459)
91. Schonegg S, Hyman AA. 2006 CDC-42 and RHO-1 coordinate acto-myosin contractility and PAR protein localization during polarity establishment in *C. elegans* embryos. *Development* **133**, 3507–3516. (doi:10.1242/dev.02527)
92. Zonies S, Motegi F, Hao Y, Seydoux G. 2010 Symmetry breaking and polarization of the *C. elegans* zygote by the polarity protein PAR-2. *Development* **137**, 1669–1677. (doi:10.1242/dev.045823)
93. Beatty A, Morton D, Kemphues K. 2010 The *C. elegans* homolog of *Drosophila* Lethal giant larvae functions redundantly with PAR-2 to maintain polarity in the early embryo. *Development* **137**, 3995–4004. (doi:10.1242/dev.056028)
94. Nishikawa M, Naganathan SR, Jülicher F, Grill SW. 2017 Controlling contractile instabilities in the actomyosin cortex. *eLife* **6**, e19595. (doi:10.7554/eLife.19595)
95. Michaux JB, Robin FB, McFadden WM, Munro EM. 2018 Excitable RhoA dynamics drive pulsed contractions in the early *C. elegans* embryo. *J. Cell Biol.* **217**, 4230–4252. (doi:10.1083/jcb.201806161)
96. Schonegg S, Constantinescu AT, Hoege C, Hyman AA. 2007 The Rho GTPase-activating proteins RGA-3 and RGA-4 are required to set the initial size of PAR domains in *Caenorhabditis elegans* one-cell embryos. *Proc. Natl. Acad. Sci. USA* **104**, 14 976–14 981. (doi:10.1073/pnas.0706941104)
97. Schmutz C, Stevens J, Spang A. 2007 Functions of the novel RhoGAP proteins RGA-3 and RGA-4 in the germ line and in the early embryo of *C. elegans*. *Development* **134**, 3495–3505. (doi:10.1242/dev.000802)
98. Spiga FM, Prouteau M, Gotta M. 2013 The TAO kinase KIN-18 regulates contractility and establishment of polarity in the *C. elegans* embryo. *Dev. Biol.* **373**, 26–38. (doi:10.1016/j.ydbio.2012.10.001)
99. Motegi F, Zonies S, Hao Y, Cuenca AA, Griffin E, Seydoux G. 2011 Microtubules induce self-organization of polarized PAR domains in *Caenorhabditis elegans* zygotes. *Nat. Cell Biol.* **13**, 1361–1367. (doi:10.1038/ncb2354)
100. Hurov JB, Watkins JL, Piwnica-Worms H. 2004 Atypical PKC phosphorylates PAR-1 kinases to regulate localization and activity. *Curr. Biol.* **14**, 736–741. (doi:10.1016/j.cub.2004.04.007)
101. Hao Y, Boyd L, Seydoux G. 2006 Stabilization of cell polarity by the *C. elegans* RING protein PAR-2. *Dev. Cell* **10**, 199–208. (doi:10.1016/j.devcel.2005.12.015)
102. Hoege C, Constantinescu A-T, Schwager A, Goehring NW, Kumar P, Hyman AA. 2010 LGL can partition the cortex of one-cell *Caenorhabditis elegans* embryos into two domains. *Curr. Biol.* **20**, 1296–1303. (doi:10.1016/j.cub.2010.05.061)
103. Bailey MJ, Prehoda KE. 2015 Establishment of Par-polarized cortical domains via phosphoregulated membrane motifs. *Dev. Cell* **35**, 199–210. (doi:10.1016/j.devcel.2015.09.016)
104. Boyd L, Guo S, Levitan D, Stinchcomb DT, Kemphues KJ. 1996 PAR-2 is asymmetrically

distributed and promotes association of P granules and PAR-1 with the cortex in *C. elegans* embryos. *Development* **122**, 3075–3084.

105. Goehring NW, Hoege C, Grill SW, Hyman AA. 2011 PAR proteins diffuse freely across the anterior–posterior boundary in polarized *C. elegans* embryos. *J. Cell Biol.* **193**, 583–594. (doi:10.1083/jcb.201011094)
106. Kotak S. 2019 Mechanisms of spindle positioning: lessons from worms and mammalian cells. *Biomolecules* **9**, 80. (doi:10.3390/biom9020080)
107. Maduro MF. 2010 Cell fate specification in the *C. elegans* embryo. *Dev. Dyn.* **239**, 1315–1329. (doi:10.1002/dvdy.22233)
108. Naganathan SR, Fürthauer S, Nishikawa M, Jülicher F, Grill SW. 2014 Active torque generation by the actomyosin cell cortex drives left–right symmetry breaking. *eLife* **3**, e04165. (doi:10.7554/eLife.04165)
109. Naganathan SR, Middelkoop TC, Fürthauer S, Grill SW. 2016 Actomyosin-driven left-right asymmetry: from molecular torques to chiral self-organization. *Curr. Opin. Cell Biol.* **38**, 24–30. (doi:10.1016/J.CEB.2016.01.004)
110. Jaffe AB, Hall A. 2005 Rho GTPases: biochemistry and biology. *Annu. Rev. Cell Dev. Biol.* **21**, 247–269. (doi:10.1146/annurev.cellbio.21.020604.150721)
111. Piekny A, Werner M, Glotzer M. 2005 Cytokinesis: welcome to the Rho zone. *Trends Cell Biol.* **15**, 651–658. (doi:10.1016/j.tcb.2005.10.006)
112. Vicente-Manzanares M, Ma X, Adelstein RS, Horwitz AR. 2009 Non-muscle myosin II takes centre stage in cell adhesion and migration. *Nat. Rev. Mol. Cell Biol.* **10**, 778–790. (doi:10.1038/nrm2786)
113. Pacquelet A. 2017 Asymmetric cell division in the one-cell *C. elegans* embryo: multiple steps to generate cell size asymmetry. In *Asymmetric cell division in development, differentiation and cancer* (eds J-P Tassan, JZ Kubiak), pp. 115–140. Cham, Switzerland: Springer International Publishing. (doi:10.1007/978-3-319-53150-2)
114. Severson AF, Baillie DL, Bowerman B. 2002 A Formin Homology protein and a Profilin are required for cytokinesis and Arp2/3-independent assembly of cortical microfilaments in *C. elegans*. *Curr. Biol.* **12**, 2066–2075. (doi:10.1016/S0960-9822(02)01355-6)
115. Velarde N, Gunsalus KC, Piano F. 2007 Diverse roles of actin in *C. elegans* early embryogenesis. *BMC Dev. Biol.* **7**, 142. (doi:10.1186/1471-213X-7-142)
116. Shivas JM, Skop AR. 2012 Arp2/3 mediates early endosome dynamics necessary for the maintenance of PAR asymmetry in *Caenorhabditis elegans*. *Mol. Biol. Cell* **23**, 1917–1927. (doi:10.1091/mbc.e12-01-0006)
117. Chartier NT, Salazar Ospina DP, Benkemoun L, Mayer M, Grill SW, Maddox AS, Labbé JC. 2011 PAR-4/LKB1 mobilizes nonmuscle myosin through anillin to regulate *C. elegans* embryonic polarization and cytokinesis. *Curr. Biol.* **21**, 259–269. (doi:10.1016/j.cub.2011.01.010)
118. Amini R, Goupil E, Labella S, Zetka M, Maddox AS, Labbé JC, Chartier NT. 2014 *C. elegans* Anillin proteins regulate intercellular bridge stability and germline syncytial organization. *J. Cell Biol.* **206**, 129–143. (doi:10.1083/jcb.201310117)
119. Pacquelet A, Uhart P, Tassan JP, Michaux G. 2015 PAR-4 and anillin regulate myosin to coordinate spindle and furrow position during asymmetric division. *J. Cell Biol.* **210**, 1085–1099. (doi:10.1083/jcb.201503006)
120. Fievet BT, Rodriguez J, Naganathan S, Lee C, Zeiser E, Ishidate T, Shirayama M, Grill S, Ahringer J. 2013 Systematic genetic interaction screens uncover cell polarity regulators and functional redundancy. *Nat. Cell Biol.* **15**, 103–112. (doi:10.1038/ncb2639)
121. Ding WY, Ong HT, Hara Y, Wongsantichon J, Toyama Y, Robinson RC, Nédélec F, Zaidel-Bar R. 2017 Plastin increases cortical connectivity to facilitate robust polarization and timely cytokinesis. *J. Cell Biol.* **216**, 1371–1386. (doi:10.1083/jcb.201603070)
122. Naganathan SR, Fürthauer S, Rodriguez J, Fievet BT, Jülicher F, Ahringer J, Cannistraci CV, Grill SW. 2018 Morphogenetic degeneracies in the actomyosin cortex. *eLife* **7**, e37677. (doi:10.7554/eLife.37677)
123. Sadler PL, Shakes DC. 2000 Anucleate *Caenorhabditis elegans* sperm can crawl, fertilize oocytes and direct anterior–posterior polarization of the 1-cell embryo. *Development* **127**, 355–366.
124. O'Connell KF, Maxwell KN, White JG. 2000 The *spd-2* gene is required for polarization of the anteroposterior axis and formation of the sperm asters in the *Caenorhabditis elegans* zygote. *Dev. Biol.* **222**, 55–70. (doi:10.1006/dbio.2000.9714)
125. Hannak E, Kirkham M, Hyman AA, Oegema K. 2001 Aurora-A kinase is required for centrosome maturation in *Caenorhabditis elegans*. *J. Cell Biol.* **155**, 1109–1116. (doi:10.1083/jcb.200108051)
126. Hamill DR, Severson AF, Carter JC, Bowerman B. 2002 Centrosome maturation and mitotic spindle assembly in *C. elegans* require SPD-5, a protein with multiple coiled-coil domains. *Dev. Cell* **3**, 673–684. (doi:10.1016/S1534-5807(02)00327-1)
127. Kemp CA, Kopish KR, Zipperlen P, Ahringer J, O'Connell KF. 2004 Centrosome maturation and duplication in *C. elegans* require the coiled-coil protein SPD-2. *Dev. Cell* **6**, 511–523. (doi:10.1016/S1534-5807(04)00066-8)
128. Cowan CR, Hyman AA. 2006 Cyclin E-Cdk2 temporally regulates centrosome assembly and establishment of polarity in *Caenorhabditis elegans* embryos. *Nat. Cell Biol.* **8**, 1441–1447. (doi:10.1038/ncb1511)
129. Noatynska A, Panbianco C, Gotta M. 2010 SPAT-1/Bora acts with Polo-like kinase 1 to regulate PAR polarity and cell cycle progression. *Development* **137**, 3315–3325. (doi:10.1242/dev.055293)
130. Wallenfang MR, Seydoux G. 2000 Polarization of the anterior–posterior axis of *C. elegans* is a microtubule-directed process. *Nature* **408**, 89–92. (doi:10.1038/35040562)
131. Sonneville R, Gönczy P. 2004 *zyg-11* and *cul-2* regulate progression through meiosis II and polarity establishment in *C. elegans*. *Development* **131**, 3527–3543. (doi:10.1242/dev.01244)
132. Reich JD, Hubatsch L, Illukkumbura R, Peglion F, Bland T, Hirani N, Goehring NW. 2019 Regulated activation of the PAR polarity network ensures a timely and specific response to spatial cues. *Curr. Biol.* **29**, 1911–1923.e5. (doi:10.1016/j.cub.2019.04.058)
133. Schumacher JM, Ashcroft N, Donovan PJ, Golden A. 1998 A highly conserved centrosomal kinase, AIR-1, is required for accurate cell cycle progression and segregation of developmental factors in *Caenorhabditis elegans* embryos. *Development* **125**, 4391–4402.
134. Toya M, Terasawa M, Nagata K, Iida Y, Sugimoto A. 2011 A kinase-independent role for Aurora A in the assembly of mitotic spindle microtubules in *Caenorhabditis elegans* embryos. *Nat. Cell Biol.* **13**, 708–714. (doi:10.1038/ncb2242)
135. Mangal S, Sacher J, Kim T, Osório DS, Motegi F, Carvalho AX, Oegema K, Zanin E. 2018 TPXL-1 activates Aurora A to clear contractile ring components from the polar cortex during cytokinesis. *J. Cell Biol.* **217**, 837–848. (doi:10.1083/jcb.201706021)
136. Wu C-F, Savage NS, Lew DJ. 2013 Interaction between bud-site selection and polarity-establishment machineries in budding yeast. *Phil. Trans. R. Soc. B* **368**, 20130006. (doi:10.1098/rstb.2013.0006)
137. De Henau S, Pagès-Gallego M, Pannekoek WJ, Dansen TB. 2020 Mitochondria-derived H_2O_2 promotes symmetry breaking of the *C. elegans* zygote. *Dev. Cell* **53**, 263–271.e6. (doi:10.1016/j.devcel.2020.03.008)
138. Moon W, Matsuzaki F. 2013 Aurora A kinase negatively regulates Rho-kinase by phosphorylation *in vivo*. *Biochem. Biophys. Res. Commun.* **435**, 610–615. (doi:10.1016/j.bbrc.2013.05.028)
139. Wirtz-Peitz F, Nishimura T, Knoblich JA. 2008 Linking cell cycle to asymmetric division: Aurora-A phosphorylates the Par complex to regulate Numb localization. *Cell* **135**, 161–173. (doi:10.1016/j.cell.2008.07.049)
140. Bell GP, Fletcher GC, Brain R, Thompson BJ. 2015 Aurora kinases phosphorylate Lgl to induce mitotic spindle orientation in *Drosophila* epithelia. *Curr. Biol.* **25**, 61–68. (doi:10.1016/j.cub.2014.10.052)
141. Carvalho CA, Moreira S, Ventura G, Sunkel CE, Morais-de-Sá E. 2015 Aurora A triggers Lgl cortical release during symmetric division to control planar spindle orientation. *Curr. Biol.* **25**, 53–60. (doi:10.1016/j.cub.2014.10.053)
142. Zaidel-Bar R, Zhenhuan G, Luxenburg C. 2015 The contractome – a systems view of actomyosin contractility in non-muscle cells. *J. Cell Sci.* **128**, 2209–2217. (doi:10.1242/jcs.170068)
143. Chugh P, Paluch EK. 2018 The actin cortex at a glance. *J. Cell Sci.* **131**, jcs186254. (doi:10.1242/jcs.186254)
144. Descovich CP, Cortes DB, Ryan S, Nash J, Zhang L, Maddox PS, Nedelec F, Maddoxa AS. 2018 Cross-linkers both drive and brake cytoskeletal remodeling and furrowing in cytokinesis. *Mol. Biol. Cell* **29**, 622–631. (doi:10.1091/mbc.E17-06-0392)

145. Maddox A, Lewellyn L, Desai A, Oegema K. 2007 Anillin and the septins promote asymmetric ingression of the cytokinetic furrow. *Dev. Cell* **12**, 827–835. (doi:10.1016/j.devcel.2007.02.018)
146. Jordan SN, Davies T, Zhuravlev Y, Dumont J, Shirasu-Hiza M, Canman JC. 2016 Cortical PAR polarity proteins promote robust cytokinesis during asymmetric cell division. *J. Cell Biol.* **212**, 39–49. (doi:10.1083/jcb.201510063)
147. Flynn JR, McNally FJ. 2017 A casein kinase 1 prevents expulsion of the oocyte meiotic spindle into a polar body by regulating cortical contractility. *Mol. Biol. Cell* **28**, 2410–2419. (doi:10.1091/mbc.E17-01-0056)
148. Singh D, Odedra D, Dutta P, Pohl C. 2019 Mechanical stress induces a scalable switch in cortical flow polarization during cytokinesis. *J. Cell Sci.* **132**, jcs231357. (doi:10.1242/jcs.231357)
149. Biswas KH, Groves JT. 2019 Hybrid live cell-supported membrane interfaces for signaling studies. *Annu. Rev. Biophys.* **48**, 537–562. (doi:10.1146/annurev-biophys-070317-033330)
150. Ganzinger KA, Schwille P. 2019 More from less – bottom-up reconstitution of cell biology. *J. Cell Sci.* **132**, jcs227468. (doi:10.1242/jcs.227488)
151. Monachino E, Spenkelink LM, van Oijen AM. 2017 Watching cellular machinery in action, one molecule at a time. *J. Cell Biol.* **216**, 41–51. (doi:10.1083/jcb.201610025)
152. Hoorens MWH, Szymanski W. 2018 Reversible, spatial and temporal control over protein activity using light. *Trends Biochem. Sci.* **43**, 567–575. (doi:10.1016/j.tibs.2018.05.004)
153. Hirsch SM, Sundaramoorthy S, Davies T, Zhuravlev Y, Waters JC, Shirasu-Hiza M, Dumont J, Canman JC. 2018 FLIRT: fast local infrared thermogenetics for subcellular control of protein function. *Nat. Methods* **15**, 921–923. (doi:10.1038/s41592-018-0168-y)
154. Martin AC, Kaschube M, Wieschaus EF. 2009 Pulsed contractions of an actin–myosin network drive apical constriction. *Nature* **457**, 495–499. (doi:10.1038/nature07522)
155. Rauzi M, Lenne PF, Lecuit T. 2010 Planar polarized actomyosin contractile flows control epithelial junction remodelling. *Nature* **468**, 1110–1115. (doi:10.1038/nature09566)
156. Roh-Johnson M *et al*. 2012 Triggering a cell shape change by exploiting preexisting actomyosin contractions. *Science* **335**, 1232–1235. (doi:10.1126/science.1217869)
157. Levayer R, Lecuit T. 2013 Oscillation and polarity of E-cadherin asymmetries control actomyosin flow patterns during morphogenesis. *Dev. Cell* **26**, 162–175. (doi:10.1016/j.devcel.2013.06.020)
158. Razzell W, Wood W, Martin P. 2014 Recapitulation of morphogenetic cell shape changes enables wound re-epithelialisation. *Development* **141**, 1814–1820. (doi:10.1242/dev.107045)
159. Maître JL, Niwayama R, Turlier H, Nedelec F, Hiiragi T. 2015 Pulsatile cell-autonomous contractility drives compaction in the mouse embryo. *Nat. Cell Biol.* **17**, 849–855. (doi:10.1038/ncb3185)
160. Vasquez CG, Tworoger M, Martin AC. 2014 Dynamic myosin phosphorylation regulates contractile pulses and tissue integrity during epithelial morphogenesis. *J. Cell Biol.* **206**, 435–450. (doi:10.1083/jcb.201402004)
161. Kumar KV, Bois JS, Jülicher F, Grill SW. 2014 Pulsatory patterns in active fluids. *Phys. Rev. Lett.* **112**, 208101. (doi:10.1103/PhysRevLett.112.208101)
162. Munjal A, Philippe JM, Munro E, Lecuit T. 2015 A self-organized biomechanical network drives shape changes during tissue morphogenesis. *Nature* **524**, 351–355. (doi:10.1038/nature14603)
163. Saha S, Nagy TL, Weiner OD. 2018 Joining forces: crosstalk between biochemical signalling and physical forces orchestrates cellular polarity and dynamics. *Phil. Trans. R. Soc. B* **373**, 20170145. (doi:10.1098/rstb.2017.0145)
164. Gorfinkiel N. 2016 From actomyosin oscillations to tissue-level deformations. *Dev. Dyn.* **245**, 268–275. (doi:10.1002/dvdy.24363)
165. Xie S, Martin AC. 2015 Intracellular signalling and intercellular coupling coordinate heterogeneous contractile events to facilitate tissue folding. *Nat. Commun.* **6**, 7161. (doi:10.1038/ncomms8161)
166. Heer NC, Miller PW, Chanet S, Stoop N, Dunkel J, Martin AC. 2017 Actomyosin-based tissue folding requires a multicellular myosin gradient. *J. Cell Sci.* **130**, 1876–1886. (doi:10.1242/dev.146761)
167. Denk-lobnig M, Heer NC, Martin AC. 2020 Combinatorial patterns of graded RhoA activation and uniform F-actin depletion promote tissue curvature. *bioRxiv*, 2020.04.15.043893. (doi:10.1101/2020.04.15.043893)
168. Banerjee DS, Munjal A, Lecuit T, Rao M. 2017 Actomyosin pulsation and flows in an active elastomer with turnover and network remodeling. *Nat. Commun.* **8**, 1121. (doi:10.1038/s41467-017-01130-1)
169. Bailles A, Collinet C, Philippe JM, Lenne PF, Munro E, Lecuit T. 2019 Genetic induction and mechanochemical propagation of a morphogenetic wave. *Nature* **572**, 467–473. (doi:10.1038/s41586-019-1492-9)
170. Mason FM, Xie S, Vasquez CG, Tworoger M, Martin AC. 2016 RhoA GTPase inhibition organizes contraction during epithelial morphogenesis. *J. Cell Biol.* **214**, 603–617. (doi:10.1083/jcb.201603077)
171. Coravos JS, Mason FM, Martin AC. 2017 Actomyosin pulsing in tissue integrity maintenance during morphogenesis. *Trends Cell Biol.* **27**, 276–283. (doi:10.1016/j.tcb.2016.11.008)
172. Padmanabhan A, Ong HT, Zaidel-Bar R. 2017 Non-junctional E-cadherin clusters regulate the actomyosin cortex in the *C. elegans* zygote. *Curr. Biol.* **27**, 103–112. (doi:10.1016/j.cub.2016.10.032)
173. Robin FB, Mcfadden WM, Yao B, Munro EM. 2014 Single-molecule analysis of cell surface dynamics in *Caenorhabditis elegans* embryos. *Nat. Methods* **11**, 677–682. (doi:10.1038/nmeth.2928)
174. Arata Y *et al*. 2016 Cortical polarity of the RING protein PAR-2 is maintained by exchange rate kinetics at the cortical-cytoplasmic boundary. *Cell Rep.* **16**, 2156–2168. (doi:10.1016/j.celrep.2016.07.047)
175. Benton R, St Johnston D. 2003 A conserved oligomerization domain in *Drosophila* Bazooka/PAR-3 is important for apical localization and epithelial polarity. *Curr. Biol.* **13**, 1330–1334. (doi:10.1016/S0960-9822(03)00508-6)
176. Mizuno K, Suzuki A, Hirose T, Kitamura K, Kutsuzawa K, Futaki M, Amano Y, Ohno S. 2003 Self-association of PAR-3-mediated by the conserved N-terminal domain contributes to the development of epithelial tight junctions. *J. Biol. Chem.* **278**, 31 240–31 250. (doi:10.1074/jbc.M303593200)
177. Feng W, Wu H, Chan LN, Zhang M. 2007 The Par-3 NTD adopts a PB1-like structure required for Par-3 oligomerization and membrane localization. *EMBO J.* **26**, 2786–2796. (doi:10.1038/sj.emboj.7601702)
178. Li B, Kim H, Beers M, Kemphues K. 2010 Different domains of *C. elegans* PAR-3 are required at different times in development. *Dev. Biol.* **344**, 745–757. (doi:10.1016/j.ydbio.2010.05.506)
179. McKinley RFA, Yu CG, Harris TJC. 2012 Assembly of Bazooka polarity landmarks through a multifaceted membrane-association mechanism. *J. Cell Sci.* **125**, 1177–1190. (doi:10.1242/jcs.091884)
180. Zhang Y *et al*. 2013 Structural insights into the intrinsic self-assembly of Par-3 N-terminal domain. *Structure* **21**, 997–1006. (doi:10.1016/j.str.2013.04.004)
181. Harris TJC. 2017 Protein clustering for cell polarity: Par-3 as a paradigm. *F1000Research* **6**, 1620. (doi:10.12688/f1000research.11976.1)
182. Lemmon MA. 2008 Membrane recognition by phospholipid-binding domains. *Nat. Rev. Mol. Cell Biol.* **9**, 99–111. (doi:10.1038/nrm2328)
183. Beers M, Kemphues K. 2006 Depletion of the co-chaperone CDC-37 reveals two modes of PAR-6 cortical association in *C. elegans* embryos. *Development* **133**, 3745–3754. (doi:10.1242/dev.02544)
184. Gotta M, Abraham MC, Ahringer J. 2001 CDC-42 controls early cell polarity and spindle orientation in *C. elegans*. *Curr. Biol.* **11**, 482–488. (doi:10.1016/S0960-9822(01)00142-7)
185. Kay AJ, Hunter CP. 2001 CDC-42 regulates PAR protein localization and function to control cellular and embryonic polarity in *C. elegans*. *Curr. Biol.* **11**, 474–481. (doi:10.1016/S0960-9822(01)00141-5)
186. Aceto D, Beers M, Kemphues KJ. 2006 Interaction of PAR-6 with CDC-42 is required for maintenance but not establishment of PAR asymmetry in *C. elegans*. *Dev. Biol.* **299**, 386–397. (doi:10.1016/j.ydbio.2006.08.002)
187. Truong Quang BA, Mani M, Markova O, Lecuit T, Lenne PF. 2013 Principles of E-cadherin supramolecular organization in vivo. *Curr. Biol.* **23**, 2197–2207. (doi:10.1016/j.cub.2013.09.015)
188. Nashchekin D, Fernandes AR, St Johnston D. 2016 Patronin/shot cortical foci assemble the noncentrosomal microtubule array that specifies the

Drosophila anterior-posterior axis. *Dev. Cell* **38**, 61–72. (doi:10.1016/j.devcel.2016.06.010)

189. Shan Z *et al*. 2018 Basal condensation of Numb and Pon complex via phase transition during *Drosophila* neuroblast asymmetric division. *Nat. Commun.* **9**, 737. (doi:10.1038/s41467-018-03077-3)
190. Ko CS, Tserunyan V, Martin AC. 2019 Microtubules promote intercellular contractile force transmission during tissue folding. *J. Cell Biol.* **218**, 2726–2742. (doi:10.1083/jcb.201902011)
191. Hird S. 1996 Cortical actin movements during the first cell cycle of the *Caenorhabditis elegans* embryo. *J. Cell Sci.* **109**, 525–533.
192. Gallo CM, Wang JT, Motegi F, Seydoux G. 2010 Cytoplasmic partitioning of P granule components is not required to specify the germline in *C. elegans*. *Science* **330**, 1685–1689. (doi:10.1126/science.1193697)
193. Weinert FM, Braun D. 2008 Optically driven fluid flow along arbitrary microscale patterns using thermoviscous expansion. *J. Appl. Phys.* **104**, 104701–104706. (doi:10.1063/1.3026526)
194. Krauss J, López de Quinto S, Nüsslein-Volhard C, Ephrussi A. 2009 Myosin-V regulates *oskar* mRNA localization in the *Drosophila* oocyte. *Curr. Biol.* **19**, 1058–1063. (doi:10.1016/j.cub.2009.04.062)
195. Hecht I, Rappel WJ, Levine H. 2009 Determining the scale of the Bicoid morphogen gradient. *Proc. Natl Acad. Sci. USA* **106**, 1710–1715. (doi:10.1073/pnas.0807655106)
196. Leibfried A, Müller S, Ephrussi A. 2013 A Cdc42-regulated actin cytoskeleton mediates *Drosophila* oocyte polarization. *Development* **140**, 362–371. (doi:10.1242/dev.089250)
197. Wang HR, Zhang Y, Ozdamar B, Ogunjimi AA, Alexandrova E, Thomsen GH, Wrana JL. 2003 Regulation of cell polarity and protrusion formation by targeting RhoA for degradation. *Science* **302**, 1775–1779. (doi:10.1126/science.1090772)
198. Chen X, Macara IG. 2005 Par-3 controls tight junction assembly through the Rac exchange factor Tiam1. *Nat. Cell Biol.* **7**, 262–269. (doi:10.1038/ncb1226)
199. Tsankova A, Pham TT, Garcia DS, Otte F, Cabernard C. 2017 Cell polarity regulates biased myosin activity and dynamics during asymmetric cell division via *Drosophila* Rho kinase and protein kinase N. *Dev. Cell* **42**, 143–155.e5. (doi:10.1016/j.devcel.2017.06.012)
200. Hannaford MR, Ramat A, Loyer N, Januschke J. 2018 aPKC-mediated displacement and actomyosin-mediated retention polarize Miranda in *Drosophila* neuroblasts. *eLife* **7**, e29939. (doi:10.7554/eLife.29939)
201. Brangwynne CP, Eckmann CR, Courson DS, Rybarska A, Hoege C, Gharakhani J, Jülicher F, Hyman AA. 2009 Germline P granules are liquid droplets that localize by controlled dissolution/condensation. *Science* **324**, 1729–1732. (doi:10.1126/science.1172046)
202. Saha S *et al*. 2016 Polar positioning of phase-separated liquid compartments in cells regulated by an mRNA competition mechanism. *Cell* **166**, 1572–1584.e16. (doi:10.1016/j.cell.2016.08.006)
203. Smith J, Calidas D, Schmidt H, Lu T, Rasoloson D, Seydoux G. 2016 Spatial patterning of P granules by RNA-induced phase separation of the intrinsically-disordered protein MEG-3. *eLife* **5**, e21337. (doi:10.7554/eLife.21337)
204. Han B, Antkowiak KR, Fan X, Rutigliano M, Ryder SP, Griffin EE. 2018 Polo-like kinase couples cytoplasmic protein gradients in the *C. elegans* zygote. *Curr. Biol.* **28**, 60–69.e8. (doi:10.1016/J.CUB.2017.11.048)
205. Wu Y, Han B, Li Y, Munro E, Odde DJ, Griffin EE. 2018 Rapid diffusion-state switching underlies stable cytoplasmic gradients in the *Caenorhabditis elegans* zygote. *Proc. Natl Acad. Sci. USA* **115**, E8440–E8449. (doi:10.1073/pnas.1722162115)
206. Wu Y, Han B, Gauvin TJ, Smith J, Singh A, Griffin EE. 2019 Single-molecule dynamics of the P granule scaffold MEG-3 in the *Caenorhabditis elegans* zygote. *Mol. Biol. Cell* **30**, 333–345. (doi:10.1091/mbc.E18-06-0402)
207. Putnam A, Cassani M, Smith J, Seydoux G. 2019 A gel phase promotes condensation of liquid P granules in *Caenorhabditis elegans* embryos. *Nat. Struct. Mol. Biol.* **26**, 220–226. (doi:10.1038/s41594-019-0193-2)
208. Wang JT, Seydoux G. 2013 Germ cell specification. *Adv. Exp. Med. Biol.* **757**, 17–39. (doi:10.1007/978-1-4614-4015-4_2)
209. Strome S, Updike D. 2015 Specifying and protecting germ cell fate. *Nat. Rev. Mol. Cell Biol.* **16**, 406–416. (doi:10.1038/nrm4009)
210. Seydoux G. 2018 The P granules of *C. elegans*: a genetic model for the study of RNA–protein condensates. *J. Mol. Biol.* **430**, 4702–4710. (doi:10.1016/j.jmb.2018.08.007)
211. Voronina E, Seydoux G, Sassone-Corsi P, Nagamori I. 2011 RNA granules in germ cells. *Cold Spring Harb. Perspect. Biol.* **3**, a002774. (doi:10.1101/cshperspect.a002774)
212. Griffin EE, Odde DJ, Seydoux G. 2011 Regulation of the MEX-5 gradient by a spatially segregated kinase/phosphatase cycle. *Cell* **146**, 955–968. (doi:10.1016/j.cell.2011.08.012)
213. Folkmann AW, Seydoux G. 2019 Spatial regulation of the polarity kinase PAR-1 by parallel inhibitory mechanisms. *Development* **146**, dev171116. (doi:10.1242/dev.171116 RESEARCH)
214. Wheeler RJ, Hyman AA. 2018 Controlling compartmentalization by non-membrane-bound organelles. *Phil. Trans. R. Soc. B* **373**, 20170193. (doi:10.1098/rstb.2017.0193)
215. Updike D, Strome S. 2010 P granule assembly and function in *Caenorhabditis elegans* germ cells. *J. Androl.* **31**, 53–60. (doi:10.2164/jandrol.109.008292)
216. Wang JT *et al*. 2014 Regulation of RNA granule dynamics by phosphorylation of serine-rich, intrinsically disordered proteins in *C. elegans*. *eLife* **3**, e04591. (doi:10.7554/eLife.04591)
217. Elbaum-Garfinkle S, Kim Y, Szczepaniak K, Chen CC-H, Eckmann CR, Myong S, Brangwynne CP. 2015 The disordered P granule protein LAF-1 drives phase separation into droplets with tunable viscosity and dynamics. *Proc. Natl Acad. Sci. USA* **112**, 7189–7194. (doi:10.1073/PNAS.1504822112)
218. Schubert CM, Lin R, De Vries CJ, Plasterk RHA, Priess JR. 2000 MEX-5 and MEX-6 function to establish soma/germline asymmetry in early *C. elegans* embryos. *Mol. Cell* **5**, 671–682. (doi:10.1016/S1097-2765(00)80246-4)
219. Pagano JM, Farley BM, McCoig LM, Ryder SP. 2007 Molecular basis of RNA recognition by the embryonic polarity determinant MEX-5. *J. Biol. Chem.* **282**, 8883–8894. (doi:10.1074/jbc.M700079200)
220. Tenlen JR, Molk JN, London N, Page BD, Priess JR. 2008 MEX-5 asymmetry in one-cell *C. elegans* embryos requires PAR-4- and PAR-1-dependent phosphorylation. *Development* **135**, 3665–3675. (doi:10.1242/dev.027060)
221. Daniels BR, Dobrowsky TM, Perkins EM, Sun SX, Wirtz D. 2010 MEX-5 enrichment in the *C. elegans* early embryo mediated by differential diffusion. *Development* **137**, 2579–2585. (doi:10.1242/dev.051326)
222. Howard M. 2012 How to build a robust intracellular concentration gradient. *Trends Cell Biol.* **22**, 311–317. (doi:10.1016/j.tcb.2012.03.002)
223. Mello CC, Schubert C, Draper B, Zhang W, Lobel R, Priess JR. 1996 The PIE-1 protein and germline specification in *C. elegans* embryos. *Nature* **382**, 710–712. (doi:10.1038/382710a0)
224. Tabara H, Hill RJ, Mello CC, Priess JR, Kohara Y. 1999 Pos-1 encodes a cytoplasmic zinc-finger protein essential for germline specification in *C. elegans*. *Development* **126**, 1–11.
225. Nishi Y, Rogers E, Robertson SM, Lin R. 2008 Polo kinases regulate *C. elegans* embryonic polarity via binding to DYRK2-primed MEX-5 and MEX-6. *Development* **135**, 687–697. (doi:10.1242/dev.013425)
226. Pecreaux J, Röper JC, Kruse K, Jülicher F, Hyman AA, Grill SW, Howard J. 2006 Spindle oscillations during asymmetric cell division require a threshold number of active cortical force generators. *Curr. Biol.* **16**, 2111–2122. (doi:10.1016/j.cub.2006.09.030)
227. Couwenbergs C, Labbé J-C, Goulding M, Marty T, Bowerman B, Gotta M. 2007 Heterotrimeric G protein signaling functions with dynein to promote spindle positioning in *C. elegans*. *J. Cell Biol.* **179**, 15–22. (doi:10.1083/jcb.200707085)
228. Nguyen-Ngoc T, Afshar K, Gönczy P. 2007 Coupling of cortical dynein and Gα proteins mediates spindle positioning in *Caenorhabditis elegans*. *Nat. Cell Biol.* **9**, 1294–1302. (doi:10.1038/ncb1649)
229. Grill SW, Gönczy P, Stelzer EH, Hyman AA. 2001 Polarity controls forces governing asymmetric spindle positioning in the *Caenorhabditis elegans* embryo. *Nature* **409**, 630–633. (doi:10.1038/35054572)
230. Grill SW, Howard J, Schäffer E, Stelzer EHK, Hyman AA. 2003 The distribution of active force generators controls mitotic spindle position. *Science* **301**, 518–521. (doi:10.1126/science.1086560)

231. Colombo K, Grill SW, Kimple RJ, Willard FS, Siderovski DP, Gönczy P. 2003 Translation of polarity cues into asymmetric spindle positioning in *Caenorhabditis elegans* embryos. *Science* **300**, 1957–1961. (doi:10.1126/science.1084146)
232. Gotta M, Dong Y, Peterson YK, Lanier SM, Ahringer J. 2003 Asymmetrically distributed *C. elegans* homologs of AGS3/PINS control spindle position in the early embryo. *Curr. Biol.* **13**, 1029–1037. (doi:10.1016/S0960-9822(03)00371-3)
233. Park DH, Rose LS. 2008 Dynamic localization of LIN-5 and GPR-1/2 to cortical force generation domains during spindle positioning. *Dev. Biol.* **315**, 42–54. (doi:10.1016/j.ydbio.2007.11.037)
234. Panbianco C, Weinkove D, Zanin E, Jones D, Divecha N, Gotta M, Ahringer J. 2008 A casein kinase 1 and PAR proteins regulate asymmetry of a PIP_2 synthesis enzyme for asymmetric spindle positioning. *Dev. Cell* **15**, 198–208. (doi:10.1016/j.devcel.2008.06.002)
235. Galli M, Muñoz J, Portegijs V, Boxem M, Grill SW, Heck AJR, van den Heuvel S. 2011 aPKC phosphorylates NuMA-related LIN-5 to position the mitotic spindle during asymmetric division. *Nat. Cell Biol.* **13**, 1132–1138. (doi:10.1038/ncb2315)
236. De Simone A, Nédélec F, Gönczy P. 2016 Dynein transmits polarized actomyosin cortical flows to promote centrosome separation. *Cell Rep.* **14**, 2250–2262. (doi:10.1016/j.celrep.2016.01.077)
237. De Simone A, Gönczy P. 2017 Computer simulations reveal mechanisms that organize nuclear dynein forces to separate centrosomes. *Mol. Biol. Cell* **28**, 3165–3170. (doi:10.1091/mbc.E16-12-0823)
238. Zhu M, Settele F, Kotak S, Luis SP, Ehret L, Ponting CP, Gönczy P, Hoffmann I. 2013 MISP is a novel Plk1 substrate required for proper spindle orientation and mitotic progression. *J. Cell Biol.* **200**, 773–787. (doi:10.1083/jcb.201207050)
239. Kschonsak YT, Hoffmann I. 2018 Activated ezrin controls MISP levels to ensure correct NuMA polarization and spindle orientation. *J. Cell Sci.* **131**, jcs214544. (doi:10.1242/jcs.214544)
240. Machicoane M, de Frutos CA, Fink J, Rocancourt M, Lombardi Y, Gare S, Piel M, Echard A. 2014 SLK-dependent activation of ERMs controls LGN-NuMA localization and spindle orientation. *J. Cell Biol.* **205**, 791–799. (doi:10.1083/jcb.201401049)
241. Kwon M, Bagonis M, Danuser G, Pellman D. 2015 Direct microtubule-binding by myosin-10 orients centrosomes toward retraction fibers and subcortical actin clouds. *Dev. Cell* **34**, 323–337. (doi:10.1016/j.devcel.2015.06.013)
242. Redemann S, Pecreaux J, Goehring NW, Khairy K, Stelzer EHK, Hyman AA, Howard J. 2010 Membrane invaginations reveal cortical sites that pull on mitotic spindles in one-cell *C. elegans* embryos. *PLoS ONE* **5**, e12301. (doi:10.1371/journal.pone.0012301)
243. Scarpa E, Finet C, Blanchard GB, Sanson B. 2018 Actomyosin-driven tension at compartmental boundaries orients cell division independently of cell geometry *in vivo*. *Dev. Cell* **47**, 727–740.e6. (doi:10.1016/j.devcel.2018.10.029)
244. Sugioka K, Bowerman B. 2018 Combinatorial contact cues specify cell division orientation by directing cortical myosin flows. *Dev. Cell* **46**, 257–270.e5. (doi:10.1016/j.devcel.2018.06.020)
245. Rosenblatt J, Cramer LP, Baum B, McGee KM. 2004 Myosin II-dependent cortical movement is required for centrosome separation and positioning during mitotic spindle assembly. *Cell* **117**, 361–372. (doi:10.1016/S0092-8674(04)00341-1)
246. Sommi P, Cheerambathur D, Brust-Mascher I, Mogilner A. 2011 Actomyosin-dependent cortical dynamics contributes to the prophase force-balance in the early *Drosophila* embryo. *PLoS ONE* **6**, e18366. (doi:10.1371/journal.pone.0018366)
247. Lázaro-Diéguez F, Müsch A. 2017 Cell–cell adhesion accounts for the different orientation of columnar and hepatocytic cell divisions. *J. Cell Biol.* **216**, 3847–3859. (doi:10.1083/jcb.201608065)
248. Lough KJ, Byrd KM, Descovich CP, Spitzer DC, Bergman AJ, Beaudoin GM, Reichardt LF, Williams SE. 2019 Telophase correction refines division orientation in stratified epithelia. *eLife* **8**, e49249. (doi:10.7554/eLife.49249)
249. Basant A, Glotzer M. 2018 Spatiotemporal regulation of RhoA during cytokinesis. *Curr. Biol.* **28**, R570–R580. (doi:10.1016/j.cub.2018.03.045)
250. Pollard TD, O'Shaughnessy B. 2019 Molecular mechanism of cytokinesis. *Annu. Rev. Biochem.* **88**, 661–689. (doi:10.1146/annurev-biochem-062917-012530)
251. Leite J, Osorio DS, Sobral AF, Silva AM, Carvalho AX. 2019 Network contractility during cytokinesis—from molecular to global views. *Biomolecules* **9**, 194. (doi:10.3390/biom9050194)
252. Nishimura Y, Yonemura S. 2006 Centralspindlin regulates ECT2 and RhoA accumulation at the equatorial cortex during cytokinesis. *J. Cell Sci.* **119**, 104–114. (doi:10.1242/jcs.02737)
253. D'Avino PP, Savoian MS, Capalbo L, Glover DM. 2006 RacGAP50C is sufficient to signal cleavage furrow formation during cytokinesis. *J. Cell Sci.* **119**, 4402–4408. (doi:10.1242/jcs.03210)
254. Verma V, Mogilner A, Maresca TJ. 2019 Classical and emerging regulatory mechanisms of cytokinesis in animal cells. *Biology* **8**, 55. (doi:10.3390/biology8030055)
255. Werner M, Munro E, Glotzer M. 2007 Astral signals spatially bias cortical myosin recruitment to break symmetry and promote cytokinesis. *Curr. Biol.* **17**, 1286–1297. (doi:10.1016/j.cub.2007.06.070)
256. Murthy K, Wadsworth P. 2008 Dual role for microtubules in regulating cortical contractility during cytokinesis. *J. Cell Sci.* **121**, 2350–2359. (doi:10.1242/jcs.027052)
257. Argiros H, Henson L, Holguin C, Foe V, Shuster CB. 2012 Centralspindlin and chromosomal passenger complex behavior during normal and Rappaport furrow specification in echinoderm embryos. *Cytoskeleton* **69**, 840–853. (doi:10.1002/cm.21061)
258. Nguyen PA, Groen AC, Loose M, Ishihara K, Wühr M, Field CM, Mitchison TJ. 2014 Spatial organization of cytokinesis signaling reconstituted in a cell-free system. *Science* **346**, 244–247. (doi:10.1126/science.1256773)
259. Su KC, Bement WM, Petronczki M, Von Dassow G. 2014 An astral simulacrum of the central spindle accounts for normal, spindle-less, and anucleate cytokinesis in echinoderm embryos. *Mol. Biol. Cell* **25**, 4049–4062. (doi:10.1091/mbc.E14-04-0859)
260. Turlier H, Audoly B, Prost J, Joanny JF. 2014 Furrow constriction in animal cell cytokinesis. *Biophys. J.* **106**, 114–123. (doi:10.1016/j.bpj.2013.11.014)
261. Uehara R, Kamasaki T, Hiruma S, Poser I, Yoda K, Yajima J, Gerlich DW, Goshima G. 2016 Augmin shapes the anaphase spindle for efficient cytokinetic furrow ingression and abscission. *Mol. Biol. Cell* **27**, 812–827. (doi:10.1091/mbc.E15-02-0101)
262. Chapa-Y-Lazo B, Hamanaka M, Wray A, Balasubramanian MK, Mishima M. 2020 Polar relaxation by dynein-mediated removal of cortical myosin II. *J. Cell Biol.* **219**, e201903080. (doi:10.1083/jcb.201903080)
263. Khaliullin RN, Green RA, Shi LZ, Gomez-Cavazos JS, Berns MW, Desai A, Oegema K. 2018 A positive-feedback-based mechanism for constriction rate acceleration during cytokinesis in *Caenorhabditis elegans*. *eLife* **7**, e36073. (doi:10.7554/eLife.36073)
264. Reymann AC, Staniscia F, Erzberger A, Salbreux G, Grill SW. 2016 Cortical flow aligns actin filaments to form a furrow. *eLife* **5**, e17807. (doi:10.7554/eLife.17807)
265. Menon VV, Soumya SS, Agarwal A, Naganathan SR, Inamdar MM, Sain A. 2017 Asymmetric flows in the intercellular membrane during cytokinesis. *Biophys. J.* 113, 2787–2795. (doi:10.1016/j.bpj.2017.10.011)
266. Li Y, Munro E. 2020 Existing actin filaments orient new filament growth to provide structural memory of filament alignment during cytokinesis. *bioRxiv*. (doi:10.1101/2020.04.13.039586)
267. Carvalho A, Desai A, Oegema K. 2009 Structural memory in the contractile ring makes the duration of cytokinesis independent of cell size. *Cell* **137**, 926–937. (doi:10.1016/j.cell.2009.03.021)
268. Dorn JF, Zhang L, Phi TT, Lacroix B, Maddox PS, Liu J, Maddox AS. 2016 A theoretical model of cytokinesis implicates feedback between membrane curvature and cytoskeletal organization in asymmetric cytokinetic furrowing. *Mol. Biol. Cell* **27**, 1286–1299. (doi:10.1091/mbc.E15-06-0374)
269. Knoblich JA. 2010 Asymmetric cell division: recent developments and their implications for tumour biology. *Nat. Rev. Mol. Cell Biol.* **11**, 849–860. (doi:10.1038/nrm3010)
270. Panbianco C, Gotta M. 2011 Coordinating cell polarity with cell division in space and time. *Trends Cell Biol.* **21**, 672–680. (doi:10.1016/j.tcb.2011.08.006)
271. Watts JL, Morton DG, Bestman J, Kemphues KJ. 2000 The *C. elegans par-4* gene encodes a putative serine-threonine kinase required for establishing embryonic asymmetry. *Development* **127**, 1467–1475.
272. Morton DG, Shakes DC, Nugent S, Dichoso D, Wang W, Golden A, Kemphues KJ. 2002 The *Caenorhabditis elegans par-5* gene encodes a 14-3-3 protein required for cellular asymmetry in the early embryo. *Dev. Biol.* **241**, 47–58. (doi:10.1006/dbio.2001.0489)

273. Basant A, Lekomtsev S, Tse YC, Zhang D, Longhini KM, Petronczki M, Glotzer M. 2015 Aurora B kinase promotes cytokinesis by inducing centralspindlin oligomers that associate with the plasma membrane. *Dev. Cell* **33**, 204–215. (doi:10.1016/j.devcel.2015.03.015)
274. Ou G, Stuurman N, D'Ambrosio M, Vale RD. 2010 Polarized myosin produces unequal-size daughters during asymmetric cell division. *Science* **330**, 677–680. (doi:10.1126/science.1196112)
275. Chien SC, Brinkmann EM, Teuliere J, Garriga G. 2013 *Caenorhabditis elegans* PIG-1/MELK acts in a conserved PAR-4/LKB1 polarity pathway to promote asymmetric neuroblast divisions. *Genetics* **193**, 897–909. (doi:10.1534/genetics.112.148106)
276. Cabernard C, Prehoda KE, Doe CQ. 2010 A spindle-independent cleavage furrow positioning pathway. *Nature* **467**, 91–94. (doi:10.1038/nature09334)
277. Cinalli RM, Lehmann R. 2013 A spindle-independent cleavage pathway controls germ cell formation in *Drosophila*. *Nat. Cell Biol.* **15**, 839–845. (doi:10.1038/ncb2761)
278. Sedzinski J, Biro M, Oswald A, Tinevez JY, Salbreux G, Paluch E. 2011 Polar actomyosin contractility destabilizes the position of the cytokinetic furrow. *Nature* **476**, 462–468. (doi:10.1038/nature10286)
279. Pittman K, Skop A. 2012 Anterior PAR proteins function during cytokinesis and maintain DYN-1 at the cleavage furrow in *Caenorhabditis elegans*. *Cytoskeleton* **69**, 826–839. (doi:10.1002/cm.21053)
280. Schenk C, Bringmann H, Hyman AA, Cowan CR. 2010 Cortical domain correction repositions the polarity boundary to match the cytokinesis furrow in *C. elegans* embryos. *Development* **137**, 1743–1753. (doi:10.1242/dev.040436)
281. Dechant R, Glotzer M. 2003 Centrosome separation and central spindle assembly act in redundant pathways that regulate microtubule density and trigger cleavage furrow formation. *Dev. Cell* **4**, 333–344. (doi:10.1016/S1534-5807(03)00057-1)
282. Bringmann H, Cowan CR, Kong J, Hyman AA. 2007 LET-99, GOA-1/GPA-16, and GPR-1/2 are required for aster-positioned cytokinesis. *Curr. Biol.* **17**, 185–191. (doi:10.1016/j.cub.2006.11.070)
283. Siegrist SE, Doe CQ. 2005 Microtubule-induced Pins/Gαi cortical polarity in *Drosophila* neuroblasts. *Cell* **123**, 1323–1335. (doi:10.1016/j.cell.2005.09.043)
284. Johnston CA, Hirono K, Prehoda KE, Doe CQ. 2009 Identification of an Aurora-A/PinsLINKER/Dlg spindle orientation pathway using induced cell polarity in S2 cells. *Cell* **138**, 1150–1163. (doi:10.1016/j.cell.2009.07.041)
285. Januschke J, Gonzalez C. 2010 The interphase microtubule aster is a determinant of asymmetric division orientation in *Drosophila* neuroblasts. *J. Cell Biol.* **188**, 693–706. (doi:10.1083/jcb.200905024)
286. Loyer N, Januschke J. 2018 The last-born daughter cell contributes to division orientation of *Drosophila* larval neuroblasts. *Nat. Commun.* **9**, 3745. (doi:10.1038/s41467-018-06276-0)
287. Hannezo E, Heisenberg CP. 2019 Mechanochemical feedback loops in development and disease. *Cell* **178**, 12–25. (doi:10.1016/j.cell.2019.05.052)
288. Liu Z *et al*. 2020 Par complex cluster formation mediated by phase separation. *Nat. Commun.* **11**, 2266. (doi:10.1038/s41467-020-16135-6)